

PURIFICATION AND MODIFICATION OF BENTONITE AND ITS USE IN
POLYPROPYLENE AND LINEAR LOW DENSITY POLYETHYLENE
MATRIX NANOCOMPOSITES

A THESIS SUBMITTED TO
THE GRADUATE SCHOOL OF NATURAL AND APPLIED SCIENCES
OF
MIDDLE EAST TECHNICAL UNIVERSITY

BY

TIJEN SEYİDOĞLU

IN PARTIAL FULFILLMENT OF THE REQUIREMENTS
FOR
THE DEGREE OF DOCTOR OF PHILOSOPHY
IN
CHEMICAL ENGINEERING

JULY 2010

Approval of the thesis:

**PURIFICATION AND MODIFICATION OF BENTONITE AND ITS USE IN
POLYPROPYLENE AND LINEAR LOW DENSITY POLYETHYLENE
MATRIX NANOCOMPOSITES**

submitted by **TİJEN SEYİDOĞLU** in partial fulfillment of the requirements
for the degree of Doctor of Philosophy in **Chemical Engineering**
Department, Middle East Technical University by,

Prof. Dr. Canan Özgen _____
Dean, Graduate School of **Natural and Applied Sciences**

Prof. Dr. Gürkan Karakaş _____
Head of Department, **Chemical Engineering**

Prof. Dr. Ülkü Yılmaz _____
Supervisor, **Chemical Engineering, METU**

Examining Committee Members:

Prof. Dr. Güngör Gündüz _____
Chemical Engineering Dept., METU

Prof.Dr. Ülkü Yılmaz _____
Chemical Engineering Dept., METU

Prof. Dr. Teoman Tinçer _____
Chemistry Dept., METU

Prof. Dr. Göknur Bayram _____
Chemical Engineering Dept., METU

Prof. Dr. Halil İbrahim Ünal _____
Chemistry Dept.,Gazi University

Date: 16 .07. 2010

I hereby declare that all information in this document has been obtained and presented in accordance with academic rules and ethical conduct. I also declare that, as required by these rules and conduct, I have fully cited and referenced all material and results that are not original to this work.

Name, Last name: **Tijen Seyidođlu**

Signature:

ABSTRACT

PURIFICATION AND MODIFICATION OF BENTONITE AND ITS USE IN POLYPROPYLENE AND LINEAR LOW DENSITY POLYETHYLENE MATRIX NANOCOMPOSITES

Seyidođlu, Tijen

Ph.D., Department of Chemical Engineering

Supervisor: Prof. Dr. Ülkü Yılmaz

July 2010, 290 pages

The potential use of Reşadiye/Tokat bentonite as a reinforcement in polypropylene (PP) and linear low density polyethylene (LLDPE) polymer matrix nanocomposites filler was investigated. At first, organoclays (OC) were prepared by cation exchange reaction (CER) between the raw bentonite (RB) and three quaternary ammonium salts with long alkyl tails (QA): hexadecyl trimethyl ammonium bromide [HMA] [Br], tetrabutyl ammonium tetrafluoroborate [TBA] [BF₄], tetrakisdecyl ammonium bromide [TKA] [Br] and one quaternary phosphonium (QP) salt: tetrabutyl phosphonium tetrafluoroborate [TBP] [BF₄]. Characterization of resulting materials by XRD, TGA, FTIR and chemical analysis confirmed the formation of organoclays. Ternary composites of PP/organoclay/ maleic anhydride grafted polypropylene (MAPP) were prepared with two different grades of PPs in a co-rotating twin screw extruder. Composites prepared with these organoclays and PPs showed microcomposite formation.

In the second part of the study, raw bentonite was purified by sedimentation, and characterization of purified bentonite (PB) by XRD, cation exchange capacity (CEC) measurement and chemical analysis (ICP)

confirmed the success of purification method. PB was then modified with two QA's: dimethyl dioctadecylammonium chloride [DMDA] [Cl], tetrakis decylammonium bromide [STKA] [Br] and one QP: tributyl hexadecyl phosphonium bromide [TBHP] [Br].

Organoclays from PB were used with the PP with lower viscosity, and ternary nanocomposites (PP/Organoclay2/MAPP5) were prepared in the extruder followed by batch mixing in an intensive batch mixer. Use of DMDA and TBHP OCs resulted in nanocomposite formation, while STKA resulted in microcomposite formation as observed by XRD and TEM. Young's modulus and yield stress of the samples were enhanced through nanocomposite formation.

In the last part of the study, ternary composites of LLDPE/Organoclay/compatibilizer, a random terpolymer of ethylene, butyl acrylate and maleic anhydride (E-BA-MAH, Lotader®3210), were prepared by melt compounding in the batch mixer at two different clay concentrations (2 and 5 wt %) and fixed compatibilizer/organoclay ratio ($\alpha=2.5$). A commercial organoclay, I34, was also used in LLDPE based nanocomposites to make a comparison. XRD and TEM analyses of the compounds prepared by DMDA and TBHP showed mixed nanocomposite morphologies consisting of partially intercalated and exfoliated layers. Young's modulus and tensile strength of nanocomposites prepared with DMDA and TBHP showed generally higher values compared to those of neat LLDPE, while results were the highest in the composites prepared with commercial organoclay I34. Parallel disk rheometry was used as a supplementary technique to XRD, TEM and mechanical characterizations, and it was shown to be a sensitive tool in assessing the degree of dispersion of clay layers in the polymer matrix.

Keywords: Bentonite purification, clay modification, quaternary alkyl ammonium/phosphonium salts, polypropylene, linear low density polyethylene, nanocomposites, extrusion, rheology.

ÖZ

BENTONİTİN SAFLAŞTIRILMASI, MODİFİYE EDİLMESİ VE POLİPROPİLEN VE LİNEER ALÇAK YOĞUNLUKLU POLİETİLEN MATRİSLİ NANOKOMPOZİTLER İÇİNDE KULLANIMI

Seyidođlu, Tijen

Doktora, Kimya Mühendisliđi Bölümü

Tez yöneticisi: Prof. Dr. Ülkü Yılmaz

Temmuz 2010, 290 sayfa

Reşadiye/Tokat bentonitinin polipropilen (PP) ve lineer alçak yoğunluklu polietilen (LAPPE) polimer matrisli nanokompozitler içinde takviye dolgu maddesi olarak kullanım potansiyeli araştırılmıştır. Öncelikle, organikkiller işlenmemiş bentonitin üç kuaterner alkil amonyum: heksadesil amonyum bromür [HMA] [Br], tetrabütil amonyum tetrafloroborat [TBA] [BF₄], tetrakisdesil amonyum bromür [TKA] [Br] ve bir kuaterner alkil fosfonyum: tetrabütil fosfonyum tetrafloroborat [TBP] [BF₄] tuzu ile katyon deđiştirme reaksiyonu ile üretilmişlerdir. Üretilen malzemelerin XRD, TGA, FTIR ve kimyasal analizleri organokkil oluşumunu doğrulamıştır. PP/organikkil/maleik anhidrit aşılınmış polipropilen (MAPP) üçlü nanokompozitler iki farklı tip PP ile ekstrüderde eriyik karıştırma yöntemi ile oluşturulmuşlardır. Karışımların XRD analizi mikrokompzit oluşumunu göstermiştir.

Çalışmanın ikinci kısmında işlenmemiş bentonit suda sedimentasyon yöntemi ile saflaştırılmış ve saf bentonitin (SB) XRD, katyon deđiştirme kapasitesi (KDK) ölçümü ve kimyasal analiz karakterizasyonları, saflaştırma yönteminin başarısını doğrulamıştır. SB, iki kuaterner alkil amonyum tuzu: dimetildioktadesil amonyum klorür [DMA] [Cl],

tetrakisdesil amonyum bromür [STKA] [Br] ve bir kuarterner fosfonyum tuzu olan tetrabütilfosfonyum bromür [TBHP] [Br] ile modifiye edilmiştir.

Organikkiller düşük viskoziteye sahip PP içinde kullanılmışlar ve üçlü nanokompozitler (PP/organobentonit/MAPP) ekstrüzyon ve devamında kesikli karıştırıcı içinde eriyik karıştırma yöntemi ile üretilmişlerdir. XRD analizleri DMDA ve TBHP ile nanokompozit oluştuğunu gösterirken, STKA ile ise mikrokompozitlerin oluştuğu gözlemlenmiştir. Young modülü ve akma gerilimleri nanokompozit oluşumu ile artmıştır.

Çalışmanın son kısmında, iki farklı kil konsantrasyonlarında (% 2 ve 5) ve sabit uyum sağlayıcı/kil oranında ($\alpha=2.5$), LAYPE/organikkil/uyum sağlayıcı, bir etilen-bütil akrilat-maleik anhidrit üçlü polimerinden (E-BA-MAH, Lotader ©3210), oluşan üçlü nanokompozitler, kesikli karıştırıcı içinde eriyik karıştırma yöntemi ile üretilmişlerdir. Bir ticari kil, I34, karşılaştırma yapılabilmesi için LAYPE bazlı nanokompozitler içinde ayrıca kullanılmıştır. DMDA ve TBHP ile üretilen karışımların XRD ve TEM analizleri kısmi aralanmış ve saçılmış karışık bir morfolojiye sahip nanokompozitlerin üretildiğini doğrulamıştır. DMDA ve TBHP ile üretilen nanokompozitlerin Young modülü ve çekme dayanımları saf LAYPE matrisine göre artış gösterirken, en yüksek değerler ticari kil I34 ile elde edilmiştir. Paralel disk reometrisi, XRD, TEM ve mekanik analizlere tamamlayıcı teknik olarak kullanılmış ve reolojik ölçümlerin kil dağılımı derecesinin tayininde duyarlı bir yöntem olduğu görülmüştür.

Anahtar kelimeler: Bentonit saflaştırılması, kilin modifiye edilmesi, kuarterner alkil amonyum/fosfonyum tuzu, polipropilen, lineer alçak yoğunluklu polietilen, nanokompozitler, ekstrüzyon, reoloji.

To my family

ACKNOWLEDGMENTS

I would like to thank sincerely my thesis advisor Prof. Dr. Ülkü Yılmaz for his trust, encouragement, understanding, guidance and help in every step of my study. He was always concerned and enthusiastic, and provided many outstanding suggestions that advanced the thesis. I sincerely appreciate the time and effort he has taken to train me in the methods of carrying out successful research.

My special thanks go to Prof. Dr. Göknur Bayram for her contributions to completion of the thesis and also for providing me every opportunity to use the instruments in her laboratory. I would also like to thank to Prof. Dr. Teoman Tinçer for his helpful advice necessary for the completion of this work.

I am sincerely grateful to Prof. Dr. Dilhan Kalyon from Stevens Institute of Technology, for giving me the opportunity to study in his Highly Filled Materials Institute (HFMI) laboratories, under his supportive and helpful supervising. My acknowledgements also go to Dr. Halil Gevgilili from HFMI Group for his help through my experiments and contributions on viscoelastic property analysis.

I would like to thank my lab mates Dr. Sertan Yeşil, Filiz Cengiz and Canan Yeniova for their help in getting me acquainted in laboratory equipments and for their friendship. In addition, I would also like to thank to my other lab mates Dr. Mert Kılınç, Dr. Özcan Köysüren, Damla Eroğlu, Wisam Abdallah, Fatma Işık Coşkunes for their friendship through the laboratory days. I would specially like to thank to Beril Korkmaz Erdural for her friendship through my study. I would also like to thank colleagues from HFMI group during my studies.

I would like to thank to Selahaddin Erdoğan from METU, Chemistry Department for his help for the sample preparation. I would also like to thank technicians Mehmet Güler from UNAM, Bilkent University for the TEM analysis, Cengiz Tan from METU, METE Department for the SEM analysis, Necmi Avcı from METU, METE Department for the X-Ray analysis, Ayşe Nur Özkan from METU, Central Laboratory for the DSC analysis, Mihrican Açıkgöz from METU, ChE Department for the TGA analysis.

Last, but not the least, my appreciations extend to my parents Mayide, and Cevdet, brother Can Gürel, for their endless, continuous support and meaning in my life.

I offer sincere thanks to my sister Aylin Met and her husband Ilker Met for their continuous encouragement, patience, advice and support during my study.

This study was partially supported by The Scientific and Technological Research Council of Turkey (TUBITAK) under scholarship code 2214-International Research Fellowship Programme.

TABLE OF CONTENTS

ABSTRACT.....	iv
ÖZ.....	vii
ACKNOWLEDGMENTS.....	x
TABLE OF CONTENTS.....	xii
LIST OF TABLES.....	xix
LIST OF FIGURES.....	xxii
LIST OF ABBREVIATIONS.....	xxxvii
CHAPTER	
1. INTRODUCTION.....	1
2. BACKGROUND INFORMATION.....	8
2.1 Composites.....	8
2.2. Polymeric Composite Materials.....	9
2.3. Nanocomposite Materials.....	9
2.4. Polymer Layered Silicate Nanocomposites (PLSN).....	11
2.4.1 Microcomposites.....	11
2.4.2 Intercalated Nanocomposites.....	12
2.4.3 Flocculated Nanocomposites.....	12
2.4.4 Exfoliated Nanocomposites.....	12
2.5 Synthesis of PLSN.....	12
2.5.1 In-Situ Method.....	12

2.5.2 Solution Polymerization	13
2.5.3 Melt Intercalation	13
2.6. Fillers	13
2.6.1 Bentonite.....	13
2.6.2 Layered Silicates and Montmorillonite.....	15
2.6.3 Cation Exchange Capacity and Modification of MMT	18
2.7 Polymer Matrices.....	20
2.7.1 Polypropylene	20
2.7.2 Polyethylene	22
2.8 Factors Affecting the PLSN Behavior.....	24
2.9. Nanocomposite Production	26
2.9.1 Extrusion.....	26
2.9.2 Batch Mixing	27
2.10 Characterization Methods	29
2.10.1 X-Ray Diffraction Analysis (XRD).....	29
2.10.2 Transmission Electron Microscopy (TEM).....	31
2.10.3 Scanning Electron Microscopy (SEM).....	33
2.10.4 Spectroscopic Analyses	34
2.10.4.1 Fourier Transform Infrared Spectroscopy (FTIR)	34
2.10.4.2. Inductively Coupled Ionic Plasma Optical Emission Spectrometer (ICP)	36
2.10.5 Thermal Characterizations	37
2.10.5.1 Differential Scanning Calorimetry (DSC).....	37
2.10.5.2 Thermogravimetric Analysis (TGA).....	38

2.10.6 Mechanical Characterization	39
2.10.6.1 Tensile Properties	39
2.10.7 Rheological Characterization.....	41
2.11 Previous Studies on MMT Modification and Their Applications in Polymer Nanocomposites	42
3. EXPERIMENTAL WORK	53
3.1 Materials	53
3.1.1 Polymer Matrix.....	53
3.1.2 Bentonite and MMTs	54
3.1.3 Elastomers	56
3.1.3.1 Maleic Anhydride Grafted Polypropylene (MAPP).....	56
3.1.3.2 Lotader®3210	56
3.1.4 Surfactants Used for Clay Modification	58
3.1.5 Heat Stabilizer	61
3.1.6 Sodium Pyrophosphate [$\text{Na}_4 (\text{P}_2\text{O}_7)$].....	62
3.2 Method.....	62
3.2.1 Purification of Bentonite.....	62
3.2.2 Modification of Bentonite	65
3.2.3 Production of Nanocomposites.....	69
3.2.3.1 Extrusion	69
3.2.3.2 Batch Mixing.....	74
3.2.4 Drying.....	79
3.2.5 Injection molding.....	79
3.2.6 Compression Molding.....	80

3.3 Characterization Techniques	81
3.3.1 Characterization of Organoclays	81
3.3.1.1 Bentonite Cation Exchange Capacity Measurement	81
3.3.1.2 X-Ray Diffraction	82
3.3.1.2.1 X-Ray Equipment (METU-METE Department)	83
3.3.1.2.2 X-Ray Equipment (Stevens Institute of Technology- HFMI Laboratory)	83
3.3.1.3 Scanning Electron Microscopy	84
3.3.1.4 Transmission Electron Microscopy (TEM).....	84
3.3.1.5 Spectroscopic Analysis	84
3.3.1.5.1 Inductively Coupled Plasma Optical Emission Spectrometer, (ICP) (Chemical Analysis for Clays).....	84
3.3.1.5.2 Fourier Transform Infrared Spectroscopy (FTIR).....	85
3.3.1.6 Thermal Analysis	85
3.3.1.6.1 Thermogravimetric Analysis (TGA).....	85
3.3.1.6.2 Differential Scanning Calorimetry (DSC)	85
3.3.1.7 Mechanical Testing	86
3.3.1.7.1 Impact Test.....	86
3.3.1.7.2 Tensile testing	88
3.3.1.8 Rheological Measurements (Stevens Ins. Tech.-HFMI)..	89
4. RESULTS AND DISCUSSION.....	91
4.1 Purification of Reşadiye Bentonite	91
4.1.1 X-Ray Analysis for Purification	91
4.1.2 X-Ray Analysis of Organoclays	94

4.1.3 TGA Analysis	101
4.1.4 FTIR Analysis	106
4.1.5 SEM and TEM Analysis of Organoclays	110
4.2 Characterization of Nanocomposites	111
4.2.1 X-Ray Analysis	111
4.2.1.1 X-Ray Analysis of Composites Prepared in SET1 (PPM/Organoclay2/MAPP2)	111
4.2.1.2 X-Ray Analysis of Composites Prepared in SET2 (PPE/Organoclay2/MAPP5)	120
4.2.1.3 X-Ray Analysis of Composites Prepared in SET-3, 4 and 5	125
4.2.1.3.1 X-Ray Analysis of Binary Nanocomposites	125
4.2.1.4 X-Ray Analysis of LLDPE Based Nanocomposites	133
4.2.1.4.1 X-Ray of Binary Nanocomposites	133
4.2.1.4.2 X-Ray Analysis of Ternary Nanocomposites	135
4.2.2 TEM Analysis	140
4.2.2.1 TEM Micrograph of PPM Based Composites	141
4.2.2.2 TEM Analysis of PPE-M Matrix Nanocomposites	143
4.2.2.3 TEM Analysis of LLDPE Based Nanocomposites	146
4.2.3 SEM Analysis	153
4.2.3.1 SEM Analysis for SET-1	153
4.2.3.2 SEM Analysis for SET 2	157
4.2.3.3 SEM Analysis for SET-4	161
4.2.3.4 SEM Analysis for SET 6	164

4.2.4 DSC Analysis	171
4.2.4.1 DSC Results of PPM and PPE Based Composites (SETs 1-4).....	171
4.2.5 Mechanical Characterization.....	175
4.2.5.1 Tensile Tests of PPM Based Composites (SET-1)	176
4.2.5.2 Tensile Tests of PPE Based Composites (SET-2).....	183
4.2.5.3 Tensile Tests of PPE Based Composites (SET-3 and 4)...	188
4.2.5.3.1 Effect of Organoclay Type	193
4.2.5.4 Mechanical Tests on LLDPE Nanocomposites.....	194
4.2.6. Linear Viscoelastic Behavior in the Melt State.....	201
4.2.6.1 Rheological Characterization of PP Based Composites	202
4.2.6.1.1 Time Sweep Test of the Samples.....	202
4.2.6.1.2 Strain Sweep Tests.....	204
4.2.6.1.3 Effect of Heat Stabilizer on Rheology	205
4.2.6.2 Frequency Test of PPE/Organoclay ² /MAPP ⁵ -M Composites.....	207
4.2.6.3 Rheological Characterization of LLDPE Based Composites.....	210
4.2.6.3.1 Time Sweep Test of LLDPE Based Nanocomposites .	210
4.2.6.3.2 Strain Sweep Test of LLDPE Based Composites.....	215
4.2.6.3.3 Frequency Sweep and Strain Amplitude Tests of LLDPE Based Composites.....	217
4.2.6.3.3.1 Effect of Organoclay Content on Rheology.....	218
4.2.6.3.3.2. Effect of Modifier Type on Rheology.....	228

5. CONCLUSIONS.....	237
5.1 Composites Prepared by Organoclays Derived from Raw Bentonite (RB)	237
5.1.1 Purification of Reşadiye Bentonite	237
5.2 Modification of Bentonite	238
5.3 PPM Based Nanocomposites (SET-1).....	239
5.4 PPE Based Nanocomposites (SET-2)	240
5.5 Composites Prepared from Organoclays Derived from PB	240
5.5.1 PPE Matrix Nanocomposites.....	240
5.5.2 LLDPE Matrix Nanocomposites.....	241
REFERENCES	244
APPENDICES.....	260
A. DSC ANALYSIS	260
B. MECHANICAL TEST RESULTS.....	276
C. RHEOLOGICAL PROPERTIES.....	285
CURRICULUM VITAE	288

LIST OF TABLES

TABLES

Table 2.1 Classifications of silicates (Bailey, 1980b; Rieder et al., 1998). Minerals that can be frequently found in bentonite or kaolin are in bold; the main components are in large typeface. Illite is a component of common soil and sediments and is classified as a mica.....	16
Table 2.2 Miliequivalent weights of common cations.....	19
Table 2.3 Studies in the literature on polymer-clay nanocomposites	47
Table 3.1 Properties of PPs and LLDPE.....	54
Table 3. 2 Chemical analysis of metal oxide composition of raw bentonite	55
Table 3.3 Properties of clays.....	55
Table 3.4 Properties of MAPP.....	56
Table 3.5 Properties of Lotader.....	57
Table 3.6 Chemical structures of surfactants.....	59
Table 3.7 Abbreviations used for organoclays used with raw and pure bentonite	67
Table 3.8 Compositions of PPM ternary and MAPP-Organoclay binary composites (Organoclays derived from RB).....	72
Table 3.9 Compositions of PPE ternary and MAPP-Organoclay binary composites (Organoclays derived from RB).....	73
Table 3.10 Compositions of PPE ternary and MAPP-Organoclay binary composites (Organoclays derived from PB).....	73

Table 3.11 Compositions of PPE ternary and MAPP-Organoclay binary composites (Organoclays derived from PB).....	75
Table 3.12 Compositions of LLDPE ternary and LOT-Organoclay binary composites.....	77
Table 3.13 Drying conditions.....	79
Table 3.14 Dimensions of impact test sample	88
Table 3.15 Dimensions of tensile sample	89
Table 4.1 Chemical analysis of bentonite	93
Table 4.2 Thermal Characterization results	105
Table 4.3 FTIR band assignment for montmorillonite clay	108
Table 4.4 Results of particle analysis by TEM analysis.....	153
Table 4.5 DSC results of PPM, PPM/MAPP blend and PPM/MAPP based composites prepared in SET-1	172
Table 4.6 DSC results PPM and its composites prepared in SET-2	173
Table 4.7 DSC results PPE and its blend and composites prepared in SETs 3-4.....	173
Table 4.8 DSC results LLDPE and its blend and composites prepared in SET-6.....	174
Table B. 1 Tensile strength data for SET-1and SET-2	276
Table B.2 Tensile strength data for SET-3, 4 and 6	277
Table B.3 Yield stress data for SET-1 and SET-2	278
Table B. 4 Young`s modulus data for SET-1 and SET-2.....	279
Table B. 5 Young`s modulus data for SET-3, SET-4 and SET-6	280
Table B. 6 Elongation at break data for SET-1, SET-2.....	281
Table B. 7 Elongation at break for SET-3, SET-4 and SET-6	282

Table B. 8 Elongation at yield data for SET-1 and SET-2	283
Table B. 9 Elongation at yield data for SET-3	284

LIST OF FIGURES

FIGURES

Figure 2.1 Schematical representation of possible composite formations with layered silicates.....	11
Figure 2. 2 a) Imaginary structure of MMT, proposed by Hoffman, Endell and Wilm, 1933, b) High aspect ratio clay platelet, c) Schematic of side view between layers.	17
Figure 2.3 Change of cation of layered silicates with cations of long chain alkyl ammonium ions.	20
Figure 2.4 Structure of PP	21
Figure 2.5 Structure of PE types.....	23
Figure 2.6 Different types of twin-screw extruders, differences between; a) intermeshing and non-intermeshing b) co and counter rotating.....	27
Figure 2.7 Banbury type internal batch mixer.....	28
Figure 2.8 Diffractions of X-Rays by planes of atoms	30
Figure 2.9 Schematic representation of TEM.....	32
Figure 2.10 Schematic view of a SEM.....	34
Figure 2.11 Infrared spectroscopy correlation table.	35
Figure 2.12 Different stretching and bending vibrations.....	36
Figure 2.13 DSC curve of a polymer	38
Figure 2.14 Structures of ionic liquids used and their names	43
Figure 3.1 Chemical structure of MAPP	56
Figure 3.2 Chemical structure of elastomer LOT	57

Figure 3.3 Chemical structure of the organic modifier of commercial clay I34, methyl dihydroxyethyl hydrogenated tallow ammonium. HT refers to hydrogenated tallow long organic molecules having ~65% C18; ~30% C16; ~5% C14.....	60
Figure 3.4 Chemical structure of the organic modifier of commercial clay Cloisite ®25A, dimethyl, hydrogenated tallow, 2-ethylhexyl quaternary ammonium and anion, methyl sulfate.....	60
Figure 3. 5 Chemical Structure of IRGAFOS 168	61
Figure 3. 6 Chemical structure of IRGANOX 1010.....	61
Figure 3. 7 Chemical structure of sodium pyrophosphate.....	62
Figure 3.8 Schematical representation of purification of bentonite	65
Figure 3. 9 Schematical representation of modification of bentonite	68
Figure 3.10 Thermo Prism TSE 16 TC twin screw extruder.....	70
Figure 3. 11 Flow chart for production route of SET-1 and SET-2.....	71
Figure 3.12 Haake Torque Rheometer with 300cc mixing head	74
Figure 3.13 Flow chart for production route of SET-3,4,5 and 6	78
Figure 3.14 DSM injection molding machine	80
Figure 3.15 Square shaped molds for X-Ray	80
Figure 3.16 CARVER compression molder	81
Figure 3. 17 Ceast Resil Impactor	87
Figure 3.18 Schematic of impact test sample	87
Figure 3.19 Schematic of tensile test sample.....	88
Figure 3.20 Rheometric Dynamic Analyzer, RDA	89

Figure 4.1 X-Ray analysis of RB, PB and PGW Nanocor (S: Smectite, Q: Quartz, C: Calcite, Cln: Clinoptilolite, F: Feldspar, OC: Opal-C).....	93
Figure 4.2 X-Ray results of modified clays a) PB, b) DMDA, c) I34, d) TBHP and e) STKA.....	96
Figure 4.3 X-Ray results of modified clays a) RB, b) TBA, c) TBP, d) HMA, e) TKA, f) TKA50 and g) PGWTKA.	97
Figure 4.4 Alkyl chain aggregation in silicates a) lateral monolayer; b) lateral bilayer; c) paraffin-type monolayer; d) paraffin-type bilayer [Vaia et al., 1994]	98
Figure 4.5 Arrangement of alkylammonium ions in the interlayer space of smectites: (a) monolayers, (b) bilayers, (c) pseudo-trimolecular layers, and (d, e) paraffin-type arrangements of dialkylammonium ions with different tilting angles of the alkyl chains.	99
Figure 4.6 Conformation of dialkylammonium ions with and without gauche bonds near the ammonium group.	100
Figure 4.7 TGA results of PB and organoclays with [different scaling in (a) and (b)]: a) PB, b) TBHP, c) I34, d) STKA and e) DMDA.....	102
Figure 4.8 TGA results of a) RB and organoclays; b) TBP, c) TBA, d) HMA, e) TKA, f) TKA50 and g) PGWTKA	103
Figure 4.9 FTIR spectra of RB.....	107
Figure 4.10 FTIR spectra of RB and organoclays	109
Figure 4.11 FTIR Spectra of PB and organoclays.....	109
Figure 4.12 SEM analysis of a) TKA, b) HMA and c) TEM analysis of TKA clay.....	110

Figure 4.13 XRD patterns for TKA and its composites PPM/TKA2/MAPP2	113
Figure 4.14 XRD patterns for HMA and its composites PPM/HMA2/MAPP2	115
Figure 4.15 XRD patterns for TBA and its composites PPM/TBA2/MAPP2	116
Figure 4.16 XRD patterns for TBP and its composites MAPP98/ TBP2 and PPM/TBP2/MAPP2.....	116
Figure 4.17 XRD patterns for HMA and its composite PPM/HMA1/MAPP3	117
Figure 4.18 XRD patterns for Cloisite®25 A and its composite PPM/Cloisite ®25A2/MAPP2.....	118
Figure 4.19 XRD patterns for HMA and its composite PPE/HMA2/MAPP5	121
Figure 4. 20 XRD patterns for TKA and its composite PPE/TKA2/MAPP5	122
Figure 4.21 XRD patterns for TKA50 and its composites PPE/TKA50- 2/MAPP5.....	123
Figure 4.22 XRD patterns for PGWTKA and its composites PPE/PGWTKA2/MAPP5.....	125
Figure 4.23 XRD patterns for DMDA and its binary composites MAPP98/DMDA2.....	126
Figure 4.24 XRD patterns for TBHP and its binary composites MAPP98/TBHP2.....	126

Figure 4.25 XRD patterns for DMDA and its ternary composites PPE/DMDA2/MAPP5 “extruded only”, extruded + batch mixed for different times.	128
Figure 4.26 XRD patterns for TBHP and its ternary composites PPE/DMDA2/MAPP5 “extruded only”, extruded + batch mixed.....	130
Figure 4.27 XRD patterns for STKA and its ternary composites PPE/STKA2/MAPP5 “extruded only”, extruded + batch mixed.....	131
Figure 4.28 XRD patterns for DMDA and its ternary composites PPE/DMDA2/MAPP5 “extruded only”, extruded + batch mixed for different time intervals.....	131
Figure 4.29 XRD patterns for TBHP and its ternary composites PPE/TBHP2/MAPP5 “extruded only”, extruded + batch mixed.....	132
Figure 4.30 XRD analysis of binary composites and associated organoclays, a) LOT98/DMDA2, b) LOT98/TBHP2, c) LOT98/I34-2, d) LOT98/STKA2.	134
Figure 4.31 Schematical representation of reaction between hydroxyl group of organoclay and maleic anhydride group of LOT [Loyens and Groeninckx, 2002].....	134
Figure 4.32 XRD analysis of DMDA organoclay and LLDPE ternary composites prepared by DMDA.....	136
Figure 4.33 XRD analysis of TBHP organoclay and LLDPE ternary composites prepared by TBHP.....	136
Figure 4.34 XRD analysis of LLDPE ternary composites prepared by organoclay I34.	140

Figure 4.35 TEM analysis of PPM/TKA2/MAPP2.....	142
Figure 4.36 TEM analysis of PPM/TKA2/MAPP2 (XRD is given in Fig. 4.13).....	142
Figure 4.37 The illustration for dispersed clay structure and the inter-fibrillar structure for PP/OrganoclayMAPP nanocomposites with different clay loading 2 % and 5 % [Adapted from Nam et al., 2001].....	143
Figure 4.38 TEM Analysis of PPE/DMDA2/MAPP5 -M.....	144
Figure 4.39 TEM Analysis of PPE/DMDA2/MAPP5–M at 100 nm magnification.....	145
Figure 4.40 TEM Analysis of PPE/DMDA2/MAPP5–M at 50 nm magnification.....	145
Figure 4.41 TEM analysis of PPE/TBHP2/MAPP5–M with different magnifications.....	146
Figure 4.42 TEM analysis of LL/TBHP2/LOT5 composites.....	147
Figure 4.43 TEM Analysis of LL/DMDA2/LOT5 composites	151
Figure 4.44 TEM Analysis of LL/I34-2/LOT5 composites.....	152
Figure 4.45 Fracture surface of PPM (a) x 250 magnification (b) x3000 magnification.....	154
Figure 4.46 Fracture surface of PPM98/MAPP2 (a) x 250 magnification (b) x3000 magnification.....	155
Figure 4.47 Fracture surface of PPM/TKA2/MAPP2 (a) x 250 magnification (b) x3000 magnification	155
Figure 4.48 Fracture surface of PPM/HMA2/MAPP2 (a) x 250 magnification (b) x3000 magnification.....	156

Figure 4.49 Fracture surface of PPM/HMA1/MAPP3 (a) x 250 magnification (b) x3000 magnification.....	156
Figure 4.50 Fracture surface of PPM/TBA2/MAPP2 (a) x 250 magnification (b) x3000 magnification	157
Figure 4.51 Fracture surface of PPM/TBP2/MAPP2 (a) x 250 magnification (b) x3000 magnification	157
Figure 4. 52 Fracture surface of PPE (a) x 250 magnification (b) x3000 magnification.....	158
Figure 4.53 Fracture surface of PPE/HMA2/MAPP5 (a) x 250 magnification (b) x3000 magnification	159
Figure 4.54 Fracture surface of PPE/TKA50-2/MAPP5 (a) x 250 magnification (b) x3000 magnification.....	160
Figure 4.55 Fracture surface of PPE/TKA2/MAPP5 (a) x 250 magnification (b) x 3000 magnification	160
Figure 4.56 Fracture surface of PPE/PGWTKA2/MAPP5 (a) x 250 magnification (b) x3000 magnification.....	161
Figure 4.57 Fracture surface of PPE-M (a) x 250 magnification (b) x3000 magnification.....	162
Figure 4.58 Fracture surface of PPE/DMDA2/MAPP5-M (a) x 250 magnification (b) x3000 magnification.....	162
Figure 4.59 Fracture surface of PPE/STKA2/MAPP5-M (a) x 250 magnification (b) x3000 magnification.....	163
Figure 4.60 Fracture surface of PPE/TBHP2/MAPP5-M (a) x 250 magnification (b) x3000 magnification.....	163

Figure 4.61 Fracture surface of LLDPE (a) x 250 magnification (b) x3000 magnification.....	164
Figure 4.62 Fracture surface of LLDPE95/LOT5 (a) x 250 magnification (b) x3000 magnification.....	165
Figure 4.63 Fracture surface of LLDPE87.5/LOT12.5 (a) x 250 magnification (b) x3000 magnification.....	165
Figure 4.64 Fracture surface of LL/DMDA2/LOT5 (a) x 250 magnification (b) x3000 magnification	167
Figure 4.65 Fracture surface of LL/DMDA5/LOT12.5 (a) x 250 magnification (b) x3000 magnification.....	167
Figure 4.66 Fracture surface of LL/TBHP2/LOT5 (a) x 250 magnification (b) x3000 magnification	168
Figure 4.67 Fracture surface of LL/TBHP5/LOT12.5 (a) x 250 magnification (b) x3000 magnification.....	168
Figure 4.68 Fracture surface of LL/I34-2/LOT5 (a) x 250 magnification (b) x3000 magnification.....	169
Figure 4.69 Fracture surface of LL/I34-5/LOT5 (a) x 250 magnification (b) x3000 magnification.....	170
Figure 4.70 Fracture surface of LL/I34-5/LOT12.5 (a) x 250 magnification (b) x3000 magnification	170
Figure 4.71 Typical stress-strain diagram of PPM	176
Figure 4.72 Effect of organoclay type on tensile strength of PPM/Organoclay2/MAPP2 and PPM/Organoclay1/MAPP3 composites prepared in SET-1	178

Figure 4.73 Effect of organoclay type on tensile stress at yield of PPM/Organoclay2/MAPP2 and PPM/Organoclay1/MAPP3 composites prepared in SET-1.	178
Figure 4.74 Effect of organoclay type on Young`s modulus of PPM/Organoclay2/MAPP2 and PPM/Organoclay1/MAPP3 composites (SET1).....	179
Figure 4.75 Effect of organoclay type on elongation at break of PPM/Organoclay2/MAPP2 and PPM/Organoclay1/MAPP3 composites.	182
Figure 4.76 Effect of organoclay type on Young`s modulus of PPE/Organoclay2/MAPP5 composites prepared in SET2.	184
Figure 4.77 Effect of organoclay type on yield stress of PPE/Organoclay2/MAPP5 composites prepared in SET-2.....	186
Figure 4.78 Effect of organoclay type on tensile strength of PPE/Organoclay2/MAPP5 composites prepared in SET-2.....	186
Figure 4.79 Effect of organoclay type on elongation yield of PPE/Organoclay2/MAPP5 composites prepared in SET-2.....	187
Figure 4.80 Effect of organoclay type on elongation at break of PPE/Organoclay2/MAPP5 composites prepared in SET-2.....	187
Figure 4.81 Representative stress-strain diagram of PPE-M based composites.....	189
Figure 4.82 Effect of organoclay type on yield stress of PPE/Organoclay2/MAPP5-M composites prepared in SETs-3 and 4.	190
Figure 4.83 Effect of organoclay type on Young`s modulus of PPE/Organoclay2/MAPP5-M composites prepared in SETs-3 and 4.	190

Figure 4.84 Effect of organoclay type on elongation at yield of PPE/Organoclay2/MAPP5-M composites prepared in SETs-3 and 4.....	192
Figure 4.85 Effect of organoclay type on elongation at break of PPE/Organoclay2/MAPP5-M composites prepared in SETs 3 and 4.....	192
Figure 4.86 Representative stres-strain diagram of LLDPE based composites.....	196
Figure 4.87 Effect of organoclay type and concentration on Young`s modulus of LLDPE based composites prepared in SET-6.....	197
Figure 4.88 Effect of organoclay type and concentration on tensile strength of LLDPE based composites (SET-6)	197
Figure 4.89 Effect of organoclay type and concentration on elongation at break of LLDPE based composites (SET-6).	199
Figure 4.90 Time sweep test of PPE subjected to different temperature histories.....	203
Figure 4.91 Time dependence of complex viscosity of PP, MAPP and their mixtures PP%95-MAPP%5.	204
Figure 4.92 Strain dependence of storage modulus of PPE/Organoclay2/MAPP5-M samples	205
Figure 4.93 Frequency dependence of complex viscosity of PP, MAPP and their mixtures PP%95-MAPP%5 with and without heat stabilizer B225 ..	206
Figure 4.94 Frequency dependence of storage modulus, G' (Pa), of PP, MAPP and their mixtures PP%95-MAPP%5 with and without heat stabilizer B225.....	206

Figure 4.95 Frequency dependence of loss modulus, G'' (Pa), of PP, MAPP and their mixtures PP%95-MAPP%5 with and without heat stabilizer B225	207
Figure 4.96 Frequency dependence of storage, G' (Pa), and loss modulus, G'' (Pa), of ternary composites of PPE/organoclay2/MAPP5-M.	208
Figure 4.97 Frequency dependence of complex viscosity, η^* (Pa.s), of ternary composites of PPE/organoclay2/MAPP5-M composites.	209
Figure 4.98 Frequency dependence of storage modulus, G' (Pa), of PPE/organoclay2/MAPP5 samples prepared by extrusion only and by extrusion followed by batch mixing. Samples prepared with organoclay a) DMDA, b) STKA and c) TBHP.	210
Figure 4.99 Time dependence of complex viscosity, η^* (Pa.s), of LLDPE and LOT mixed for different times.	211
Figure 4.100 Time dependence of complex viscosity, η^* (Pa.s), of LLDPE and LLDPE95/LOT5 binary mixtures batch mixed for different time intervals. a) 5 min mix, b) 10 min mix, c) 15 min mix, d) 20 min mix and e) 25 min mix.	213
Figure 4.101 Frequency dependence of η^* (Pa.s), of LLDPE, LLDPE/LOT mixtures, LL/organoclay2/LOT5 composites batch mixed for different time durations with a) I34, b) DMDA	214
Figure 4.102 Strain dependence of storage modulus (G') of LLDPE and LL/Organoclay/LOT composites ($T=190\text{ }^{\circ}\text{C}$, $\omega = 5\text{ rad/s}$).	216
Figure 4.103 Strain dependence of storage modulus of LOT and LOT 98/Organoclay2 nanocomposites.	217

Figure 4.104 Frequency dependence of storage modulus $G'(\text{Pa})$, loss modulus $G''(\text{Pa})$ and complex viscosity η^* ($\text{Pa}\cdot\text{s}$) of LLDPE, LOT and the blend LLDPE95-LOT5	218
Figure 4.105 Frequency dependence of a) $G'(\text{Pa})$; b) $\eta^*(\text{Pa}\cdot\text{s})$ of LLDPE/DMDA/LOT composites with 2 wt % and 5 wt % clay	220
Figure 4.106 Frequency dependence of a) G' of PLSN containing DMDA relative to the $G'(\omega)$ of the matrix. b) η^* of PLSN containing DMDA relative to the $\eta^*(\omega)$ of the matrix	221
Figure 4.107 Frequency dependence of a) $G'(\text{Pa})$; b) $\eta^*(\text{Pa}\cdot\text{s})$ of LLDPE/TBHP/LOT composites with 2 wt % and 5 wt % clay	223
Figure 4. 108 Frequency dependence a) G' of PLSN containing TBHP relative to the $G'(\omega)$ of the matrix. b) η^* of PLSN containing TBHP relative to the $\eta^*(\omega)$ of the matrix	224
Figure 4.109 Frequency dependence of a) storage modulus, $G'(\text{Pa})$; b) complex viscosity, $\eta^*(\text{Pa}\cdot\text{s})$ of LLDPE/I34/LOT composites with 2 wt % and 5 wt % clay.....	226
Figure 4. 110. Frequency dependence a) G' of PLSN containing I34 relative to the $G'(\omega)$ of the matrix. b) η^* of PLSN containing I34 relative to the $\eta^*(\omega)$ of the matrix	227
Figure 4.111 Frequency dependence of a) $G'(\text{Pa})$; b) $\eta^*(\text{Pa}\cdot\text{s})$ of LLDPE/Organoclay2/LOT5 composites	231
Figure 4. 112 Frequency dependence of a) G' of PLSN containing 2 % of clay relative to the $G'(\omega)$ of the matrix. b) η^* of PLSN containing 2 % of clay	232

Figure 4.113 Frequency dependence of a) $G'(\text{Pa})$; b) $\eta^*(\text{Pa.s})$ of LLDPE/Organoclay5/LOT12.5 composites	233
Figure 4. 114 Frequency dependence of a) G' of PLSN containing 5 % of clay relative to the $G'(\omega)$ of the matrix. b) η^* of PLSN containing 5 % of clay relative to the $\eta^*(\omega)$ of the matrix	234
Figure 4.115 Loss modulus as a function of storage modulus for LLDPE/Organoclay2/LOT5 composites	235
Figure 4.116 Loss modulus as a function of storage modulus for LLDPE/Organoclay5/LOT12.5 composites	236
Figure A.1 DSC thermogram of PPM	260
Figure A.2 DSC thermogram of PPM98/MAPP2.....	261
Figure A.3 DSC thermogram of PPM/TBA2/MAPP2.....	261
Figure A.4 DSC thermogram of PPM/TBP2/MAPP2.....	262
Figure A.5 DSC thermogram of PPM/HMA2/MAPP2.....	262
Figure A.6 DSC thermogram of PPM/TKA2/MAPP2.....	263
Figure A.7 DSC thermogram of PPM/Cloisite25A2/MAPP2	263
Figure A.8 DSC thermogram of PPM/HMA1/MAPP3.....	264
Figure A.9 DSC thermogram of PP/TKA1/MAPP3.....	264
Figure A.10 DSC thermogram of PPE.....	265
Figure A.11 DSC thermogram of PPE/HMA2/MAPP5	265
Figure A.12 DSC thermogram of PPE/TKA2/MAPP5	266
Figure A.13 DSC thermogram of PPE/TKA50-2/MAPP5.....	266
Figure A.14 DSC thermogram of PPE/PGWKIS2/MAPP5.....	267
Figure A.15 DSC thermogram of PPE/DMDA2/MAPP5.....	267
Figure A.16 DSC thermogram of PPE/TBHP2/MAPP5.....	268

Figure A.17 DSC thermogram of PPE/STKA2/MAPP5.....	268
Figure A.18 DSC thermogram of PPE-M	269
Figure A.19 DSC thermogram of PPE/DMDA2/MAPP5-M	269
Figure A.20 DSC thermogram of PPE/TBHP2/MAPP5-M	270
Figure A.21 DSC thermogram of PPE/STKA2/MAPP5-M.....	270
Figure A.22 DSC thermogram of LLDPE	271
Figure A.23 DSC thermogram of LLDPE95/LOT5	271
Figure A.24 DSC thermogram of LLDPE87.5/LOT12.5	272
Figure A.25 DSC thermogram of LL/DMDA2/LOT5	272
Figure A.26 DSC thermogram of LL/DMDA5/LOT12.5.....	273
Figure A.27 DSC thermogram of LL/TBHP2/LOT5	273
Figure A.28 DSC thermogram of LL/TBHP5/LOT12.5.....	274
Figure A.29 DSC thermogram of LL/I34-2/LOT5	274
Figure A.30 DSC thermogram of LL/I34-5/LOT5	275
Figure A.31 DSC thermogram of LL/I34-5/LOT12.5	275
Figure C.1 Frequency dependence of storage modulus, η^* (Pa.s), of PPE/organoclay2/MAPP5 samples prepared by extrusion only and by extrusion followed by batch mixing. Samples prepared with organoclay DMDA	285
Figure C.2 Frequency dependence of storage modulus, η^* (Pa.s), of PPE/organoclay2/MAPP5 samples prepared by extrusion only and by extrusion followed by batch mixing. Samples prepared with organoclay STKA.....	286

Figure C.3 Frequency dependence of storage modulus, η^* (Pa.s), of PPE/organoclay2/MAPP5 samples prepared by extrusion only and by extrusion followed by batch mixing. Samples prepared with organoclay TBHP	286
Figure C.4 Frequency dependence of loss modulus, G'' (Pa) of LLDPE mixed for different durations.	287
Figure C.5 Frequency dependence of complex viscosity, η^* (Pa.s) of LLDPE mixed for different durations	287

LIST OF ABBREVIATIONS

[DMDA] [Cl]	Dimethyldioctadecyl ammonium chloride
[HMA] [Br]	Hexadecyltrimethyl ammonium bromide
[TBA] [BF ₄]	Tetra butyl ammonium tetrafluoroborate
[TBHP] [Br]	Tributylhexadecyl phosphonium bromide
[TBP] [BF ₄]	Tetrabutyl phosphonium tetrafluoroborate
[TKA] [Br]	Tetrakisdecyl ammonium bromide
ASTM	American Society for Testing and Materials
B	Width of the specimen, mm
Btyl	Butyl
CCD	Charge coupled device
CEC	Cation exchange capacity
CER	Cation exchange reaction
D	Distance between grips, mm
d	Interlayer spacing, nm
D	Barrel diameter, mm
DMDA	Organoclay produced by [DMDA] [Cl] and PB
DSC	Differential Scanning Calorimetry
E-BA-MAH	Ethylene-Butyl Acrylate-Maleic Anhydride
EthOH	Ethylene hydroxide
F	Force, N
FTIR	Fourier Transform Infrared Spectroscopy
G''	Loss modulus, MPa

G'	Storage modulus, MPa
G` _m	Storage modulus of base polymer (LLDPE)
HMA	Organoclay produced by [HMA] [Br] and RB
HT	Hydrogenated tallow
I34	Commercial organoclay
ICP	Inductively Coupled Plasma Spectrometer
L	Length of impact test specimen, mm
L	Length of the extruder barrel, mm
LLDPE	Linear low density polyethylene
LOT	Lotader
MAPP	Maleic anhydride grafted polypropylene
MFI	Melt flow index
MMT	Montmorillonite
Me	Methyl
Min	Minute
OC	Organoclay
PB	Purified bentonite
PCN	Polymer Clay Nanocomposites
PHR	Parts per hundred
PP	Polypropylene
PPE	Polypropylene-EH 241
PGW	Commercial montmorillonite
PPM	Polypropylene-MH418
PSN	Polymer Layered Silicate Nanocomposites

QA	Quaternary alkyl ammonium salt
QP	Quaternary alkyl phosphonium salt
RB	Raw bentonite
RDA	Rheological Dynamic Analyzer
sec	Seconds
SEM	Scanning Electron Microscopy
STKA	Organoclay produced by [TKA] [Br] and PB
T	Tallow
TBA	Organoclay produced by [TBA] [BF ₄] and RB
TBHP	Organoclay produced by [TBHP] [Br] and PB
TBP	Organoclay produced by [TBP] [BF ₄] and RB
TEM	Transmission Electron Microscopy
TKA	Organoclay produced by [TKA] [Br] and RB
TS	Tensile strength
XRD	X-Ray Diffraction
YM	Young`s modulus, MPa
YS	Yield stress

CHAPTER 1

INTRODUCTION

Polymer layered silicate nanocomposites (PLSN) are a new class of nanocomposites created by dispersing a refined form of nanoclay into polymer resins. Polymer/clay nanocomposites were first utilized by Toyota in 1990 when they developed a clay/nylon-6 nanocomposite to produce timing belt covers [Usuki et al., 1993]. Later, other automotive applications for nanocomposites were developed such as a clay/nylon-6 nanocomposite cover for Mitsubishi engines and a clay/polyolefin nanocomposite step assistant for General Motors vehicles. Presently, polymer/clay nanocomposites have attracted many researchers owing to remarkable improvement in product properties compared to pure polymer through addition of small amount of organoclay (2-5% by weight). Improvements include increase in mechanical properties i.e., higher modulus, increase in strength [Quintanilla et al., 2006; Lee et al., 2005; Chow et al., 2003; Ratnayake 2006; Contreras et al., 2006; Jin et al., 2009; Stoeffler et al., 2008 (b)], increase in thermal properties [Alexandre and Dubois, 2000], decreased permeability [Osman et al., 2004; Osman et al., 2007], and decreased flammability [Qin et al., 2005; Smart et al., 2008]. The extent of these improved polymer properties is dependent upon the interfacial interactions between the polymer and the modified clay.

Montmorillonite (MMT) is the most commonly used silicate in the PLSN due to its weak cation exchange capacity (CEC) compared to other type of clays which leads to reduced ionic interactions holding the clay layers

together. This character allows easy delamination or separation of MMT layers. Other clays such as vermiculate with high CEC are difficult to delaminate making the modification process difficult [Tjong, 2008]. MMT belongs to 2:1 type smectite family with one octahedral alumina layer inserted between two tetrahedral silica sheets. Stacking of these layers leads to van der Waals gaps or galleries. As a result of the isomorphous substitution within the layers (e.g. tetrahedral Si^{4+} replaced by Al^{3+} or octahedral Al^{3+} replaced by Mg^{2+}), a charge deficiency is generated and this deficiency is compensated by the exchangeable cations (i.e., Na^+ , Ca^{2+} , K^+) [Kim et al., 2006, Awad et al., 2004, Xie et al., 2001].

The name “bentonite” is used for a mineral which contains large amounts (80-90 wt %) of MMT and other clay and non-clay impurities together. Beneficiation of bentonite to obtain pure MMT has attracted interest [Onal et al., 2003] since MMT with high degree of purity and organoclays derived from it has many application areas such as medication [Carretero et al., 2009], membrane [Liangxiong et al., 2003], carbonless copy paper [Caine et al., 2001], catalyst [Kannan et al., 1997], groundwater and wastewater treatment [Wiles et al., 2005], compacted landfill liner [Met et al., 2005], electrorheological studies [Erol et al., 2010]. Turkey has vast amounts of bentonite mineral deposits and its estimated reserve is 280 million tons according to a research done in 1989 by Mineral Research and Exploration Institute of Turkey. Intensive research is necessary to investigate the possible application areas of this local mineral, since use of local sources are always better than the use of commercially available organoclays when economy is concerned.

Separation of clay and non-clay parts from raw bentonite (RB) to obtain pure MMT has paramount importance, especially for PLSN, because degree of purity of MMT affects delamination of clay layers in polymer matrices where non-purities and non-exchangeable cations apart from Na^+ may act as trapping points in the matrix [Bergaya et al., 2006]. Onal et al., 2003 purified the Reşadiye bentonite by sedimentation method and

found that settlement of bentonite suspension for various time intervals was successful in isolating the Na⁺-smectite similar to Na⁺-MMT. This study aims to purify Tokat/Reşadiye bentonite to obtain MMT.

The process of dispersing clay layers into the polymer matrix is heavily dependent upon polymer-clay compatibility. It is very difficult to separate the individual clay platelets in non-polar polymers such as polyolefins owing to the natural polarity and hydrophilicity of the clay. In order to achieve this separation, clay is made more organophilic by pretreating it with amino acids, quaternary long alkyl length ammonium or phosphonium salts, tetra organic phosphonium solution and ionic liquids. Several studies were conducted on the modification of montmorillonite with quaternary alkyl ammonium and phosphonium ions [Kozak et al., 2004; Lee et al., 2004; Hedley et al., 2007; Calderon et al., 2008; Massinga et al., 2010] dealing with the success of the modification and thermal stability of the organoclays which has profound effects in dispersion of clays and in final properties of polymer composites. However, even in the modified form, organoclays cannot easily be dispersed in non-polar polyolefins without the help of a compatibilizer which increases the interfacial interactions between the clay layers and the polymer matrix. Compatibilizers have functional groups on their backbone providing sufficient polarity to interact with silicate surfaces and also making dispersion in the polymer matrix easier. Compatibility between the compatibilizer and clay has primary importance since firstly clay layers should be intercalated within the compatibilizer and then within the matrix. Maleic anhydride grafted polyolefins, mainly, polypropylene (PP) and polyethylene (PE), are the most widely used compatibilizers used in many studies [Kawasumi et al., 1997; Hasegawa et al., 1998; Hotta and Paul, 2004; Quintanilla et al., 2006; Stoeffler et al., 2008 (a); Samyn et al., 2008].

The final structure of the polymer/clay nanocomposite is either exfoliated, intercalated or flocculated [Ray and Okamoto, 2003]. Exfoliation occurs

when the nanoclay platelets separate from one another in a polymer matrix. Intercalation occurs when the polymer penetrates into the clay gallery space, but does not separate the individual clay platelets. Flocculation occurs when intercalated and stacked silicate layers are flocculated due to hydroxylated edge-edge interaction of the silicate layers [Ray and Okamoto, 2003]. Literature research reveals that the diffusion of polymer chains into the galleries of layered silicate and consequent delamination and dispersion of the layered silicates in the polymer matrix is affected by the chemistry and initial d-spacing of the clay, rheology of polymer melt and shear forces applied during the production process and processing conditions. During the processing of PLSN, applied shear forces break and delaminate clay agglomerates into separated layers leading to diffusion of the clay layers within the matrix. Establishment of better clay dispersion, i.e., evolution of organoclay to an intercalated hybrid necessitates conveying of polymer chains into the interlayer of silicate layers. Considering the TEM analysis, Vaia et al., 1995 explained the structure of clay particles as agglomerates of small, oblong-shaped (primary particles) particles where these particles have a lateral dimension from 1 to 10 μm . In order to have intercalation, the polymer must be transported from the agglomerate-polymer interface to the primary particles and to the edges of the tactoids.

Vaia et al., 1996 explained the lack of XRD usage alone, in assessing the degree of dispersion in the silicate layers and proposed that XRD provides precise measurements of silicate layers but it does not provide information about the spatial distribution of silicate layers because all its data are averaged over the whole region of the specimen. Additionally, some layered silicates do not initially exhibit well-defined basal reflections. Clay dilution, peak broadening and preferred orientation of clay layers can mislead the results of XRD [Tjong 2006; Eckel et al., 2004]. Meanwhile, TEM analysis provides information about the morphology and spatial distribution of clay layers in a specific area [Vaia et al., 1996]. Hence, XRD and TEM analysis should be used together in analyzing the state of clay

dispersion. Nevertheless, the major problem by TEM is that the volume probed is very small and may not be representative of the nanocomposite as a whole. Consequently, bulk properties such as rheological/mechanical properties should be analyzed in addition to using both TEM and XRD observations [Kim and Paul, 2007].

Polyolefins used in the present study are polypropylene (PP) and linear low density polyethylene (LLDPE), which are the most widely used commodity polyolefin polymers through the world. Polyolefin based nanocomposites provide many advantages for different applications owing to their low cost, relatively high mechanical properties and commercial potential of the market of various polyolefin products [Demirkol and Kalyon 2007; Hasegawa et al., 1998; Hasegawa et al., 2000; Kato et al., 1997; Nam et al., 2001; Maiti et al., 2002].

The processing of polymer nanocomposites necessitates knowledge on their rheology. Since rheological properties of particulate suspensions are responsive to the feature of the dispersed phase, it provides information about the internal microstructure of nanocomposites, such as the state of dispersion of clay and the confinement effect of silicate layers on the motion of polymer chains [Wu et al., 2005(c); Prasad et al., 2006]. Incorporation of organoclay to a polymer matrix enhances the rheological functions, i.e, storage modulus, $G'(\text{Pa})$, by several order of magnitudes and alter the shear thinning behavior at low frequencies to indicate a transition from liquid-like ($G' \propto \omega^2$) to solid-like ($G', G'' \propto \omega^0$) rheological behavior. These enhancements are believed to indicate the degree of dispersion of the silicate layers. This has been attributed to the arrangement, in the quiescent state, of a percolated network superstructure of exfoliated layers or stacks of intercalated layers called tactoids [Kim and Paul, 2007]. Consequently, it can be used as a supplementary tool to other characterization techniques such as XRD, TEM and mechanical testing. Superior to these traditional methods, rheological properties are measured in the melt state, but they provide

information on the hybrid structure only indirectly [Solomon et al., 2001]. Conventional composite systems give rheological responses at higher filler contents than clays used in PLSN, since addition of only 3-5 % clay can give considerable rise in rheological properties. Rheological characterization has been performed by many authors to assess the degree of dispersion of clay layers [Li et al., 2003 (a)-(b); Stoeffler et al., 2008 (a); Galgali et al., 2001; Durmus et al., 2007; Wu et al., 2005 (a), (b), (c); Krishnammoorti and Giannelis ,1997] .

In the light of these discussions, this study is aimed to investigate potential use of local Tokat, Reşadiye bentonite in PP and LLDPE based matrix nanocomposites. At first, raw bentonite was modified with HMA, TKA, TBA and TBP alkyl salts and the resulting organoclays were characterized by XRD, Fourier Transform Infrared Spectroscopy (FTIR), Thermogravimetric Analysis (TGA) and by Inductively Coupled Plasma Optical Emission Spectrometer, (ICP). Then, these organoclays were used in two different grades of PP`s. PP/organoclay/ MAPP composites were prepared in a co-rotating twin screw extruder. Although there have been studies on use of HMA cation in organoclay production and its application in PP matrix nanocomposites; TKA, TBA and TBP were not used in PP nanocomposite production.

In the second part of the study, raw bentonite (RB) was purified by sedimentation method and rather pure bentonite (PB) that was rich in MMT was obtained. Then, PB was modified with DMDA, TKA and TBHP modifiers. Different quaternary compounds were used to see the effect of alkyl chain structure on the formation of nanocomposites. Characterizations of clays were done by XRD, FTIR, TGA and, ICP. CEC of RB and SB were determined by methylene blue test method (MB). TEM and SEM analysis of TKA clay produced from RB was also performed. These organoclays were used in production of PP/organoclay/MAPP ternary composites with the extruder and then they were further sheared in an intensive batch mixer. Organoclays produced were also used in

production of LLDPE/ organoclay/compatibilizer (LOT) ternary composites in an intensive batch mixer. In addition, one commercial clay, I34, was used in this set of experiments. Hitherto, no studies were conducted on the use of organoclays DMDA, TKA and I34 in preparation of LLDPE matrix based nanocomposites. Stoeffler et al., 2008 (a) used TBHP clay in LLDPE matrix and characterized it with XRD, TEM, rheometer, DSC, TGA, but not with mechanical testing.

Morphological characterizations of composites were done by XRD, SEM and TEM. Crystallization behavior of the composites was studied by Differential Scanning Calorimetry (DSC). Mechanical behavior of the nanocomposites was evaluated by measuring tensile properties (tensile strength, Young`s modulus, % elongation at break). Rheological properties of the samples were determined by a parallel disk rheometer [Rheometric Dynamic Analyzer (RDA)].

CHAPTER 2

BACKGROUND INFORMATION

2.1 Composites

A composite is a structural material which consists of two or more constituents combined at a macroscopic level and not soluble in each other [Kaw, 1997]. This combination is formed to attain properties that the individual constituents cannot attain by themselves [Chung, 2004]. One constituent is named as *the reinforcing phase* and the one in which it is embedded is named as the *matrix*. The reinforcing part can be in either shape like fiber, flake or particles [Kaw, 1997]. Many examples of composites naturally occurring can be found. As an example, coconut palm leaf can be given where it can be considered as a cantilever using the idea of fiber reinforcement. Wood is a fibrous composite: cellulose fibers in a lignin matrix. The cellulose fibers have high tensile strength but are very flexible (i.e., low stiffness), while the lignin matrix connects the fibers and renders the stiffness. Bone can be given as another example of natural composite that holds the weight of body. It consists of short and soft collagen fibers inserted in a mineral matrix called apatite [Chawla, 1998]. In addition to these naturally occurring composites, there are many other engineering materials that are composites in a general way. The origin of the demand for the composite materials can be given as the beginning of the 1960s. Since the early of the 1960s, there has been increasing demand for materials that are stiffer and stronger, yet lighter, in fields as diverse as aerospace, energy, and civil construction. An example is a lightweight structural composite that is obtained by incorporating continuous carbon fibers in one or more orientations in a polymer matrix.

The fibers give the strength and stiffness, while the polymer acts as the binder [Chung, 2004].

In general, composites are classified according to their matrix material. The main classes of composites are polymer-matrix, cement-matrix, metal-matrix, carbon-matrix and ceramic-matrix composites [Chung, 2004]. Polymer and cement matrix composites are the most commonly used composites due to the low fabrication cost. Polymer-matrix composites are mainly used for lightweight structures (aircraft, sporting goods, wheelchairs etc.) in addition to vibration, damping, electronic enclosures, asphalt solder replacement and so on.

2.2. Polymeric Composite Materials

The most common advanced composites are polymer composites consisting of a polymer (e.g., polyester, polyolefins, epoxy, urethane) reinforced by thin fillers (e.g., fibers, flakes, aramids, boron). Their vast usage is due to their low cost, high strength and simple production principles. For example, epoxy/graphite composites are five times stronger than steel on a weight-for-weight basis.

2.3. Nanocomposite Materials

Nanomaterials, and in particular, nano reinforcement for polymer composites have in recent years been the subject of intense research, development and commercialization. A remarkable 1959 talk by Nobel Laureate Richard Feynman has been accepted as a prominent step in the history of nanotechnology by many scientists. Feynman had foreseen the development of nanomaterials, nanolithography, nanoscale digital storage and molecular electronics by his famous `there is plenty of room at the bottom` quote.

Nanocomposite materials are composites prepared with filler having at least one dimension in nanoscale. Nanomaterials not only have very small physical dimensions, but also possess some unique properties owing to their small size, and moreover the producers of these materials have control over the dimensions of the materials and the subsequent property improvements [Gupta, Kennel E. and Kim, 2010].

Alexander and Dubois, 2000 classified the type of the nanocomposites depending on the how many dimensions of the embedded particles are in the nanometer scale.

a) If three dimensions are in the nano range, *isodimensional nanoparticles* are the area of interest. Examples include spherical silica nanoparticles obtained by in situ sol-gel methods and semiconductor nanoclusters.

b) If two dimensions are in nanorange and the third one is larger, forming an elongated structure, for example carbon nanotubes and cellulose whiskers which are generally used as reinforcing fillers, the resulting materials can have remarkable properties.

c) The third type of nanocomposites consists of filler in the form of sheets of one to a few nanometer thick, from hundreds to thousands nanometer long. This class of nanocomposites are mainly called as *polymer-layered crystal* nanocomposites. These materials are formed by the intercalation of a polymer inside the galleries of clay.

Investigating nanoproperties of fillers requires knowledge on their chemical structure. Since clay mineral structure and its intercalation behavior have been studied and known for a long time, third types of polymer nanocomposites mentioned above are the most widely studied types of nanocomposites [Alexander and Dubois, 2000].

2.4. Polymer Layered Silicate Nanocomposites (PLSN)

Layered silicates form various types of composite formation through polymeric matrices. These structures are schematically given in Figure 2.1.

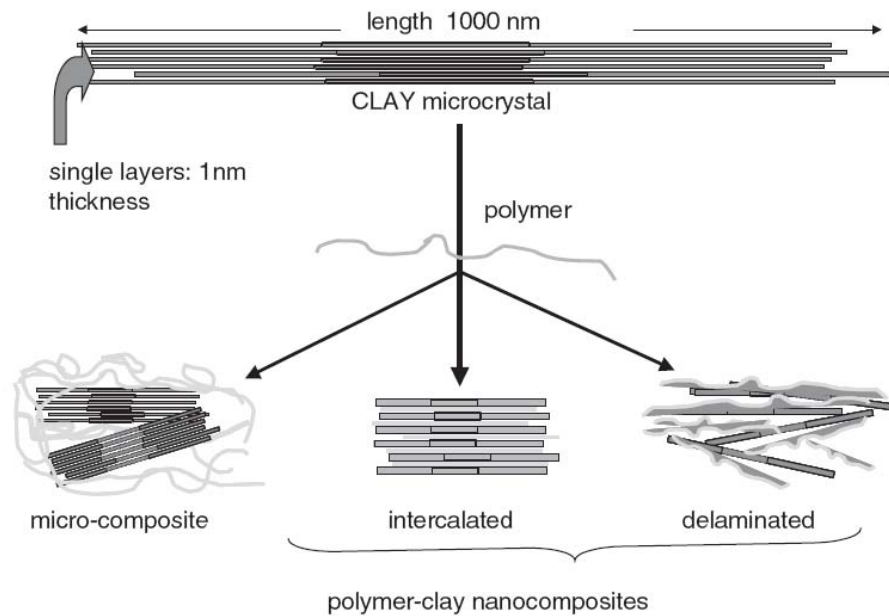


Figure 2.1 Schematical representation of possible composite formations with layered silicates [Ruitz, 2006].

2.4.1 Microcomposites

The silicates layer behave as conventional filler, and intercalation can not occur with polymer matrix. Conventional microcomposites require large amounts of filler (% 20-40) to achieve enhanced composite properties, e.g., stiffness [Tjong, 2006].

2.4.2 Intercalated Nanocomposites

Polymer matrix intercalation through silicate layers occurs in a crystallographically regular fashion, regardless of the clay to polymer ratio. Intercalated nanocomposites are obtained when one or a few molecular layers of polymers are inserted into the interlayer space of the layered silicates [Lim and Park, 1999].

2.4.3 Flocculated Nanocomposites

The structure of flocculated nanocomposites resembles to that of intercalated nanocomposites, but silicate layers are sometimes flocculated due to hydroxylated edge–edge interaction of the silicate layers [Okamoto et al., 2001].

2.4.4 Exfoliated Nanocomposites

The individual silicate layers are scattered and separated in a continuous polymer matrix by an average distance that depends on clay loading. Generally, clay concentration of an exfoliated nanocomposite is much lower than that of intercalated nanocomposites. Polymer separates the clay layers by 8-10 nm or more.

2.5 Synthesis of PLSN

Synthesis of PLSN can be divided into three main groups; in situ intercalative polymerization of monomers, polymer intercalation by the solution method and melt intercalation.

2.5.1 In-Situ Method

In situ polymerization involves the insertion of a suitable monomer into the clay galleries followed by polymerization [Tjong, 2006]. Thermoset-clay nanocomposites are generally prepared by this formation method. Process begins with swelling of organoclay in the monomer. This step

involves a specific amount of time depending on the polarity of the monomer molecules, the surface modification of organoclay and the swelling temperature. Then, the reaction is started by addition of initiators. For thermosets, i.e., epoxies or unsaturated polyesters, a curing agent or peroxide is used as the initiator. For thermoplastics, the polymerization can be started by addition of a curing agent or by an increase in temperature [Kornman, 2001].

2.5.2 Solution Polymerization

The layered silicates are exfoliated into single layers using a solvent in which the polymer (or a prepolymer in case of insoluble polymers such as polyimide) is soluble [Alexandre and Dubois, 2000]. Clay minerals can be easily dispersed in a proper solvent, owing to the weak forces that stack the layers together. Then, the polymer, dissolved in the solvent, is added to the solution and intercalates between the clay layers. In the final step, solvent is evaporated under vacuum. Nanocomposites based on high-density polyethylene, polyimide, and nematic liquid crystal polymers have been synthesized by this method [Kornman, 2001].

2.5.3 Melt Intercalation

The layered silicate is melt mixed with the polymer in the molten state. If the layer surfaces are sufficiently compatible with the chosen polymer, the polymer can enter into the basal space under shearing, and form either an intercalated or an exfoliated nanocomposite. In this technique, no solvent is required [Alexandre and Dubois, 2000].

2.6. Fillers

2.6.1 Bentonite

Bentonite is an aluminum phyllosilicate generated frequently from the alteration of volcanic ash, consisting predominantly of smectite minerals, mostly MMT (80-90 % by weight). Other smectite group minerals include hectorite, saponite, beidelite, quartz, feldspar, calcite and gypsum. The

name “bentonite” originates from the discovery of this type of clay near Fort Benton, USA, in the 19th Century. This was a natural sodium bentonite, and has been mined extensively for many years in Wyoming and Dakota for oil well drilling applications.

Two types of bentonite exist: swelling bentonite which is also called sodium bentonite and non-swelling bentonite or calcium bentonite.

Bentonites have a wide spectrum of application areas. They are either used directly or after treatment. For example, in areas such as the preparation of drilling fluids, pelletizing iron ores, the casting industry, purification of discharge waters, building applications and pet litter production, bentonites are used directly, whereas for the bleaching of edible oils acid activated bentonites are used. Clays are the major minerals in bentonites. In addition, some nonclay minerals and other clay minerals are contained in bentonites. The quality and characteristics of a bentonite depend largely on the quality and quantity of the clay, which is a micro-mesoporous material. High purity smectites obtained by purification of bentonites are used in a wide variety of areas such as carbonless copy paper, selective adsorbent, medication, membrane, organoclay, polymeric clay, pillared clay, and nanoclay and catalyst production. Thus, the isolation of some clay group minerals from bentonites is of great importance. Some of these minerals that are porous materials are MMT, beidellite, nontronite, saponite and hectorite. A specific purification method for each bentonite needs to be developed depending upon the properties of its clay and non-clay minerals. The particle sizes of these agglomerated smectite particles are smaller than 2 μm in aqueous suspensions. This property is of great importance in the purification of bentonites since it permits separation of smectites from bentonites. Onal et al., 2003 used this property in order to isolate clay from a Na^+ -bentonite (Tokat/Reşadiye) by precipitating bentonite in water. Their XRD analysis revealed that the isolated clay formula obtained by chemical analysis was very similar to Na^+ -MMT.

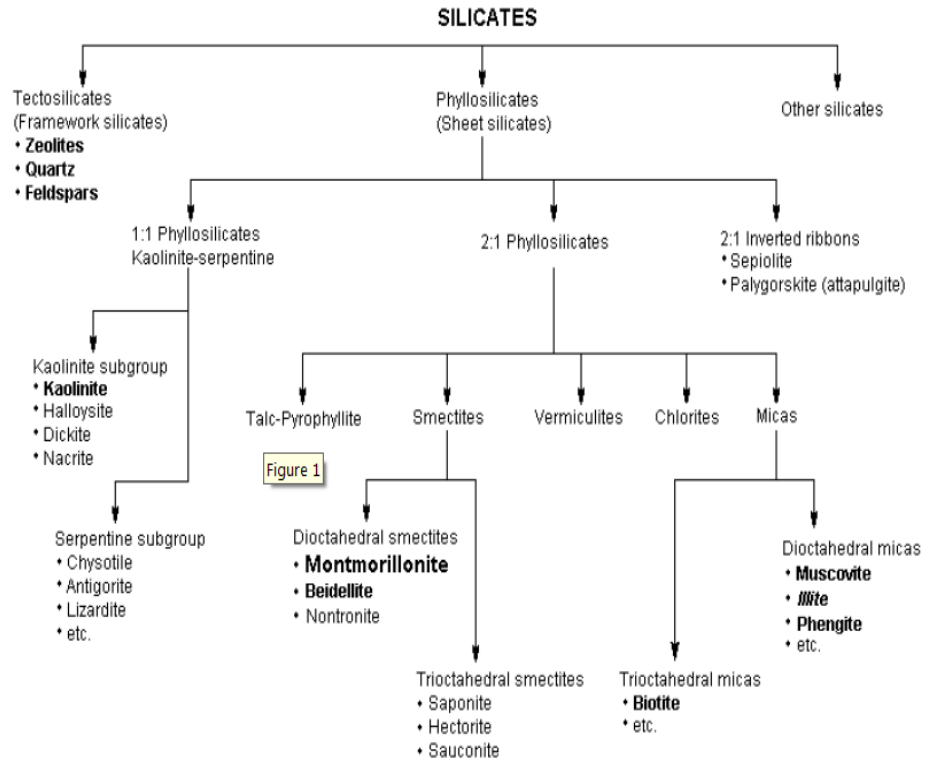
Bentonite is an abundant mineral in Turkey. The production in 1998 was 607,156 tons; estimated reserves are 280 million tons according to Mineral Research and Exploration Institute of Turkey. Bentonite has been an attractive mineral which naturally contains at least %70 MMT.

2.6.2 Layered Silicates and Montmorillonite

Clay minerals are phyllosilicates or sheet silicates with stacking of octahedral and tetrahedral sheets which are the two basic building blocks making up the basic structural units. Depending on the combination of these tetrahedral and octahedral sheets, the clay mineral structures may be of type 1:1, 2:1 and 2:1:1 type. 1:1 types consist of one octahedral sheet and one tetrahedral sheet. The 2:1 type is formed with the stacking of an octahedral sheet sandwiched between two tetrahedral sheets. The 2:1:1 structure consists of a 2:1 layer arrangement with an additional octahedral sheet between the 2:1 layers. Classification of silicates is given in Table (2.1).

The commonly used layered silicates for the preparation of PLSN's belong to the same general family of 2:1 phyllosilicates. MMT, hectorite and saponite are the most commonly used layered silicates. Mostly used clay type in polymer nanocomposites is *MMT* due to its lower cation exchange capacity. MMT belongs to 2:1 type smectite family with one octahedral alumina layer inserted between two tetrahedral silica sheets (Figure 2.2). Stacking of these layers leads to van der Waals gaps or galleries. As a result of the isomorphous substitution within the layers (e.g. tetrahedral Si^{4+} replaced by Al^{3+} or octahedral Al^{3+} replaced by Mg^{2+}), a charge deficiency is generated and this deficiency is compensated by the exchangeable cations (i.e., Na^+ , Ca^{2+} , K^+) [Kim et al., 2006, Awad et al., 2004, Xie et al., 2001].

Table 2.1 Classifications of silicates (Bailey, 1980b; Rieder et al., 1998). Minerals that can be frequently found in bentonite or kaolin are in bold; the main components are in large typeface. Illite is a component of common soil and sediments and is classified as a mica



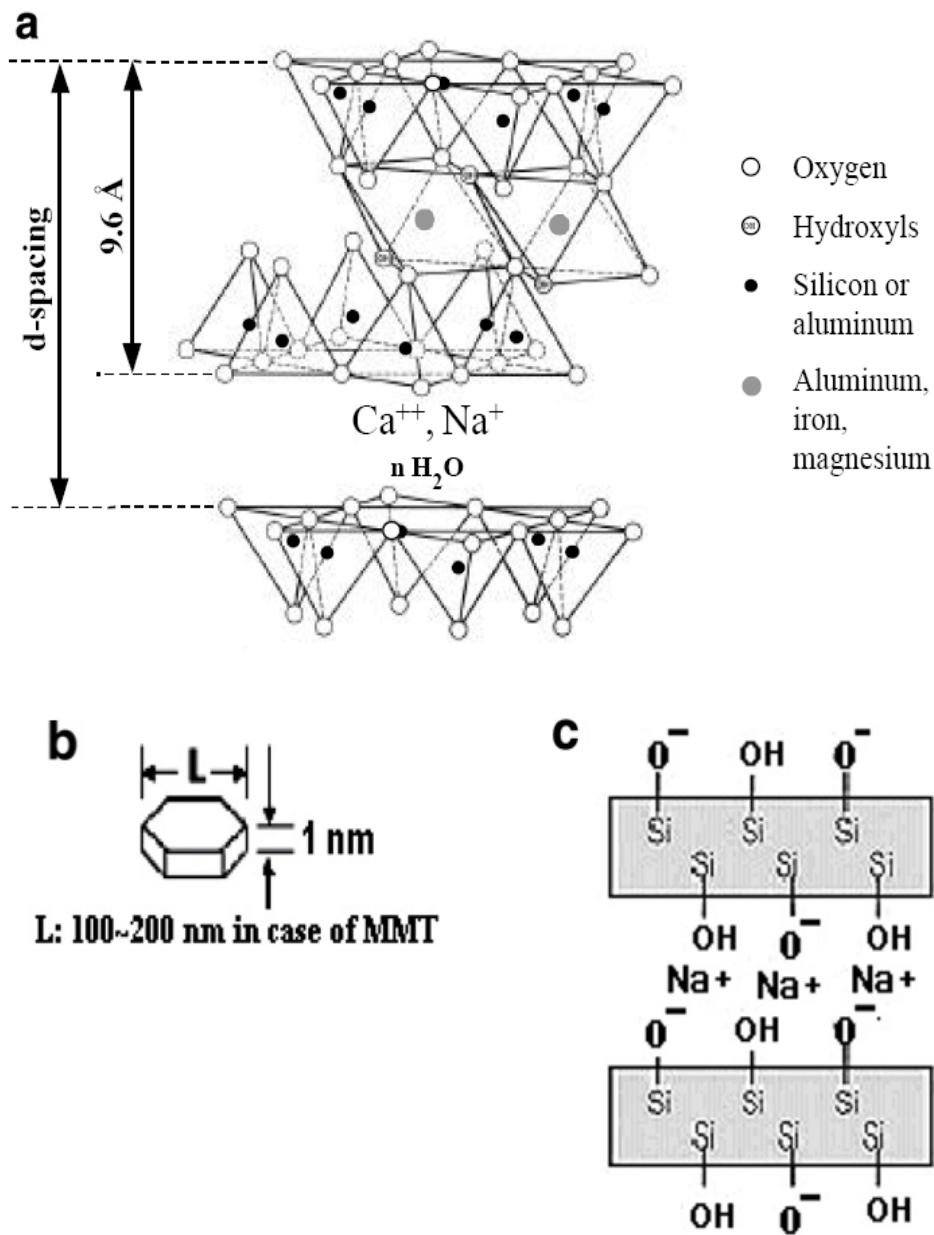


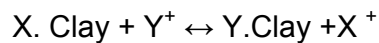
Figure 2. a) Imaginary structure of MMT, proposed by Hoffman, Endell and Wilm, 1933 [Adapted from Kornman, 2001], b) High aspect ratio clay platelet, c) Schematic of side view between layers [Adapted from Kim et al., 2006].

Beidellite and saponite are di- and trioctahedral smectites, respectively, with mainly tetrahedral substitution. MMT and hectorite are di- and trioctahedral smectites, respectively with mainly octahedral substitution. The interlayer of MMT is less expandable than hectorite, but is more easily expanded than saponite, beidellite or vermiculite.

2.6.3 Cation Exchange Capacity and Modification of MMT

A distinguished property of MMT is the ability to absorb certain cations and retain them in an exchangeable state. These intercalated cations can be exchanged by treatment with other cations in a water solution. The most exchangeable cations are Na^+ , Ca^{2+} , Mg^{2+} , K^+ and NH_4^+ [Kornman, 2001].

If the clay is added to a solution of a given electrolyte, an exchange reaction occurs between the ions of the clay X^+ and those of electrolyte (Y^+) as given by the following reaction:



For a given clay, the maximum amount of cations that can be taken up is constant and is known as the cation exchange capacity (CEC). It is measured in millimol per 100 gram (mmol/100g). The CEC of montmorillonite varies from 80 to 150 mmol/100g. In Table 2.2, meq weights of common cations are given. As CEC value of clay increases, its ability to sorb certain cations increases as well.

Table 2.2 Milliequivalent weights of common cations

MEQ Weight of Common Cations Element				
Element	K	Na ⁺	Ca ⁺⁺	Mg ⁺⁺
Valence	1	1	2	2
Atomic Wt. g	39	23	40	24
MEQ Wt. g	.039	.023	.020	.012

The efficiency of the MMT in improving the properties of the polymeric materials is primarily determined by the degree of its dispersion in the polymer matrix. Presence of positive ions on the surface of the silica sheets increases the d-spacing of the clay crystals, but it also makes the clay crystal hydrophilic. This hydrophilic nature of the MMT surface impedes homogeneous dispersion in the organic polymer phase (Awad et al., 2004). Therefore, surface modification of the clay is required to render it organophilic and thereby miscible with many common polymers. Surface modification is typically performed by ion-exchange reactions using primary, secondary, tertiary, and quaternary alkylammonium or alkylphosphonium (onium) cationic surfactants [Figure 2.3]. The number of surfactant molecules that reside in the galleries is determined by CEC of the MMT. Therefore higher CEC value of the clay is required for more successful cation exchange reaction. As a result, the basal spacing of the MMT is expanded, allowing for improved intercalation of polymer into the intergallery and providing better physical interaction between the clay and polymer.

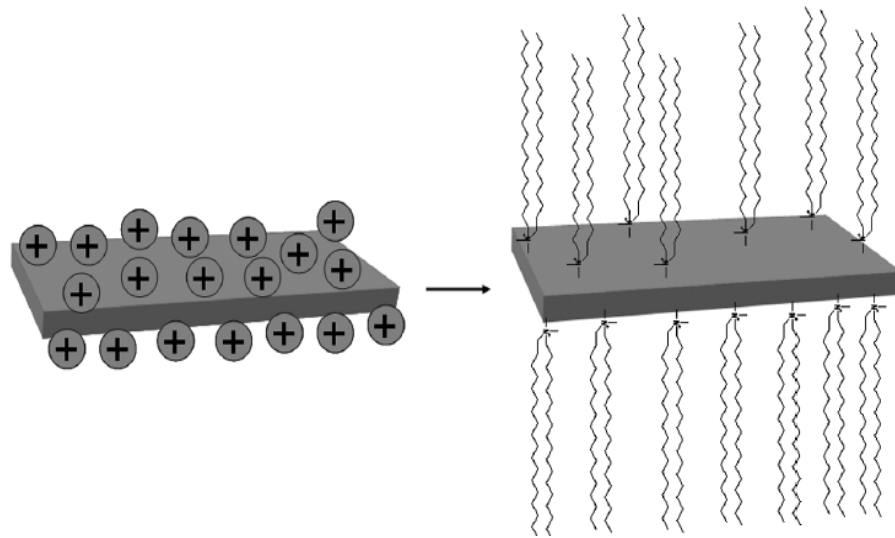


Figure 2.3 Change of cation of layered silicates with cations of long chain alkyl ammonium ions [Mittal, 2010].

2.7 Polymer Matrices

2.7.1 Polypropylene

Polypropylene is a crystalline thermoplastic and one of the major members of the polyolefins family. It is the lightest of the widely used thermoplastics with the exception of plastic foams. The structure of polypropylene is shown in Figure 2.4. With a specific gravity of less than one, polypropylene will float on water. Polypropylene, while having excellent chemical resistance to a very wide range of chemicals, is attacked however by strongly oxidizing reagents, e.g., concentrated nitric and sulphuric acid, dry chlorine and bromine gas. In the presence of certain organic solvents such as benzene, toluene and mineral oils, some swelling may occur with polypropylene at room temperature due to absorption.

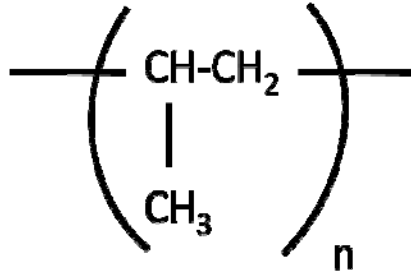


Figure 2.4 Structure of PP

Polypropylene was invented in the mid 1950's by Guilio NATTA's group in Italy through the polymerization of propylene (C_3H_6) in the presence of titanium tetra chloride (TiCl_4) and triethyl aluminium (AlEt_3) catalysts. Three types of polypropylene are used commercially: homopolymers, copolymers and random copolymers. The choice between these will depend on the end use requirements and specifications. Similarly, the molecular weight of PP can be varied to suit a particular end product since this will have a major effect on many of polypropylene's properties.

Polypropylene is a thermoplastic material offering a combination of lightness, rigidity, toughness, chemical resistance and high surface gloss. This combination of properties rates the material suitable for the production of a wide range of articles from housewares and industrial mouldings to fiber fabrics and clear packaging film.

Polypropylene is extensively used in many household items including tableware and picnic ware, mixing bowls and buckets. Other applications include drink crates, electrical components such as dishwasher or washing machine parts, outdoor furniture, automotive components including car battery cases, toys, hospital equipment and many building components.

2.7.2 Polyethylene

Polyethylene is a polyolefin polymer consisting of long chains of the monomer ethylene. The advantages of polyethylene are its low price, good processability, excellent electrical insulation properties, good chemical resistance, toughness, light weight, and flexibility. PE can be divided into three classes by the extent, statistical distribution and length of side chains (branches) covalently bound to the linear backbone chain. Branching can be controlled within a wide range by the selection of the thermodynamic conditions in the reactor during the polymerization process, the choice of the catalyst or the addition of higher alkenes as comonomers to the ethylene base monomer [Michler and Calleja, 2005]. PE is divided mainly into three groups depending on resin density and its melt index.

- 1) Low density polyethylene (LDPE)
- 2) Linear low density polyethylene (LLDPE)
- 3) High density polyethylene (HDPE)

LDPE is so called because they have significant concentration of branches that hinder the crystallization process, resulting in relatively low densities. The branches consists of ethyl and butyl groups together with some long chain branches. Structure of LDPE is given in Figure 2.5 (a). Since high pressure polymerization is applied for production of LDPE, the ethyl and butyl branches are frequently clustered together, seperated by lengthy sets of unbranched backbone. During polymerization, the long-chain branches can themselves be branched. These vast amount of branches inhibit their ability to crystallize, reducing resin density relative to HDPE. LDPE resins have generally densities between 0.9-0.94 g/cm³. Low density polyethylene (LDPE) is generally applied in packaging films owing to its good processability and mechanical properties [Wang et al., 2009; Peacock, 2000].

HDPE is chemically the most close structure to pure PE. It has primarily unbranched molecules with very few flaws to mar its linearity. Its structure is given in Figure 2.5 (b). With an extremely low level of defects to hinder organization, a high degree of crystallinity can be achieved, resulting in resins that have a high density (relative to other types of PE). HDPE resins generally have densities between 0.94-0.97 g/ cm³ [Wang et al., 2009; Peacock, 2000]. Table 2.3 gives the comparison of properties of general PE types.

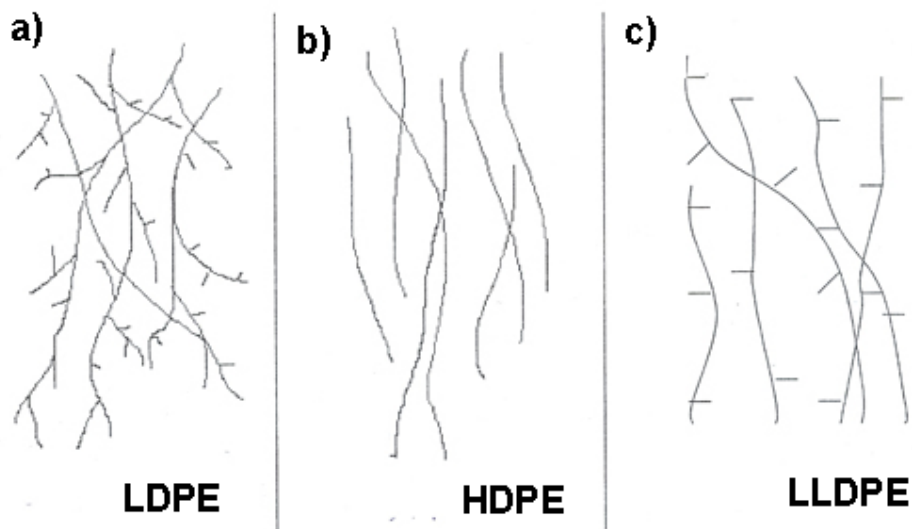


Figure 2.5 Structure of PE types

LLDPE resins comprise of molecules with linear PE backbones to which short alkyl groups are attached at random intervals. LLDPE is produced by copolymerization of ethylene and α -olefin, thus it contains short chain branches. Schematical structure of LLDPE is given in Figure 2.5 (c). The branches most commonly used are ethyl, butyl or hexyl groups. These alkyl substituents cannot be accommodated in the crystalline lattice, resulting in lower crystallinity. The crystallinity of LLDPE is higher than that of LDPE. LLDPE has been widely used as plastic films and in injection molding due to its excellent mechanical properties such as tear and impact strength as well as high tensile strength. By blending LDPE with

LLDPE, the good processability, excellent mechanical properties, and high crystallinity can be obtained [Wang et al., 2009; Peacock, 2000].

2.8 Factors Affecting the PLSN Behavior

There are many factors affecting the behavior of PLSN. First and most important one is the chemical compatibility between the components of PLSN, i.e., clay, polymer matrix and compatibilizer (if any). Chemical attraction between the phases creates and increases the adhesion and formation of a strong physical network through the matrix which in turn enhances many properties of the matrix compared to the neat matrix. After chemical compatibility, high and homogeneous level of dispersion of silicate layers is required to achieve nanocomposite formation and property enhancements. Following discuss the parameters affecting the PLSN.

Basal length or d-spacing of organoclays is an important parameter affecting the intercalation/exfoliation behavior of silicates. Higher d-spacing make diffusion of polymer chains between the clay spacing easier in the case of compatibility between the phases. While higher d-spacing is required, individual structures residing between the spaces show different behavior. Xiao et al., 2003, studied the influence of various kinds of alkyl-amines and modifying time on the intergallery distance of organoclays. Their study resulted with the following consequences:

- 1) As modifying time increases during the cation exchange reaction, d-spacing of the clay increases regardless of the alkyl-amine (ammonium) used. After 0.5h, the increase of the d-spacing is very little.
- 2) In the case of primary amines (n-butylamine, n-octylamine, dodecylamine, hexadecylamine, octadecylamine), the d-spacing of the MMT increases with increasing carbon numbers of the main chains of the primary amines, that is $d_{18} > d_{16} > d_{12} > d_8 > d_4$ (subscripts

abbreviate the carbon numbers of the main chain of the primary amines).

- 3) Comparison between the quaternary and primary amines with same carbon numbers indicated that, quaternary ones resulted in higher d-spacing compared to secondary types.

Calderon et al., 2008 mentioned that, during cation exchange process, at least a surfactant concentration equivalent to 1xCEC was necessary to assure the optimum interlayer distance. Janek and Lagaly, 2003 reported that the content of organic cations required for the alteration from fine to voluminous flocs of organically modified clay correspond to the CEC. In addition, Kadar et al., 2006 mentioned that a small amount of surfactant does not cover the entire surface of the clay d-spacing and leaves high-energy surface uncovered, and results in large surface tension, while excessive amounts may dissolve or disperse in the polymer, leading to inferior properties [Kadar et al., 2006]. Therefore, MMT was modified with the surfactants at concentrations equivalent to 1.1xCEC in this study. One ammonium cation was prepared with 1.5 x CEC to see the effect of high concentration usage of surfactant (TKA50).

As previously stated, the role of the ammonium or phosphonium cations is to lower the surface energy of the MMT and improve the wetting characteristic with the polymer. Lan et al., 1995 indicated that in systems with epoxy matrix, organoclays also catalyze the polymerization reaction for making the intergallery polymerization rate comparable to the rate of extragallery polymerization. This effect is increased by the acidity of the surface modifier, i.e., $[\text{CH}_3(\text{CH}_2)_{17}\text{NH}_3^+ > \text{CH}_3(\text{CH}_2)_{17}\text{N}(\text{CH}_3)_2\text{H}_2^+ > \text{CH}_3(\text{CH}_2)_{17}\text{N}(\text{CH}_3)_2\text{H}^+ > \text{CH}_3(\text{CH}_2)_{17}\text{N}(\text{CH}_3)_3^+]$.

Flaws and impurities of the MMT also play important part in the mechanical performance of nanocomposite systems. When a system has no impurities, the mechanical behavior of a composite depends on the magnitude of forces that bind atoms together and the adhesion force

between the filler and matrix phases. In the layered silicates, the common contaminants are grits and amorphous silicates, i.e., quartz, silica, feldspar, gypsum, albite, anorthite, apatite, halite, calcite dolomite, sodium carbonate, siderite, biotite, muscovite, chlorite, stilbite, pyrite, kaolinite, hematite and many others. Commercial polymer-grade bentonites are laboriously purified, but they may still contain <5% of nonsmectite impurities [Gupta, Kennel and Kim, 2010].

2.9. Nanocomposite Production

Compounding can be achieved by two broad classes, batch or continuous mixers.

2.9.1 Extrusion

Continuous mixers comprise single and twin screw extruders and a number of modified variants constructed particularly for mixing.

The twin screw extrusion processing is one of the foremost processing methods for transferring solids, melting, mixing, devolatilization, pressurization and shaping through die flows of polymeric melts, gels, dispersions and suspensions. Various types of twin-screw extruders are compared by [Kalyon, 1989]. Modes of twin-screw extruders can be in co rotating or counter-rotating (screws rotating in the same or opposite directions) and can be fully-intermeshing or non-intermeshing (tangential mode). The different types of extruders are shown Figure 2.6.

Intermeshing twin screws can be regarded to be self-wiping, i.e., all the surfaces within the processing chamber are wiped of polymer. In the use of materials that are sensitive to heat, self-wiping characteristic is important. It is advantageous to the operational economics as the screws need much less downtime for cleaning. Efficient self-wiping ensures that no material is stagnant in the machine and can be demonstrated by a short residence time distribution for the material being processed [Shennoy, 1999].

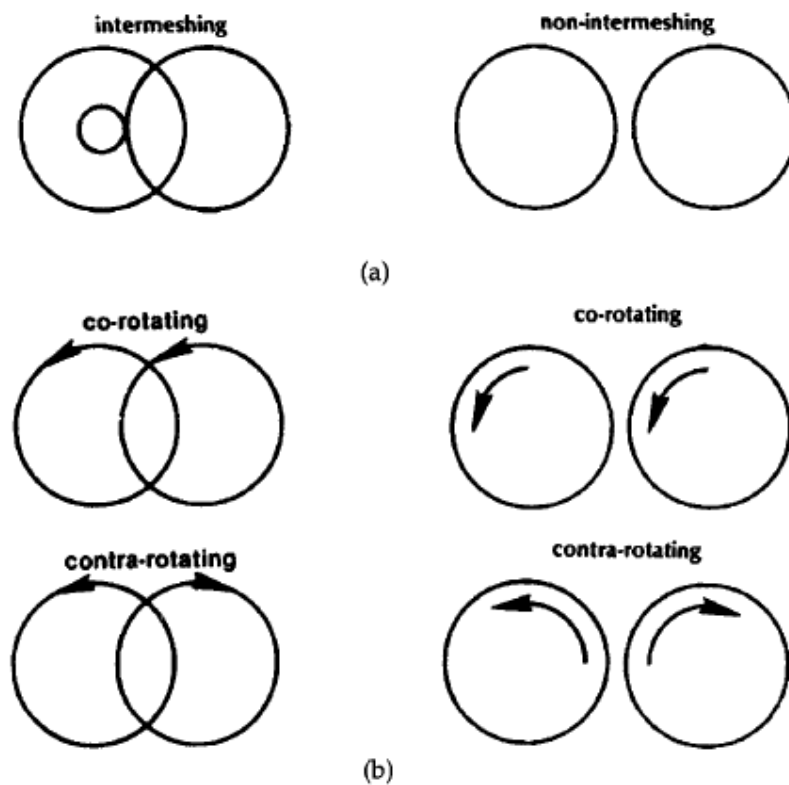


Figure 2.6 Different types of twin-screw extruders, differences between; a) intermeshing and non-intermeshing b) co and counter rotating.

The residence time in the co-rotating twin screw extruder is in general narrower than that in the single screw extruder. Because of that uniformity, it is possible with a twin screw mixer, to achieve the desired degree of mix with less mechanical energy input and, therefore, less heat buildup than with other mixers [Shennoy, 1999].

2.9.2 Batch Mixing

Batch mixers used in polymer production can be classified as nonplasticating equipment, which mix particulate solids, doughs or liquid polymers, and plasticating mixers such as the two-roll mill and internal

mixers which are capable of melting and mixing polymers [Wilkinson and Ryan, 1989].

The internal mixer (Figure 2.7) is one of the oldest components of the mixer family. It has adopted the open mill mixing rule but has an entirely enclosed mixing chamber in which two rotors are mounted. The rotors are sealed at each end to avoid leakage of material from the chamber. In batch mixers, the end of the mixing operation is normally adjudged by the observed steadiness of the torque level in the mixer's motor drive unit after a definite length of time. A constant torque indicates internal homogeneity of the mixture that is accomplished within the system's capability limits [Shennoy, 1999].

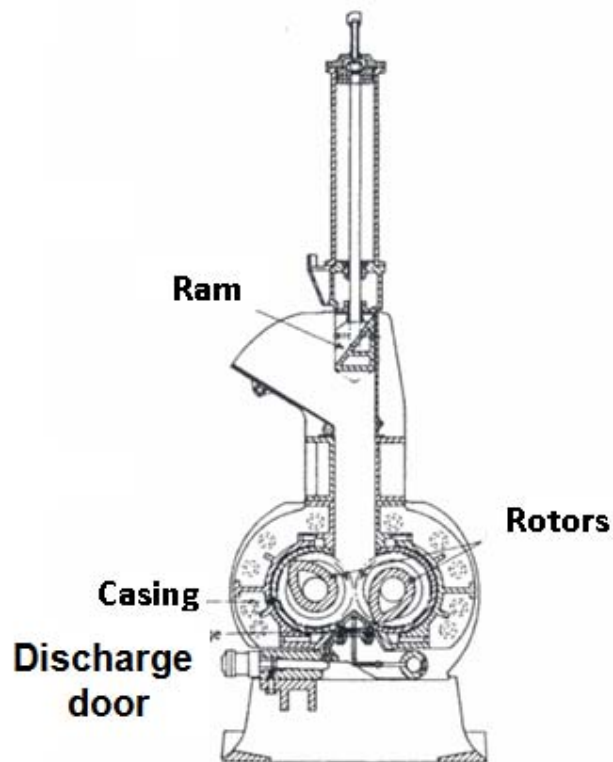


Figure 2.7 Banbury type internal batch mixer [Adapted from Wilkinson and Ryan, 1989].

Mixer/torque mixers are used partially full, usually at a degree of fill of 70%. The torque, T , and hence the specific energy, E_s , input generated during the mixing process could be monitored as:

$$E_s = \frac{\Omega \int_0^{t_m} T dt}{M_t} \quad (2.1)$$

where Ω is the rotational speed of the blades of the mixer, t is time, M_t is the total weight of the mixture in the mixer and t_m is the duration of the batch mixing. In batch mixing experiments, the total duration of the mixing process, t_m , can be varied systematically in order to assess the effects of the specific energy input, expanded during the mixing process [Demirkol, 2005].

2.10 Characterization Methods

2.10.1 X-Ray Diffraction Analysis (XRD)

X-Ray Diffraction (XRD) method has been used to determine the arrangement of atoms within a crystal and to define the crystallographic structure determination. It is aimed to understand a variety of issues like crystal structure of solids such as geometry, crystal lattice spacings, crystal size and perfection, and the crystallinity [Cao, 2004]. In this experimental method, a beam of X-Rays strikes a crystal and diffracts into many specific directions (Figure 2.8). The energetic X-rays can penetrate deep into the materials and provide information about the bulk structure. Thus, the degree of preferred orientation in polycrystalline samples is determined. To explain why the cleavage faces of crystals appear to

reflect X-ray beams at certain angles of incidence (θ , λ), Bragg's Law refers to the simple equation:

$$n\lambda = 2d \sin\theta \quad (2.2)$$

where the variable d is the distance between atomic layers in a crystal, and the variable λ is the wavelength of the incident X-ray beam; n is an integer [Jens, 2001; Sperling 2006]. Diffraction occurs according to Bragg's law and at any given position a multiplicity of Bragg's reflections is excited with the crystalline sample and gathered data are recorded [Sperling 2006; Ramakrishna, 2005].

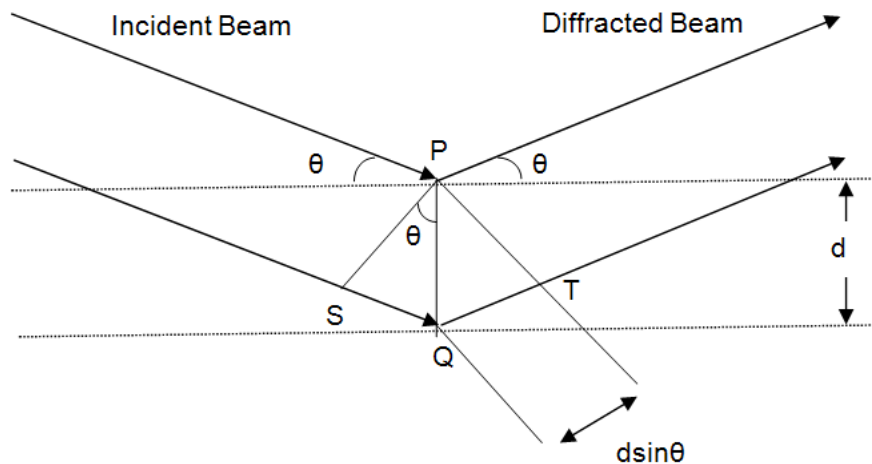


Figure 2.8 Diffractions of X-Rays by planes of atoms [Callister, 1997; Callister and William, 2003].

X-ray is a form of electromagnetic radiation that has high energy and short wavelength. X-rays are generally produced by either x-ray tubes, or synchrotron. X-rays scattered from different electrons that interfere with each other produces a diffraction pattern which varies with scattering angle [Billmeyer, 1984]. X-rays transfer some of their energy to the electrons and the scattered x-rays will have different wavelength than the incident x-rays. When a beam of x-rays impinges on a solid material, a portion of this beam will be scattered in all directions. If the wavelength of these scattered x-rays does not change, the process is called elastic

scattering. In the elastic scattering process, only momentum is transferred [University of California, www.mrl.ucsb.edu].

Depending on the scale of the studied features, X-ray diffraction techniques can be categorized into two main groups. These two techniques are; Wide Angle X-Ray Scattering (WAXS) and Small Angle X-ray Scattering (SAXS). WAXS detects the changes in crystallinity and orientation by which spatial arrangement of atoms is described, whereas SAXS detects fibrillar and lamellar structures and cavities [Seymour, 1996]. By observing the position, shape, and intensity of basal reflections from the distributed silicate layers obtained by WAXS, the nanocomposite structure may be identified.

2.10.2 Transmission Electron Microscopy (TEM)

Transmission Electron Microscopy (TEM), allowing a qualitative understanding of the internal structure, distribution of the various phases, and views of the defect structure through direct visualization at levels down to atomic dimensions (a few angstroms, 10^{-10} m) with thin materials (less than 100 nm thick) [Bower, 2002] is a valuable characterization tool for studying heterogeneous catalysts. Energy dispersive x-ray data in conjunction with microprobe analysis has enabled the metal composition of the particles to be examined [Tajammul, 1996]. For TEM analysis, the specimen prepared is required to be thinned to dimensions typically 100 nm. Thus, the passage of electron beam through the material is allowed. The provided electron diffraction data can be used to calculate the molecular spacing of the crystalline phases in the polymer.

It is possible to compare TEM analysis with XRD and Scanning Electron Microscopy (SEM) analysis. In X-Ray diffraction analysis it is not possible to gather a precise definition of the chain-packing dimensions and orientation; thus, the type of information obtained by TEM is quite complimentary to that obtained by XRD [Kroschwitz and Mark, 2003]. SEM is used to study the surface morphology, whereas TEM provides

information about the internal structure of thin specimens in much higher magnifications [Goodhew, Humphreys and Beanland, 1975].

Schematic representation of TEM is given in Figure 2.9 [http://nobelprize.org]. As can be seen from the figure, electrons that travel through vacuum in the column of the microscope are emitted by a "light source" which is at the top of the microscope. TEM uses electromagnetic lenses to focus the electrons into a very thin beam instead of glass lenses focusing the light in the light microscope. The electron beam travels through the specimen which is studied. Depending on the density of this specimen, some of the electrons are scattered and disappear from the beam. The unscattered electrons hit a fluorescent screen at the bottom of the microscope and thus a shadow image of the different parts of the specimen is displayed in varied darkness according to their density. Operator can directly study this image or it is possible to photograph this image [http://nobelprize.org/educational games]. With the use of a charge coupled device (CCD), the data recording system tends to be digital, allowing quantitative data processing and quantification [Wang, 2001].

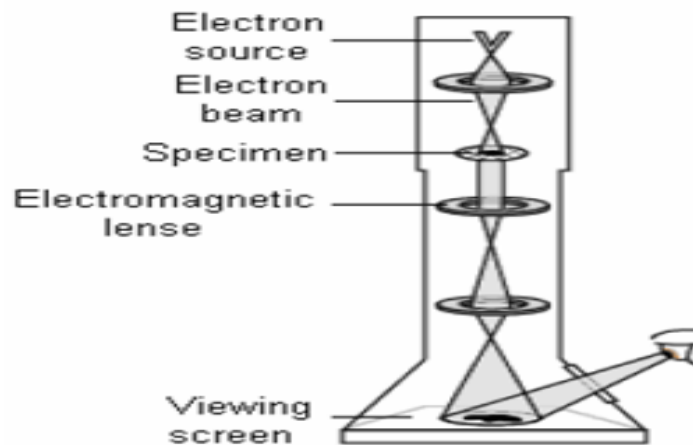


Figure 2.9 Schematic representation of TEM [http://nobelprize.org/educational_games/physics]

2.10.3 Scanning Electron Microscopy (SEM)

SEM is primarily used for examining the surface, near surface morphology and structure of bulk specimens [Goodhew, Humphreys and Beanland, 1975]. In SEM, an incident electron beam is scanned across the sample's surface, and the resulting electrons emitted from the sample are collected to form an image of the surface. The image on the screen, which may be photographed, represents the surface features of the specimen [Callister, 1997]. Thus, fracture surfaces, crack initiation and propagation, microdomains of blends and nanodispersion of fillers can be detected by this technique. The surface must be electrically conductive; therefore a very thin metallic surface coating must be applied to nonconductive materials. Imaging with backscattered electrons gives contrast based on atomic number to resolve microscopic composition variations, as well as, topographical information [<http://www.mee-inc.com/sem.html>]. The magnification of the SEM images is in between the optical microscope and transmission electron microscope (TEM). More specifically, magnifications ranging from 10 to in excess of 50,000 diameters are possible [Goodhew, Humphreys and Beanland, 1975].

An electron source (electron gun) accelerates the electrons to a higher energy level in a SEM instrument. Then, proper magnifications is adjusted. Radiation reflected from specimen surface and detected low energy secondary electrons are recorded. Meanwhile, the spot of a cathode ray tube (CRT) is scanned across the screen and brightness is modulated. Three dimensional images are obtained as a result of electron beam and CRT spot both being scanned [Goodhew, Humphreys and Beanland, 1975]. Schematic view of SEM is shown in Figure 2.10.

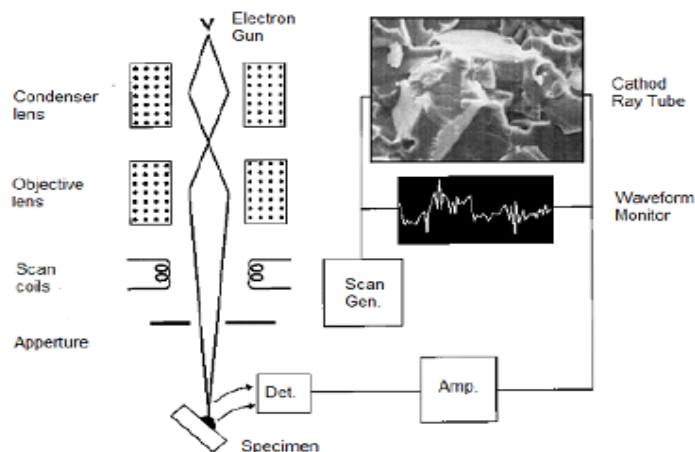


Figure 2.10 Schematic view of a SEM [Goodhew, Humphreys, Beanland, 1975].

Since SEM only requires the sample to be conductive, it is relatively easy to prepare samples for SEM instrument. The surface of the specimen is coated with a gold-platinum containing solution with a sputter coater under vacuum in order to make the surface conductive [<http://www.mse.iastate.edu/microscopy/whatsem.html>.; Bower, 2002] and to avoid the loss of resolution as a consequence of the build up of trapped charge [Kroschwitz and Mark, 2003]. Identification of inorganic fillers and their dispersion in compounds, as well as inorganic impurities on surfaces can be made by SEM method [Sandler, 1998].

2.10.4 Spectroscopic Analyses

2.10.4.1 Fourier Transform Infrared Spectroscopy (FTIR)

FTIR is an important tool for analyzing types of chemical bonds in a molecule by generating an infrared absorption spectrum that is similar to molecular "fingerprint".

Molecular bonds vibrate at a several frequencies depending on the elements and the type of bonds. For any given bond, there are several specific frequencies which it can vibrate (Figure 2.11). According to quantum mechanics, these frequencies correspond to the ground state (lowest frequency) and several excited states (higher frequencies). One way to cause the frequency of a molecular vibration to increase is to excite the bond by having it absorb light energy. For any given transition between two states, the light energy (determined by the wavelength) must exactly equal to the difference in the energy between the two states [usually ground state (E_0) and the first excited state (E_1)].

All the motions of moving atoms can be described in terms of two types of vibrations, stretching and bending. Stretching can be defined as a rhythmic movement along the line between the atoms. Bending can be formed due to a change in bond angle. These two bendings can also be divided into different kinds of variations; where a stretch may be symmetric or asymmetric and bending can occur in the plane of the molecule or out of plane; it can be scissoring, like blades of a pair of scissors, or rocking, where two atoms move in the same direction.

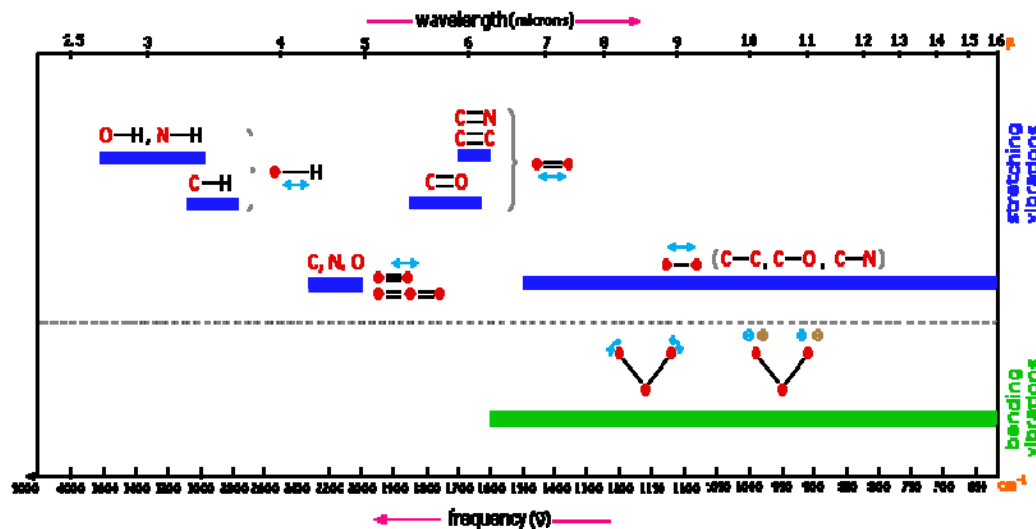


Figure 2.11 Infrared spectroscopy correlation table [http://en.wikipedia.org/wiki/Infrared_spectroscopy].

Different stretching and bending vibrations can be imagined by considering the CH₂ group in hydrocarbons. The arrows in Figure 2.12 refer to the direction of motion. The stretching motions necessitate more energy than the bending ones and high wavenumber (high energy) required to produce these motions. The bending motions are sometimes defined as wagging or scissoring motions [www.cartage.org.lb/.../OrganicCompound.htm].

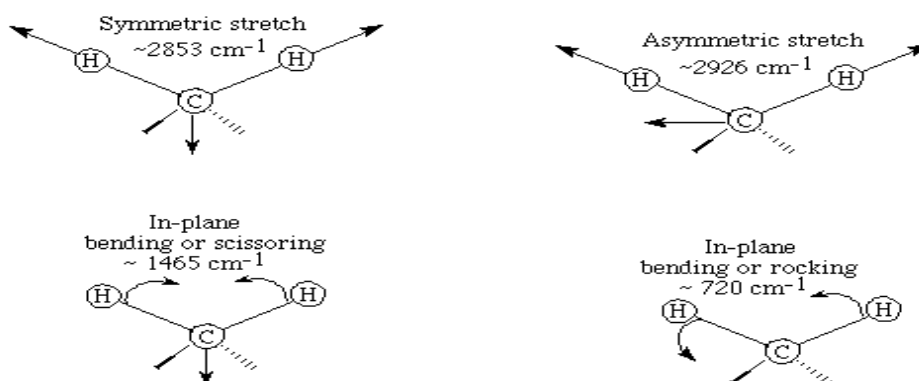


Figure 2.12 Different stretching and bending vibrations [www.cartage.org.lb/.../OrganicCompound.htm].

2.10.4.2. Inductively Coupled Ionic Plasma Optical Emission Spectrometer (ICP)

ICP is an analytical technique used for the detection of trace metals in certain samples. The ultimate aim of ICP is to have elements to emit characteristic wavelength specific light which can then be measured. ICP technology was first invented in the early 1960's with the purpose of improving crystal growing techniques.

ICP hardware is planned to produce plasma, which is a gas in which atoms are in an ionized state. Framework of ICP includes three concentric tubes, most often made of silica. These tubes, defined as outer loop, intermediate loop and inner loop collectively make up the torch of the ICP. The torch is situated within a water-cooled coil of a radio frequency produced. As gases are passed into the torch, the radio frequency field is activated and the gas in the coil region is made electrically conductive. This cycle of events generate the plasma.

2.10.5 Thermal Characterizations

2.10.5.1 Differential Scanning Calorimetry (DSC)

DSC is one of the most widely used techniques to measure glass transition (T_g), melting temperature (T_m) and heat of fusion of polymers (ΔH_f). DSC analysis was developed by E.S. Watson and M.J. O'Neill in 1960, and introduced commercially at the 1963 Pittsburgh Conference on Analytical Chemistry and Applied Spectroscopy [<http://en.wikipedia.org>].

In the DSC analysis, the difference in the amount of heat required to increase the temperature of a sample and reference is measured as a function of temperature. This method comprises individual heaters to maintain identical temperatures for two small platinum holders: one contains a small polymer sample (5 to 10 mg) mechanically sealed in a small aluminum pan and the other contains an empty (reference) pan. The sample and reference are heated at the same rate during the analysis. When the polymer experiences a thermal transition, the power which is given to the two heaters is adjusted to keep their temperatures constant, and a signal proportional to the power variation is plotted on the axis of the recorder. The thermodynamic property monitored here is the enthalpy vs. temperature [Rosen, 1982]. The area under the curve is a direct measure of the heat transition and this area can be converted to percent

crystallinity (X_c) if heat of fusion for the 100 % crystalline polymer is known.

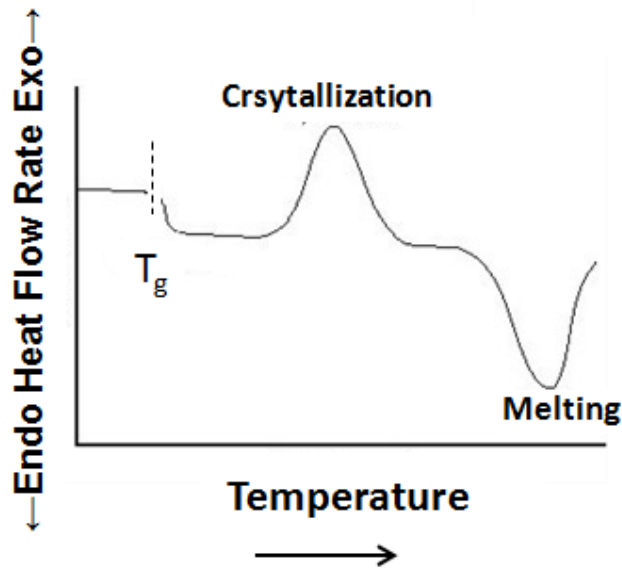


Figure 2.13 DSC curve of a polymer

Figure 2.13 displays a typical thermogram of a polymer. At T_g polymer goes from a hard, glass like state to a rubber like state. The heat capacity of the sample suddenly increases, requiring more power (relative to the reference) to keep the temperature the same. This endothermic differential heat flow to the sample causes a drop in the DSC curve. At T_m , the sample crystals want to melt at constant T , so a sudden input of large amounts of heat is required to keep the sample T even with the reference T . This results in the characteristic endothermic melting peak. Crystallization, in which large amounts of heat are given off at constant T , gives rise to a similar but exothermic peak. Heat capacities and heat of fusions can be determined by measuring the net energy flow to or from the sample [Rosen, 1993].

2.10.5.2 Thermogravimetric Analysis (TGA)

TGA is a technique which measures the weight loss (or weight gain) of a sample as a function of temperature. As materials experience heat, they

can lose weight from a simple process such as drying, or from chemical reactions that release gasses. Through heating, some materials can gain weight by reacting with atmosphere. TGA measures the amount and the rate of weight change in a material as a function of increasing temperature in a controlled atmosphere. This data give the stability information of the material as a function of increasing temperature, and this information can also be used to characterize the materials exhibiting a weight change and to detect weight changes due to decomposition, oxidation, or dehydration [Billmeyer, 1984].

In TGA analysis, a sample of the test material is located into an alumina cup that is supported on, or suspended from an analytical balance located outside the furnace chamber. The balance is set o zero, and the sample cup is heated according to a predetermined thermal cycle. The balance transmits the weight signal to the computer for storage, along with the sample temperature and the elapsed time. The result of TGA curve is the signal converted to percent weight change on the y-axis versus the reference material temperature on the X-axis [Seymour and Carraher, 1984].

2.10.6 Mechanical Characterization

Mechanical characterizations are used to measure the force response when a material is strained, compressed or sheared at a constant rate. Results of mechanical testing give a means to characterize the mechanical properties of a polymer in terms of modulus, strength and elongation to failure.

2.10.6.1 Tensile Properties

In a tensile test, the sample with the shape of a dogbone is clamped at one end and pulled at a constant rate of elongation until the center of specimen fails. Standards of tensile testing is specified by ASTM D 638

Method. The tensile response is plotted as engineering stress (σ) versus engineering strain (ε) [Fried, 1995].

The length of the center section is defined as the initial gauge length L_o . The force F is measured at the fix end as a function of elongation. Engineering stress (σ) is given by the relationship,

$$\sigma = \frac{F}{A_o} \quad (2.3)$$

where F is the instantaneous load applied perpendicular to the specimen cross section in Newtons, A_o (mm^2) is the original cross-sectional area before any load is applied.

Engineering strain, ε is defined according to;

$$\varepsilon = \frac{L_i - L_o}{L_o} = \frac{\Delta L}{L_o} \quad (2.4)$$

where L_o is the initial gauge length (mm), L_i is instantenous length (mm) and ΔL is the change in sample length (mm).

Tensile strength (MPa) is the maximum tensile stress sustained by the specimen. It is calculated from the maximum load beared during a tension test and the original cross-section area of the specimen [Callister, 1997].

Tensile modulus (Young`s modulus) is the tensile stress divided by the strain within the proportional range. In addition, it is calculated by the slope of the tangent to the initial portion of the stress-strain curve [ASTM D638-03, 2004].

2.10.7 Rheological Characterization

The rheological material functions are characterized using viscometers with well-defined flow dynamics, generally involving simple shear flow in which only one component of the velocity vector exists and changes only in one direction. Examples include “pressure driven flows” in which the fluid is pressurized to flow into slit or capillary (cylindrical) dies or “drag induced flows” in which there is one surface moving at constant velocity while the other surface is held stationary (steady torsional flow in between a cone and plate or between two parallel disks, or Couette flow in between two cylinders one of which is rotating). The motion can also be cyclic in nature (for example small-amplitude oscillatory shear in which the motion of a disk varies in a cyclic fashion between clockwise and counter clockwise rotation). In this thesis, the principle rheological characterization methods used were the steady torsional flow in between two disks and small-amplitude oscillatory shear.

The shear stress is proportional to the amplitude of the shear strain in the linear viscoelastic region, however the maxima in the shear stress are not coincident with the maxima in the shear strain or the shear rate. The term which is proportional to the shear strain is called the *storage modulus*, G' , and represents the stored elastic energy and the term which is proportional to the shear rate is called the *loss modulus*, G'' , and is indicative of the energy dissipated in one cycle of deformation. The ratio G''/G' is called the loss tangent or $\tan \delta$. This ratio, G''/G' , is high for liquid-like materials and is low for materials which are solid-like. The magnitude of the *complex viscosity*, η^* is defined as: $\eta^* = [(G'/\omega)^2 + (G''/\omega)^2]^{1/2}$. The magnitude of the complex viscosity approaches the zero shear viscosity, η_0 , (the limiting value of shear viscosity as the shear rate approaches zero) as the frequency is reduced to zero (Cox-Merz rule).

2.11 Previous Studies on MMT Modification and Their Applications in Polymer Nanocomposites

The initial structure of the MMT contains many stacked layers with a lateral dimension of 100-200 nm, a layer thickness of around 1 nm, and an interlayer spacing of around 1 nm. If these stacked layers are then separated into individual clay platelets they have individual aspect ratios on the order of 100 – 200. These very high aspect ratios provide significant surface area to volume of the particles and hence substantially increase many properties of the polymer at particularly low loading levels. In addition, several factors can be accounted affecting the properties (mechanical, permeability, thermal stability, flammability) of polymer nanocomposites such as concentration of clay used as reinforcement, the effects of polymer immobilization by adsorption on clay surfaces, weak crosslink due to bridging molecules between clay tactoids, and the alternation in the crystallinity of polymer [Chen et al., 2005]. Therefore, the elucidation of property improvements necessitates inclusive research on these factors.

Production of organoclay has attracted many researchers. Summary of the literature review is given in detail by Table 2.3 with structures of surfactants used for modification. Tiwari et al., 2008 synthesized novel organoclays with three different amines, and observed increase in the basal spacing of the clay while thermal analysis showed that these organoclays could be used in PLSN. Kim et al., 2006 used different alkylimidazolium salts in modification of MMT and characterized the resulting organoclays by FTIR, XRD and TGA. The organoclays were used in PP-clay composite production. Awad et al., 2004 synthesized a series of alkyl-imidazolium modified organoclays and studied thermal degradation process of organoclays in detail using TGA and thermal

desorption mass spectroscopy. They observed that as the chain length of the alkyl groups increased from propyl, butyl, decyl, hexadecyl, octadecyl to eicosyl, the thermal stability decreased. Lee and Lee, 2004 analyzed the thermal properties of MMT modified with a series of alkyl amines and ammonium salts and revealed that thermal stability of organoclay depends on the nature and arrangement of the surfactant between the MMT layers. Patel et al., 2007 purified Indian bentonite by sedimentation and then modified the product with seven different QP salts followed by characterization with XRD, FTIR, and TGA. It was found that phenyl group substituted phosphonium salt had the highest thermal stability. Calderon et al., 2008 and Xie et al., 2002 studied thermal stability of organoclays modified with QA and QP and found that phosphonium ions are more thermally stable than ammonium ions.

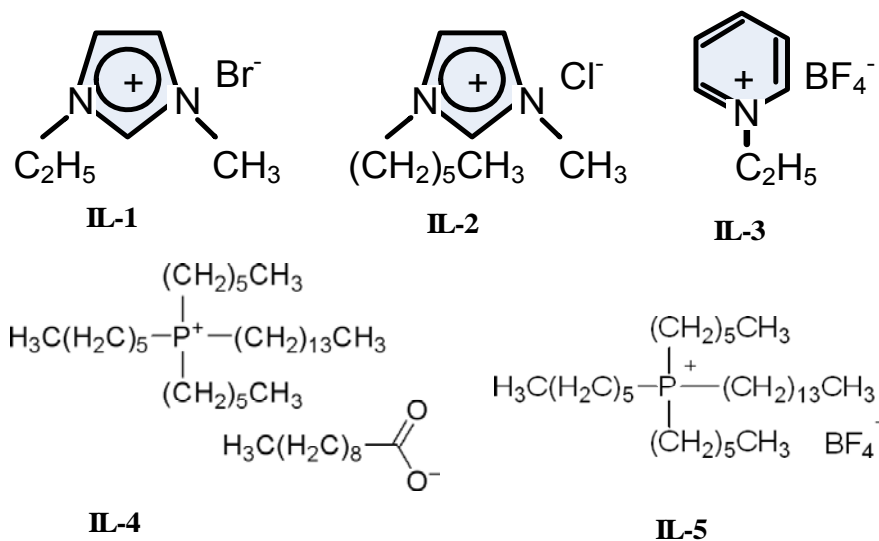


Figure 2.14 Structures of ionic liquids used and their names

IL-1. 1-ethyl-3-methylimidazolium bromide [EMIM] [Br]: MW 191.07

IL-2. 1-hexyl-3-methylimidazolium chloride [HXMIM] [Cl]: MW 202.72

IL-3. N-ethyl pyridinium tetrafluoroborate [Etpy] [BF₄]: MW 194.8

IL-4, Trihexyl tetradecyl phosphonium decanoate, [THTDP] [DE]: MW 655.13

IL-5 Trihexyl tetradecyl phosphonium tetrafluoroborate, [THTDP] [BF₄]:
MW 570.68

Kim et al. 2006, used pyridinium and imidazolium based ionic liquids shown in Figure 2.14 to modify pristine Na⁺ MMT clay in order to use in PP based nanocomposites. TGA results revealed that thermal stability of trialkyl imidazolium decreases as the length of the alkyl group attached to the nitrogen increases. This analysis further proved that the thermal stability of the commercial clays is lower than that of their samples. In spite of improvements in thermal stability, visual observation of PP samples mixed with ionic liquid modified clays revealed very little clay dispersion and the presence of agglomerates which shows that the modified clays having low carbon chain lengths are much less efficient in promoting dispersion in the PP matrix than commercial organoclays. Their results also showed that the d-spacing of the clays after compounding increased only by an insignificant amount. They concluded that further work is needed to obtain the proper structure of the ionic liquids.

Kadar et al. 2006 studied the surface characteristics of layered silicates to obtain more information on the effects of interfacial interactions on exfoliation and composite properties. They used six surfactants which are listed in Table 2.3. The surface tension of Na-MMT and organophilized clays (OMMT) was determined by inverse gas chromatography (IGC), and decrease in surface tension in MMT after modification was observed. Increase in interlayer gallery was high in the case of Nanofil 948 which has two long alkyl chains compared to others. They pointed out that, the amount of surfactant located in the galleries and the orientation of the molecules should significantly influence the structure and properties of layered silicate/polymer nanocomposites.

Lopez et al., 2005 used MMT and bentonite in polyamide-6 nanocomposite formation to see the effects of bentonite usage which is much cheaper than the MMT. They purified bentonite firstly dispersing in

water, then eliminating supernatant organic phases, wet sieving, milling with steatite balls and then applying high shear dispersion in a machine. They used octadecyl ammonium ion for the ion exchange reaction. XRD and TEM results showed that, nanocomposites of MMT and bentonite resulted in intercalated/exfoliated structures with slight differences. They concluded that, mechanical properties of all nanocomposites prepared by bentonite showed similar tensile modulus, slightly lower in comparison to that of MMT based nanocomposites, and significantly lower heat deflection temperature than that of MMT based nanocomposites.

Leuteritz et al., 2005 used four different types of smectite clay and modified with dimethyldistearylammonium chloride to make nanocomposites using a batch technology, via master-batch of organoclay and MAPP. Their analyses showed that the smallest *d*-spacing belonged to the clay with the lowest CEC. Their mechanical properties indicated the influence of the CEC on the strength and the modulus, when comparable clays were used. MMT with the lowest CEC gave the lowest impact strength in the corresponding nanocomposite, while the MMT with the highest CEC showed the highest impact strength. Their analyses also revealed that the surface tension of the modified clays were mainly dependent on the differences in the organic modifiers, not on the CECs of the clays.

Filho et. al., 2005 modified bentonite with hexadecyltrimethylammonium bromide and used it in PP based nanocomposites. Their XRD analysis suggested that the compound was formed as a nanocomposite together with a microcomposite. Other techniques such as TEM and mechanical characterization were not included in the study. Kozak et al., 2004, studied the modification of MMT with several quaternary ammonium surfactants and analyzed the organoclays with X-Ray, FTIR, and TGA. Hedley et al., 2007 used three phosphonium and three ammonium salts in modification of MMT and used the same analyses for examining the organoclays. Ren et al. 2000, modified MMT with dimethyldioctadecylammonium ion and used in

it polystyrene (PS) based nanocomposites. Their study mainly focused on the linear viscoelastic behavior of the nanocomposites.

Stoeffler et al., 2008 (a) modified Na^+ -MMT (Cloisite Na^+) with imidazolium, pyridinium and phosphonium (tributylhexadecylphosphonium bromide) based salts and investigated the effects of intercalating agent characteristics on the clay dispersion in LLDPE matrix by studying XRD, SEM, TEM, DSC and rheology of composites while mechanical properties were not studied. Their study revealed that highly thermally stable organoclays were prepared with dialkyl imidazolium salts compared to the one prepared with dialkyl ammonium modified organoclays. They suggested that these high thermally stable organoclays can be used together with polymers such as polyethylene terephthalate (PET) and polyamides which require high processing temperatures. Jin et al., 2009 used trimethoxysilyl-modified organosilane as a compatibilizer between LLDPE and organoclays with different modifiers. They used DCP which is known to react with organosilane producing free radicals which can also react with LLDPE, therefore increase the polarity of the LLDPE. They correlated XRD with mechanical properties, and improved mechanical properties were observed in LLDPE nanocomposite foams.

Table 2.3 Studies in the literature on polymer-clay nanocomposites

Clay type	Modifier	Application
Kato et al., 1997		
Purified MMT (Kunipia)	Octadecylamine (Stearylamine)	- PP - MAPP
Ishida et al., 2000		
Bentonite (Southern Clay Prod.)	12 aminododecanic acid	Polyisobutylene Polyisoprene Polydimethylsiloxane Polystyrene- acrylonitrile Nylon 12 Polyvinylalcohol Polynivylacetate Poly 1- butadiene Poly 1-butene Polychloropen Polyisoprene Polyisobutylene Polyethylmethacrylate Polybutyl methacrylate PE PS PC PP Nylon6 PVC PTFE PMMA Polyethyleneglycol Polyvinylimidazole Polyoxymethylene Polyoctadecyl methacrylate
Tjong et al., 2002		
Vermiculite	HCl Dicumyl Peroxide (DCP)	- (PP) - (MAPP)

Table 2.3. (continued)

Clay type	Modifier	Application
Xie et al., 2002		
-Na ⁺ -MMT (Southern Clay)	-Triphenyldodecyl phosphonium bromide -Tributyltetradecyl phosphonium bromide -Tributylhexadecyl phosphonium bromide -Tributyloctadecyl phosphonium bromide -Tetraphenyl phosphonium bromide -Tetraoctyl phosphonium bromide -Tetraoctylammonium bromide	-No use in polymer -Organoclay prepared by cation exchange reaction (CER)
Gilman et al., 2002		
-Na ⁺ -MMT (Southern Clay)	-Series of imidazolium salts	-Polystyrene -Polyamide-6
Tang et al., 2003		
-MMT (Keyan Company, China)	-Octadecylammonium -Hexadecyltrimethyl ammonium	-PP
Arroya et al., 2003		
-Sepiolite from Mihaliccik, Eskisehir, Turkey -Na ⁺ -MMT (Tolsa, Spain)	Octadecylammonium chloride	Natural rubber composites
Xiao et al., 2003		
-MMT (Institute of Chem., Chines Academy of Sciences)	- <i>n</i> -butylamine - <i>n</i> -octylamine, - Dodecylamine, - Hexadecylamine, - Octadecylamine -Hexadecyltrimethyl ammonium bromide	-No use in polymer -Organoclay prepared by (CER)
Bongiovanni et al., 2003		
MMT	Imidazolium salts	Polystyrene (PS)
Celik et al., 2004		
Purified Reşadiye bentonite	--	-Glycidyl Methacrylate (GMA)

Table 2.3. (continued)

Clay type	Modifier	Application
Sanchez-Solis et al., 2004		
Na ⁺ -MMT (Nanocor)	-MAPP -Pentaerythritol -Decacylammonium chloride -Dodecylammonium chloride -Tetradecylammonium chloride -Octadecylammonium chloride	-PET
Lee and Lee, 2004		
Ca ⁺² -Bentonite (Kampo, Korea)	-Hexadecylamine -Octadecylamine -Cetyltrimethylammonium Br -Octadecylammonium Br	Epoxy matrix -Diglycidyl ether of bisphenol A
Awad et al., 2004		
-Na ⁺ -MMT (Southern Clay)	-Series of imidazolium salts	-No use in polymer -Organoclay prepared by (CER)
Lopez et al., 2005		
Na ⁺ - Bentonite	Octadecylammonium ion	Polyamide6
Yapar et al., 2005		
Bentonite from Reşadiye (Tokat, Turkey)	-Tetradecyl trimethyl ammonium Br -Hexadecyl trimethyl ammonium Bromide	Study of phenol adsorption
Velasco et al., 2005		
Ca-Bentonite purified to have Na ⁺ -MMT	Undecyl Ammonium Chloride	-PP-PET Blend -MAPP
Kim and White, 2005		
-Na ⁺ -Cloisite -Cloisite 30B -Cloisite 20A	-12-aminolauric acid -Dioctylamine -Trioctylamine	-PP, PS, SAN, PMMA, PVDF, NBR
Leuteritz et al., 2005		
-Nanofil 757 -Nanofil 918 -Cloisite Na+ -Somasif ME	Dimethyldistearylammonium chloride (DSQ)	-PP-PET Blend -MAPP

Table 2.3. (continued)

Clay type	Modifier	Application
Kim et al., 2006		
1)MMT- Na ⁺ (Southern Clay Prod..)	Ionic Liquids: -1 ethyl- 3- methylimidazolium Br -1- hexyl- 3- methylimidazolium Cl 1-N- ethyl pyridinium tetrafluoroborate	- PP
2)Cloisite 15A : Dimethyl, dehydrogenated tallow, quaternary ammonium		- MAPP
3) Cloisite 30 B : Methy, tallow, bis-2- hydroxyethyl, quaternary ammonium		
Mravčáková et al., 2006		
- MMT- Na ⁺ (Kunimine Industries, Japan) - Organommodified bentonite, (modified with distearyldimethyl -ammonium chloride, Sud Chemi)	Oxidant: FeCl ₃ Surfactant: Dodecylbenzenesulfonic acid (DBSA)	- Polypyrrole
Lee et al., 2006		
- Na ⁺ -MMT (CEC= 95meq/100g	Distearyldimethyl ammonium bromide	- PP - MAPP

Table 2.3. (continued)

Clay type	Modifier	Application
Velasco et al., 2006		
- Ca rich Bentonite (purification is applied) - Commercial Bentonite modified with DMDHT	- 11- Undecylammonium chloride (UD)	- PP - MAPP - Maleic Anhydride – grafted poly(styrene-co-ethylenebutylene-b-styrene) - Poly(ethylene terephthalate-co-isophthalate (PET)
Kulshreshtha et al., 2006		
- Bentonite Clay used as received (Na based Bentonite from S.M. Chemicals)		- PP - MAPP
Ding et al., 2006		
MMT- Na ⁺ (Qinghe Clay, China)	Ionic Liquid : 1 methyl- 3-tetradecylimidazolium chloride (prepared)	- PP
Quintanilla et al., 2006		
-Cloisite Na ⁺ -Cloisite 20A -Cloisite 30B	-Commercial organic modification	-PP -GMA - MAPP -Acrylic Acid (AA)
Akçay, 2006		
Bentonite from Reşadiye (Tokat, Turkey)	-Tetraethylammonium iodide -Tetrabutylammonium bromide	Study of adsorption of pchlorophenol
Patel et al., 2007		
-Indian Bentonite (Akli Mines, Barmer, Rajasthan) purified by sedimentation	-Tetrabutylphosphonium Br -Hexadecyl tributylphosphonium Br -Tetradecyl tributylphosphonium Br -Tetraphenylphosphonium Br -Methyl triphenylphosphonium Br -Ethyl triphenylphosphonium Br -Propyl triphenylphosphonium Br	-No use in polymer -Organoclay prepared by cation exchange reaction (CER)

Table 2.3. (continued)

Clay type	Modifier	Application
Hedley et al., 2007		
MMT (Kunimine Indust., Japan)	-Tetrabutylphosphonium Br -Butyltriphenylphosphonium Br -Hexadecyltributyl phosphonium Br -Octadecyltrimethylammonium Br	-No use in polymer -Organoclay prepared by (CER)
Tiwari et al., 2007		
-Na ⁺ -MMT (Southern Clay)	-β-dimethyl-aminopropiophenone ammonium -N-phenyldiethanolammonium -glycine-n-hexylester ammonium	-No use in polymer -Organoclay prepared by (CER)
Stoeffler et al., 2008		
Na ⁺ -MMT (Southern Clay)	-Hexadecyl pyridinium bromide -1-vinyl hexadecyl imidazolium bromide -1- vinyl octadecyl imidazolium bromide -Tributyl hexadecyl phosphonium bromide -Dihexadecyl imidazolium bromide -Dioctadecyl imidazolium bromide -Dimethyl dioctadecyl ammonium chloride	-Linear Low Density Polyethylene (LLDPE) -Organoclay prepared by cation exchange reaction (CER)
Calderon et al., 2008		
-Na ⁺ -MMT (Southern Clay) -Cloisite 10-A (modifier= dimethyl benzyl, hydrogenated tallow ammonium Cl) -Cloisite 15-A (Dimethyl di-hydrogenated tallow ammonium Cl)	- Tributyl-tetradecyl-Ph ⁺ Cl ⁻ - Tributyl-tetradecyl-Ph ⁺ Cl ⁻ - Tetra n-octyl Ph ⁺ Br ⁻ -Tetra n-octyl Ph ⁺ Cl ⁻	-No use in polymer -Organoclay prepared by cation exchange reaction (CER)

CHAPTER 3

EXPERIMENTAL WORK

3.1 Materials

3.1.1 Polymer Matrix

Two types of Polypropylenes were purchased from Petkim Petrokimya Holding A.Ş., İzmir, Turkey. The trade names of the PPs are MH-418 and EH-241, and they are sold in the form of pellets in 25 kg bags. PP-MH418 is referred as PPM and PP-EH241 is referred as PPE in this study.

Linear Low Density Polyethylene (LLDPE) is a product of ExxonMobil, USA. The trade name of the LLDPE is LL-1001 Blown Film Resin (previous name MMA-042). Properties of LLDPE and PPs given by the companies are listed in Table 3.1.

Table 3.1 Properties of PPs and LLDPE

Property	Value
PP-MH 418 (PPM)	
Melt Flow Index MFI, g/10 min 2.160g, 230 °C, ASTM D-1238	4-6
Tensile Strength at Yield (MPa) ASTM D-638	35
PP-EH 241 (PPE)	
Melt Flow Index MFI, g/10 min 2.16 kg, 230 °C, ASTM D-1238	20-28
Tensile Strength at Yield (MPa) ASTM D-638	36.5
LLDPE (LL)	
Melt Flow Index MFI, g/10 min 2.16 kg, 230 °C, ASTM D-1238	1
Tensile Strength at Yield (MPa) ASTM D-638	22
Density, g/cm ³	0.918

3.1.2 Bentonite and MMTs

Bentonite was supplied by Karakaya Bentonit A.Ş., Ankara, in yellow powder form. The source of the mineral is Tokat/Reşadiye, Turkey. Its chemical analysis given in Table 3. 2, determined by Inductively Coupled Plasma Optical Emission Spectrometer (ICP), shows high levels of SiO₂ and MgO indicating a high amount of MMT in it [Filho et al., 2005]. Loss on ignition and insoluble residue of the bentonite, which constitute almost 20 w % of bentonite, are not included in the chemical analysis result. The CEC of the bentonite was determined as 67.5 mmol/100 g clay by methylene blue method (ASTM C0837/99, Standard Test Method for Methylene Blue Index of Clay). Commercial pure NaMMT (Cloisite-Na⁺)

was purchased from Southern Clay Products Inc., Texas, USA. Another pure MMT was purchased from Nanocor Inc., USA with a brand name G105 also called as PGW. Properties of the clays are given in Table 3.3.

Table 3. 2 Chemical analysis of metal oxide composition of raw bentonite

Components	Weight percent (%)
	Raw Bentonite (RB)
MgO	1.85
CaO	2.60
Fe ₂ O ₃	3.21
Al ₂ O ₃	15.6
Na ₂ O	2.69
K ₂ O	0.78
SiO ₂	54.97

Table 3.3 Properties of clays

Property	Value
Raw Bentonite (RB)	
Cation Exchange Capacity (mmol/100g of clay) ^a	67.5
Purified Bentonite (PB)	
Cation Exchange Capacity (mmol/100g of clay) ^a	100
Cloisite-Na⁺(Southern Clay Products Inc.)	
Cation Exchange Capacity (mmol/100g of clay) ^b	92.6
PGW (Nanocor, Inc.)	
Cation Exchange Capacity (mmol/100g of clay) ^b	145
Aspect Ratio ^b	200-400
Specific Gravity ^b	2.6

^aDetermined by Methylene Blue Method

^bGiven by the producer

3.1.3 Elastomers

3.1.3.1 Maleic Anhydride Grafted Polypropylene (MAPP)

Maleic anhydride grafted polypropylene (MAPP) was purchased from Polyram Israel with a brand name of Bondyram 1001 with an 85/15(PP/MA) wt ratio. Chemical structure is shown in Figure 3.1. Properties of MAPP given by the producer are listed in Table 3.4.

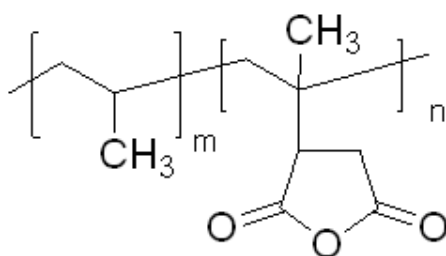


Figure 3.1 Chemical structure of MAPP

Table 3.4 Properties of MAPP

Property	ASTM Test Method	Unit	Bondyram® 1001
MFI	D-1238, 190° C/2.16 kg	g/10min	100
Density	D-792	g/cm ³	0.90
Melting Point	DSC	°C	160
Maleic Anhydride Level	FTIR	%	1

3.1.3.2 Lotader®3210

Lotader®3210 (LOT) was kindly provided by Arkema Inc., Philadelphia, USA. It is a terpolymer of Ethylene (E), Butyl Acrylate (BA) and Maleic Anhydride (MAH), and it was used in the LLDPE based composites. LOT is effectively compatible with many of the thermoplastics as well as

polyethylenes and nylons, owing to the functional groups on its backbone. Chemical structure of LOT is shown in Figure 3.2. Properties of LOT given by the producer are listed in Table 3.5.

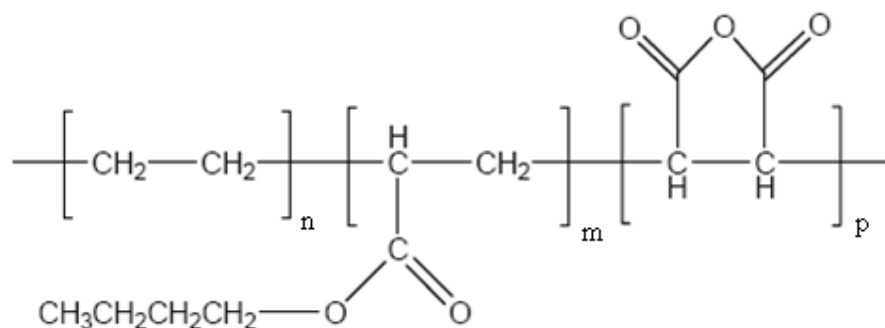


Figure 3.2 Chemical structure of elastomer LOT

Table 3.5 Properties of Lotader

Property	Method-Standard- Unit	Lotader® 3210
MFI	(190°C, 2.16 kg ASTM D 1238) (g/10 min)	5
n-Butyl Acrylate Content	(FTIR) (%wt)	6
MAH Content	(FTIR) (%wt)	3
Melting Point	(ASTM D 2117) (°C)	107
Vicat Softening Point	(ASTM D 1525-82) (°C)	80
Flexural Modulus	(ASTM D 790) (MPa)	120
Tensile Strength at Break	(ASTM D 638) (MPa)	12
Elongation at Break	(ASTM D 638) (%)	600

3.1.4 Surfactants Used for Clay Modification

All ammonium and phosphonium based quaternary salts (surfactants) were purchased from Sigma-Aldrich Company.

- 1) Hexadecyltrimethylammonium bromide, [HMA] [Br]
- 2) Tetra(kis)decylammonium bromide, [TKA] [Br]
- 3) Tetrabutylammonium tetrafluoroborate, [TBA] [BF₄]
- 4) Tetrabutylphosphonium tetrafluoroborate, [TBP] [BF₄]
- 5) Dimethyldioctadecylammonium chloride [DMDA] [Cl]
- 6) Tetrabutylhexadecylphosphonium bromide [TBHP] [Br]

Chemical structures of the surfactants are given in Table 3.6.

In addition to these clays produced by different modifiers, one commercial organoclay with a trade name of I34TCN, Nanocor Inc., was used in preparation of LLDPE based nanocomposites, while another commercial clay Cloisite 25A was used in PPE based composites. The surfactant of I34 TCN is methyl dihydroxyethyl hydrogenated tallow ammonium, while the modifier of Cloisite®25A is dimethyl, hydrogenated tallow, 2-ethylhexyl quaternary ammonium and the anion is methyl sulfate. Chemical structures of I34 and Cloisite®25A are given in Figure 3.3 and Figure 3.4 respectively.

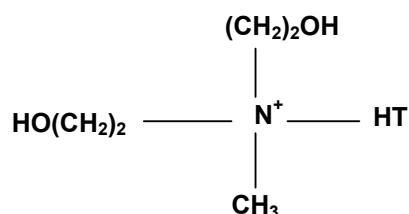


Figure 3.3 Chemical structure of the organic modifier of commercial clay I34, methyl dihydroxyethyl hydrogenated tallow ammonium. HT refers to hydrogenated tallow long organic molecules having ~65% C18; ~30% C16; ~5% C14.

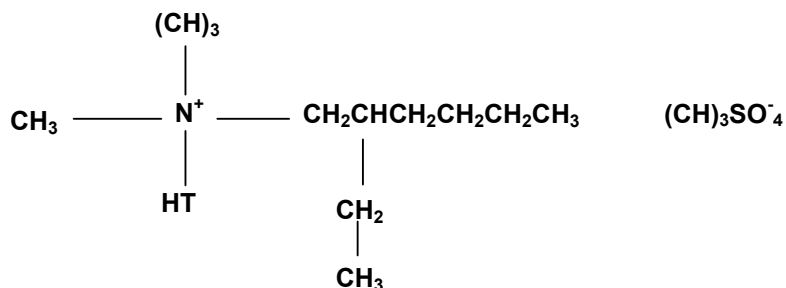


Figure 3.4 Chemical structure of the organic modifier of commercial clay Cloisite®25A, dimethyl, hydrogenated tallow, 2-ethylhexyl quaternary ammonium and anion, methyl sulfate.

3.1.5 Heat Stabilizer

IRGANOX® B 225 was used as a heat stabilizer in the PP based nanocomposites. It is a product of Ciba Specialty Chemicals Inc., and is in white powder form. It is a synergistic blend of %50 IRGAFOS 168 and % 50 IRGANOX 1010, the chemical structure which are given in Figure 3.5 and 3.6 respectively. Irganox B225 provides low color formation and long-term heat stability. It is used in polyolefins and olefin-copolymers such as polyethylene, polypropylene, polybutene and ethylene-vinylacetate copolymers. The heat stabilizer Irganox-B225 is referred as B225 in this study.

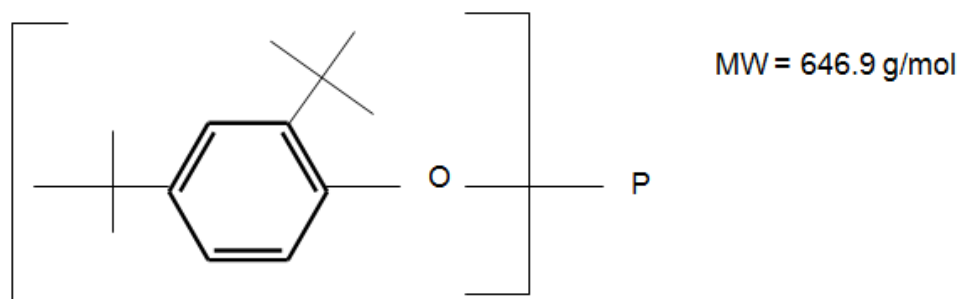


Figure 3. 5 Chemical Structure of IRGAFOS 168

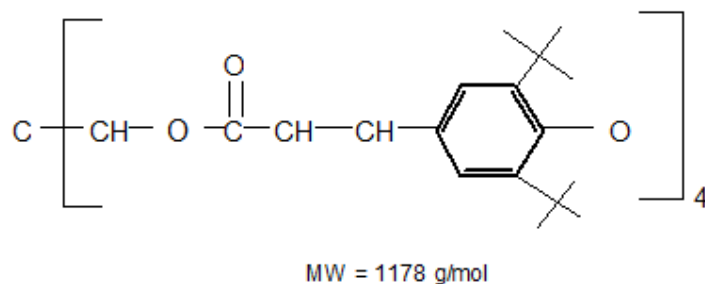


Figure 3. 6 Chemical structure of IRGANOX 1010

3.1.6 Sodium Pyrophosphate [Na₄(P₂O₇)]

Sodium Pyrophosphate was purchased from Sigma-Aldrich and used as a dispersant in preparing the bentonite suspension with water. It has been shown that Na₄(P₂O₇) can be used effectively as a dispersant in beneficiation of MMT from bentonite ore [Song et al., 2005]. Tendency of coagulation of MMT is high in the aqueous solution, because of the strong electrical double layer attraction between the planes and the edges of the fine particles [Song et al., 2005]. Chemical structure of Na₄(P₂O₇) is given in Figure 3.7.

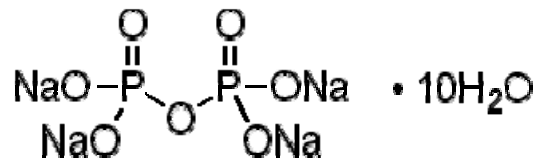


Figure 3. 7 Chemical structure of sodium pyrophosphate

3.2 Method

3.2.1 Purification of Bentonite

Bentonite is the name for the ore whose major constituent (%50-90) is the clay mineral MMT. In addition to MMT, bentonite may contain mostly smectite minerals such as MMT, beidellite, nontronite, saponite and other non-clay impurities such as analcime (An), calcite (C), clinoptilolite (Cln), dolomite (D), feldspar (F), illite (I), opal-C (OC), quartz (Q) in it [Onal et al., 2003; Tabak et al., 2007] depending on the geological deposit. Properties and quality of a bentonite depend largely on the quality and quantity of the smectite in it. Particle size of the MMT is approximately 2 μm and other non-clay parts have in a diameter scale of approximately 10 μm. Also, MMT particles swell in water, leading to a much smaller density than the gangue particles. Thus, by sedimentation process,

montmorillonite can be obtained as supernatant, while the gangue minerals are removed as sediment [Crozier, 1992].

Sedimentation of bentonite for purification is based on Stoke`s law. According to this law, a spherical particle falling in a viscous liquid with a sufficiently small velocity quickly reaches a constant velocity called the terminal velocity, which is the maximum attainable velocity under the circumstances, and where the effective weight of the particle is balanced by the frictional force exerted on it by the liquid [Rahaman, 2007].

The frictional force F on the particle is given by Stoke`s law;

$$F = 6 \pi \eta r u_t \quad (3.1)$$

where η is the viscosity of the liquid (Pa.s)

r is the radius of the particle (m)

u_t is the terminal velocity (m/s)

Equating F to the effective weight of the particle gives;

$$u_t = \frac{gD_p^2(\rho_p - \rho_l)}{18\eta} \quad (3.2)$$

where D_p is the diameter of sphere particle (m)

ρ_p is the density of the particle (kg/m³)

ρ_l is the density of the liquid (kg/m³)

g is the acceleration due to gravity ($g= 9.81 \text{ m/s}^2$)

According to Eq. 3.2 particle with a diameter of 2 μm ($\rho_p = 2.6 \text{ g/cm}^3$) will settle 10 cm at the end of 500 min, and thus non-clay minerals that have higher density than MMT will settle as sediment at the bottom of the flask, before the MMT particles with lower density. Then, MMT can be beneficiated from the liquid suspension in the upper 10 cm of the flask.

Siphoning and then centrifugation of this supernatant liquid gives MMT as sediment. The purification procedure is as follows:

- 1) 50g of vacuum dried (90°C, 12 h) bentonite and 3 g of $\text{Na}_4(\text{P}_2\text{O}_7)$ are mixed in 5lt of water and mechanically mixed with a mixer for 4 h. $\text{Na}_4(\text{P}_2\text{O}_7)$ prevents agglomeration of the clay particles in water.
- 2) After fully dispersed slurry is obtained, the suspension is left for sedimentation.
- 3) At the end of 8 h, supernatant liquid is siphoned and centrifuged with a Hitach High-Speed Refrigerated Centrifuge (8 polyethylene bottles of 500 ml were used in each centrifuge step) at 7500 rpm for 15 min.
- 4) Sediment obtained in centrifuge tubes is smeared from the bottom of each bottle.
- 5) Sediment obtained in step 4 is air dried for 24 h and then vacuum dried at 120 °C for 72 h.
- 6) Samples are ground in mortar and then ground in disk-grinder (present in the METU Central Lab.) to obtain fine particles. Resultant sample is named as pure bentonite (PB).
- 7) Procedure is continued until a 1000 g of sediment is collected. For modification of the purified bentonite with one surfactant, approximately 200 g of purified MMT is needed.

Purification procedure is also shown schematically in Figure 3.8.

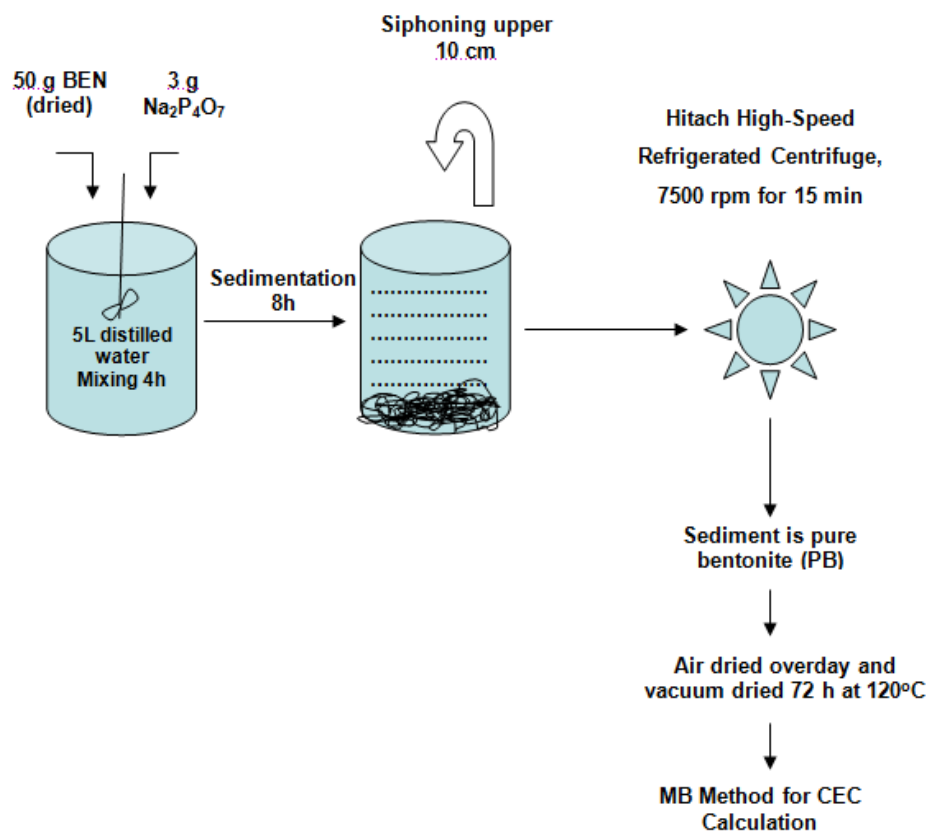


Figure 3.8 Schematical representation of purification of bentonite

3.2.2 Modification of Bentonite

Raw (RB) and purified (PB) bentonite were both used in the modification process. At first, modification of RB was performed with [HMA] [Br], [TBA] [BF₄], [TBP] [BF₄] and [TKA] [Br]. Modification of pure bentonite (PB) was performed with [DMDA] [Cl], [TBHP] [Br] and [TKA] [Br]. Organoclays are abbreviated by the cation of the modifier. Organoclay modified with [DMDA] [Cl] is called DMDA. While organoclay prepared with PB and [TKA][Br] is named as STKA, one prepared with RB and [TKA][Br] is named as TKA.

In the modification process, 5 wt % bentonite (RB or PB) was dispersed in water - ethanol (4:1, v/v) mixture and stirred with a mechanical stirrer for 4 h to obtain a well dispersed mixture of clay. The mixture was heated to 80

°C in a jacketed heater. 1.1 x CEC of the salt was dissolved and stirred in a water-ethanol (4:1 v/v) mixture and poured into the bentonite dispersion. The amount of surfactant (mg) was determined with the following equation for 50 g of bentonite;

$$\frac{CEC (mmol)}{100 g \text{ bentonite}} \times 1.1 \times \frac{1 mol}{1000 mmol} \times \frac{MW (g) \text{ of surfactant}}{1 mol} \times \frac{1000 mg}{1 g} \times 50 g \text{ bentonite} = A (mg \text{ of surfactant})$$

If CEC of PB is 98 mmol/100 g of and MW of surfactant [HMA] [Br] is 364.46 g/ mol, then the amount of surfactant for 50 g of PB is calculated as;

$$\frac{98 mmol}{100 g \text{ PB}} \times 1.1 \times \frac{1 mol}{1000 mmol} \times \frac{364.46 g}{1 mol} \times \frac{1000 mg}{1 g} \times 50 g \text{ of PB} = 17,900 \text{ mg of [HMA] [Br] or } 17.9 \text{ g of [HMA] [Br]}$$

In the preparation of one organoclay sample, concentration of [TKA] [Br] salt was used as 1.5 x CEC to observe the effects of salt usage at high concentration. This clay was named as TKA50. In the case of [TKA] [Br], isopropyl alcohol was used, since [TKA] [Br] has low solubility in ethanol-water solution. The mixture was stirred for 4 h at 70-80 °C. After mixing, the solution was filtered through a Buchner funnel filtration system, washed with 4-5 liters of hot water-ethanol (1:1, v/v) mixture to have a bromide/chloride ion free paste. Absence of bromide ion was tested with AgNO₃ test. Washing was stopped when a white precipitate was not observed when a few drops of 0.1 N AgNO₃ were added to the filtrate. The paste was smeared in a large glass plate and air dried overnight. Then, it was dried in a vacuum oven for 24 h at 80 °C. The dried clay was ground and stored in a desiccator. Abbreviations used for modified bentonite are given in Table 3.7. Figure 3.9 schematizes the procedure.

Sample with PGW, commercial pure MMT, was also modified with [TKA] [Br] at (1.1x CEC) to compare it with samples modified with bentonite. This sample is named as PGWTKA.

Table 3.7 Abbreviations used for organoclays used with raw and pure bentonite

Abbreviation	Modifier Name
Raw Bentonite (RB)	
HMA	Hexadecyltrimethylammonium
TKA	Tetra(kis)decylammonium
TKA50	Tetra(kis)decylammonium with 1.5XCEC
TBA	Tetrabutylammonium
TBP	Tetrabutylphosphonium
Purified Bentonite (PB)	
DMDA	Dimethyldioctadecylammonium
TBHP	Tributylhexadecylphosphonium
STKA	Tetra(kis)decylammonium
PGW	
PGWTKA	Tetra(kis)decylammonium

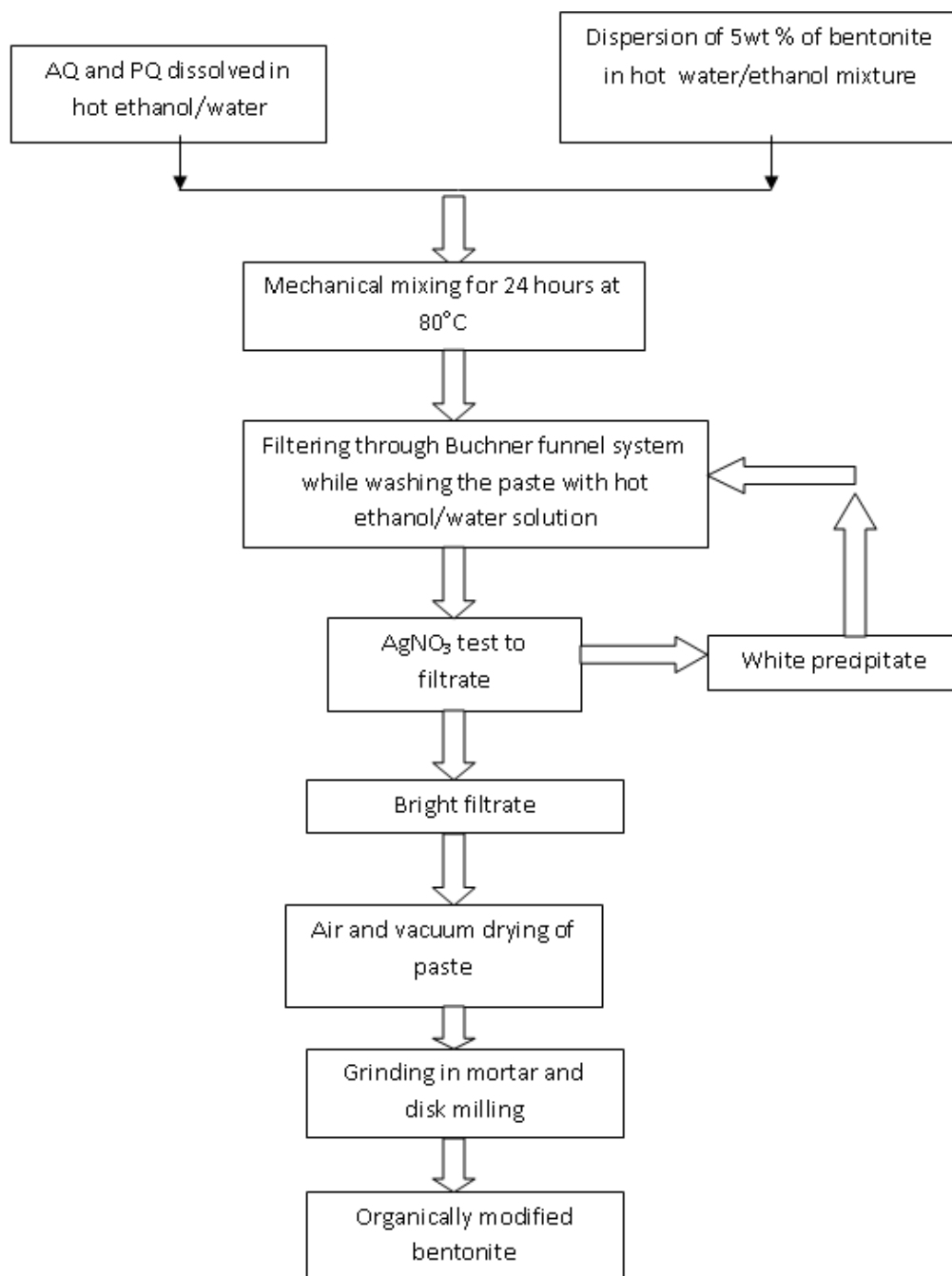


Figure 3. 9 Schematical representation of modification of bentonite

3.2.3 Production of Nanocomposites

3.2.3.1 Extrusion

In the production of ternary composites, a co-rotating twin screw extruder (Thermoprism TSE 16 TC with L/D = 24, screw diameter = 16 mm) was used (Figure 3.10). The length and diameter of the barrel are 384 mm and 16 mm, respectively.

Table 3.8 gives the compositions of samples prepared in SET-1. For the production of PPM based nanocomposites (SET 1); 400g mixture of organoclay (2 wt %), MAPP (2 wt %) and PPM were fed to the extruder simultaneously through the hopper. Four organoclays: HMA, TBP, TBA, TKA, and Cloisite®25A were used in this set. In addition to these concentrations, nanocomposites with TKA and HMA clays were prepared with a clay content of (1 wt %), MAPP (3 wt %) and PPM. These samples were abbreviated as PPM/Organoclay1/MAPP3. Temperature profile was 210°C throughout the extruder and the screw speed was 150 and 80 rpm in the first and second melt processing steps respectively. The extrudates obtained were passed through a water bath and then pelletized. Pelletized samples were dried in vacuum oven for 4 hrs at 100°C prior to the second extrusion process. Samples were dried in vacuum oven for 12 hrs at 100°C before injection molding.



Figure 3.10 Thermo Prism TSE 16 TC twin screw extruder

Table 3.9 gives the compositions of samples prepared in SET-2. In these set of experiments, (SET 2), organoclay (2 wt %), MAPP (5 wt %) and PPE were feed to the extruder with the help of Retsch/DR100 vibrating type feeder at a feed rate of 15-20 g/min. Four different organoclay types (HMA, TKA, TKA50 and PGWTKA) were used in this set. Temperature profile was 180°C throughout the extruder and the screw speed was 350 rpm in the first and second melt processing steps respectively. Figure 3.11 gives production routes for SET-1 and SET-2

Organoclays prepared by RB and cations of HMA, TKA,

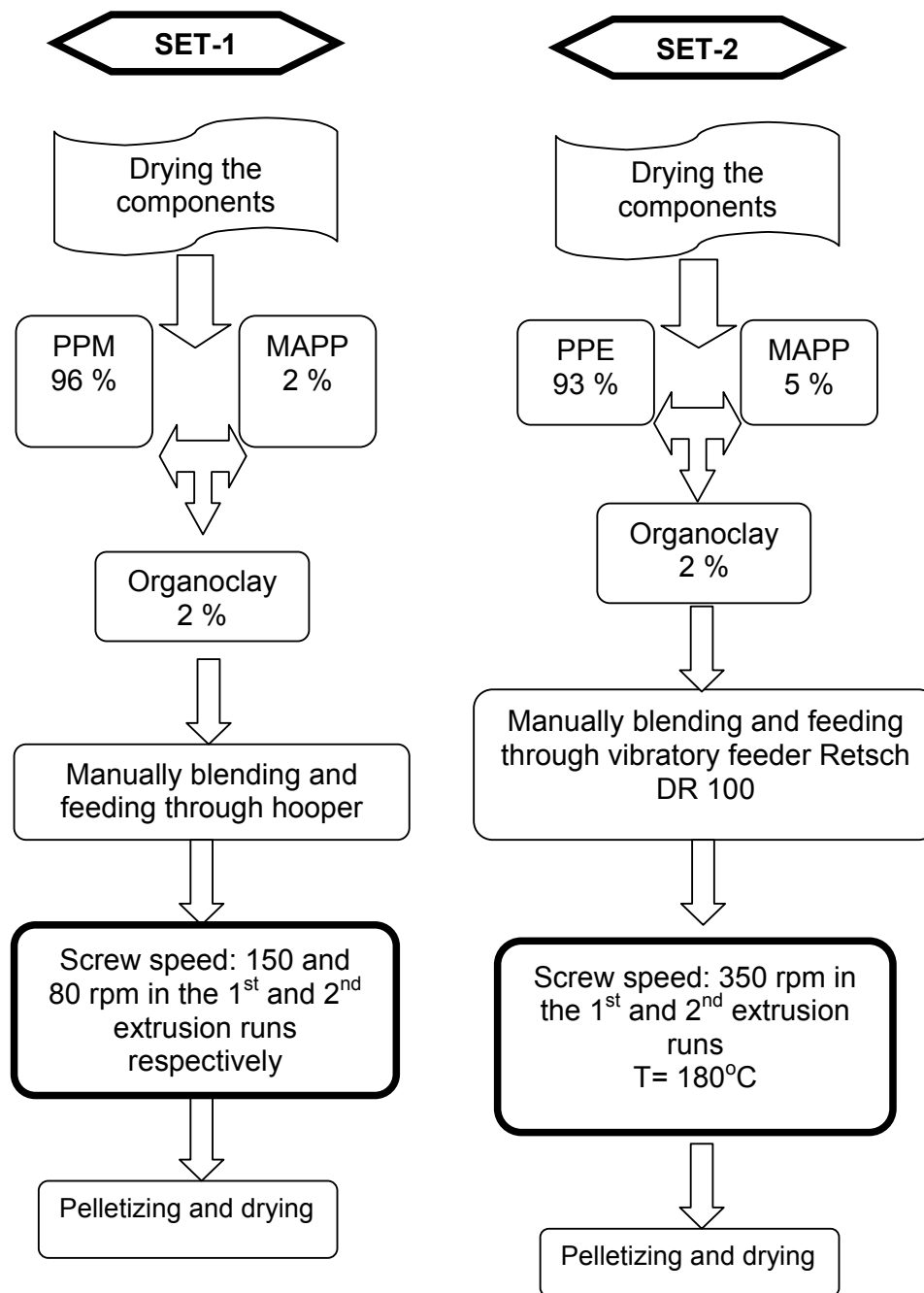


Figure 3. 11 Flow chart for production route of SET-1 and SET-2

Table 3.8 Compositions of PPM ternary and MAPP-Organoclay binary composites (Organoclays derived from RB)

	Concentration (%)		
SET-1			
Two Step Extrusion-150 rpm and 80 rpm in 1st and 2nd extrusion steps, 210°C			
Composition	PPM	MAPP	Organoclay
PPM	100		
PPM95/MAPP5	98	2	-
PPM/TBA2/MAPP2	96	2	2
PPM/TBP2/MAPP2	96	2	2
PPM/HMA2/MAPP2	96	2	2
PPM/TKA2/MAPP2	96	2	2
PPM/Cloisite®25A2/MAPP2	96	2	2
PPM/HMA1/MAPP3	96	1	3
PPM/TKA1/MAPP3	96	1	3

Table 3.9 gives the compositions of samples prepared in SET 3. In the third set of experiment (SET3), a mixture of organoclay (2 wt %), MAPP (5 wt %) and PPE were fed to the extruder through the vibratory feeder Retsch/DR100. Organoclays used in this set were DMDA, TBHP and STKA. Temperature profile was 180°C throughout the extruder and the screw speed was 350 rpm in both of the melt processing steps. The extrudates obtained were passed through a water bath and then pelletized. Pelletized samples were dried in vacuum oven for 4 hrs at 100°C prior to the second extrusion process. Production route for SET-3 is given in Figure 3.13

Table 3.9 Compositions of PPE ternary and MAPP-Organoclay binary composites (Organoclays derived from RB)

	Concentration (%)		
SET-2			
Two Step Extrusion-350 rpm at 180°C			
Composition	PPE	MAPP	Organoclay
PPE	100		
MAPP98/TBA2	-	98	2
MAPP98/TBP2	-	98	2
MAPP98/HMA2	-	98	2
MAPP98/TKA2	-	98	
MAPP98/TKA50-2		98	2
PPE/HMA2/MAPP5	93	2	5
PPE/TKA2/MAPP5	93	2	5
PPE/TKA50-2/MAPP5	93	2	5
PPE/PGWTKA2/MAPP5	93	2	5

Table 3.10 Compositions of PPE ternary and MAPP-Organoclay binary composites (Organoclays derived from PB).

	Concentration (%)		
SET-3			
Two Step Extrusion-350 rpm at 180°C			
Composition	PPE	MAPP	Organoclay
PPE	100		
PPE/DMDA2/MAPP5	93	2	5
PPE/TBHP2/MAPP5	93	2	5
PPE/PTKA2/MAPP5	93	2	5

3.2.3.2 Batch Mixing

Compositions and process conditions of PPE based composites prepared with batch mixing (SET 4 and 5) are given in Table 3.11. Extruded composite materials produced in SET 3 were further sheared by melt mixing of samples in an intensive batch mixer/torque rheometer, manufactured by Haake Buchler Instruments, Inc., Saddle Brooke, NJ (EU-5V) with a mixing volume capacity of 300 ml (Figure 3.12). Composites prepared in this system are named as SET 4 thereafter. Samples prepared in SET 4 are abbreviated with an M (referring the mixing) at the end of the sample name such as, PPE/DMDA2/MAPP5-M. Binary composites of 98 wt % MAPP and 2 wt % clay with 1 phr (part per hundred of the polymer matrix) Irganox®B225 were also prepared in batch mixer by melt blending to observe MAPP and clay compatibility (SET-5). Samples prepared by mixing in the batch mixer only are abbreviated with a B (referring the batch mixing), such as MAPP98/DMDA2-B. Based on the time sweep tests of the matrix, which will be mentioned later in detail, it was realized the PPE had a degradation tendency at the processing temperature. It was decided to use the heat stabilizer Irganox ®B225 which is a product of Ciba Company to avoid further degradation of PPE. This material was used at 1 phr of the composites in batch mixing experiment. In all mixing steps, temperature and blade speed were kept at 190°C and 32 rpm, respectively.

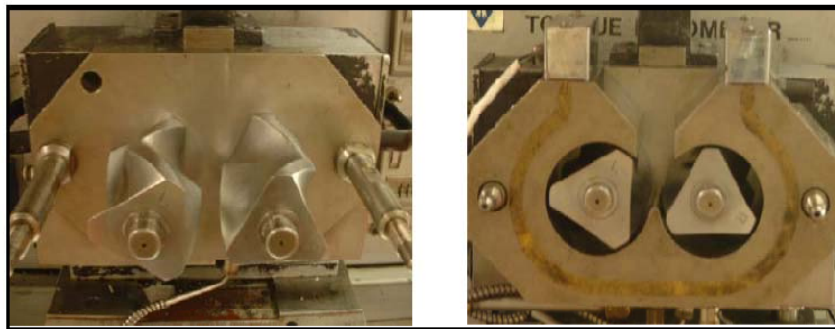


Figure 3.12 Haake Torque Rheometer with 300cc mixing head

Table 3.11 Compositions of PPE ternary and MAPP-Organoclay binary composites (Organoclays derived from PB).

	Concentration (%)		
SET-4			
Melt mixing of nanocomposites prepared in SET3 in the batch mixer at 190 °C and 32 rpm for 15 min with 1 phr IrganoxB225			
Composition	PPE	MAPP	Organoclay
PPE-M	100		-
PPE/DMDA2/MAPP5-M	93	2	5
PPE/TBHP2/MAPP5-M	93	2	5
PPE/PTKA2/MAPP5-M	93	2	5
SET-5			
Melt mixing in the batch mixer at 190 °C and 32 rpm for 15 min with 1 phr Irganox B225			
Composition	PPE	MAPP	Organoclay
PPE-B	100	-	-
PPE95/MAPP5-B	95	5	-
MAPP98/DMDA2-B	-	98	2
MAPP98/TBHP2-B	-	98	2

LLDPE based nanocomposites (SET 6) were directly prepared by melt mixing in Haake Haake Buchler Instruments, Inc., Saddle Brooke, NJ (EU-5V) mixer at 190°C and 32 rpm for 15 min. LOT was used as the compatibilizer between organoclay and LLDPE. In this part of the experiments, DMDA, TBHP, STKA and I34TCN organoclays were used. Compositions of the nanocomposites produced in SET-6 are given in Table 3.12.

At first, binders (polyolefin and compatibilizer) were fed into the batch mixer followed by the clay particles. The mixtures were kept in a desiccator to avoid humidity for 24 h before the characterization experiments. Production route for SET 4, 5 and 6 are given in Figure 3.13.

Table 3.12 Compositions of LLDPE ternary and LOT-Organoclay binary composites

	Concentration (%)		
SET 6			
Melt mixing in the batch mixer at 190 °C and 32 rpm for 15 min			
Composition	LLDPE	LOT	Org-Clay
LLDPE	100		
LOT	100		
LLPE95/LOT5	95	5	
LL87.5/LOT12.5	87.5	12.5	
LOT98/DMDA2		98	2
LOT98/TBHP2		98	2
LOT98/TKA2		98	2
LOT98/I34-2		98	2
LL/DMDA2/LOT5	93	5	2
LL/DMDA5/LOT12.5	82.5	12.5	5
LL/TBHP2/LOT5	93	5	2
LL/TBHP5/LOT12.5	82.5	12.5	5
LL/I34-2/LOT5	93	5	2
LL/I34-5/LOT12.5	82.5	12.5	5
LL/I34-5/LOT5	90	5	5

Organoclays prepared by PB and cations of DMDA, TBHP, TKA and I34

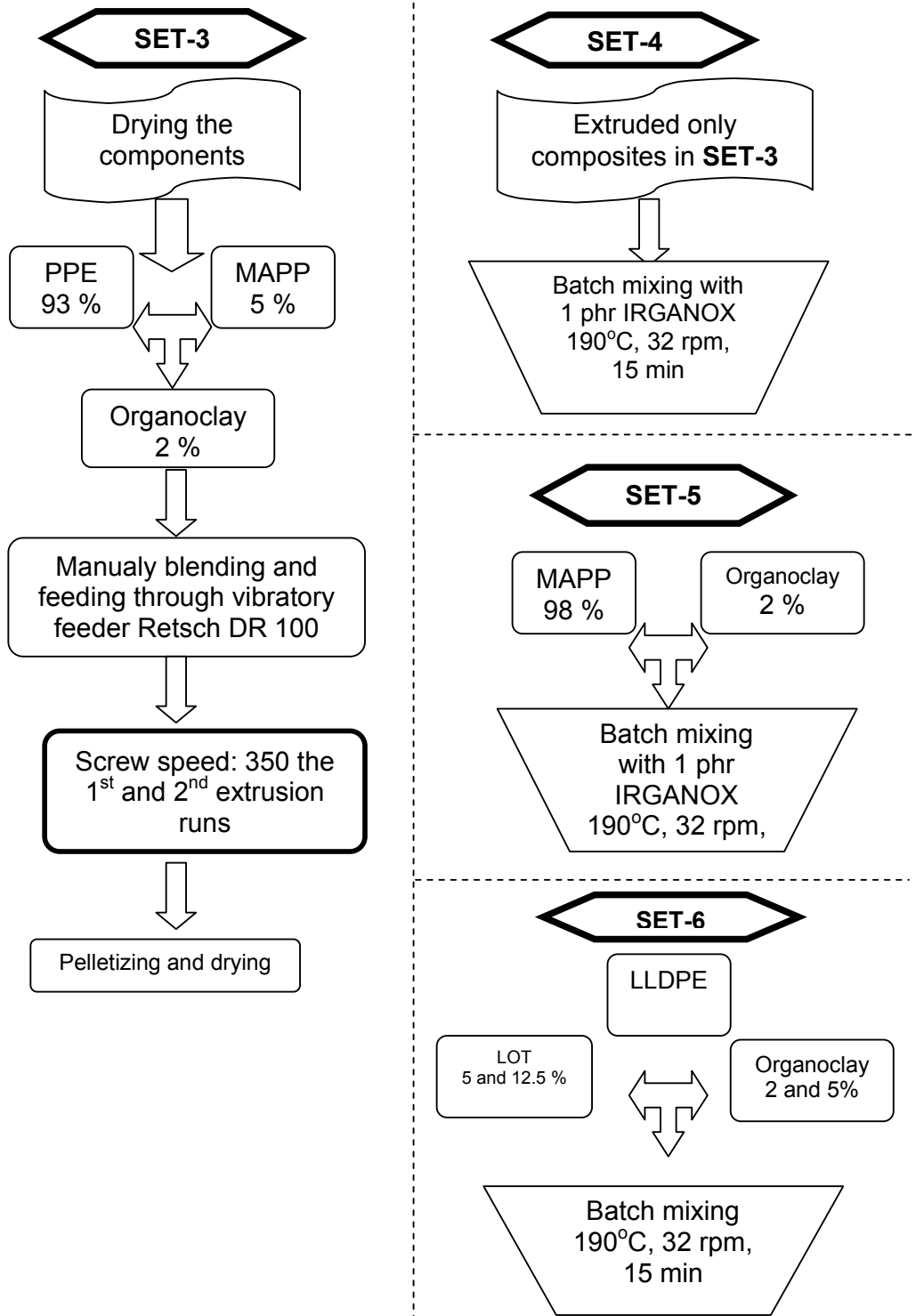


Figure 3.13 Flow chart for production route of SET-3,4,5 and 6

3.2.4 Drying

Before all at the extrusion processes, samples (PP, MAPP, LLDPE, LOT and organoclays) were dried in a vacuum oven. Drying conditions are given in Table 3.13.

Table 3.13 Drying conditions

Sample	Drying Temperature (°C)	Drying Time (h)
Before Extrusion and Batch Mixing		
PP	80	
LLDPE	80	
MAPP	80	12-15
LOT	80	12-15
Organoclays	80	12-15
Before 2nd Extrusion Run		
PPE/Organoclay/MAPP	100	4
PPM/Organoclay/MAPP	100	4
MAPP98/Organoclay2	80	4
Before Injection Molding		
All samples	100	12-15

3.2.5 Injection molding

Samples for tensile testing and impact tests were prepared by injection molding. For injection molding, DSM Micro 10 cc Injection Molding Machine shown in Figure 3.14 was used. PPM and PPE based composites were injection molded at barrel temperature of 220°C and melt temperature of 25 °C, with hold time of 4 min. and 40 sec.. LLDPE based

nanocomposites were molded at barrel temperature of 200°C and melt temperature of 25 °C where hold time was 3 min. and 40 sec.



Figure 3.14 DSM injection molding machine

3.2.6 Compression Molding

For X-Ray analysis conducted in HFMI laboratories, samples were compression molded between two teflon sheets in square shaped molds shown in Figure 3.15 using CARVER compression molder (Figure 3.16). Temperature was kept between 190-200°C during the experiment. At first, materials were heated for 5 min. for melting. Then, the melt was pressed at 2 psi for 1 min. Molds were cooled with tap water with an internal water circulation system for 8 min under pressure. Then, the pressure was released and the materials were taken out.

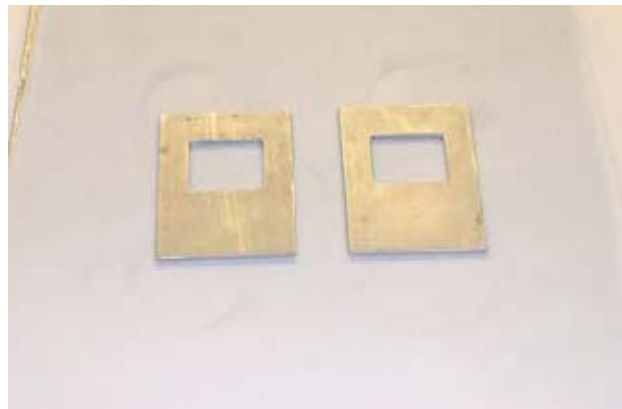


Figure 3.15 Square shaped molds for X-Ray



Figure 3.16 CARVER compression molder

For rheological analysis, nanocomposites were molded between two teflon sheets in disk shaped molds with a diameter of 25 mm and thickness of 1 mm. The same temperature history was applied as used in sample preparation for X-Ray measurement.

3.3 Characterization Techniques

3.3.1 Characterization of Organoclays

3.3.1.1 Bentonite Cation Exchange Capacity Measurement

Although cation exchange capacity (CEC) of the Reşadiye bentonite (RB) has been given by researchers (Onal et al., 2003; Can et al., 2007; Cinku et al., 2007), in this thesis, it was determined by methylene blue (MB) procedure for confirmation. For MB test, ASTM/C837 – 99 procedure given as follows was used: 2.00 g of clay that was dried at 105 °C was placed in a 600-mL beaker. 300 mL of distilled water was added to the

beaker and stirred with the mixer until the clay was uniformly dispersed. The pH of the slurry was adjusted to 2.5-3.8 with sufficient sulfuric acid. Stirring was continued while the pH was adjusted and continued 10 to 15 min after the last addition of acid. With the slurry still being mixed, the buret was filled with 0.1 N methylene blue solution and added to the mixture in 5 ml increments, then the mixture was stirred for 1 to 2 min. A drop of the slurry was placed at the edge of the filter paper with a glass stirring rod. The end point was indicated by the formation of a light blue halo around the drop. Addition of the methylene blue solution to the slurry was continued in 1.0-mL increments with 1 to 2 min of stirring after each addition, followed by testing, until the end point was reached.

CEC was calculated with the following equation,

$$MBI = \frac{E \times V}{W} \times 100 \quad (3.3)$$

where

MBI = methylene blue index for the clay in meq/100 g clay,

E = milliequivalents of methylene blue per milliliter

V = milliliters of methylene blue solution required for the titration

W = grams of dry material.

The CEC of the bentonite (RB) was determined as 67.5 meq/100 g clay. The CEC of raw Reşadiye bentonite was determined as 65 mmol/100g by Onal et al., 2003; 75 mmol/100g by Cinku et al., 2007; 78 mmol/100g by Can et al., 2007. All of these results were determined by MB method.

3.3.1.2 X-Ray Diffraction

Two types of Xray equipments, one present in METU-METE Department and one present in Stevens-HFMI laboratories were used for XRD analysis.

3.3.1.2.1 X-Ray Equipment (METU-METE Department)

The X-Ray of bentonites samples and composites obtained in a 100 kV Philips twin tube X-ray diffractometer (PW/1050) using CuK_α radiation, which generate a voltage of 40 kV and current of 40 mA ($\lambda = 1.54\text{\AA}$). The diffraction angle 2θ was scanned from 1° to 10° at a scanning rate of $1^\circ/\text{min}$ and a step size of 0.01° . X-Ray analysis of clay samples were done in powder form. Tensile bars obtained by injection molding were used for analyzing the morphology of the nanocomposites by XRD.

3.3.1.2.2 X-Ray Equipment (Stevens Institute of Technology-HFMI Laboratory)

Part of the samples were analyzed by the X-Ray equipment present in HFMI laboratory. X-Ray diffraction (XRD) patterns were obtained using a Rigaku Miniflex diffractometer equipped with Cu-K_α source (1.5406\AA) operating at 30 kV and 15 mA. This analyses were done at HFMI laboratory in Stevens Institute of Technology.

The diffraction patterns were collected as the Bragg angle, 2θ , range of $2-5^\circ$ at a scanning rate of $0.1^\circ/\text{min}$ and using a step size of 0.01° . Interlayer spacing (d -spacing) was calculated from Bragg's law: $n\lambda = 2d \sin\theta$ where n is an integer, λ is the wavelength, θ is the measured diffraction angle, and d refers to the interlayer spacing.

3.3.1.3 Scanning Electron Microscopy

SEM analysis of fractured surfaces was performed by a low voltage Scanning Electron Microscope (JEOL JSM-6400). The sample surfaces were coated with gold to prevent electrostatic charging during analyzing.

3.3.1.4 Transmission Electron Microscopy (TEM)

Morphology, i.e., dispersion of clay layers were analyzed by TEM. Two different TEM equipments were used for characterization. The first one was in DSM, Holland (Philips CM200), and it used an accelerating voltage of 120 kV. Second equipment was located in the UNAM facilities, Bilkent University, Ankara with a brand name of Tecnai™ G2 F30 produced by FEI Company, and use an accelerating voltage of 300kV. The 300 kV electron beam of the Tecnai G2 F30 delivers higher resolution for a given objective lens geometry, a higher beam current and better sample penetration compared to a 200 kV TEM.

Ultra thin sections of 70 nm in thickness were cryogenically cut with a diamond knife at a temperature of 100 °C. All samples were trimmed parallel to the molding direction.

3.3.1.5 Spectroscopic Analysis

3.3.1.5.1 Inductively Coupled Plasma Optical Emission Spectrometer, (ICP) (Chemical Analysis for Clays)

ICP analysis of the clay samples was done by Perkin Elmer Optima 4300DV in METU-Central Laboratory. Specifications of the equipment given by the METU-Central Laboratory are as follows:

- Torch: Demountable design using one-piece quartz tubing for plasma and auxiliary gas flow. 2 mm alumina injector corrosion resistant to all acids, including HF and aqua regia.
- Spray Chamber: Scott-type, constructed of Ryton, resistant to most acids, including HF and organic solvents.
- Nebulizer: Cross-flow design. The system is compatible for use with other nebulizers.
- Polychromator: The high energy (f/6.7) echelle-based polychromator is PE design.
- Detector: The patented PE segmented-array charge-coupled device.

3.3.1.5.2 Fourier Transform Infrared Spectroscopy (FTIR)

Fourier Transform Infrared Spectroscopy (FTIR) analyses of bentonites were conducted with an IR Prestige-21 Shimadzu equipment operating in the range of 400-4000 cm^{-1} . Clay specimens were prepared by mixing a small amount of clay with KBr followed by cold pressing to form discs.

3.3.1.6 Thermal Analysis

3.3.1.6.1 Thermogravimetric Analysis (TGA)

TGA analysis was done by a Shimadzu DTG-60H thermal analyzer using a scanning rate of 15 $^{\circ}\text{C}/\text{min}$ under nitrogen atmosphere, from room temperature up to 1000 $^{\circ}\text{C}$.

3.3.1.6.2 Differential Scanning Calorimetry (DSC)

Differential scanning calorimetry (DSC) measurements were carried out with DSC-60 Shimadzu (Metu-CHE) and General V4.1.C DuPont 2000 (METU-Central Laboratory) differential scanning calorimeter under N_2

atmosphere, with a scan speed of 5°C/min, in order to evaluate the crystallinity of the nanocomposites. A typical sample weight was about 5 mg. PP based composites were analyzed from 25°C to 230°C. LLDPE based composites were analyzed from 0°C to 200°C.

Crystallinity was determined using the heat of fusion of the sample (ΔH_{sample}) given by the DSC analysis. Percent crystallinity (%) values were calculated as the proportion of the heat of fusion (ΔH_{sample}) values of the specimen divided by weight fraction of the polymer (w) in the nanocomposite and the heat of fusion of the pure crystalline form of the polymer ($\Delta H^{\circ}_{\text{sample}}$). Heat of fusions of purely crystalline polypropylene and polyethylene were taken as 209 J/g and 293 J/g, respectively [Chen et al., 2007]

3.3.1.7 Mechanical Testing

Mechanical properties of the samples were measured by tensile testing. Mechanical properties of the samples give information about the reinforcement, delamination of clay particles in the matrix and compatibility between the phases present in the polymer matrix.

Tensile analyses were all done at 23 °C. At least 5 samples were tested and the averages and the standard deviations are reported.

3.3.1.7.1 Impact Test

Charpy impact strength of notched (2 mm) and unnotched samples were measured by Ceast Resil Impactor (Fig.3.17) according to ISO 179-2. Sample shapes and dimensions used for the impact tests are given in Figure 3.18 and Table 3.14 respectively.



Figure 3. 17 Ceast Resil Impactor

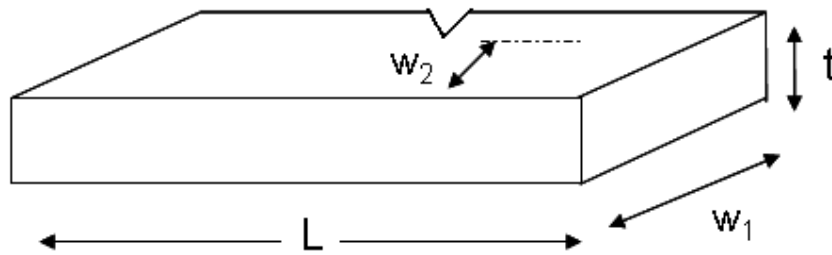


Figure 3.18 Schematic of impact test sample

Table 3.14 Dimensions of impact test sample

Designation	Dimensions (mm)
Length, L	80
Total width- w_1	10
Unnotched width- w_2	8
Thickness, t	4
Notch Type and angle	V, 45°

3.3.1.7.2 Tensile testing

Tensile properties were measured with Lloyd LR 30 K Universal Testing and Shimadzu AG-SN type machines according to ASTM D638-03 using dog bone type injection molded samples shown in Figure 3.19 (Tensile test samples were prepared according to ISO 527-5A standard). Dimensions of the dog bone specimen are given in Table 3.15. Gauge length, crosshead speed and strain rate were 30 mm, 15 mm/min and 0.5 min^{-1} respectively. Young's modulus, tensile strength and elongation at break values were measured from the stress-strain diagram. The Young's modulus (YM) of the samples were determined from the first tangent of the each plot in initial elastic region.

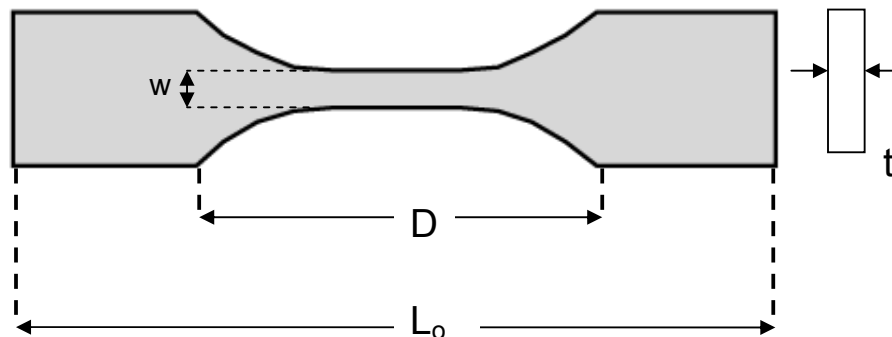


Figure 3.19 Schematic of tensile test sample

Table 3.15 Dimensions of tensile sample

Designation	Dimensions, mm
Distance between grips, D	30
Overall Length, L_0	74
Thickness, t	2.1
Width of narrow section, W	4

3.3.1.8 Rheological Measurements (Stevens Ins. Tech.-HFMI)

Linear viscoelastic behavior of LLDPE samples were analyzed by a dynamic oscillatory rheometer in the melt state as a function of time, strain and frequency. The Rheometric Dynamic Analyzer (Rheometric Scientific, NJ) (RDA) (Figure 3.20) was used in conjunction with 25 mm parallel disk fixtures for the small-amplitude oscillatory shear experiments.



Figure 3.20 Rheometric Dynamic Analyzer, RDA

All measurements were performed at 190°C and 5 rad/s. The gap height was set at 1 mm. Frequency sweep rheological measurements were performed at a frequency range from 1 to 100 rad/s. All runs were repeated for three times and averages of them are reported together with confidence intervals. To ensure that the experiments are conducted in the linear viscoelastic region, the strain amplitude was set at 10 % in LLDPE (SET 6) and 40 % in PPE (SET 4-5); elastic moduli (G'), loss moduli (G'') and complex viscosity (η^*) were obtained. G' is called as the elastic (storage) modulus and represents the stored elastic energy. G'' is called as the loss modulus and represents the amount of energy irreversibly given off by the substance to the environment.

Rheological analyses were done in HFMI laboratory in Stevens Institute of Technology.

CHAPTER 4

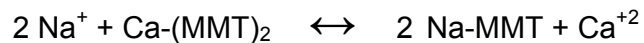
RESULTS AND DISCUSSION

4.1 Purification of Reşadiye Bentonite

4.1.1 X-Ray Analysis for Purification

The analysis of the RB, PB and commercial high purity MMT, PGW are shown in Figure 4.1. RB showed mainly the presence of smectite (S) Na⁺MMT together with non-clay impurities such as clinoptilolite (Cln), opal-C (OC) and feldspar (F) [Onal et al., 2003, Tabak et al., 2007]. XRD of PB show non-clay parts that were mainly smaller and it had peaks similar to PGW. CEC of the PB was determined by methylene blue method as 100 mmol/100g of clay, while that of RB was 67.5 mmol/100g. This increase also shows the increase in the MMT content and absorption capacity of the bentonite upon purification. X-Ray analysis, together with increase in the CEC of the bentonite, show that purification applied in this study is an adequate method to obtain pure MMT. Purification of Reşadiye bentonite was also done by Onal et al., 2007 and their analysis showed increase in the CEC of the sample from 65 mmol/100g to 108 mmol/100g. Another purification procedure was done by Can et al., 2007 and the CEC of Reşadiye bentonite was increased from 78 mmol/100g of clay to 97.8 mmol/100g. In one other study done by Boylu et al., 2007, Reşadiye bentonite was purified by hydrocylcone technology and the CEC of it after purification was measured as 104 mmol/100g. Yucel et al. 2007, determined the CEC of enriched Reşadiye bentonite as 78 mmol/100g. All of these studies show purification of Reşadiye bentonite resulted in increase in the CEC, and the values of CEC are consistent with one determined in this study.

Delamination of smectite layers is an important process in polymer-clay nanocomposites, since it leads to enhancement of several polymer properties. Impurities, non-clay parts and other ions which are not exchangeable during the cation exchange reaction may reside between the galleries as immobilized points. Other ions apart from the Na⁺ (or Li⁺), in particular Ca⁺², need also be removed, because they act as reservoirs of multivalent cations [Lagaly, 2006(b)]. Chemical analysis of clays shows (Table 4.1) reduced content of CaO in PB compared to RB, since addition of Na₄(P₂O₇) leads to exchange of Ca⁺² ions with Na⁺ [Song et al., 2005]. In the presence of high Na⁺, MMT replaces its Ca⁺² ions with Na⁺ according to following equation,



Since Na₄(P₂O₇) was added during the sedimentation process, suspension was rich in Na⁺ content. Ca⁺² may act as a trapped point and may lead to the reduction in the CEC of the clay and further lead to failure in the dispersion of clay layers in the polymer matrix. Thus, purification and fractionating of bentonite is an important step in producing an organoclay that can be used in polymer-matrix nanocomposites.

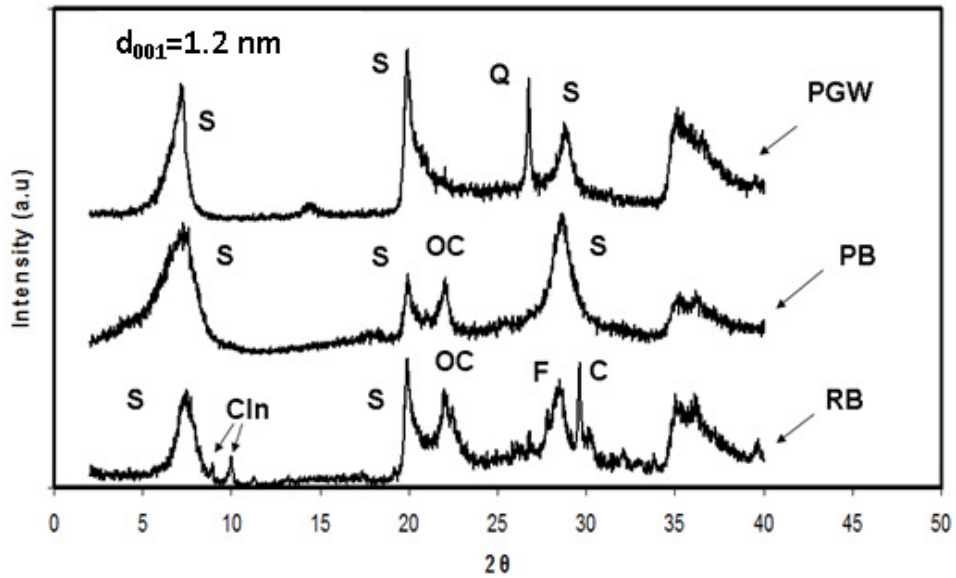


Figure 4.1 X-Ray analysis of RB, PB and PGW Nanocor (S: Smectite, Q: Quartz, C: Calcite, Cln: Clinoptilolite, F: Feldspar, OC: Opal-C).

Table 4.1 Chemical analysis of bentonite

Components	Weight Percent (%)			
	Raw Bentonite (RB)	Purified Bentonite (PB)	DMDA in PB	HMA in RB
MgO	1.85	2.15	1.51	1.66
CaO	2.60	0.33	0.1	2.19
Fe ₂ O ₃	3.21	3.91	2.7	2.85
Al ₂ O ₃	15.6	16.83	11.8	13.85
Na ₂ O	2.69	2.18	0.04	0.48
K ₂ O	0.78	0.28	0.13	0.61
SiO ₂	54.97	61.1	41.88	48.36

4.1.2 X-Ray Analysis of Organoclays

In this study, raw and purified bentonites were used for organoclay preparation. As shown in the Table 3.7, modification of pure bentonite was done with [DMDA] [Cl⁻], [TBHP][Br⁻] and [TKA][Br⁻] while modification of RB was done with [TBA][BF₄], [TBP][BF₄], [HMA][Br⁻] and [TKA][Br⁻].

DMDA was chosen as an organic modifier because it has 18C atoms in its two tails and the other two have methyl groups. These two long alkyl tails may increase the d-spacing of the bentonite to a sufficient extent and reduce the attractive forces between the silicate layers so it may become more compatible in the polymer matrix. Osman and Rupp, 2005 claimed that DMDA has alkyl chains with similar chemical structure and solubility parameter to PE. TBHP cation has one long alkyl tail with 16 C atoms while the other tails have chains with 3C (butyl groups). In total DMDA has 38 C atoms and TBHP has 28 C atoms. Bulkier C groups in DMDA with respect to TBHP allow comparison of the effect of number of C groups. In addition, phosphonium ion usage in TBHP allows comparison of its effect on the thermal stability of the organoclay. Branching present in TBHP cation allows to make a comparison with DMDA which has relatively low branching.

HMA has one long alkyl tail with 16 C atom and methyl groups on other three tails. TKA has 10C atoms in its four tails and these long and crowded C environment in it allows to make a comparison with HMA cation.

The effect of phosphonium ion comparison was made by the use of TBA and TBP since they have the same number of C (four) atoms in each tail. While TBA is ammonium based, TBP is a phosphonium based cation.

Figure 4.2 shows that the organoclays DMDA, TBHP, STKA and I34 have diffraction angles shifted to the left in comparison to the unmodified PB, indicating increase in the d-spacing of the clay according to Bragg's law: $d = \lambda n / (2 \sin \theta)$. All of the modified three clays show higher d-spacing compared to PB and commercial clay I34. The increase in d-spacing of the clays indicate that the organic modifiers have diffused between the silicate layers [Kim and White, 2005] and modification is effectively accomplished. Success of modification is also confirmed by the chemical analysis of the DMDA (Table 4.1) where concentration of Na^+ decreased after the modification compared to PB, revealing exchange of Na^+ ions. Gallery distance of the PB increased from 1.22 nm ($2\theta = 7.2^\circ$) to 2.64 nm ($2\theta = 3.34^\circ$), 2.24 nm ($2\theta = 3.94^\circ$) and 2.71 nm ($2\theta = 3.26^\circ$) after modification with [DMDA] [Cl^-], [TBHP] [Br^-] and [TKA] [Br^-] respectively. Increased d-spacing and reduced surface energy lead to easier exfoliation, since the amount of surfactant residing in the galleries and the orientation of the molecules interfere with the structure and the properties of polymer-clay nanocomposites. The highest d-spacing belongs to STKA which has a relatively bulkier cation compared to other alkyl cations with long alkyl tails. DMDA has closer d-spacing to STKA since total C atoms in each modifier are similar. Although two tails of DMDA have 18C atoms, STKA with 10C in each tails resulted in higher d-spacing. Different d-spacings in the organoclays may occur due to dissimilar amounts of surfactant between the galleries or different structure or orientation of the organic molecules [Kadar et al., 2006]. Longer and bulkier C groups in DMDA (total 38 C) resulted in higher d-spacing compared to TBHP (total 28). In the literature, d-spacing of the MMT modified with DMDA cation is given as 1.43 nm by Vaia et al., 1994; 3.15 nm by Majdan et al., 2008 and 2.4 nm by Ren et al., 2000, thus our result is consistent with the last study. To our best knowledge, no research is conducted with TKA cations. Stoeffler et al., 2008 (a) modified Na^+ -MMT (Cloisite- Na^+) with [TBHP] [Br^-] and the d-spacing of the clay was determined as 2.19 nm which is close to our calculated value., i.e., 2.24 nm for the same modifier.

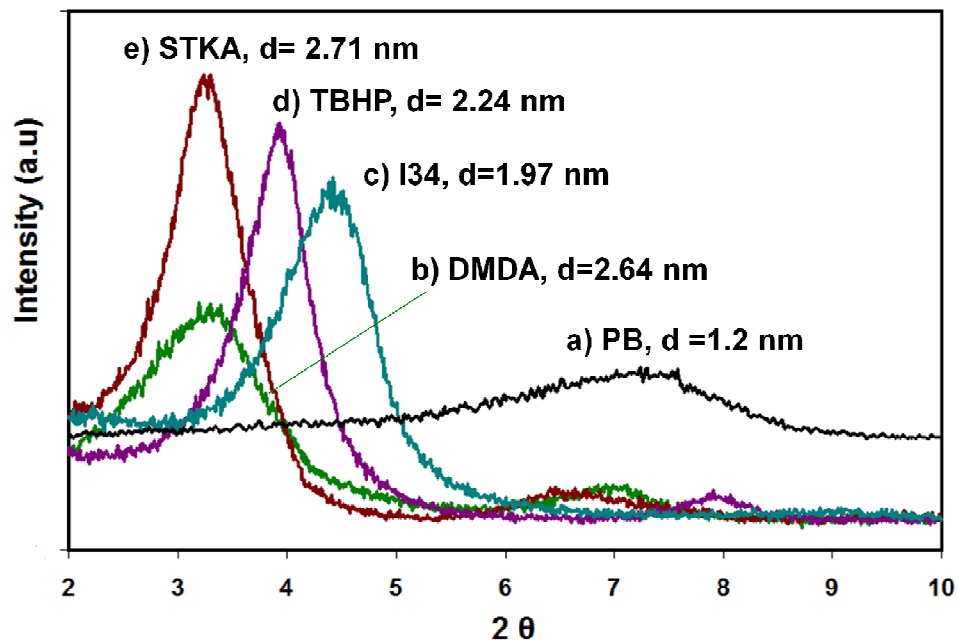


Figure 4.2 X-Ray results of modified clays a) PB, b) DMDA, c) I34, d) TBHP and e) STKA.

Figure 4.3 shows the XRD analysis of organoclays prepared with RB. X-Ray analysis shows increase in d-spacing of RB from 1.2 nm to 1.78 nm, 2.56 nm, 1.48 nm and 1.64 nm after modification with [HMA][Br], [TKA][Br], [TBA][BF₄] and [TBP][BF₄] respectively. XRD of organoclay prepared by excess (1.5 x CEC) of TKA50 shows relatively higher d-spacing (2.67 nm) compared to the one prepared with 1.1XCEC, revealing excess usage of material may cause increase in the d-spacing, since more bulky alkyl groups intercalate through the clay layers. However, it is mentioned in the literature that using excess surfactant with respect to the cation exchange capacity of the clay induces plasticization of the surfactant layer in pure organoclays and appears to reduce the tendency for intercalation [Panek et al., 2006]. Effect of excess surfactant usage will provide comparison on the effect of surfactant loading. For comparison, commercial pure Na⁺-MMT PGW was modified with TKA which is abbreviated as PGWTKA. The d-spacing of PGWTKA is the highest

among all the clays ($d=2.83$ nm) which is most probably due to high degree purity of PGW as shown by its high CEC value (145 mmol/100g of clay). High CEC of the clay indicates that the clay can absorb high amount of cation because its exchangeable cation content, i.e., Na^+ , is high. TBP and TBA show similar d-spacing values, since they have the same number of carbon atoms. Increase in the d-spacing of the modified bentonites confirms the occurrence of intercalation of salt molecules between the bentonite layers. Ion exchange between the Na^+ ions of clay and ions of HMA can also be seen from the chemical analysis given in Table 4.1. Decrease in Na^+ content in RB after modification with $[\text{HMA}][\text{Br}]$ also confirms this exchange reaction. Note that in Table 4.1, DMDA should be compared with PB and HMA should be compared with RB.

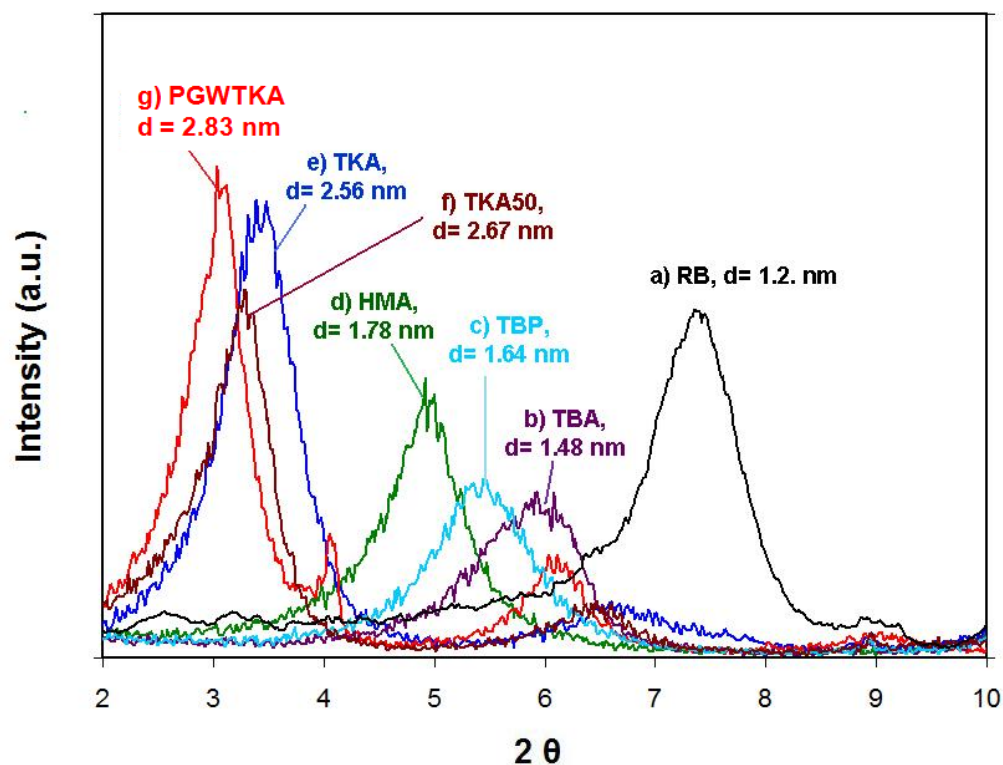


Figure 4.3 X-Ray results of modified clays a) RB, b) TBA, c) TBP, d) HMA, e) TKA, f) TKA50 and g) PGWTKA.

Depending on the packing density, temperature and chain length, the arrangement and confinements of alkyl chains between the galleries of clay are assumed to form mono or bilayers or radiate away from the surface, forming extended (paraffin-type) mono or bimolecular arrangements as shown in Figure 4.4 [Vaia et al., 1981; Vaia et al., 1994; Weiss, 1996].

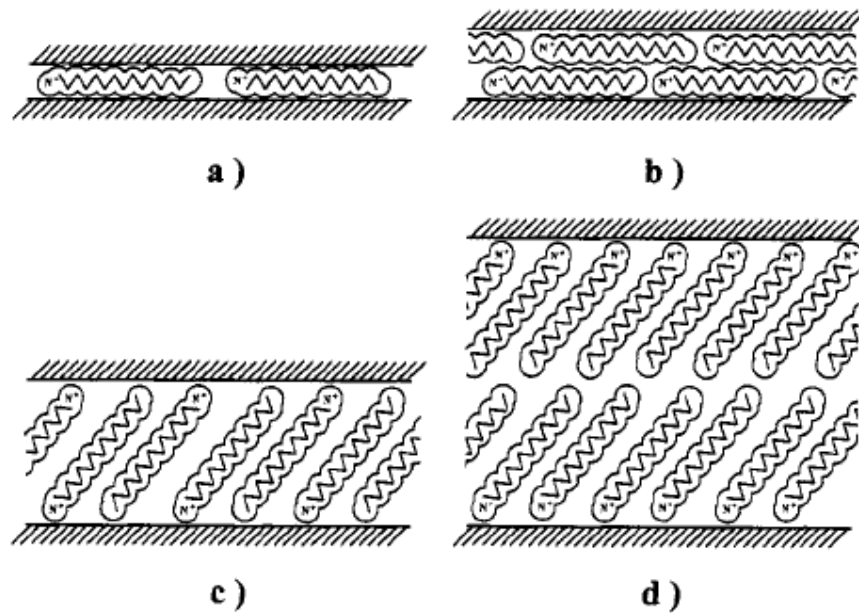


Figure 4.4 Alkyl chain aggregation in silicates a) lateral monolayer; b) lateral bilayer; c) paraffin-type monolayer; d) paraffin-type bilayer [Vaia et al., 1994]

Short chain alkylammonium ions are arranged in monolayers, longer chain alkylammonium ions in bilayers with the alkyl chain axes parallel to the silicate layers. The monolayer has a basal spacing of 1.4 nm, where the bilayer of 1.8 nm. Therefore, the values of 1.48 nm for TBA and 1.64 nm for TBP are consistent with a mono-layer arrangement of the quaternary alkyl and ammonium ions in the interlayer space. The d-spacing of 1.78 nm for HMA is consistent with a bilayer arrangement of intercalated surfactant [Hedley et. al, 2007; Lagaly, 2006 (a)].

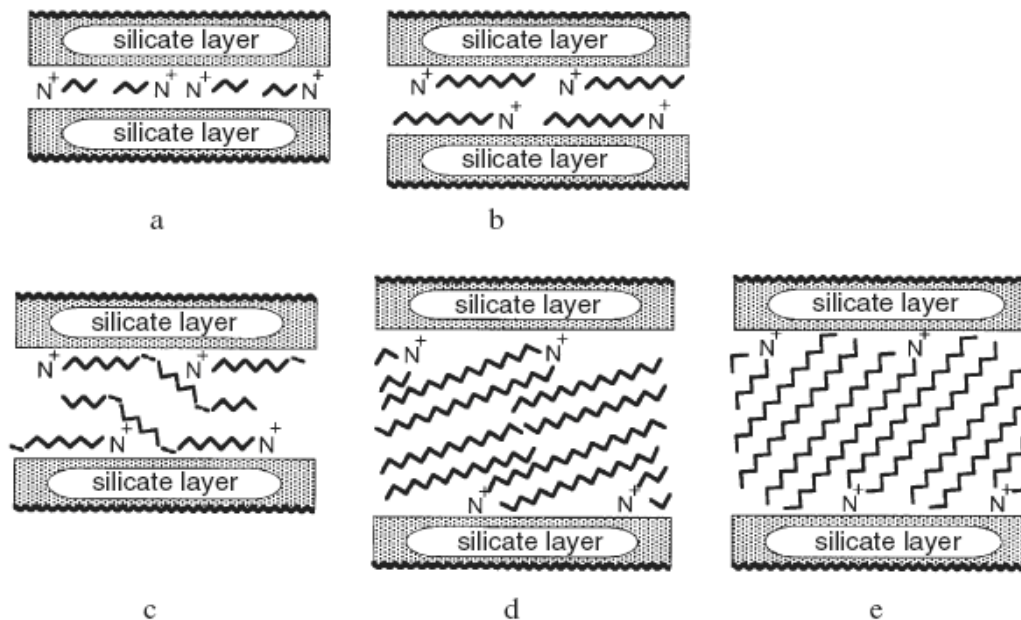


Figure 4.5 Arrangement of alkylammonium ions in the interlayer space of smectites: (a) monolayers, (b) bilayers, (c) pseudo-trimolecular layers, and (d, e) paraffin-type arrangements of dialkylammonium ions with different tilting angles of the alkyl chains [Lagaly, 2006].

Three-layer structures of twirled alkyl chains are seen with highly charged smectites and/or long surfactant cations. This pseudotrimolecular arrangement shows a basal spacing around 2.2 nm. Therefore, the values of 2.56 nm for TKA, 2.67 nm for TKA50, 2.83 nm for PGWTKA, 2.24 nm for TBHP, 2.71 nm for STKA and 2.64 nm for DMDA is consistent with a paraffin-type/ pseudotrimolecular arrangement. The term pseudo is used because the positive surfactant groups are attached on the silicate layers whereas the alkyl chains adopt a trimolecular arrangement by formation of kinks (Figure 4.5 c). Paraffin-type arrangements (Figure 4.5, d and e) in the d-spacing of layered silicates are formed by quaternary alkylammonium/phosphonium ions with two or more long alkyl chains. If all C–C bonds are in trans-conformation, the dialkylammonium ions are V-shaped. An almost parallel orientation of the chains is attained by formation of gauche-bonds near the ammonium group (Figure 4.6).

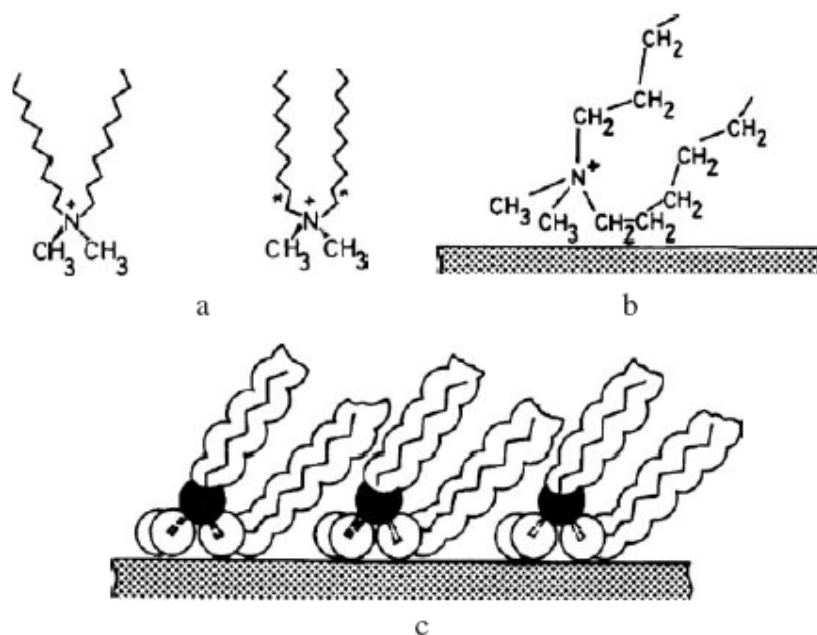


Figure 4.6 Conformation of dialkylammonium ions with and without gauche bonds near the ammonium group [Lagaly, 2006 (a)].

Apart from the orientation of surfactant molecules in the galleries, the amount used for organophilization is also important in the determination of surface properties and behavior. Small amount of modifier does not cover the entire surface, yields high-energy surface uncovered, and results in large surface tension, while excessive amounts may dissolve or disperse in the polymer, leading to lower properties [Kadar et al., 2006]. Kadar et al., 2006 showed that excess modifier added to the silicate during modification, i.e., the amount above 100% CEC, cannot be located inside the spacing between the clay layers, but only among the particles. Therefore, immoderate modifier maybe dissolved or dispersed in the polymer and might change its properties considerably.

4.1.3 TGA Analysis

TGA of PB and modified MMT's given in Figure 4.7 showed that the thermal stability of the organoclays can be classified as I34<DMDA<TKA<TBHP implying higher thermal stability of phosphonium ion compared to ammonium alkyl ions [Xie et al, 2002]. Overall weight loss of PB and modified MMTs are 6.6 %, 33 %, 38.7 %, 35 % and 29 % for the PB, I34, DMDA, TKA and TBHP respectively. Note that commercial organoclay I34 has the lowest thermal stability, e.g., first decomposition temperature, compared to other organoclays. TGA analysis of RB and modified bentonites with RB (Figure 4.8) showed that the thermal stability of the organoclays can be classified as PGWTKA<TKA50<TKA<HMA<TBA< TBP depending on their first decomposition temperatures which are summarized in Table 4.2. Initial weight loss of RB and PB at 30°C-150°C is attributed to residual water evaporation, which is adsorbed by the cations in the interlayer of the bentonite. The second loss is related to the dehydration of water molecules from the crystal lattice of MMT. Modified bentonite weight losses between 30°C-600°C are due to dehydration of water molecules in the crystal structure and the decomposition of organic salts. The organophilization of modified bentonites can be seen in both Fig. 4.7 and Fig. 4.8, since unmodified bentonites, RB and PB have higher initial weight losses due to evaporation of water in comparison to modified ones [Lee and Lee, 2004].

Decomposition of PB and RB manifest themselves in two steps. Initial weight loss in the first step at 30°C-150°C is attributed to residual or free water evaporation [Xie et al., 2001; Filho et al., 2005; Lee and Lee, 2004; Kim and White, 2005], which is adsorbed by the cations in the interlayer of the PB. The second loss is related to the dehydroxylation of structural water molecules from the crystal lattice of MMT [Tiwari et al., 2008; Hedley et al., 2007; Xie et al., 2001]. It is remarkable to observe that the overall weight losses of all the modified MMT's are higher than those of

PB and RB which are due to decomposition of intercalated alkyl tails of surfactants within the galleries of MMTs.

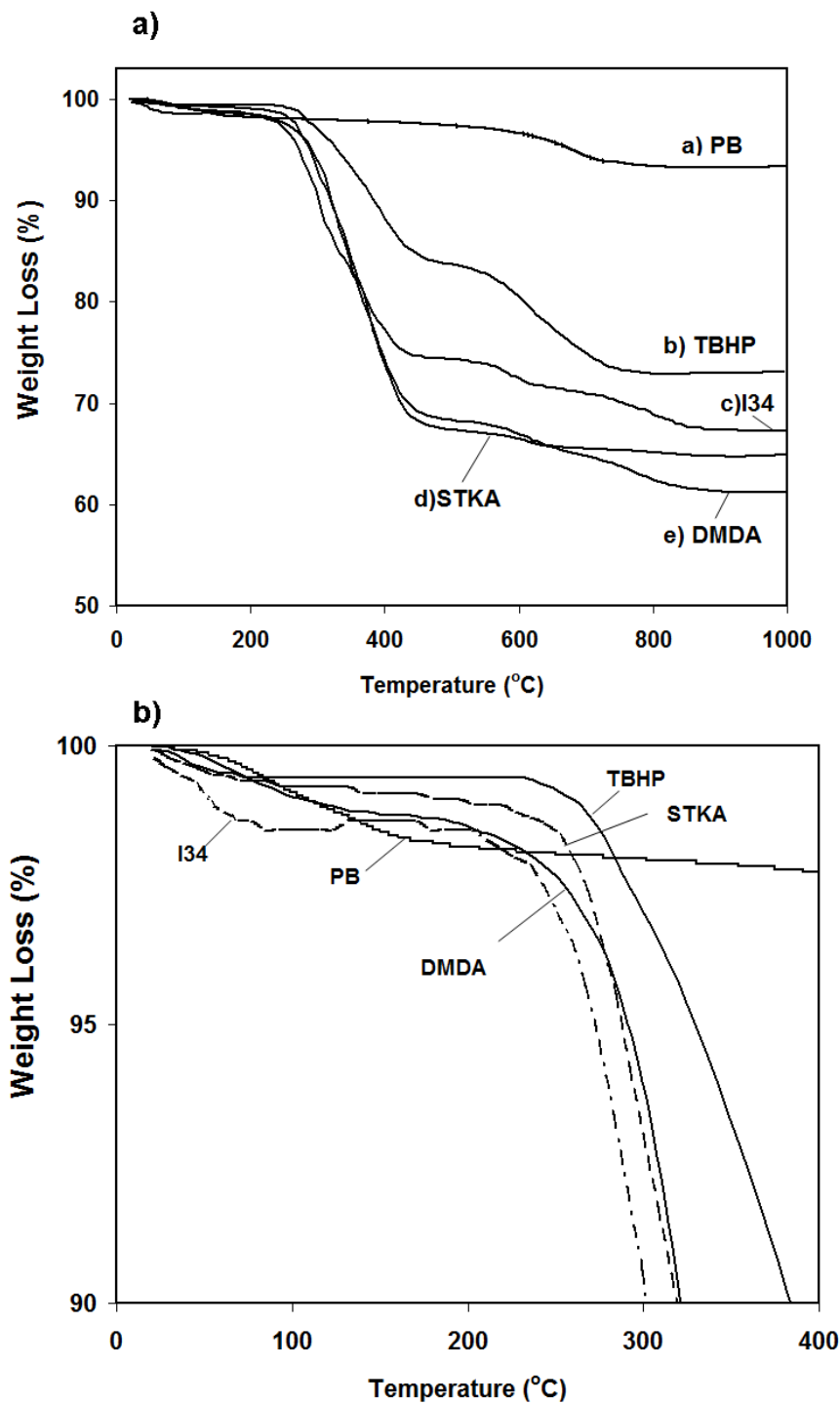


Figure 4.7 TGA results of PB and organoclays with [different scaling in (a) and (b)]: a) PB, b) TBHP, c) I34, d) STKA and e) DMDA

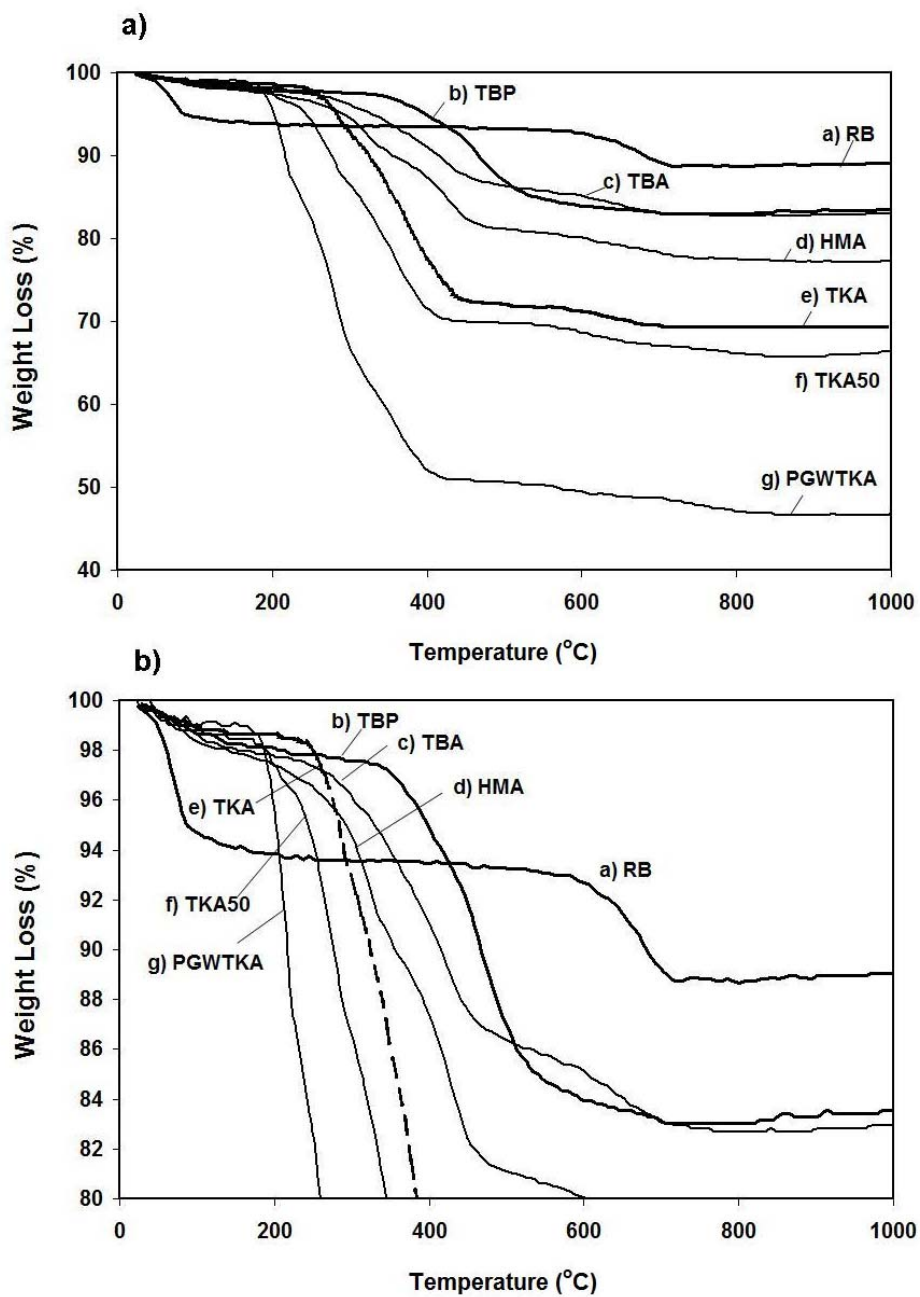


Figure 4.8 TGA results of a) RB and organoclays; b) TBP, c) TBA, d) HMA, e) TKA, f) TKA50 and g) PGWTKA

The first weight losses of modified MMTs between 30°C-700°C are referred to the decomposition of organic salts and dehydroxylation of MMT layer. After 700°C residual carbonaceous product formation begins [Xie et al., 2002, Hedley et al., 2007; Lee et al., 2004; Tiwari et al., 2008]. Xie et al., 2002 analyzed the decomposition behavior of organoclays and divided it into four different steps where free water evolves in the first step between 30-150°C. In the region between 150-550°C, decomposition of organic salts occurs then hydroxylation of MMTs layers take place between 550 and 700 °C. After 700 °C, residual carbonaceous product formation begins. Xie et al., 2002 indicated that the first and second decomposition steps of modified MMTs are the most important parts, since formation of decomposition products may affect the interfacial interactions between the MMTs and polymer. Figure 4.7 and 4.8 show that first decomposition temperatures of modified bentonites are greater than 210°C permitting their use as organoclays in melt processing of many polyolefins such as PP, PE and PS.

Table 4.2 Thermal Characterization results

	Initial Decomposition T (°C)	Temperature at 50 % Mass Loss	Final Decomposition Temperature (°C)	Max % weight loss at 1000°C
Organoclays with RB				
RB	77	-	712	10
TBP	323	-	533	16.5
TBA	218	-	668	17.1
HMA	210	-	700	22.8
TKA	208	-	793	22.8
TKA50	180	-	773	33.7
PGWTKA	157	400	810	53.4
Organoclays with PB				
PB	162	-	710	6.6
DMDA	203	-	804	38.7
TBHP	232	-	718	29
STKA	220	-	616	35
I34	198	-	835	33

The effect of excess modifier manifest itself in the reduction of the decomposition temperature of organoclay TKA50 which was prepared with 150 % x CEC of the organoclay. As mentioned in the XRD analysis earlier, excess modifier added to the silicate during modification, i.e., the amount above 100 % CEC, cannot be located inside the spacing between the clay layers, but only among the particles. This comment is confirmed since thermal stability, i.e., first decomposition temperature, of TKA50 is

lower than that of TKA which is probably due to excess modifier that cannot be located between the galleries but among the particles. This situation further leads to higher quantity of decomposition products formed during melt processing and considerably changes the properties of PLSN. Awad et al., 2004 studied the thermal stability of montmorillonite clay modified by both alkyl ammonium and imidazolium based cations. TGA-FTIR study of imidazolium based composites showed carbon dioxide, water and hydrocarbon as the main decomposition products.

Awad et al., 2004 studied the thermal stability of modified MMTs with alkyl imidazolium salts and showed that as alkyl chain length of salts increases, thermal stability decreases. This concept is also seen in this study, since TKA has the longest alkyl chain length and the lowest thermal stability in comparison to the other three. Higher thermal stability of bentonite modified with phosphonium salt TBP, compared to ammonium salt TBA, which has the same carbon atoms as TBP can also be seen from Figure 4.8. High thermal stability, i.e., first decomposition temperature, of phosphonium based cation is also seen in Figure 4.7 for TBHP. This high thermal stability over the other organoclays can be considered as an advantage, since high thermal stability prevents formation of decomposition products which may adversely effect the certain PLSN properties. TEM, rheological characterization and mechanical analysis of composites prepared with TBHP show superior properties compared to other samples which will be mentioned in the proceeding pages.

4.1.4 FTIR Analysis

FTIR is a useful technique for identifying certain bonds in a molecule by producing an infrared absorption spectrum that is like a molecular fingerprint. It was used for identifying formation of new bonds in the modified bentonites in comparison to unmodified ones. This analysis also helped to assess the success of modification procedure applied in this study.

FTIR spectra of RB and PB and modified bentonite were obtained using KBr pellets. Tyagi et al, 2006 studied the FTIR spectra of Indian MMT and attributed FTIR bands to certain interactions given in Table 4.3.

In FTIR spectra of RB (Figure 4.9) and of PB, the band near 3620cm^{-1} is attributed to OH group bound with Al^{+3} in bentonite which is a characteristic peak for MMTs with high amounts of Al in the octahedra. Free water of bentonite gives bands near 3440 cm^{-1} and 1639 cm^{-1} and are attributed to stretching and bending vibrations of OH groups of water. Characteristic band of MMT at 1114 cm^{-1} shows Si-O out-of-plane stretching vibration. The band at 1033 cm^{-1} is attributed to Si-O in-plane stretching and the band at 529 cm^{-1} is due to Si-O bending vibrations. Bending vibration of hydroxyl groups with Al (AlAlOH) is given by the band at 910 cm^{-1} , while the band at 871 cm^{-1} is attributed to AlFe-OH . Moreover, the band at 696 cm^{-1} shows presence of quartz in the bentonite [Patel et al., 2007; Tyagi et al., 2006; Madejova, 2003].

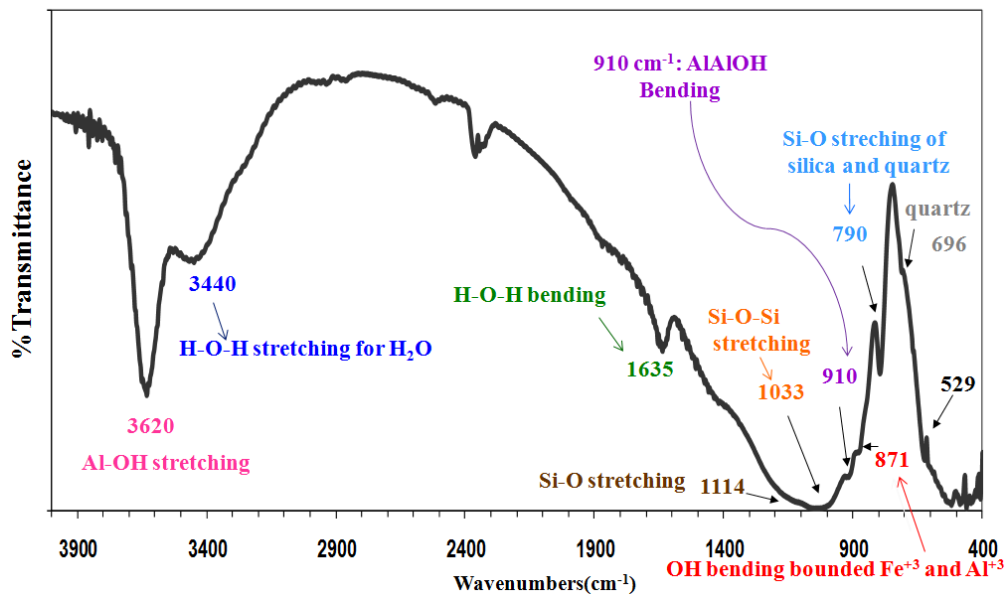


Figure 4.9 FTIR spectra of RB

In FTIR spectra of alkylammonium cations, C-H stretching usually gives bands between the wavenumbers of 3020-2800 cm^{-1} [Madejova, 2003]. FTIR spectra of RB and modified bentonites are given in Figure 4.10 displaying different absorption bands near 2931 cm^{-1} ($\nu_{\text{as}}(\text{CH}_2)$, asymmetric stretching of CH_2) and 2854 cm^{-1} ($\nu_{\text{s}}(\text{CH}_2)$, symmetric stretching) due to intercalated cations between the MMT layers [Kozak et al., 2004]. New absorption band in modified bentonite at 1487 cm^{-1} is attributed to flexural vibrations of CH_3 ($\delta_{\text{as}}(\text{C-H})$) which arises due to the cation $(\text{CH}_3)_4\text{N}^+$ [Kozak et al., 2004]. New band formation trends are seen in the all modified bentonites prepared by RB and PB shown by Figure 4.10 and Figure 4.11. FTIR analysis supports the intercalation of salts within the bentonite layers with these new bands observed in the modified bentonites [Filho et al., 2005].

Table 4.3 FTIR band assignment for montmorillonite clay

Wavenumber (cm^{-1})	- Assignments
3623	Al-OH stretching
3440	H-O-H stretching, hydration
1639	H-O-H bending
1113	Si-O stretching, out-of-plane
1035	Si-O, in-plane
915	AlAlOH
875	AlFeOH
836	AlMgOH
793	Platy form of tridymite
692	Quartz
529	Si-O bending

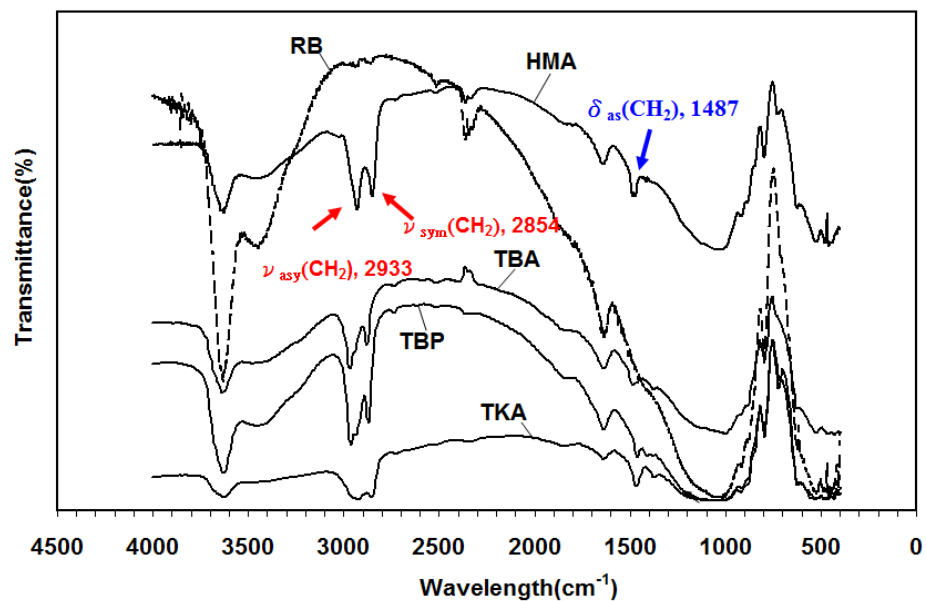


Figure 4.10 FTIR spectra of RB and organoclays

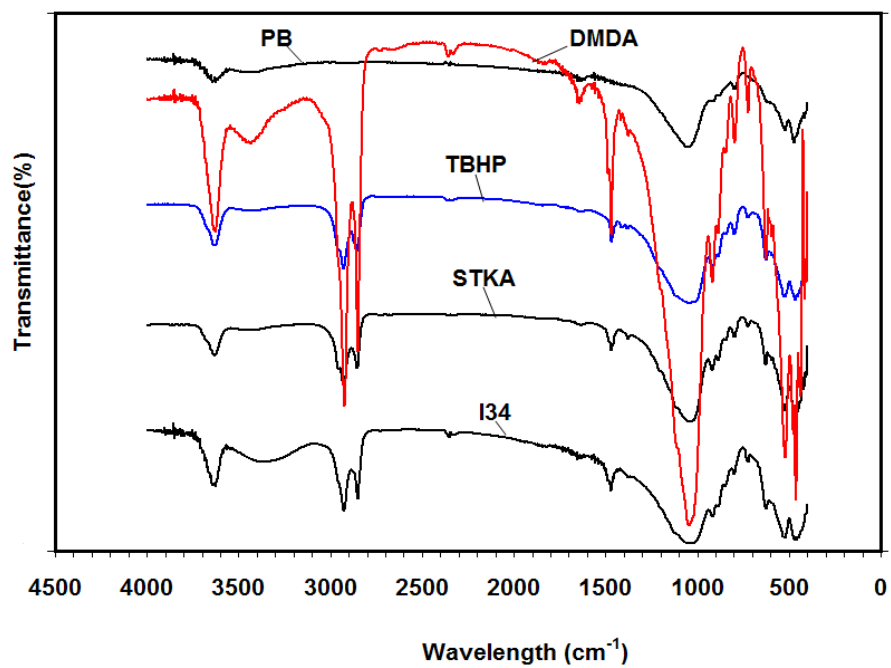


Figure 4.11 FTIR Spectra of PB and organoclays

4.1.5 SEM and TEM Analysis of Organoclays

Fig. 4.12 shows scanning electron micrograph of clay particles of HMA and TKA, showing agglomerates of 5–20 μm size. TEM analysis of TKA (Fig.4.12 c) shows platelets with high aspect ratio clay layers in a uniform structure. TEM analysis of TKA organoclay shows structure of montmorillonite layers are preserved after modification with organic surfactant.

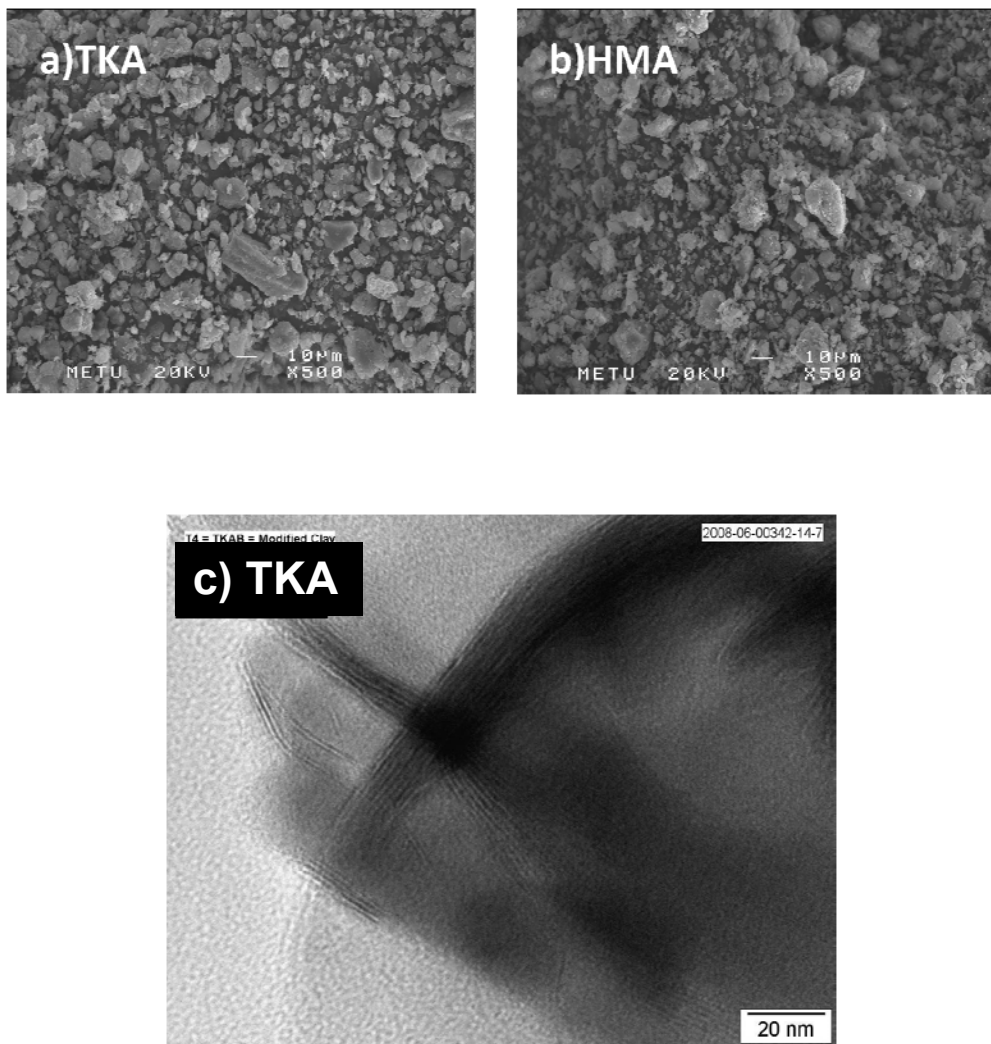


Figure 4.12 SEM analysis of a) TKA, b) HMA and c) TEM analysis of TKA clay

4.2 Characterization of Nanocomposites

4.2.1 X-Ray Analysis

XRD analysis was used to analyze the structure of PP/clay and LLDPE/clay nanocomposites. XRD diffractograms are widely used and useful techniques to assess dispersion of clay layers qualitatively, however, sole use of it to examine the degree of intercalation is not an adequate analysis and it must be supported by other characterization techniques.

4.2.1.1 X-Ray Analysis of Composites Prepared in SET1 (PPM/Organoclay2/MAPP2)

Figure 4.13 shows the XRD patterns of TKA and its ternary nanocomposites of PPM/TKA2/MAPP5. The figure shows that original d-spacing of clay did not change significantly with this clay as it increased from 2.56 to 2.65 nm with compounding. Slight increase indicates limited dispersion of TKA clay. The effect of the halide is a possible explanation of the low degree of interaction behavior of TKA in PLSN as well. At the end of the modification procedure, the final paste was washed to get rid of any halide ions. During washing, the excess cations could also be easily desorbed by washing with water or alcohol-water mixtures. This is easier for the polar cations (small R group), but harder for the less polar cations (long chain R group) which will resist the washing procedure [Awad et al., 2004]. In addition, long aliphatic tails in TKA may limit the diffusion and access of PP chains through the silicate layers [Kadar et al., 2006].

PP is a resin with low polarity, thus exfoliation and homogeneous dispersion of the clay layers is difficult at the nanometer level. This situation arises from the fact that the silicate layers have polar hydroxyl

groups and are compatible only with polymers with functional groups. However, successful preparation of PP-clay nanocomposites has been shown by some studies [Kato et al., 1997; Kawasumi et al., 1997] where maleic anhydride grafted PP was used. In the processing of PLSN with melt compounding, the exfoliation and dispersion of organoclays in the polymer matrix depend on the organic modifier of the clay, the initial d-spacing, the concentration of functional groups in the compatibilizer and its overall concentration in the composite, the viscosity of the binder, the processing conditions, such as screw configurations of extruders, rpm, temperature, residence time, shear applied during compounding etc. The general consensus is that, after many studies published in the literature on factors affecting the dispersion, sufficient long residence time is necessary to intercalate or exfoliate the organoclays in the polymer matrix. Insufficient mixing in the extruder may result in poor dispersion of TKA clay in the PP matrix. Even though shear is an important factor to obtain fine dispersion of layers, shear alone is not enough to furnish nanometric dispersion of the clay and interfacial adhesion between the components (compatibility between the clay layers and matrix, compatibilizer) present in the matrix [Quintanilla et al., 2006].

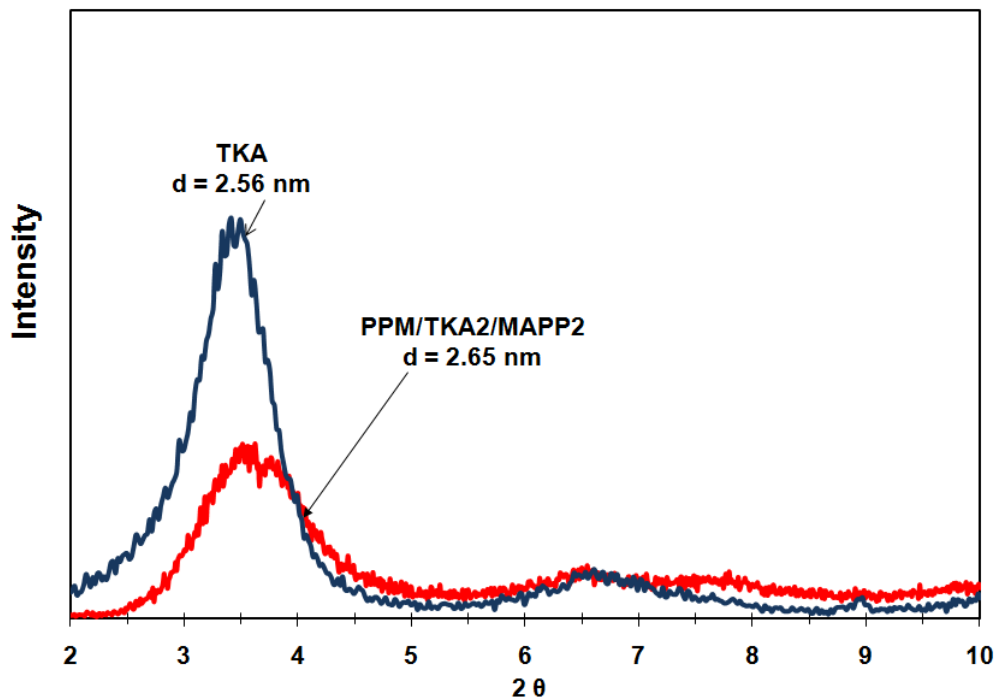


Figure 4.13 XRD patterns for TKA and its composites PPM/TKA2/MAPP2

Beside thermal stability; structure, concentration and orientation of the modifier is also important in delamination process. Kadar et al., 2006 mentioned that modifiers with bulky alkyl tails may locate between the particles of clay layers and not in between the galleries which may induce plasticization effect at processing temperature and decrease the composite properties. This explanation can be valid for TKA, since the modifier has four long alkyl tails with 10 C atoms in each tail. Higher d-spacing of clay is also supposed to induce diffusion of polymer chains into galleries readily; nevertheless high d-spacing of clay did not lead to delamination and dispersion of clay layer.

Figure 4.14 shows the XRD patterns of HMA and MAPP98/HMA2 binary composites and PPM/HMA2/MAPP2 ternary composites. This organoclay with a single alkyl tail has a d-spacing of 1.78 nm with no visible secondary reflections. Strangely, HMA peak is shifted to larger 2θ upon mixing with MAPP or with PPM/MAPP mixture. The shift to larger angles shows that the d-spacing decreases after melt mixing. This situation has

been explained by the thermal decomposition and loss of surfactant mass from the clay galleries at high melt processing temperature [Yoon et al., 2003]. However as previously explained in the case of TKA, the processing temperature is not so high, since it was 180 °C. One explanation can be given in terms of insufficient residence time during the extrusion. The external force utilized on the silicate agglomerates from the melt depends on shear rate, melt viscosity of polymer matrix, surface area of clay and surface tension at polymer-clay interface, whereas the diffusion of macromolecules relies among others on temperature, interlayer spacing, residence time, and type/concentration of surfactant modifiers at the clay surface (Vaia et al. 1995; Vaia and Giannelis, 1997; Balazs et al, 1998; Isik, 2007). The effect of halide may be taken into consideration as well, but since this organoclay with one alkyl tail is supposed not to resist washing with water/alcohol mixture, this effect may be less plausible compared to case of TKA. Chemical incompatibility and poor adhesion of clay layer with polymer matrix can be another explanation of decreased d-spacing.

Hasegawa et al., 1998 and Kawasumi et al., 1997 reported that higher content of PP-MA favors intercalation and clay dispersion in the PP matrix, and there should be an optimum compatibilizer/clay ratio for achieving dispersion of clay layers. Low concentration of PP-MA used in this set of compatibilizer might reduce the chance of formation of possible interactions between the silicate layers and polymer matrix.

Figure 4.15 shows the XRD patterns of TBA and MAPP98/TBA2 binary composites and PPM/TBA2/MAPP2 ternary composites. Figure 4.16 shows the XRD patterns of TBP and MAPP98/TBP2 binary composites and PPM/TBP2/MAPP2 ternary composites. These two organoclays show no intercalation of clay layers in the matrix based on the XRD analysis. TBP and TBA have 4 C atoms in each of the tails compared to cations TKA and HMA with higher number of C atoms. Low number of alkyl tails lead to smaller d-spacing in the original clay. These small d-spacings of

TBA and TBP impede diffusion of polymer chains into organoclay layers. Possibly, again insufficient residence time is the reason for poor dispersion with these clays. Phosphonium ion usage did not show significant difference in the XRD patterns of the composites.

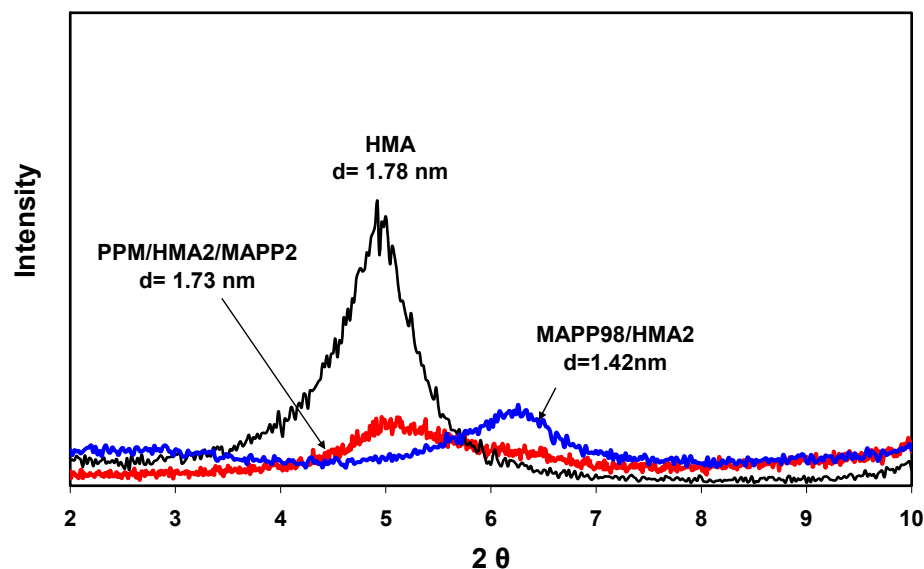


Figure 4.14 XRD patterns for HMA and its composites PPM/HMA2/MAPP2

These results may indicate to the possibility of insufficient mixing of clay, PP-g-MA and PP. It is known that, the compatibilizer (in our case PP-g-MA) improves the exfoliation/intercalation of the clay in the composites. Possibly, short alkyl chain lengths of TBA and TBP could not enhance the intercalation of PP layers. Although HMA has longer alkyl chain length compared to TBA and TBP, it also could not aid the dispersion of clay layers within the polymer matrix. Experimental observations obtained from this part of the study reveal the importance of chemical compatibility between the polymer matrix and organoclay, and also the chemistry of the clay modification in intercalation/exfoliation mechanism. SET-1 samples were prepared in extruder and the shear strength in the extruder could only reduce the tactoid particles or the size of the intercalated stacks when the chemical compatibility was not strong enough (Cho and Paul,

2001). XRD results given in Figures 4.15 and 4.16 show microcomposite formation in PPM/TBA2/MAPP2 and PPM/TBP2/MAPP2 compositions.

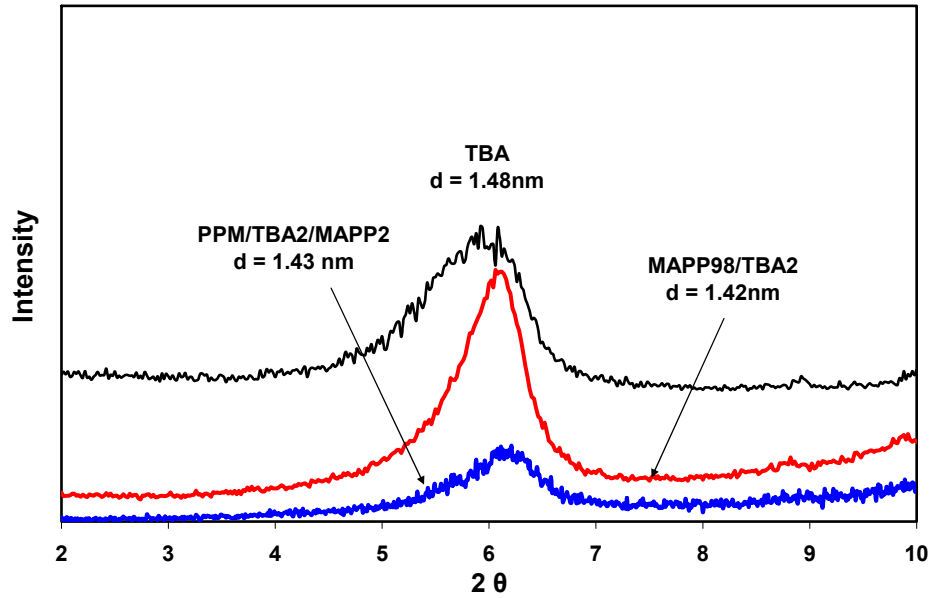


Figure 4.15 XRD patterns for TBA and its composites PPM/TBA2/MAPP2

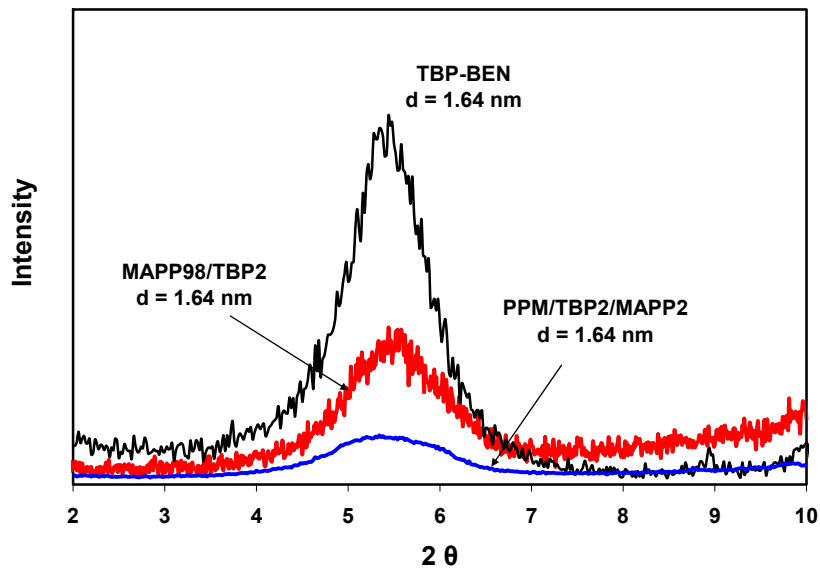


Figure 4.16 XRD patterns for TBP and its composites MAPP98/ TBP2 and PPM/TBP2/MAPP2

Kim et al., 2007 studied the effect of MAPP concentration and the ratio of MAPP/organoclay in PP based organoclay nanocomposites and the results revealed that increased MAPP concentration and higher MAPP/organoclay ratio further leads to exfoliation mechanism owing to enhanced attraction of MAPP on the silicate layers permitting easy delamination of layers during shearing. Thus, PPM/HMA1/MAPP3 composition was prepared to be able to have delamination of layers. Figure 4.17 shows XRD of this composition and HMA clay revealing higher level of delamination and insertion of clay layers compared to composites prepared with MAPP/HMA = 1 shown in Figure 4.14. Reduced intensity and broadened XRD peak in Figure 4.17 indicates a more delaminated and increased disorder of silicate layer structure compared to Figure 4.14 [Modesti et al., 2005]. This result confirms that increased MAPP/organoclay ratio enhances the exfoliation of organoclay layers in PP matrix as well.

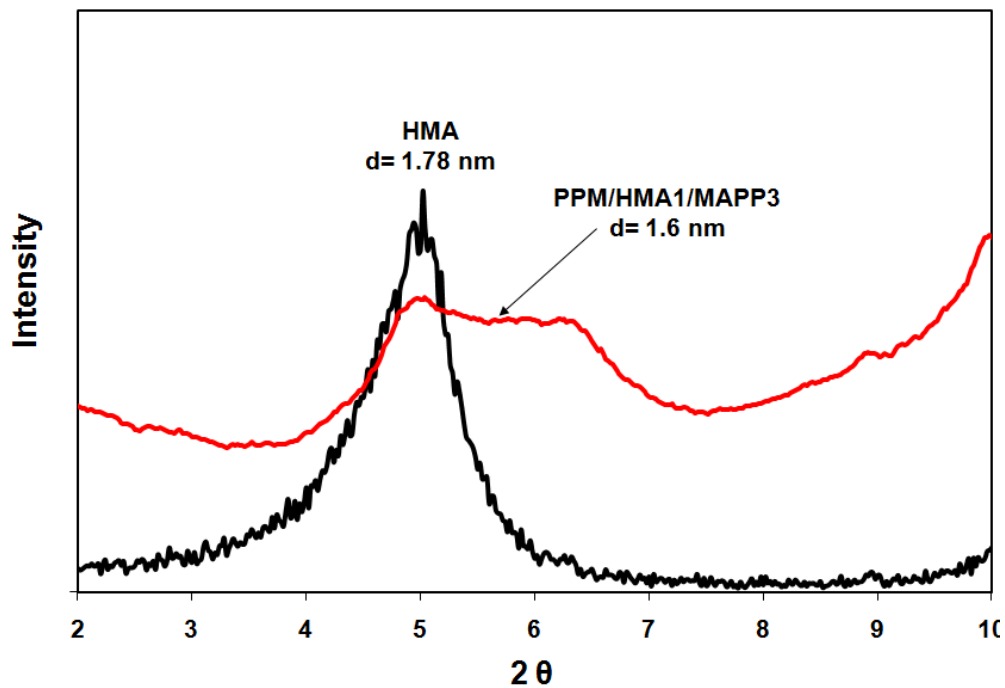


Figure 4.17 XRD patterns for HMA and its composite PPM/HMA1/MAPP3

This study was aimed to investigate the opportunity of using local silicates in PLSN. Comparison with commercial organoclays was carried out by preparing samples with commercial organoclay Cloisite®25A in PP based composites. Figure 4.18 shows XRD diffractogram of organoclay Cloisite® 25 and its ternary composites PPM/Cloisite®25A2/ MAPP2. Reduced intensity indicates some intercalation and delamination of aggregates while the slight change in 2θ degree in composites reveals no intercalation. This result may also indicate that low MAPP/organoclay ratio is responsible for lack of intercalation or exfoliation of clay layers through the matrix.

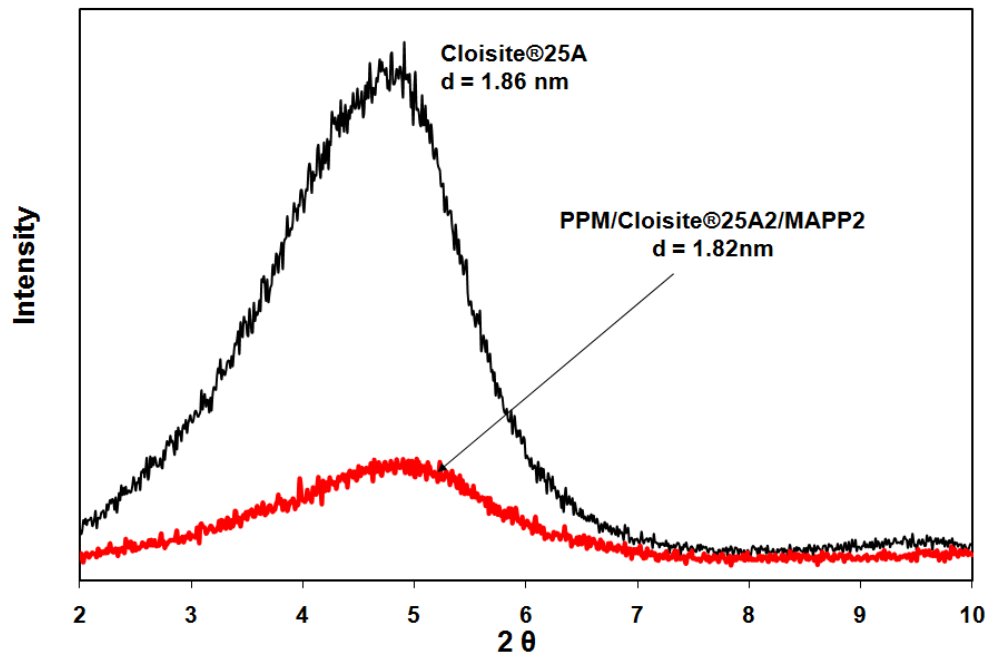


Figure 4.18 XRD patterns for Cloisite®25 A and its composite PPM/Cloisite®25A2/MAPP2

Considering the samples prepared in SET 1, low screw speed (100 rpm in the first run and 80 rpm in the second run), may not be enough to have high shear needed for delamination of layers. Also, the high viscosity of PPM (at a temperature of 210 °C), may have impede the diffusion of layers through the PP matrix. To overcome the effect of high viscosity of

PPM, another PP, with high melt index was used in order to facilitate diffusion of PP chains into the interlayer's of clay.

From processing point of view, two parameters are important. During melt blending of clay into a polymer, organoclay layers slide apart from each other depending on the shear applied. Clay layer delamination can also be increased by diffusion of polymer chains into the spacing between the clay layers [Modesti et al., 2005]. In the work of Modesti et al., 2005 better properties in PP based composites were achieved at low temperature and high screw speed (low residence time) and it was concluded that the controlling factor for their system was the intensity of shear applied to the polymer instead of the diffusion process, probably due to high melt index (i.e., high fluidity) of the their PP (MFI = 12 g/10 min). Due to high viscosity of PPM used in this study, silicate layers may have been subjected to higher shear stress but the diffusion of PP chains may have been limited and as a result, effect of fillers on the mechanical properties have been insignificant. To overcome the affect of high viscosity of PPM, another PP with lower viscosity (PPE) was used in preparation of composites with different processing conditions (higher screw speed and lower T compared to SET-1).

Ternary composites of PPE/Organoclay2/MAPP5 were prepared at a screw speed of 350 rpm and 180°C in SET-2. PPE has a melt flow index of 20-24 g/10 min which is higher compared to PP with an MFI of 2-4 g/10 min which was used in SET-1. Since the aim of this study is to investigate the potential use and delamination of local organoclay in PP matrix, a clear comparison between the two sets (SET-1 and SET-2) cannot be done because of the differences in compositions, PP type and processing conditions. Note that MAPP/organoclay ratio was changed in this set, from 1 in SET-1 to 2.5 in SET-2.

4.2.1.2 X-Ray Analysis of Composites Prepared in SET2 (PPE/Organoclay2/MAPP5)

Fig.4.19 shows XRD patterns of pure HMA, MAPP98/HMA2 binary composite and PPE/HMA2/MAPP5 ternary nanocomposite. Similar to the nanocomposite PPM/HMA2/MAPP2 shown in Fig.4.14, organoclay d_1 spacing in Figure 4.18 was not changed. The binding forces between the silicate layers and the polymer matrix are very effective in the delamination of clay layers. Absence of such an interaction, as also seen in the binary composite MAPP98/HMA2, caused clay platelets to remain as tactoids without penetration of polymer chains between them. Differences between the PPE/HMA2/MAPP5 (Fig.4.19) and PPM/HMA2/MAPP2 (Fig.4.14) are PP, the ratio of MAPP/HMA and processing conditions. Increased MAPP addition was supposed to enhance the dispersion of clay layers. Lower viscosity of PPE in comparison to PPM was also supposed to ease of diffusion of polymer chains into galleries. Increase in applied shear and reduced temperature (SET-2 was prepared at 350 rpm and 180 °C) were also supposed to increase the dispersion of clay platelets within the matrix. Since none of the changes explained above could achieve the required enhancements, these experimental results showed the importance of chemical compatibility between the polymer matrix and organoclay, the chemistry of cation used for clay modification and purity of the clay used for modification in delamination process. Also, duration of mixing may not be sufficient in both cases. The lack of intercalation shown in Figure 4.19 may also be attributed to degree of purity of bentonite used in these series of organoclay. Although, RB has mainly MMT as shown by ICP analysis given by Table 4.1, the impurities may stay as immobilized points during the modification which may act as defects leading to limiting the dispersion of clay layers in PPE matrix [Lagaly, 2006 (b)]. Removing of impurity minerals, especially carbonates, is also necessary, because they may behave as reservoirs of multivalent cations. Organic materials can also limit the dispersion. Therefore, optimum dispersion of clay layers

within the polymer matrix can be achieved when the bentonites are purified and fractionated [Lagaly, 2006 (b)]. Flaws and impurities like quartz present in the clay act as stress concentrators, allowing crack initiation and propagation, decreasing consequently the mechanical performance of the nanocomposite [Lopez et al., 2003].

Low degradation temperature ($\sim 220^{\circ}\text{C}$) of HMA which is close to the processing temperature, may also cause the clay layers to collapse, and also increase the surface tension, leading to stronger platelet-platelet and particle to particle interactions responsible for clay aggregation [Perrin-Sarazin et. al., 2005]. It was also claimed in the studies of Kim et. al., 2001; Ton-That et al. 2004; Perrin-Sarazin et al., 2005; Rohlmann et al., 2008 that, due to high processing temperature, organization of the alkyl chains may change and rearrange from bilayer to monolayer leading to the decrease in the d-spacing.

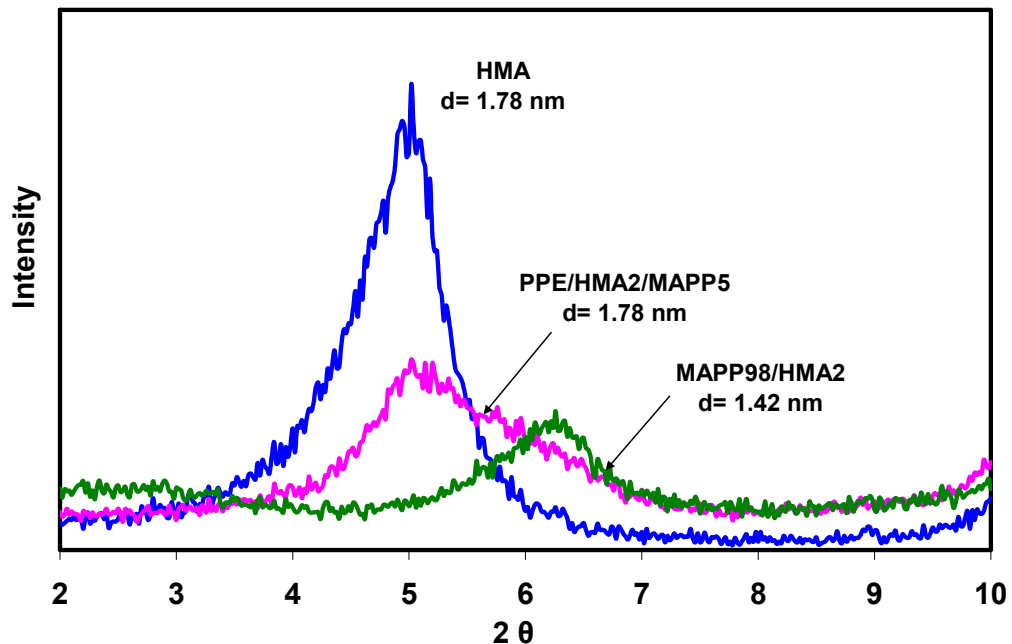


Figure 4.19 XRD patterns for HMA and its composite PPE/HMA2/MAPP5

Figure 4.20 gives the XRD patterns of pure TKA and its ternary composites PPE/TKA2/MAPP5 showing reduced d-spacing of clay in the composites system. When structures of HMA and TKA are compared, HMA has one long (C16) tail while TKA has four long alkyl tails (4C10) in its backbone. Although one alkyl tail of HMA is more favorable which would not impede and limit the diffusion of polymer layers in contrast to long alkyl tails of TKA, delamination of clay layers was not achieved in HMA based composites.

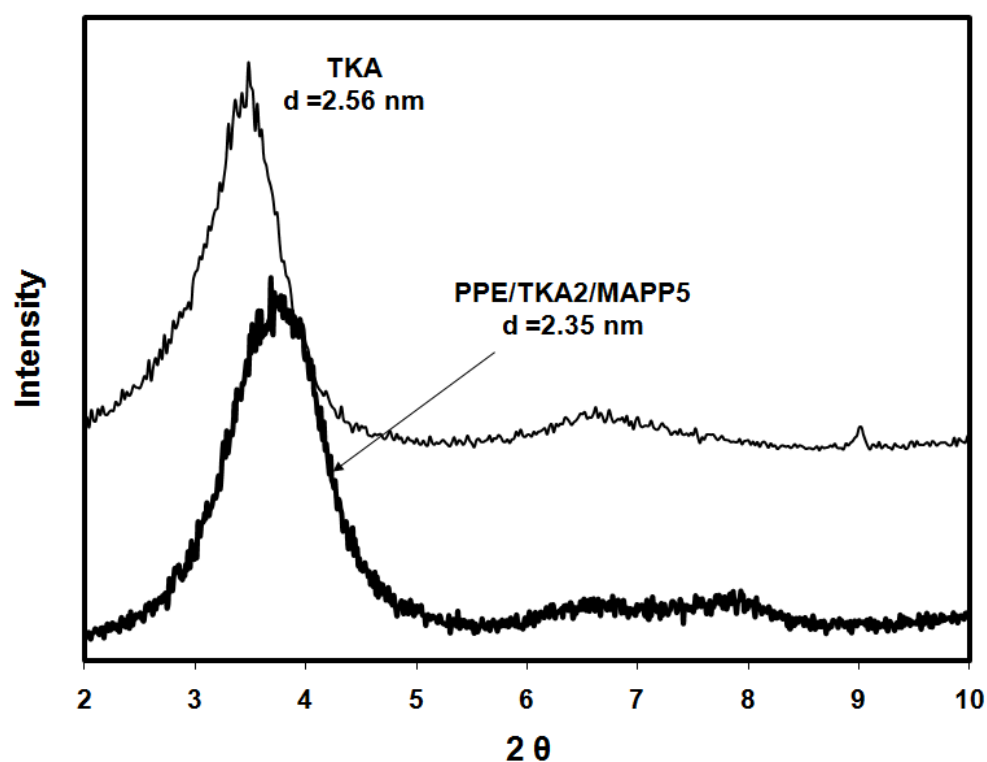


Figure 4. 20 XRD patterns for TKA and its composite PPE/TKA2/MAPP5

Figures 4.20- 4.22 show the XRD data of organoclays prepared from TKA, TKA50 and PGWTKA and their ternary composites PPE/Organoclay2/MAPP5 respectively. The amount of surfactant added to the bentonite is referred as milliequivalent ratio (MER) and it is different in TKA and TKA50, allowing comparison of different MER loading. TKA was prepared with a surfactant concentration of 1.1 x CEC, while TKA50

was prepared with a surfactant concentration of 1.5 x CEC. As expected, addition of more surfactant during the exchange reaction promoted intercalation of more cations through the clay layers and expanded d-spacing to a greater extent. While TKA clay has a d-spacing of 2.56 nm, TKA50 has a d-spacing of 2.67 nm. Figure 4.19 and Figure 4.20 indicated that excess surfactant was not advantageous in terms of dispersion [Fornes et al., 2002].

PGWTKA in Figure 4.22 was prepared with pure commercial MMT clay PGW with a CEC of 145 mmol/100g of clay, while RB has a CEC of 65 mmol/100g of clay. PGWTKA was also prepared with a surfactant concentration of 1.1 x CEC. High purity clay is supposed to lead dispersion of clay layers in the polymer matrix due to effects mentioned previously. Although d spacing of the PGWTKA (2.83 nm) is higher than TKA (2.56 nm), it also showed lack of delaminated clay layers in PPE/MAPP matrix.

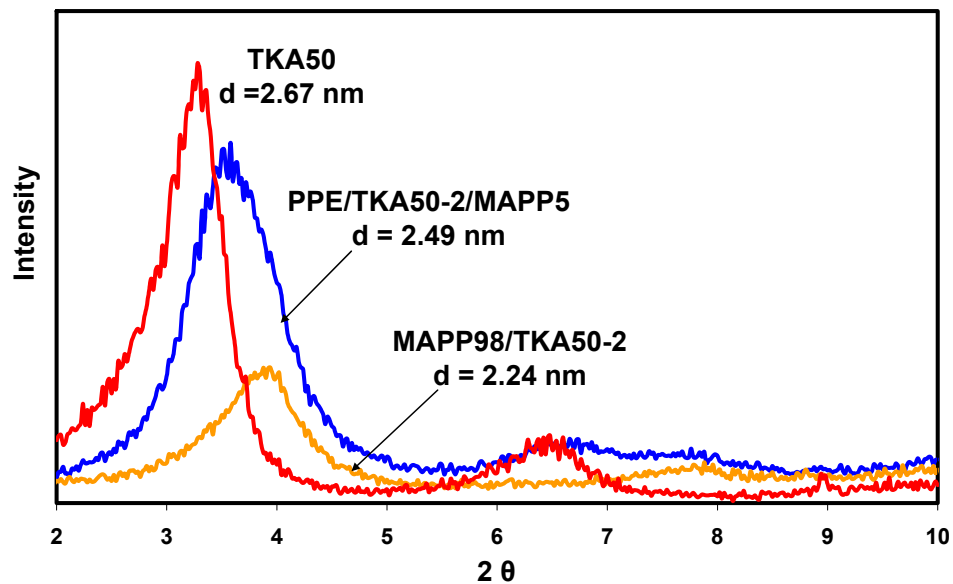


Figure 4.21 XRD patterns for TKA50 and its composites PPE/TKA50-2/MAPP5

There have been studies concerning the effect of surfactant type used in modification of organoclays and their effects in the final properties of PLSN. Fornes et al., 2002 studied a number of organoclays derived from surfactants with different alkyl tails on the morphology and mechanical properties of nylon-6 nanocomposites. Their comparison between one alkyl tail and two alkyl tails showed that better dispersion and mechanical enhancements were achieved with clay with one alkyl tail. The explanation was that: as the number of alkyl tails increases it limits the entry of polymer segments into the clay layers more, therefore sheltering the polymer-organoclay interactions and generation of a more hydrocarbon-like environment. This explanation can be taken as an evidence for the effect of TKA based organoclays in the PP matrix, since TKA cation has four long alkyl tails with 10C in each of them the entry of polymer chains through clay layers was severely limited.

Reichert et al., 2000 investigated the effects of alkyl group on the modification of sodium fluoromica as well as the morphology and mechanical properties of PP/Organoclay/MAPP composites. Their results indicated that minimum 12 C or more are necessary to achieve exfoliation in conjunction with MAPP.

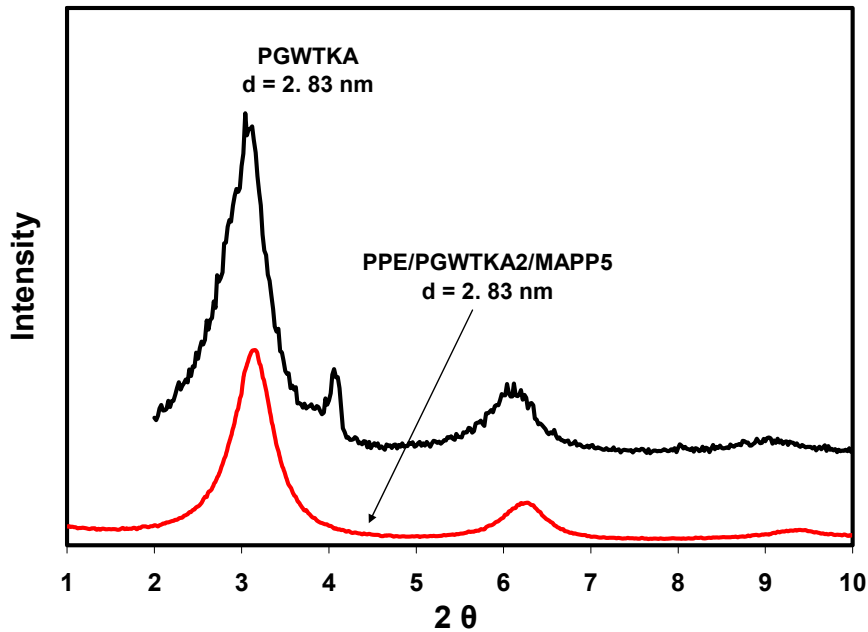


Figure 4.22 XRD patterns for PGWTKA and its composites PPE/PGWTKA2/MAPP5

4.2.1.3 X-Ray Analysis of Composites Prepared in SET-3, 4 and 5

4.2.1.3.1 X-Ray Analysis of Binary Nanocomposites

Binary mixtures of DMDA and TBHP clays with MAPP (MAPP98/Organoclay2) were prepared in the batch mixer at 190 °C and 32 rpm for 15 min with 1 phr % of Irganox®B225. Figure 4.23 shows the XRD diffractograms of DMDA and binary composites MAPP98/DMDA2. The original DMDA clay has a peak at $2\theta=3.34^\circ$ corresponding to a d-spacing of 2.64 nm and it was shifted to lower angles ($2\theta=2.62^\circ$) indicating expansion of layers to 3.4 nm and compatibility between the clay and MAPP. This case is also seen in Figure 4.24 with TBHP clay. Original TBHP clay has a peak at $2\theta=3.94^\circ$ corresponding to a d-spacing of 2.23 nm, while its composite with MAPP shows a peak at $2\theta = 3.18^\circ$ and a d-spacing of $d=2.78$ nm. Compatibility between MAPP and organoclay is important since it helps delamination and intercalation of clay layers in the main PP matrix. At first, the compatibilizer intercalates

between the clay layer increasing adhesion and then allows diffusion of PP through the intercalated system.

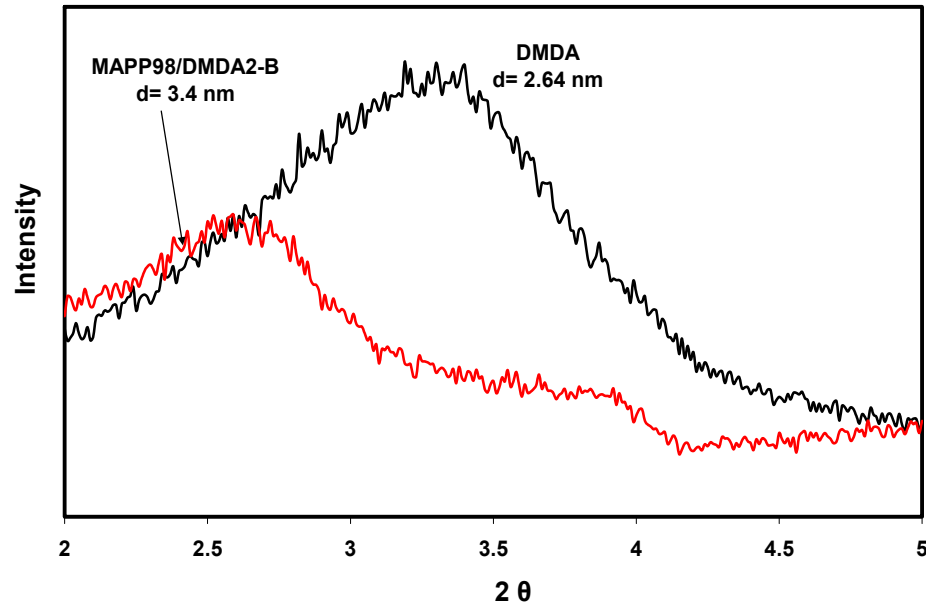


Figure 4.23 XRD patterns for DMDA and its binary composites MAPP98/DMDA2.

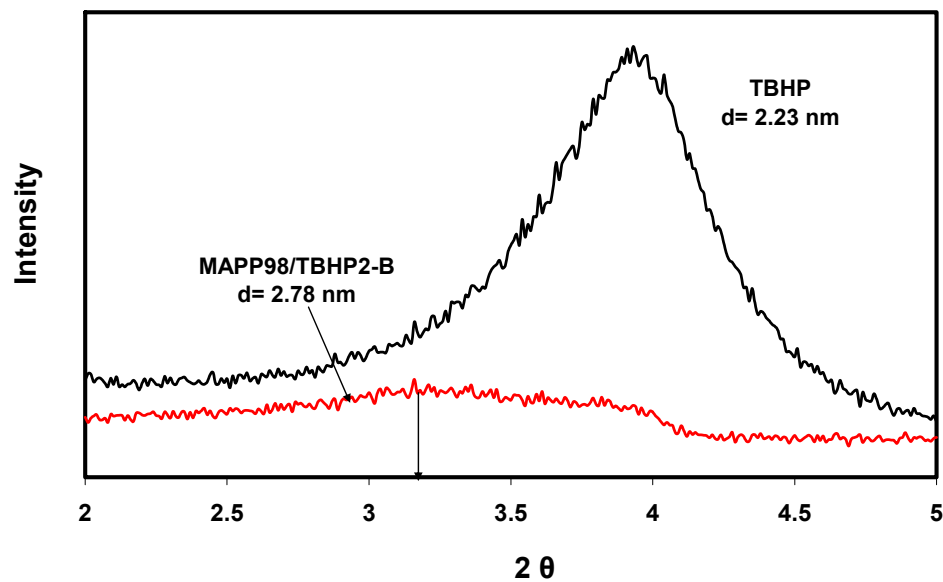


Figure 4.24 XRD patterns for TBHP and its binary composites MAPP98/TBHP2

PPE/DMDA2/MAPP5 composition shown in Figure 4.25 was prepared in two step extrusion and further sheared in the batch mixer present in the Stevens IT.- HFMI laboratories. During the batch mixing, samples were taken from the melt in different time intervals (5, 10 and 15 min) to see the effect of applying more shear to the composite system. Samples taken were analyzed by XRD and also by rheometry to determine the optimum mixing time for the composite system which will cause the highest d-spacing according to XRD and enhancements in the rheological properties. Depending on the time sweep tests of binders, which will be mentioned later in detail in the rheology section, it was realized that the PPE had a degradation tendency at the processing temperature. It was decided to use the heat stabilizer Irganox ®B225 which is a product of Ciba Company to avoid further degradation of PPE. This material was used at 1 phr of the composites in the batch mixing experiments. During preparation of all the PPE and MAPP based samples in batch mixing, the heat stabilizer Irganox® B225 was added to the system.

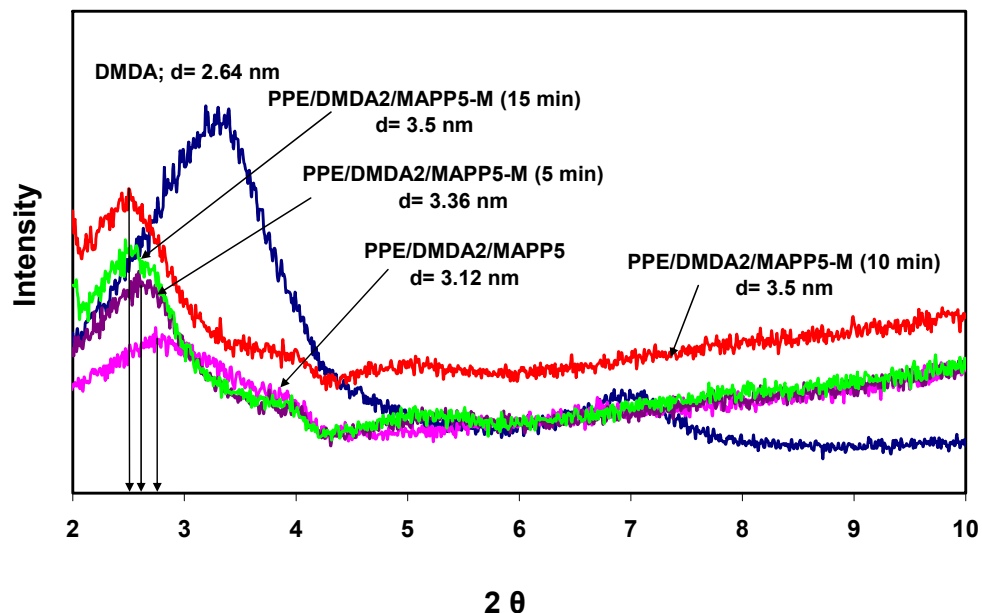


Figure 4.25 XRD patterns for DMDA and its ternary composites PPE/DMDA2/MAPP5 “extruded only”, extruded + batch mixed for different times.

Figure 4.25 shows that “extruded only” composite shows a peak at $2\theta=2.83^\circ$ with $d=3.12$ nm, while the peak of DMDA is at $2\theta=3.34^\circ$ and d-spacing of $d=2.64$ nm. In contrast to the samples prepared in SET-2, intercalation could be achieved only by extrusion in this set of materials. This result may be due to the fact that bentonite was purified before the modification process, since processing conditions and composition of constituents are the same except for the organoclay type. Higher level of intercalation may be also explained by high chemical attraction between the matrix and the surfactant of DMDA which has two long alkyl tails. As explained before, chemical attraction and affinity between the organoclay surfaces and polymer matrix is a key factor in achieving delamination and separation of clay layers through the matrix. As it can be seen in Figure 4.25, further mixing in batch mixer for 15 min mixing shifted the clay peak further to the left w.r.t. 5 min of mixing. While the clay peak is at $2\theta = 3.34^\circ$ and $d = 2.64$ nm, the peaks of composites mixed for 5 and 15 min are at $2\theta = 2.62^\circ, 2.52^\circ$ and $d = 3.36, 3.5$ nm respectively. 32 % increase in the d-

spacing was achieved after 15 min batch mixing of the extruded samples. The general conclusion in the PLSN is that, besides the chemical affinity, sufficient long residence time is necessary to intercalate or exfoliate the organoclays in the polymer matrix. Application of more shear after extrusion resulted in fracture the clay particles into smaller aggregates and the sample exhibited delamination [Macosko et al., 2007; Demirkol and Kalyon, 2007]. It seems that short residence time in the extrusion process could not lead to sufficient delamination of the clay layers in the matrix. After this finding, the samples were mixed for 15 min in the batch mixer in the other ternary systems.

Figure 4.26 shows XRD diffractogram of TBHP and its ternary composites, PPE/TBHP2/MAPP5, prepared only by extrusion, and composites, PPM/TBHP2/MAPP5-M, both extruded and melt mixed in the batch mixer for 15 min. Original TBHP clay and “extruded only” composites have peaks at the same $2\theta = 3.94^\circ$ and $d = 2.24$ nm. This shows that the extruded samples with TBHP have no intercalation of the clay layers. Additional 15 min mixing in batch mixer resulted in a shift to smaller angles in X-ray and in increase of the d-spacing of the TBHP based clay layers. Further batch mixed composite has a peak at $2\theta = 3.25^\circ$ and $d = 2.72$ nm which shows a % 22 increase in the d-spacing wrt clay peak showing delamination, but not fully exfoliated clay layers. TBHP organoclay has also exfoliated single layers which will be shown in the TEM analysis.

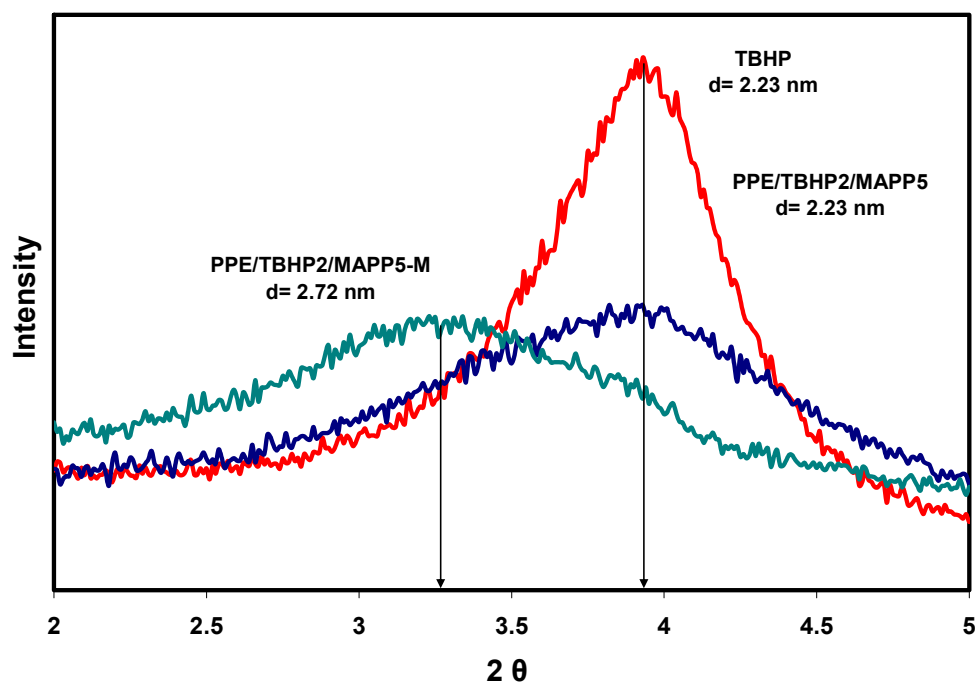


Figure 4.26 XRD patterns for TBHP and its ternary composites PPE/DMDA2/MAPP5 “extruded only”, extruded + batch mixed.

Figure 4.27 shows STKA and its ternary composites PPE/STKA2/MAPP5 prepared by “extrusion only” and composite, PPM/STKA2/MAPP5-M, both extruded and melt mixed in the batch mixer for 15 min. Original STKA clay has a peak at $2\theta = 3.26^\circ$ and a $d = 2.71$ nm and its extruded composite has a peak at $2\theta = 3.3^\circ$, $d = 2.67$ nm revealing chemical incompatibility of the TKA cation with PPE. Mixed composite shows a peak at $2\theta = 3.61^\circ$ and $d = 2.44$ nm. These results show a decrease in the d-spacing as the material was further processed with mixing. Chemical incompatibility of TKA cation with PP matrix was previously explained and the same conclusions can be taken as the cause of microcomposite formation with this clay. As it can be seen from the results given in Figure 4. 20 and Figure 4.27, bentonite purification has no effect in this case, since both samples prepared with RB and PB (with TKA cation) resulted in microcomposite formation in the PPE matrix at the same processing conditions and compositions.

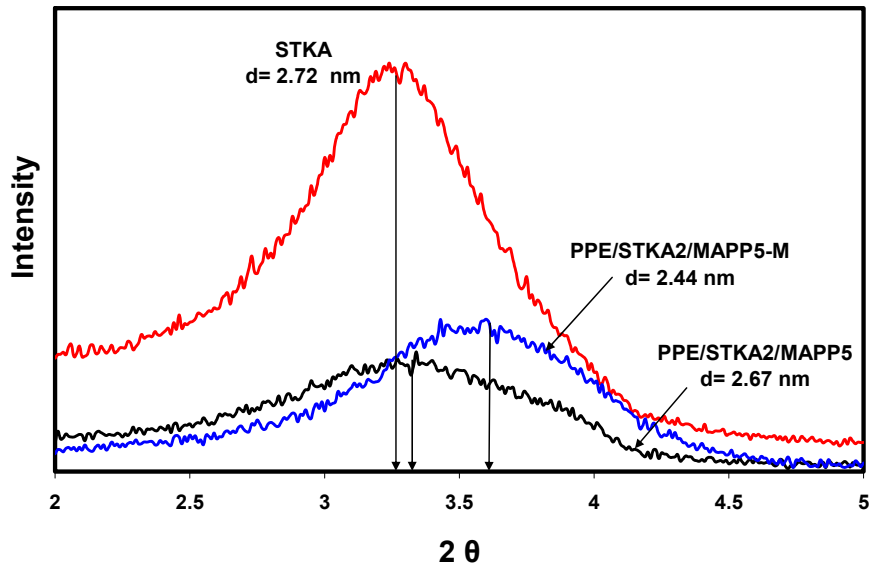


Figure 4.27 XRD patterns for STKA and its ternary composites PPE/STKA2/MAPP5 “extruded only”, extruded + batch mixed

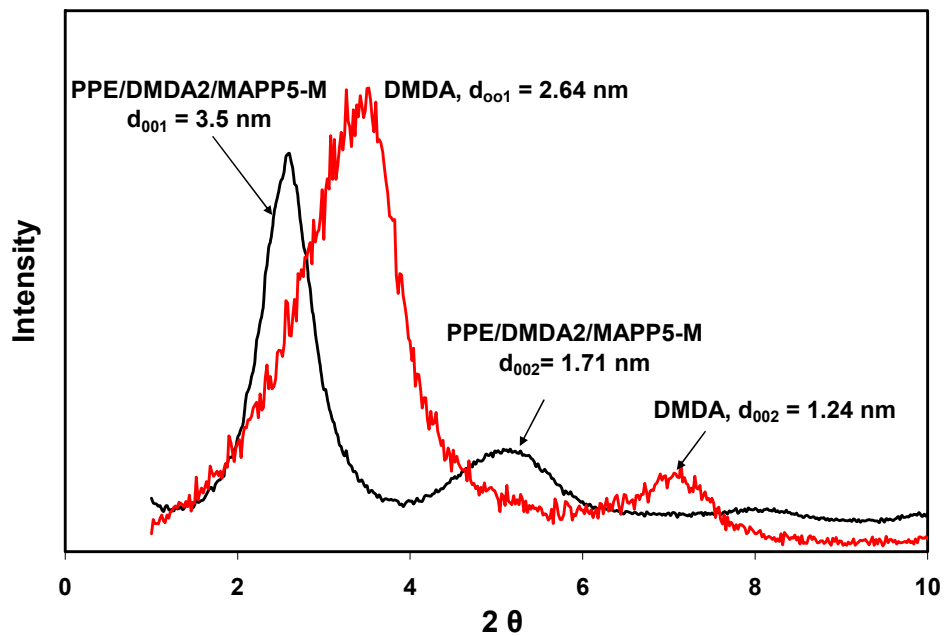


Figure 4.28 XRD patterns for DMDA and its ternary composites PPE/DMDA2/MAPP5 “extruded only”, extruded + batch mixed for different time intervals

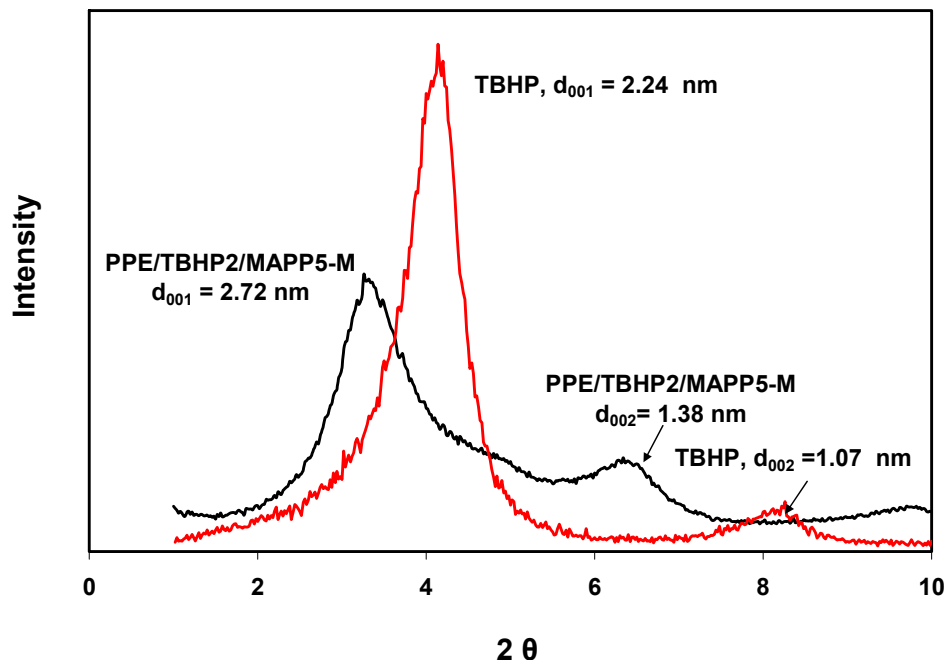


Figure 4.29 XRD patterns for TBHP and its ternary composites PPE/TBHP2/MAPP5 “extruded only”, extruded + batch mixed.

Fig. 4.28 exhibits the same composition shown in Fig. 4.25 while Fig. 4.29 exhibits the same compositions shown in Fig. 4.26 where XRD diffractograms were obtained from the second XRD machine present in METU-METE Department. It is important to keep in mind that these samples were prepared by injection molding, instead of compression molding. Secondary reflections are seen in both Figure 4.28 and Fig.4.29 showing that the systems have both partially intercalated/flocculated clay tactoids. TEM analysis of these samples shown later also indicate the presence of single exfoliated layers in PPE/TBHP2/MAPP5-M samples. Exfoliation and better dispersion in samples PPE/TBHP2/MAPP5-M compared to PPE/DMDA2/MAPP5-M was also confirmed by rheology and mechanical testing which will be given later. These results indicate that the use of XRD solely is not a good way to judge the degree of dispersion of clay layers. Results must be supported by TEM, rheology or mechanical testing.

4.2.1.4 X-Ray Analysis of LLDPE Based Nanocomposites

4.2.1.4.1 X-Ray of Binary Nanocomposites

Figure 4.30 shows XRD patterns of organoclays and their binary composites with LOT. Compatibility between LOT and clay is important, because clay cannot be easily dispersed within the non-polar LLDPE matrix without the help of a compatibilizer. Reactive groups on the LOT e.g., maleic anhydride and acrylate can form chemical bonds as shown in Figure 4.31 with the hydroxyl groups of organoclay which further help the dispersion of clay layers between LLDPE matrix. Figure 4.30 a shows the XRD diffractogram of pure DMDA and its binary composite LOT98/DMDA2. The clay peak is shifted to the left from 3.34° to 2.35° revealing increase in the d-spacing from 2.64 to 3.75 nm. The XRD patterns of binary composites show that the elastomer chains are intercalated between the clay galleries revealing DMDA is compatible with LOT. The same conclusions can be envisaged from the X-Ray analysis of TBHP (Figure 4.30 b) and I34 (Figure 4.30 c) clay. While TBHP clay has peak at $2\theta = 3.94^\circ$ corresponding a d- spacing of 2.24 nm, its composite with LOT has a peak at $2\theta = 2.72^\circ$ corresponding to a d-spacing of 3.24 nm.

Insertion of clay galleries through LOT layers increase the d-spacing of the clay layers so that intercalated binary composites can be formed with TBHP. Figure 4.30 c shows XRD of organoclay I34 and its binary composites LOT98/I34-2 where clay has a peak at $2\theta = 4.47^\circ$ corresponding a d-spacing of 1.97 nm, while a remnant of a peak was observed at $2\theta = 4^\circ$ corresponding to a d-spacing of 2.2 nm revealing not fully exfoliated but an intercalated structure of I34 in the compatibilizer LOT.

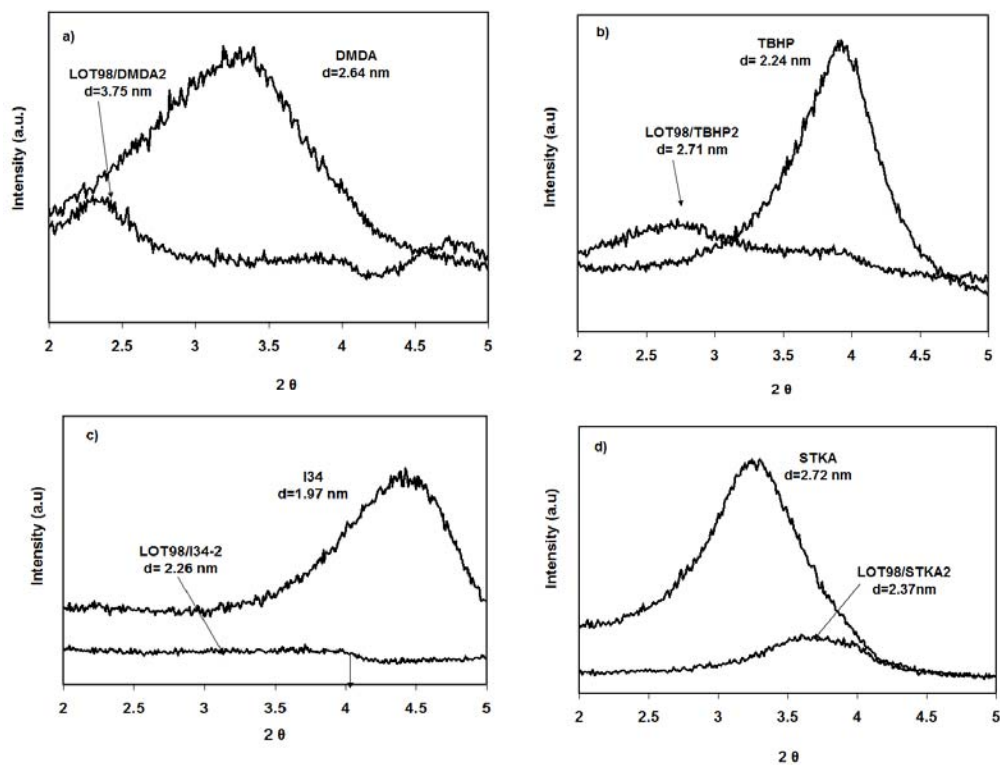


Figure 4.30 XRD analysis of binary composites and associated organoclays, a) LOT98/DMDA2, b) LOT98/TBHP2, c) LOT98/I34-2, d) LOT98/STKA2.

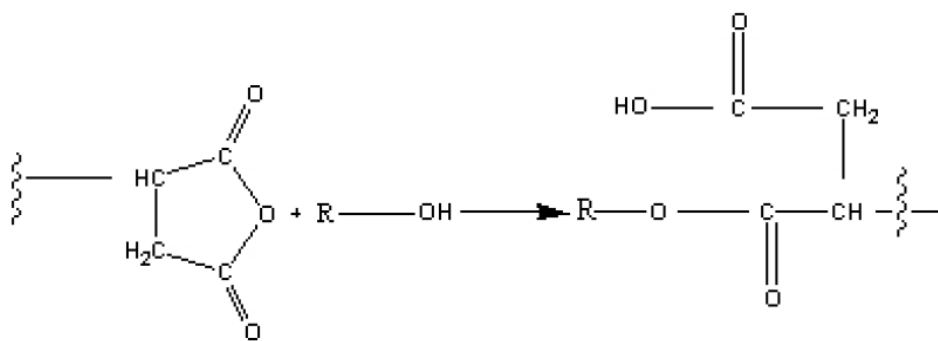


Figure 4.31 Schematical representation of reaction between hydroxyl group of organoclay and maleic anhydride group of LOT [Loyens and Groeninckx, 2002].

STKA clay (Figure 4.30 d) has a peak at $2\theta = 3.26^\circ$ and $d = 2.71$ nm while its composite has a peak at $2\theta = 3.73^\circ$ and $d = 2.37$ nm revealing that the location of the clay peak is shifted to higher angles with upon melt compounding. Decrease in the d-spacing of the STKA shows that delamination and dispersion of clay layers could not be achieved within LOT revealing that neither exfoliation nor intercalation occurred with STKA. This result shows that STKA is not compatible with LOT, so it cannot form nano dispersion within LLDPE/LOT matrix. Thus, STKA was not used in preparation of ternary nanocomposites. Experimental observations obtained in this study showed that TKA cation is not a suitable cation to be used in polyethylene or polypropylene PLSN's since it did not give intercalated/delaminated structures as shown by XRD. Long alkyl tails of TKA cations impede the diffusion of polymer chains into clay galleries in both PP and LLDPE based composites.

4.2.1.4.2 X-Ray Analysis of Ternary Nanocomposites

Figure 4.32 shows XRD patterns of pure DMDA clay, ternary nanocomposites LL/DMDA2/LOT5 and LL/DMDA5/LOT12.5. Two diffraction peaks are observed for the DMDA clay corresponding to basal spacings of $d_{001} = 2.64$ nm ($2\theta = 3.34^\circ$) and $d_{002} = 1.26$ nm ($2\theta = 6.96^\circ$). The second peak observed in DMDA clay is due to the unmodified clay during the modification, since the angle is not half of the first peak and it is the same as the angle of PB peak. The second peak can be attributed to a second silicate layer if 2θ is approximately twice the value of the first characteristic peak of the clay. If it is not half of the first peak, it may be attributed to a reflection from a portion of the clay where the inorganic cations of the smectite clay are not fully intercalated by the organic ions, if

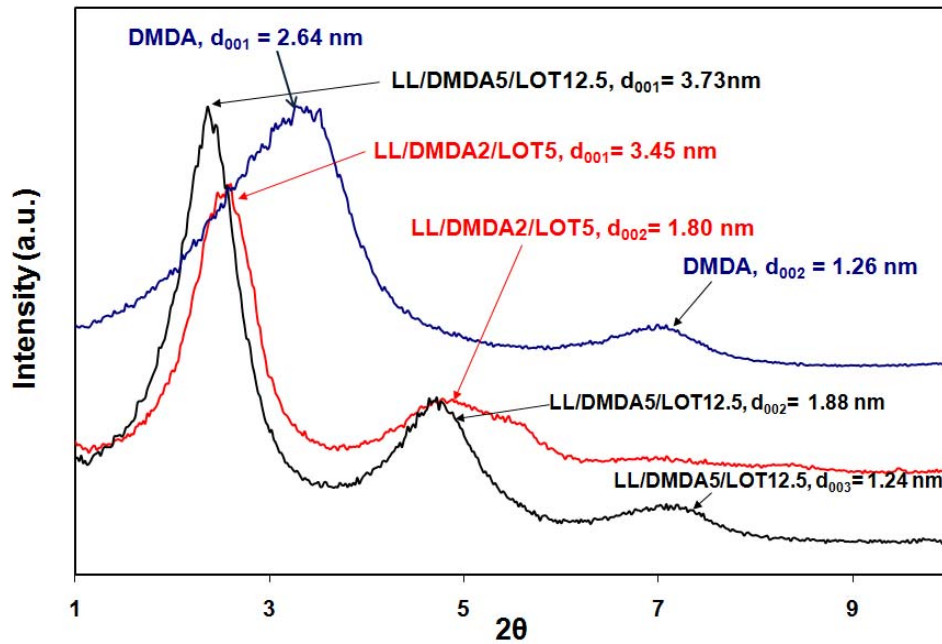


Figure 4.32 XRD analysis of DMDA organoclay and LLDPE ternary composites prepared by DMDA.

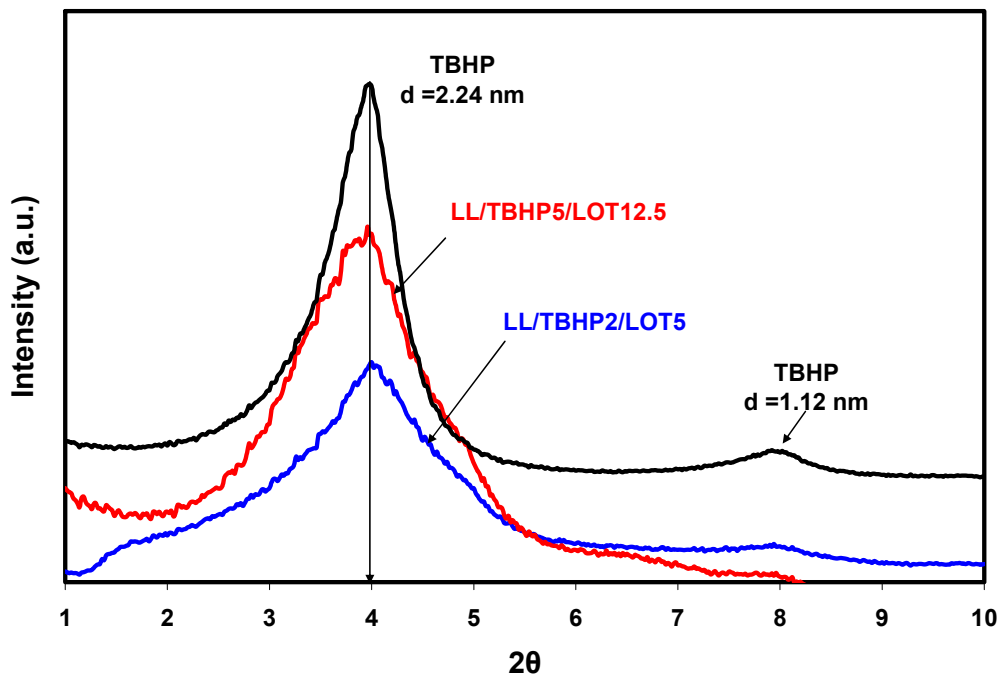


Figure 4.33 XRD analysis of TBHP organoclay and LLDPE ternary composites prepared by TBHP.

2θ is about 2θ for the unmodified clay (Mehrabzadeh and Kamal, 2004; Finnigan et al., 2005). The first two basal spacings observed in LL/DMDA5/LOT12.5 represent the harmonic series for clay itself, since the second one is at a degree of half of the first one, i.e., $d_{001} = 3.73$ nm ($2\theta = 2.36^\circ$) and $d_{002} = 1.88$ nm ($2\theta = 4.68^\circ$). The third peak observed in LL/DMDA5/LOT12.5 samples ($2\theta = 7.12^\circ$; $d_{003} = 1.24$ nm) belongs to unmodified clay which stayed as tactoids in the LLDPE matrix. Surprisingly, this third peak disappeared in the LL/DMDA2/LOT5 which may be attributed to the low clay loading. The clay peak was also shifted to lower angles in LL/DMDA2/LOT5 samples and the d-spacing was increased to 3.45 nm. Again, a second peak was observed in this composite system which may approximately represent the organoclay secondary peak, ($2\theta = 4.9^\circ$; $d = 1.80$ nm). These two peaks suggest that there are intercalated structures with different d-spacings, which were formed during the intercalation of the LLDPE throughout the clay layers and more disordered structures were obtained which will also be shown by the TEM analysis. As in the case of 5 wt % of clay composition, this system shows partially intercalated layers and flocculated structure through the matrix. LOT is a polyethylene based compatibilizer, thus is miscible with LLDPE matrix. It has both maleic anhydride and butylacrylate functional groups which may interact with the hydroxyl groups of clay layers enhancing the possible delamination mechanism. Bulky functional groups of LOT can also increase the d-spacing of the galleries and reduce the interaction between the clay layers resulting in easier dispersion. PE like nature of LOT also increases the affinity between the clay and polymer which in turn increases the delamination mechanism.

Figure 4.33 shows XRD patterns of pure TBHP, ternary nanocomposites LL/TBHP2/LOT5 and LL/TBHP5/LOT12.5. The clay peak and the peak of nanocomposites are seen at the same 2θ degree indicating that TBHP clay could not be delaminated in LLDPE and it remained as tactoids in the polymer matrix.

Morgan and Gilman, 2003 found that while XRD of polyetherimide nanocomposites samples showed immiscible clay layers through the matrix, TEM analysis of the same material showed that it had a large number of exfoliated single layers, and the material that was shown to be intercalated by XRD had both exfoliated single layers and intercalated regions. Morgan and Gilman 2003 also examined PS and MAPP organoclay nanocomposites and realized that while X-Ray analysis showed intercalated structures, TEM analysis of samples revealed that they both had single exfoliated clay layers and intercalated tactoids. Although MAPP had higher clay content (8 wt %) compared to PS (5 wt %), very broad and low intensity XRD peak in MAPP was attributed to the higher number of exfoliated single layers present in it compared to PS. In addition, it should be kept in mind that, the brittle PS-organoclay composite was ground to the powder form while solid monolith of MAPP was used for XRD analysis. The low intensity broad peak observed in the MAPP composites may be due to sample preparation technique which was also shown by cyanate-ester-organoclay composites in their study. They concluded that peak broadening can also be caused by the clay, due to defects and lattice strain in the clay [Reynolds, 1989], as well as finite distribution of clay stack sizes [Klug, 1974]. Smart et al, 2008 found that while XRD of PP prepared with organoclay and MAPP showed no intercalated structure, e.g., no change in the clay peak position in the composites, rheological analysis (e.g., increase in the complex viscosity) suggested improved clay dispersion contradictory to the XRD results. Prasad et al., 2006, studied ethylene-vinyl acetate-Cloisite 30B organoclay nanocomposites. XRD analysis of composites showed absence of clay peak while TEM images showed mixed intercalated/exfoliated morphologies where presence of stacks of silicate layers showed intercalation while individual layers suggested exfoliation. Other authors also accepted that data provided by the XRD alone are insufficient [Lertwimolnun and Vergnes, 2006; Lee et al., 2006; Navarchian and Ardakani 2009; Liu et al., 2007; Tjong 2008; Eckel et al.,

2004; Vaia et al., 1996] and either used other techniques such as TEM or rheology to explain the state of dispersion of the clay layers. Similar contradictory results for XRD were obtained in this study for LL/TBHP2/LOT5 composite where its XRD analysis indicates no intercalation, however its TEM analysis shown later indicate that clay layers were dispersed in the LLDPE matrix and there were also exfoliated single clay layers. Rheological property enhancements were also confirmed by the higher viscosity of TBHP/LOT/LLDPE based composites compared to DMDA/LOT/LLDPE based composites. These results will be given in later.

Figure 4.34 shows the XRD patterns of pure I34, ternary nanocomposites containing LL/I34-2/LOT5, LL/I34-5/LOT5 and LL/I34-5/LOT12.5. All composites show a peak at the same 2θ degree similar to pure I34, showing some unintercalated clay tactoids in the systems. Comparison of LL/I34-5/LOT12.5 and LL/I34-5/LOT5 allows analyzing the effect of addition more compatibilizer, LOT, to the system since clay contents are the same in both of the compositions, however the LOT/Organoclay ratio is different. Results indicated that incorporation of more compatibilizer, LOT, to the system increases the delamination of clay layers which may be realized from the reduced intensity of the peak in LL/I34-5/LOT12.5, where LOT/organoclay ratio is 2.5. More compatibilizer increases the chance of formation of new bands and affinity between the LOT and hydroxyl group of I34. First peaks in the LL/I34-2/LOT5 and LL/I34-5/LOT5 may have resulted from the intercalation of silicate layers through the LLDPE matrix. These systems show partially intercalated layers with tactoids of clay layers. Further analysis should be connected with TEM and rheological analysis which will be given in detail later.

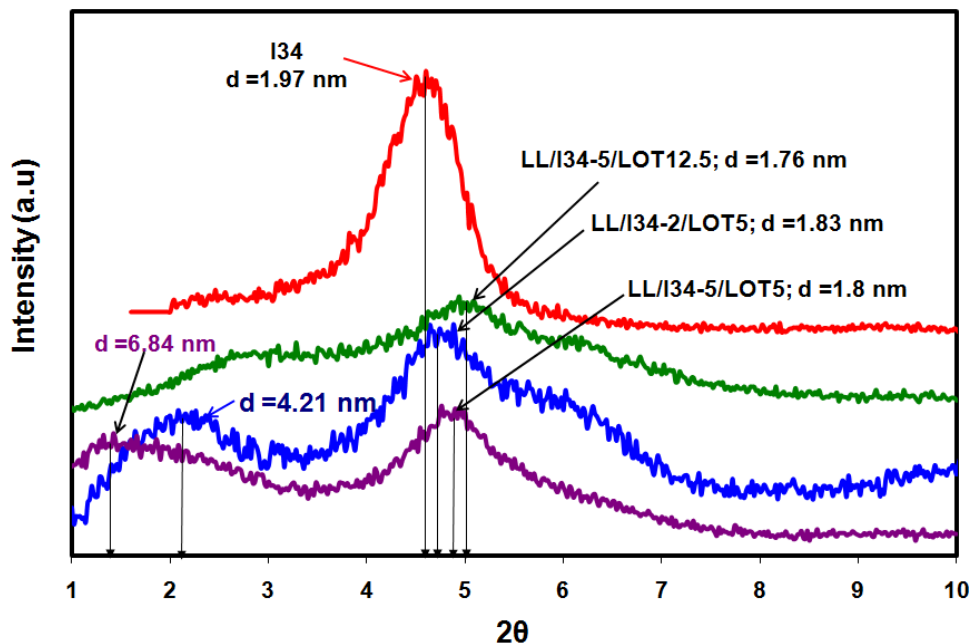


Figure 4.34 XRD analysis of LLDPE ternary composites prepared by organoclay I34.

4.2.2 TEM Analysis

XRD is an intensively used technique in PLSN, yet it is a controversial issue in the literature to decide the degree of the distribution of the silicate layers or any structural inhomogeneity in nanocomposites by XRD alone. Vaia et al., 1994; Morgan and Gilman, 2003 explained the lack of XRD alone to characterize the state of dispersion of clay layers and stated that it should be definitely used with TEM. They stated that, the absence of a peak may be misconceived in cases where no peak is seen. Depending on the problems due to sampling, orientation, clay dilution, peak broadening, preferred orientation and poor calibration of most XRD instruments at very low angles, XRD diffractograms can yield wrong conclusions for intercalated and immiscible PLSNs [Vaia et al., 1994; Morgan and Gilman, 2003; Eckel et al., 2004; Tjong 2006]. Clay dilution and peak broadening can lead to the misleading conclusion that exfoliation has happened. However, preferred orientation effects can result in the false conclusion that exfoliation has not occurred. XRD does

not give the data relating to the spatial distribution of the clay layers in the polymer matrix, because all of the data are averaged over the whole regions of the specimen. TEM can give practical information in a localized area on the morphology, structure and spatial distribution of the dispersed clay layers in the PLSN [Tjong, 2006]. Thus, XRD must be supported with TEM.

In the TEM micrographs, the dark areas point out the individual clay layers or agglomerates (tactoids), gray-white areas represent the matrix polymers.

4.2.2.1 TEM Micrograph of PPM Based Composites

Figures 4.35 and 4.36 show TEM micrographs of PPM/TKA2/MAPP2 composites prepared in SET-1, and its X-Ray analysis is given by Figure 4.13. Micrographs display stacked silicate layers as darker lines. Hotta and Paul, 2004 applied a limited image analysis for TEM images of LLDPE/clay nanocomposites. Nam et al., 2001 studied the TEM image of PP/clay nanocomposites, and the factors used in the image analysis are schematized in Figure 4.37. In this analysis, L_{clay} and d_{clay} represent the length and the thickness of dispersed clay particles and ξ_{clay} represents the correlation length between the dispersed clay particles. Only L_{clay} and d_{clay} were measured manually with help of a ruler from the print-out of images, and a limited, semiquantitative analysis of TEM image analysis is conducted in this study. Figure 4.36 shows a tactoid of 71 nm in thickness and a length of 230nm. Seven particles in the same figure show an average L_{clay} of 220 nm with a standart deviation of 75 nm. Although the X-Ray analysis showed little increase in the d-spacing (from 2.56 nm to 2.65 nm) in this composite system, TEM analysis shows partially intercalated and exfoliated layers in it.

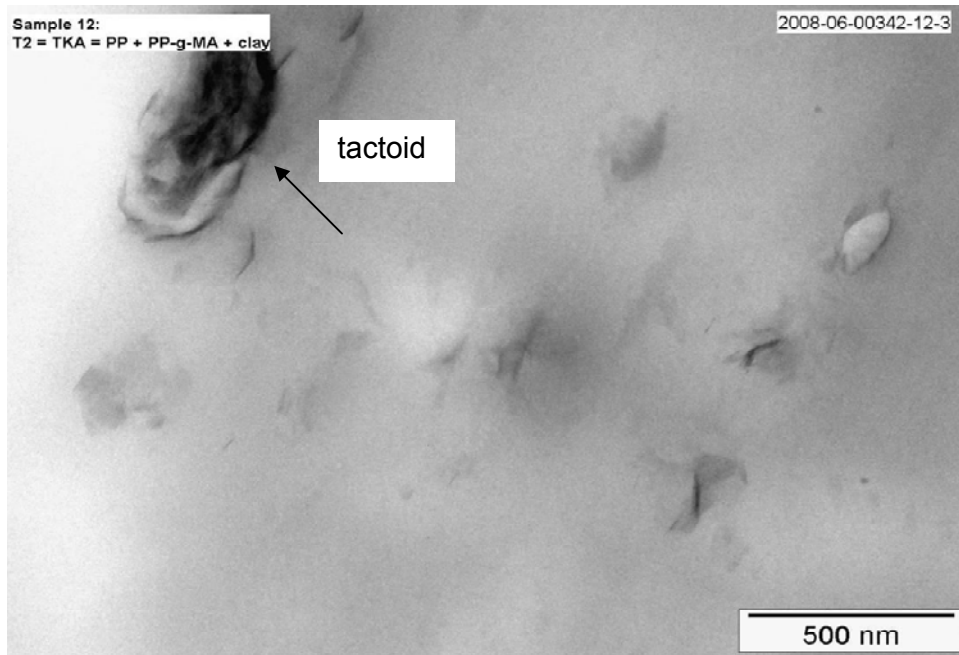


Figure 4.35 TEM analysis of PPM/TKA2/MAPP2.

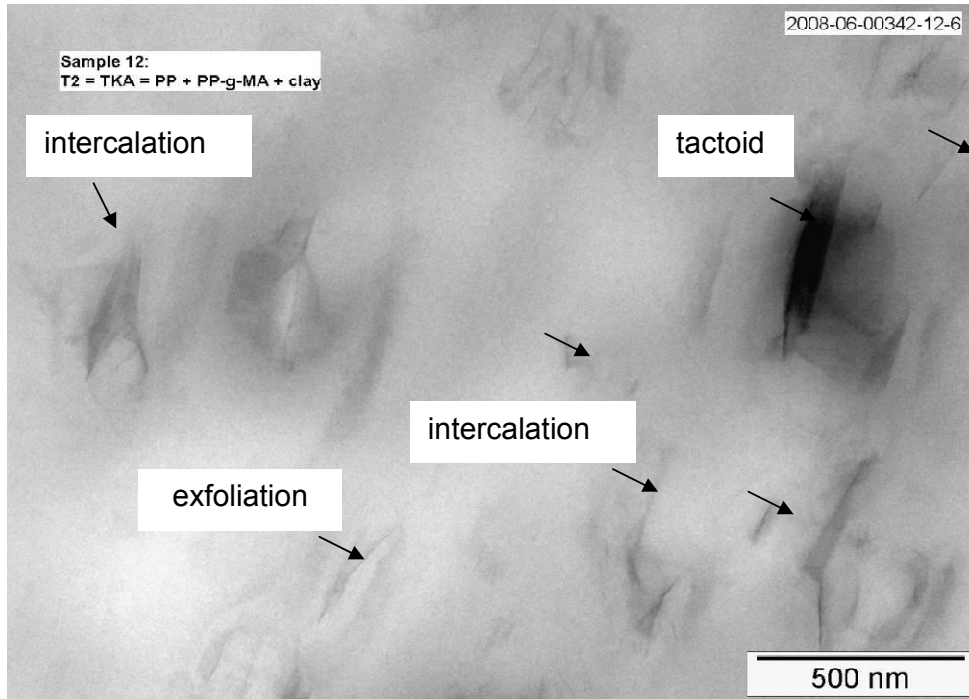


Figure 4.36 TEM analysis of PPM/TKA2/MAPP2 (XRD is given in Fig. 4.13)

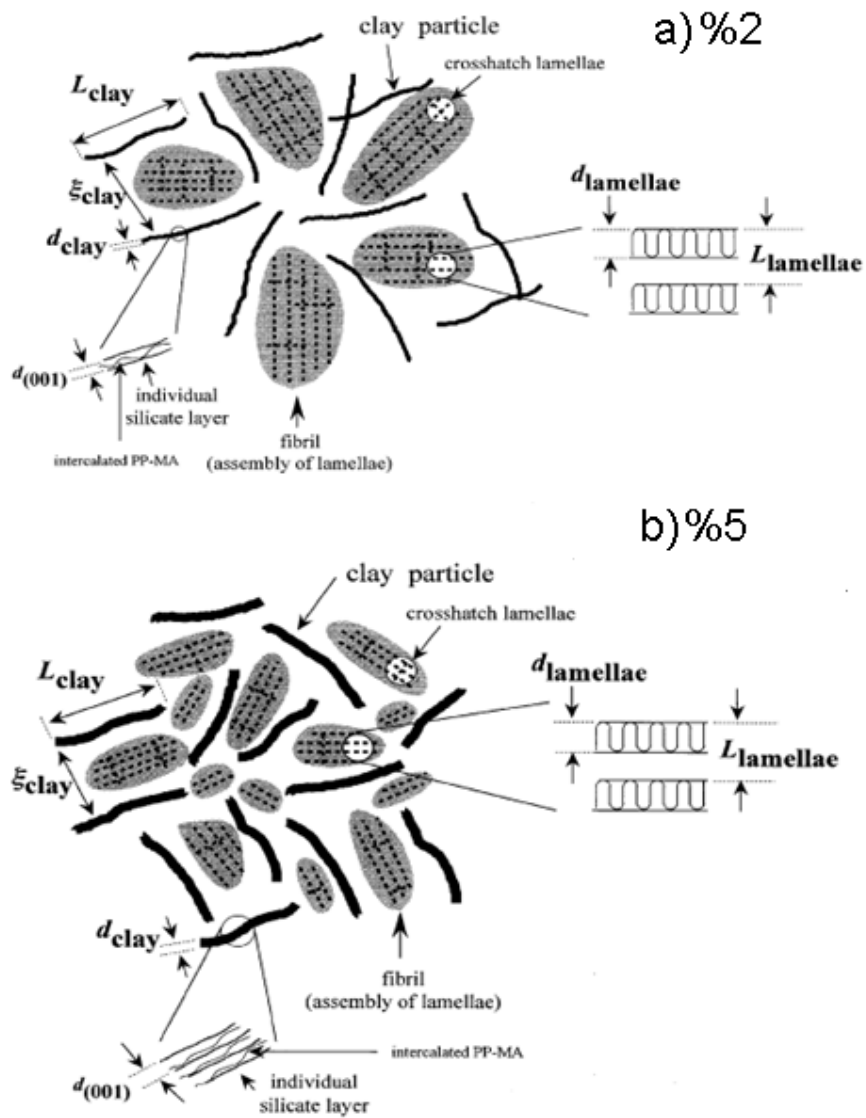


Figure 4.37 The illustration for dispersed clay structure and the inter-fibrillar structure for PP/OrganoclayMAPP nanocomposites with different clay loading 2 % and 5 % [Adapted from Nam et al., 2001].

4.2.2.2 TEM Analysis of PPE-M Matrix Nanocomposites

Figures 4.38 and 4.40 show the TEM micrographs of the sample PPE/DMDA2/MAPP5-M with different magnifications. Figure 4.38 (a) clearly shows intercalated layers of clays in a coherent order. Figure 4.38

(b), and Figure 4.39 (a), (b), (c) and (d) show stacked clay layers as darker lines, while intercalated and also few exfoliated regions are also observed, indicating a mixed morphology. Exfoliated single layers can be observed in Figure 4.38 (c) and (e) as shown by arrows and circles. L_{clay} in Figure 4.40 (b) is measured as 84 ± 39 nm, while it is measured as 79 ± 42 nm in Figure 4.40 (d).

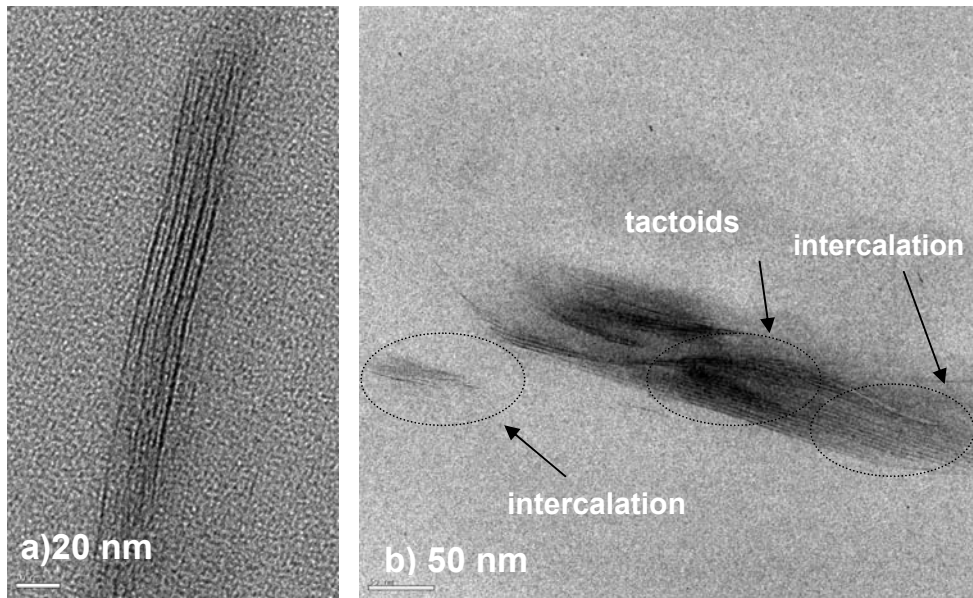


Figure 4.38 TEM Analysis of PPE/DMDA2/MAPP5 -M

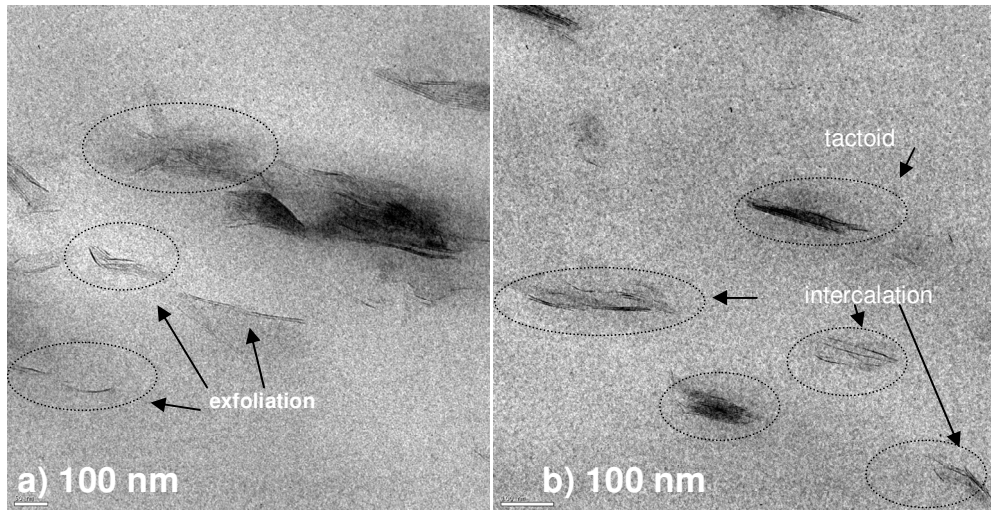


Figure 4.39 TEM Analysis of PPE/DMDA2/MAPP5-M at 100 nm magnification

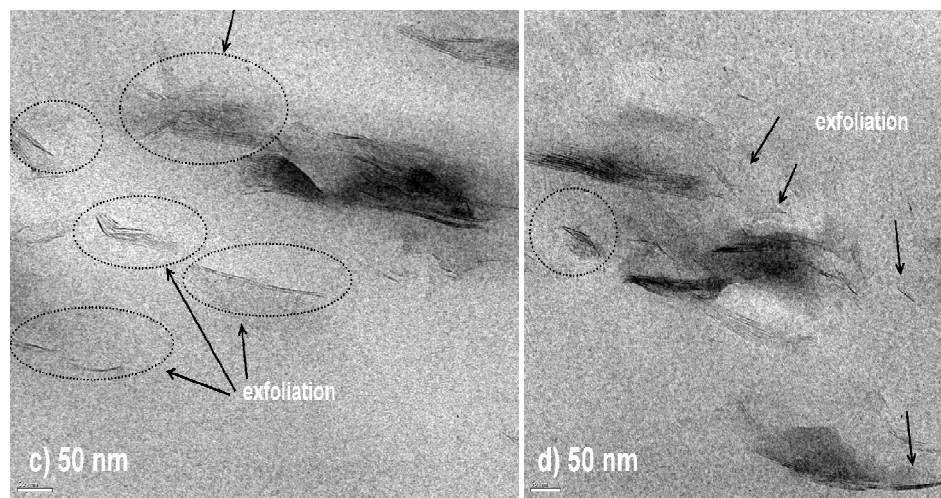


Figure 4.40 TEM Analysis of PPE/DMDA2/MAPP5-M at 50 nm magnification

Figure 4.41 shows representative TEM images for PP ternary composites of PPE/TBHP2/MAPP5-M. Figure 4.41 (a) and (b) display clear images of clay layers at 20 nm scale. Figure 4.41 (d) shows a mixed morphology structure, i.e., a combination of tactoids about 10-30 nm in thickness and

about 300 nm in length are dispersed in the matrix randomly. Figure 4.41 (c) shows that tactoids about 10-30 nm in thickness and about 100-300 nm in length are dispersed in the matrix. Micrographs of samples with TBHP clearly show much more coherent ordering/alignment compared to one prepared with DMDA.

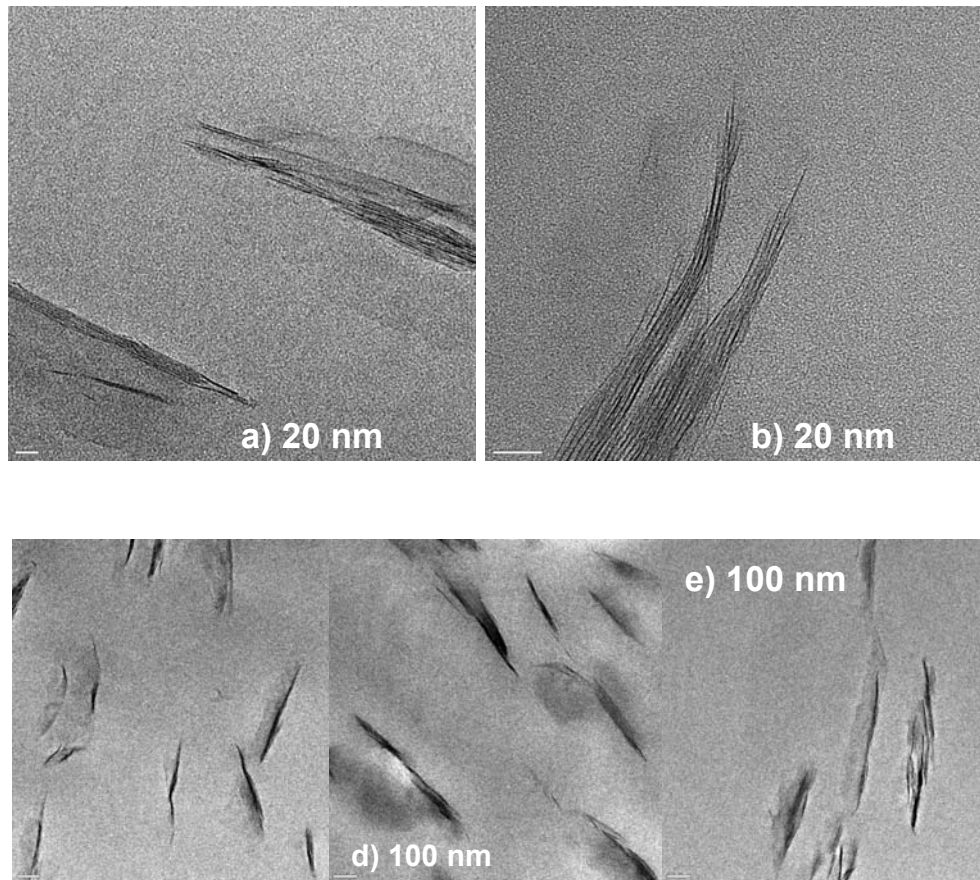


Figure 4.41 TEM analysis of PPE/TBHP2/MAPP5-M with different magnifications.

4.2.2.3 TEM Analysis of LLDPE Based Nanocomposites

Figure 4.42 (a) through (m) show the TEM images of LL/TBHP2/LOT5 nanocomposite with different magnifications. Although XRD analysis of this nanocomposite showed no change in the d-spacing of clay in the matrix, images clearly show individual exfoliated, partially intercalated and

tactoids of clay layers. Thus, the need for TEM confirmation can be seen clearly. Figures 4.41 (a) through (i) display intercalated clay layers and also exfoliated single layers of TBHP. L_{clay} of Figure 4.42 (j) is 100 nm with a standard deviation of 69 nm. Especially, single exfoliated layers are seen in Figure 4.42 (j). High aspect ratio of intercalated layers, with high L_{clay} (162 nm with a standard deviation of 78.5 nm), is seen in Figure 4.42 (k) which further indicates to high aspect ratio. Figure 4.42 (l) and (m) show a disordered clay layer structure.

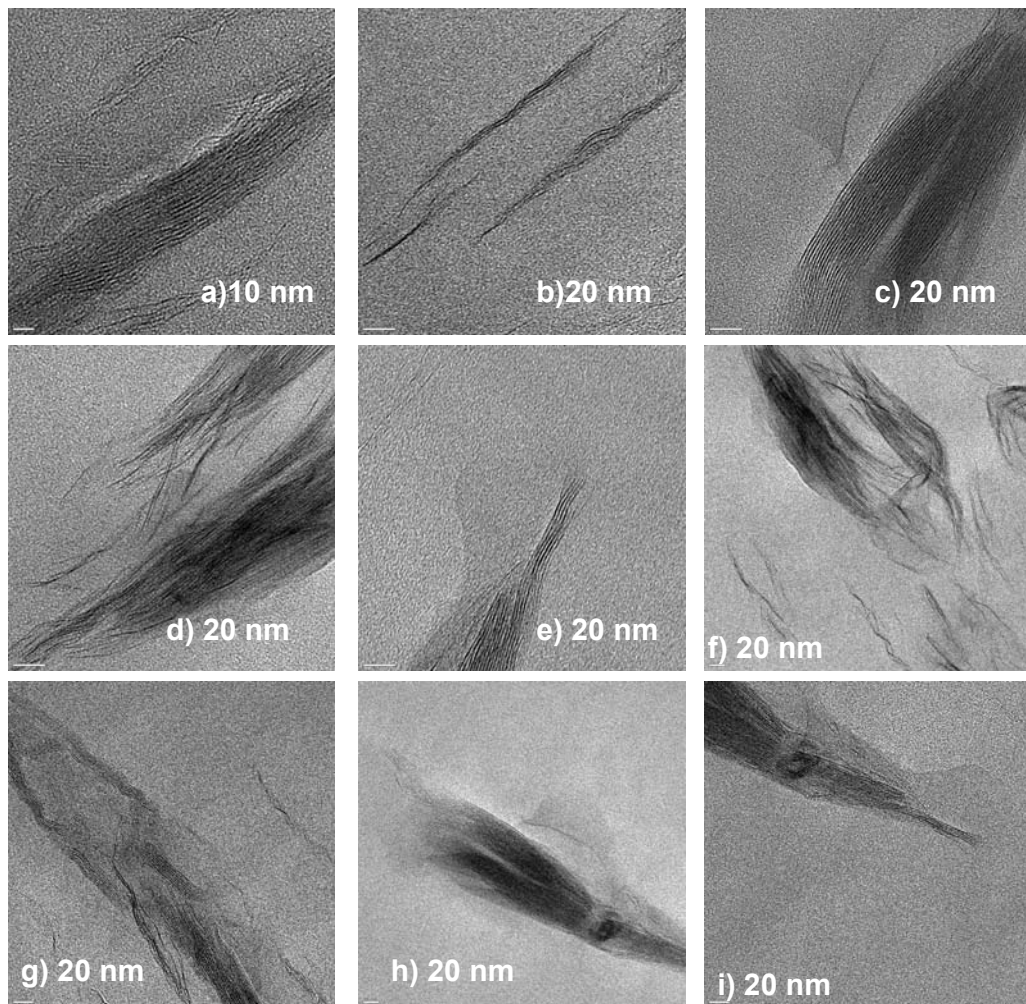


Figure 4.42 TEM analysis of LL/TBHP2/LOT5 composites

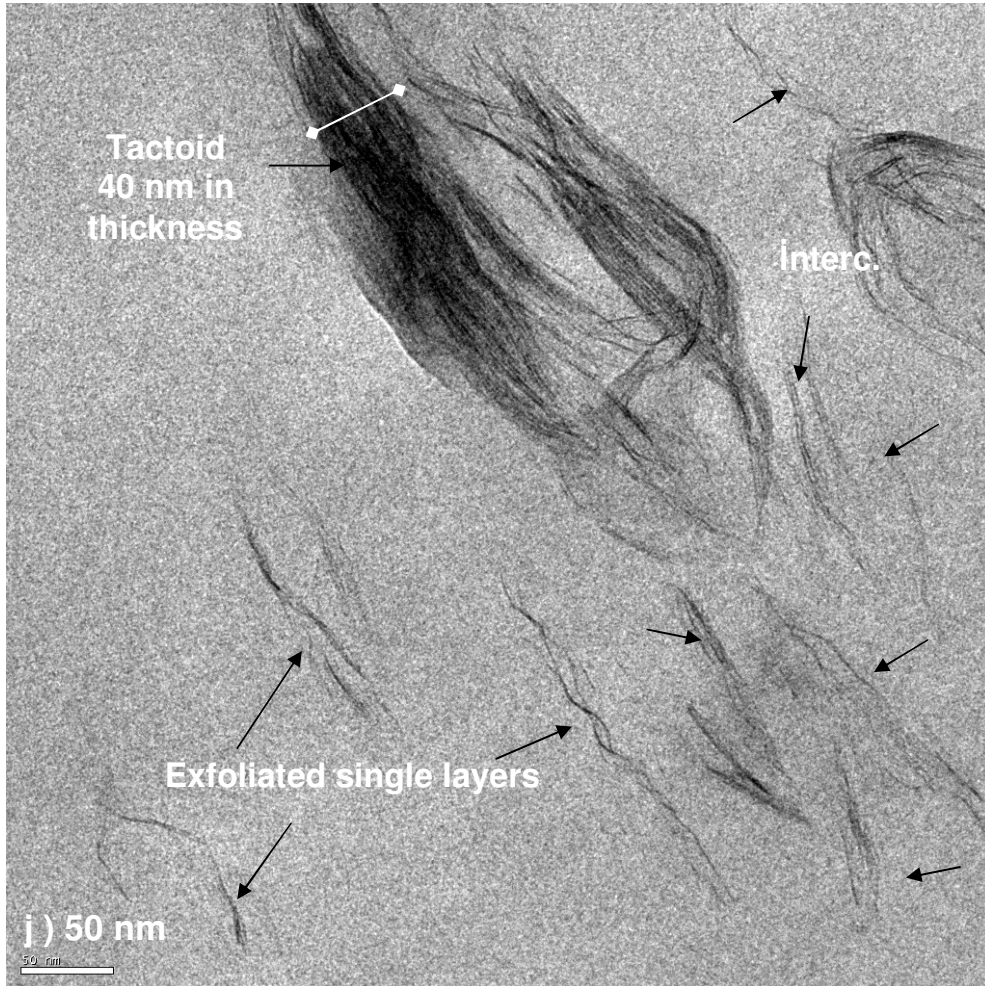


Figure 4.42 TEM Analysis of LL/TBHP2/LOT5 composites (continued)

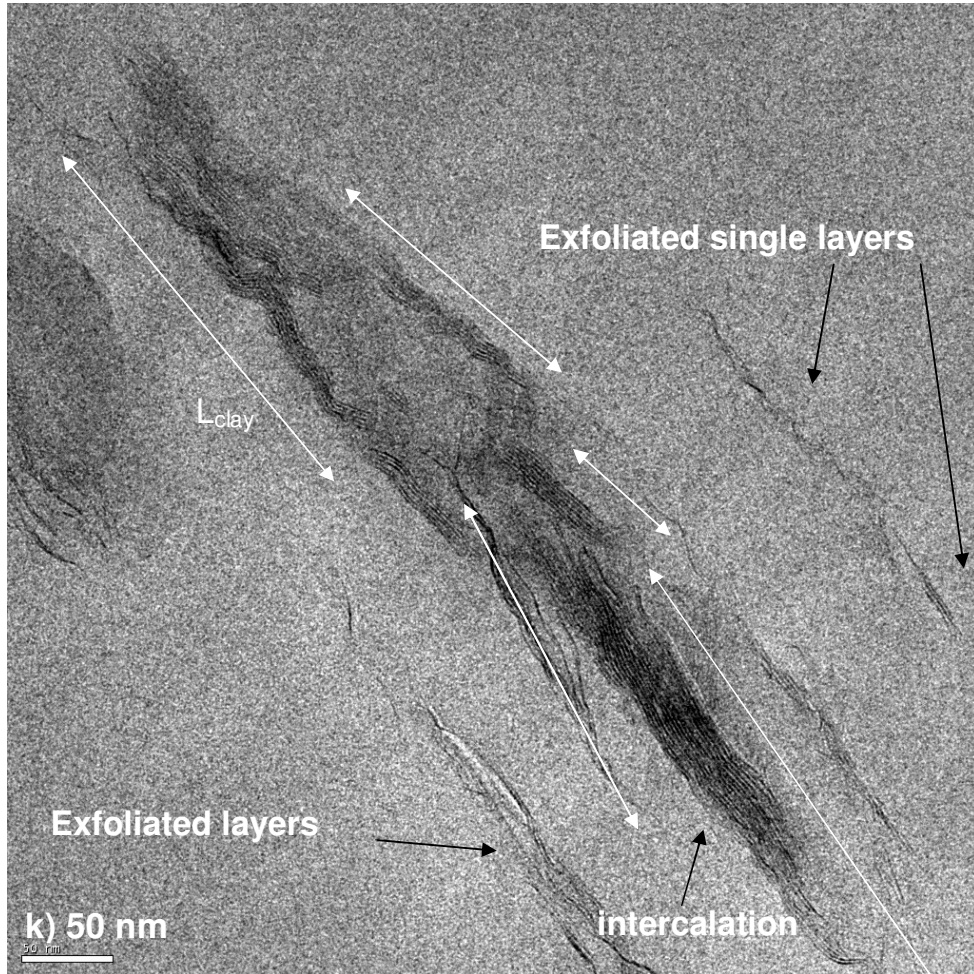


Figure 4.42 TEM Analysis of LL/TBHP2/LOT5 composites (continued).

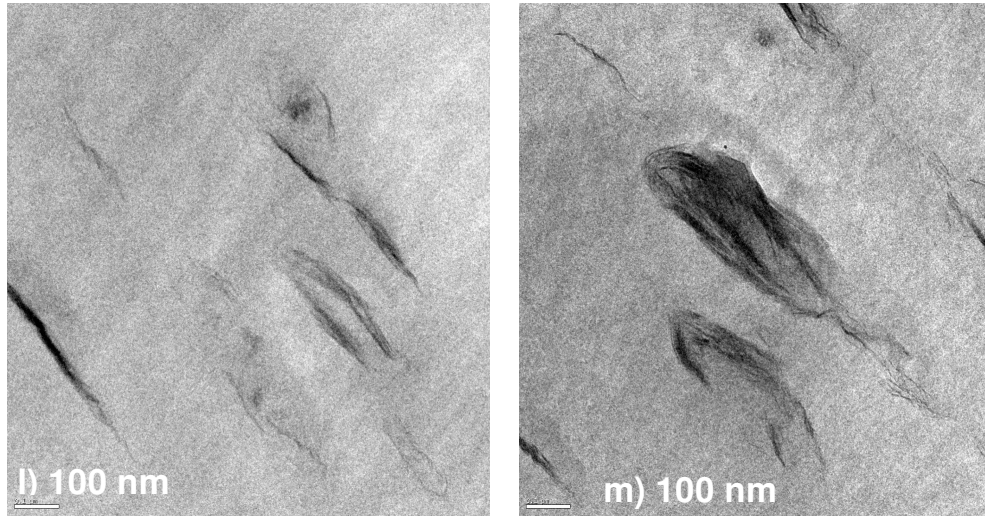


Figure 4.42 TEM Analysis of LL/TBHP2/LOT5 composites (continued)

Figure 4.43 (a)-(c) show the TEM micrographs of LL/DMDA2/LOT5 with different magnification of different regions of the sample. Average L_{clay} in Figure 4.43 (a) is about 118.8 nm with a standard deviation of 21 nm indicating high aspect ratio of dispersed clay layers. XRD analysis showed intercalation for this set of composite, but when it is compared with TEM analysis of LL/TBHP2/LOT5, much more dispersed clay layers are seen in the matrix with TBHP. Figure 4.43 (c) shows tactoids with an average thickness of 35.5 nm and indicate more ordered tactoids than micrographs of LL/TBHP2/LOT5 (Figure 4.42 (l) and (m)).

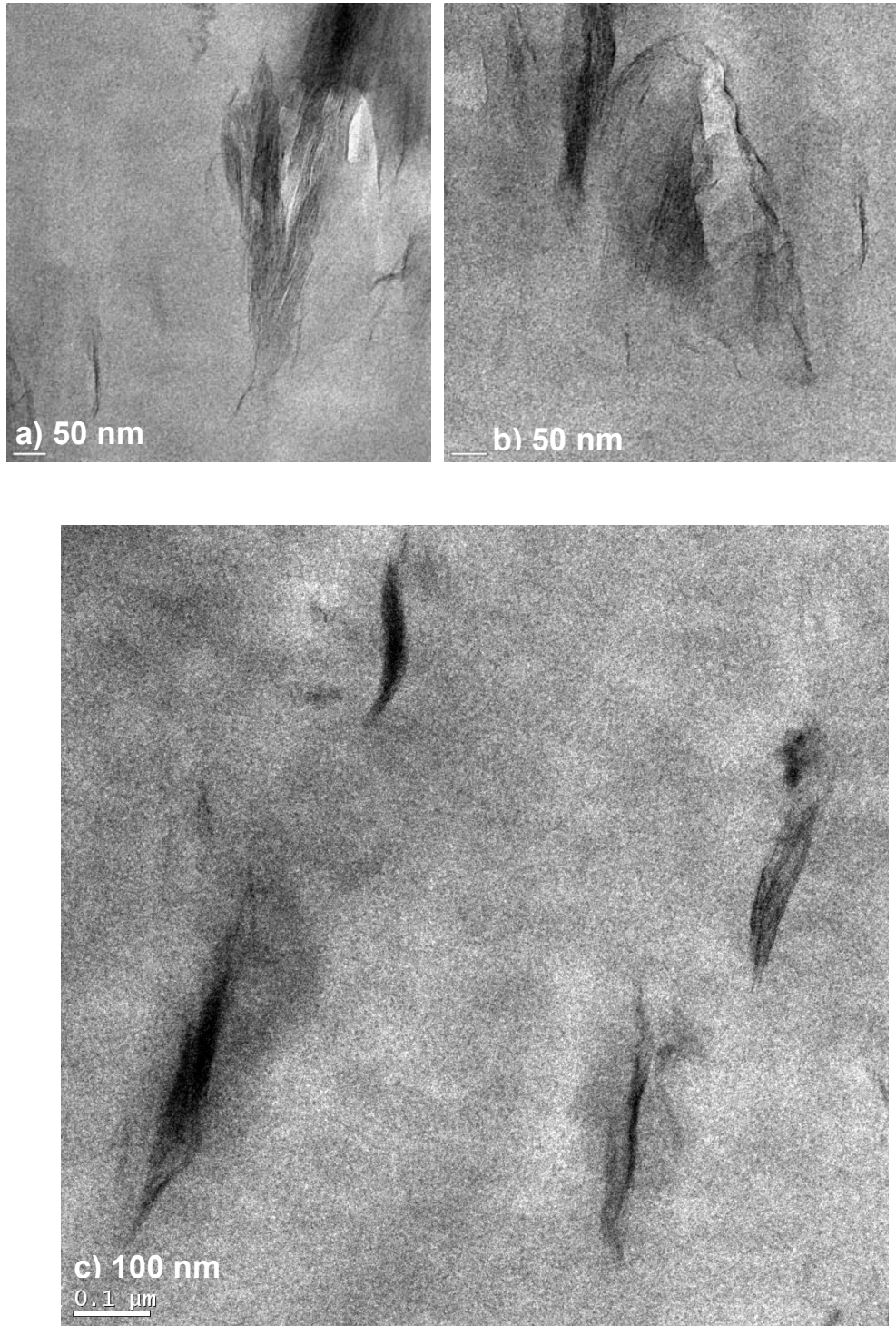


Figure 4.43 TEM Analysis of LL/DMDA2/LOT5 composites

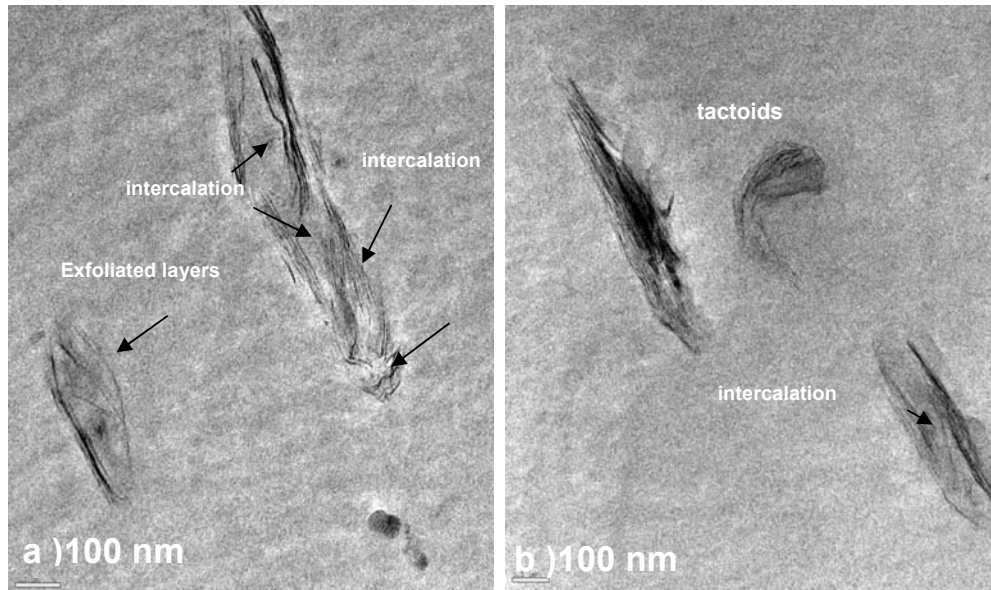


Figure 4.44 TEM Analysis of LL/I34-2/LOT5 composites

Figure 4.44 (a) and b show TEM micrograph of LL/I34-2/LOT5 samples. L_{clay} is 193.9 nm with a standard deviation of 87.24 nm. Partially intercalated, exfoliated layers are seen in Figure 4.44 (a) while tactoids are observed in Figure 4.44 (b). XRD analysis had shown two different diffraction peaks in XRD of this sample, and this situation is also confirmed by TEM analysis.

Table 4.4 summarizes the particle analysis obtained by TEM analysis.

Table 4.4 Results of particle analysis by TEM analysis

Property	Figure	L _{clay} (nm)	Tactoid	
			Thickness (nm)	L(nm)
PPM/TKA2/MAPP2	36	220±75	71	230
LL/TBHP2/LOT5	38. j	100±69		
	38. k	162±79		
LL/DMDA2/LOT5	39.a	119±21		
	39.c		35.5	
LL/I34-2/LOT5	40.a	194±87		
PPE/DMDA2/MAPP5-M	42.b	84±39		
	42.d	79±42		
PPE/TBHP2/MAPP5-M	44.d		10-30	300
	44.c		10-30	100-300

4.2.3 SEM Analysis

Morphological characterization of composites was done by SEM technique where fractured surfaces of the composite samples were analyzed. This analysis was also conducted to observe the distribution of elastomer phase in the matrix, since it is important in the toughening mechanism. Samples prepared either by extrusion or batch mixing were injected molded, and rectangular shape of samples were broken in order to obtain surfaces by fracture. These surfaces were coated by gold and then analyzed at different magnifications. This section presents the SEM images of the composites with magnifications of x250 and x3000 in order to analyze the surfaces in detail.

4.2.3.1 SEM Analysis for SET-1

Figure 4.45 shows the SEM micrograph of featureless and smooth surface of the neat PPM at magnifications of x 250 and x 3000, respectively. The SEM micrographs show that low energy may be disseminated during the

impact of this material due to its featureless structure [Bao, 2007]. Figure 4.46 shows that incorporation of MAPP into the PPM matrix diminished the featureless structure of PPM and increased its roughness indicative of increase in the ability to absorb more energy during fracture.

Figure 4.47 shows SEM micrograph of PPM/TKA2/MAPP2 samples, showing uniformly dispersed clay particles in the matrix; the average lateral dimension of clay is about 500-1000 nm. However, SEM micrographs of composites prepared with HMA (Figure 4.48 and 4.49), TBA (Figure 4.50) and TBP (Figure 4.51) do not show clay tactoids at these magnifications.

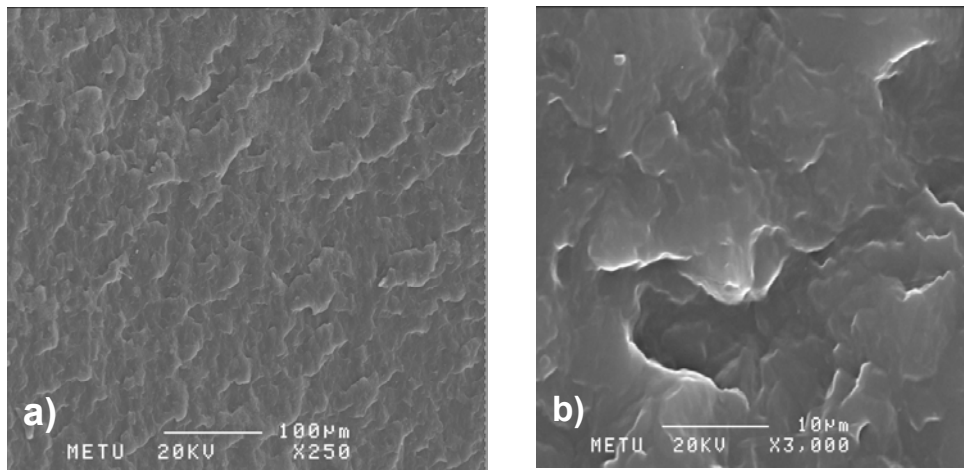


Figure 4.45 Fracture surface of PPM (a) x 250 magnification (b) x300 magnification

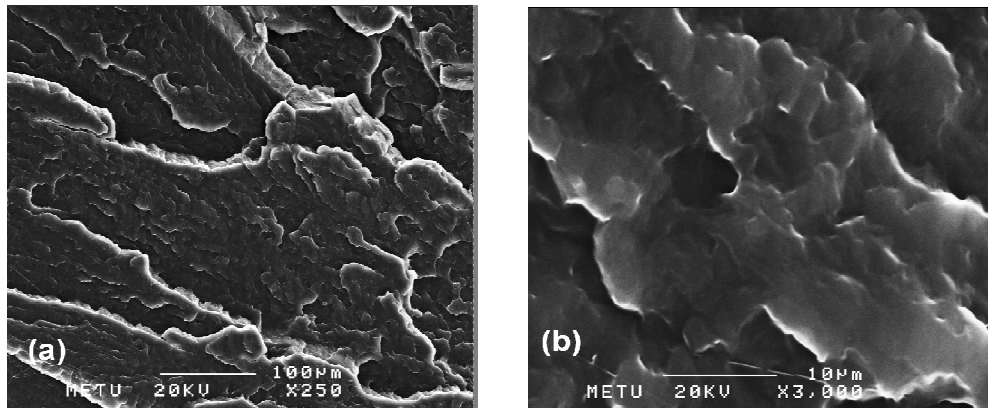


Figure 4.46 Fracture surface of PPM98/MAPP2 (a) x 250 magnification (b) x3000 magnification

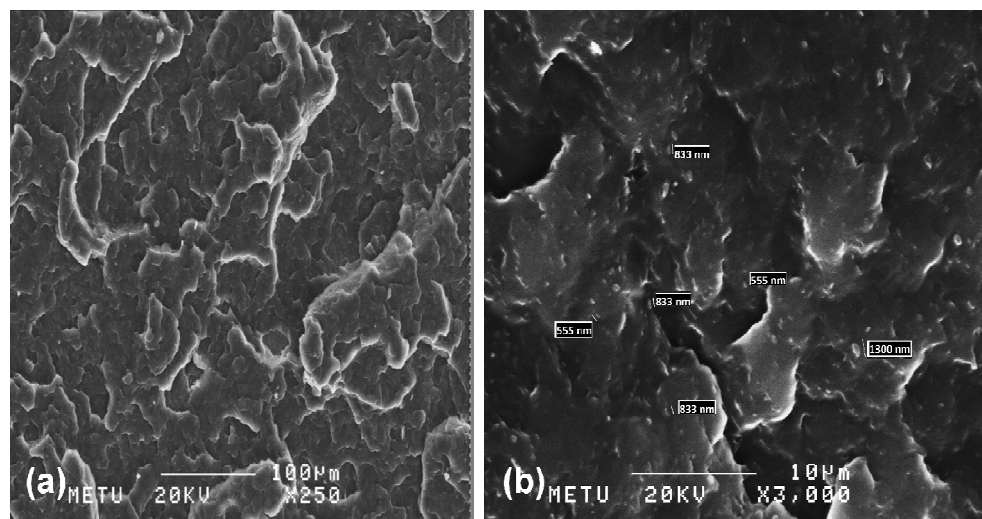


Figure 4.47 Fracture surface of PPM/TKA2/MAPP2 (a) x 250 magnification (b) x3000 magnification

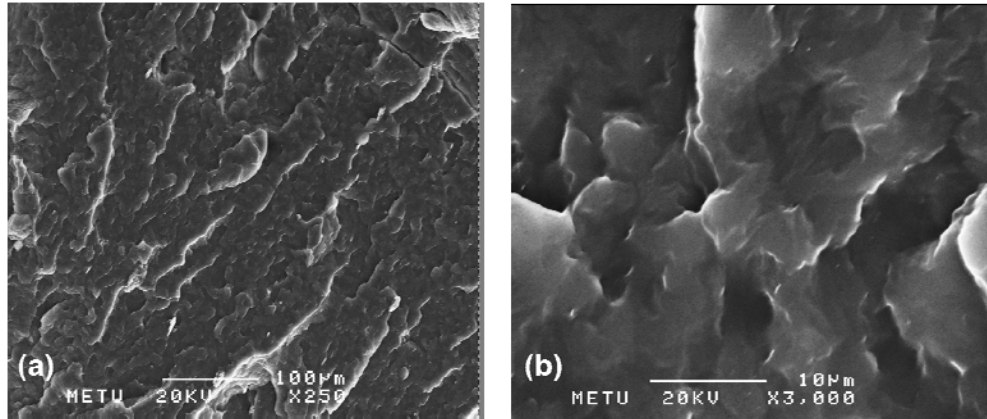


Figure 4.48 Fracture surface of PPM/HMA2/MAPP2 (a) x 250 magnification (b) x3000 magnification

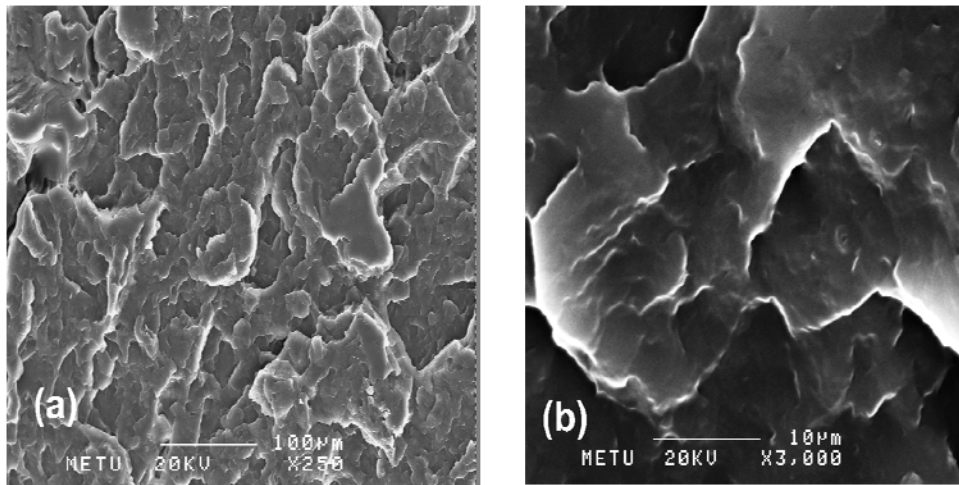


Figure 4.49 Fracture surface of PPM/HMA1/MAPP3 (a) x 250 magnification (b) x3000 magnification

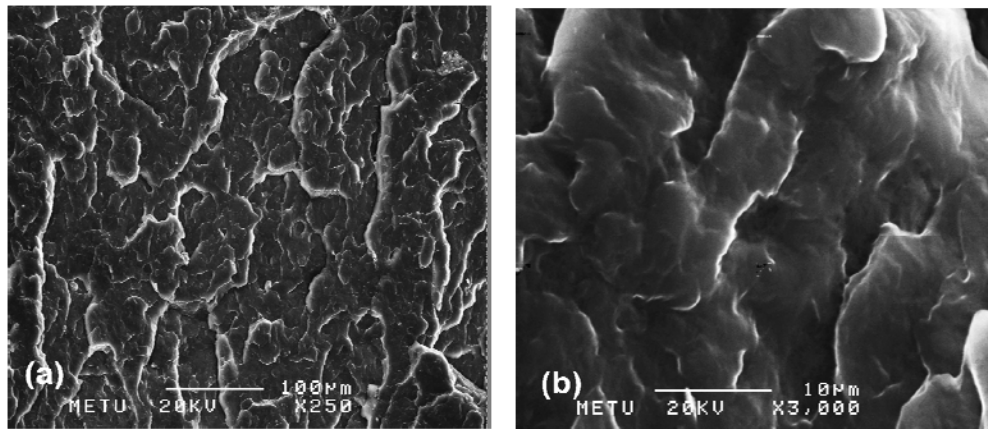


Figure 4.50 Fracture surface of PPM/TBA2/MAPP2 (a) x 250 magnification (b) x3000 magnification

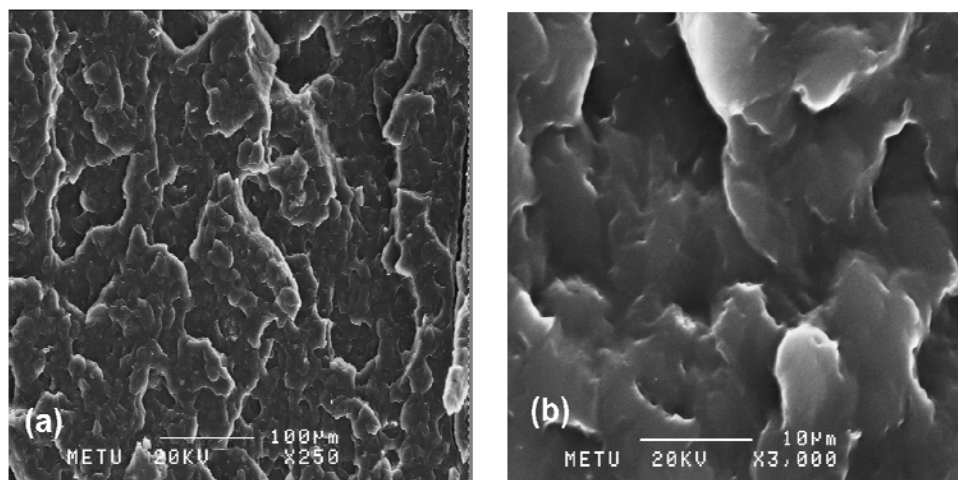


Figure 4.51 Fracture surface of PPM/TBP2/MAPP2 (a) x 250 magnification (b) x3000 magnification

4.2.3.2 SEM Analysis for SET 2

Figure 4.52 shows the SEM micrograph of neat PPE at magnifications x250 and x3000. Figure 4.53 through Figure 4.56 show SEM micrographs of ternary composites prepared by HMA, TKA, TKA50 and PGWTKA organoclay respectively prepared by extruding twice at 350 rpm and 180 °C. Featureless surface of PPE is clearly observed from the micrographs,

while through ternary composite formation crack lines on the surface of the composites became shorter and denser.

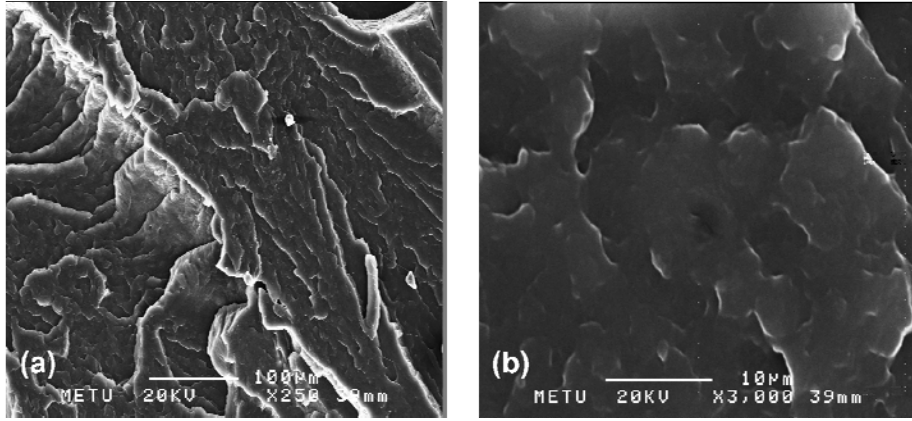


Figure 4. 52 Fracture surface of PPE (a) x 250 magnification (b) x3000 magnification

Tactoids of clay are not clearly observable in composites prepared by HMA (Figure 4.53), while larger tactoids are seen in composites prepared by TKA50 (Figure 4.54) (x3000 magnification). Clay tactoids have lateral dimensions changing from 100 to 500 nm, indicating poor dispersion and interfacial bonding between the matrix and clay phases, as also confirmed by X-Ray analysis. TKA50 was prepared with an excess surfactant concentration, while TKA was prepared by moderate surfactant concentration. SEM micrographs of composites prepared by TKA display visible tactoids with lateral dimensions of 200-600 nm supporting the XRD results. Visual observation of TKA and TKA50 composites indicate that more homogeneously distributed and smaller clay tactoids are present in the one prepared with lower TKA clay concentration. This result points out to the unnecessary use of excess surfactant for the modification of bentonite clay.

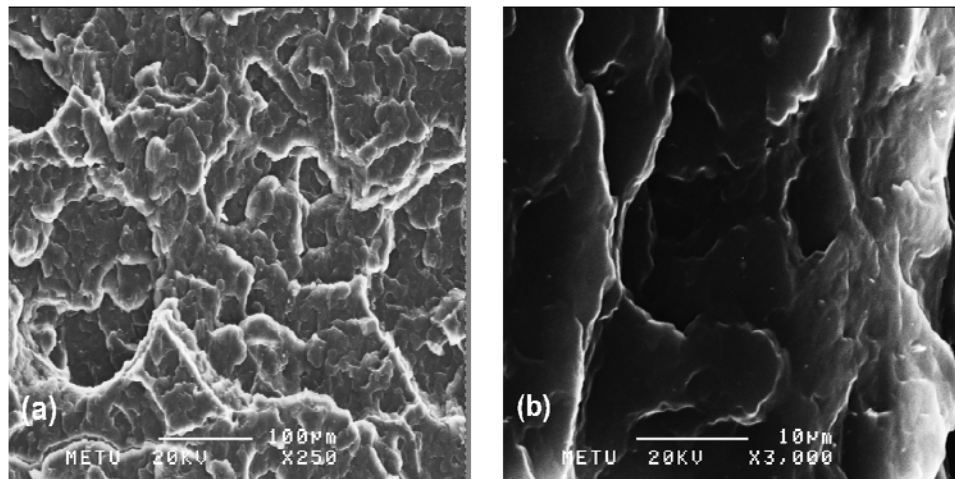


Figure 4.53 Fracture surface of PPE/HMA2/MAPP5 (a) x 250 magnification (b) x3000 magnification

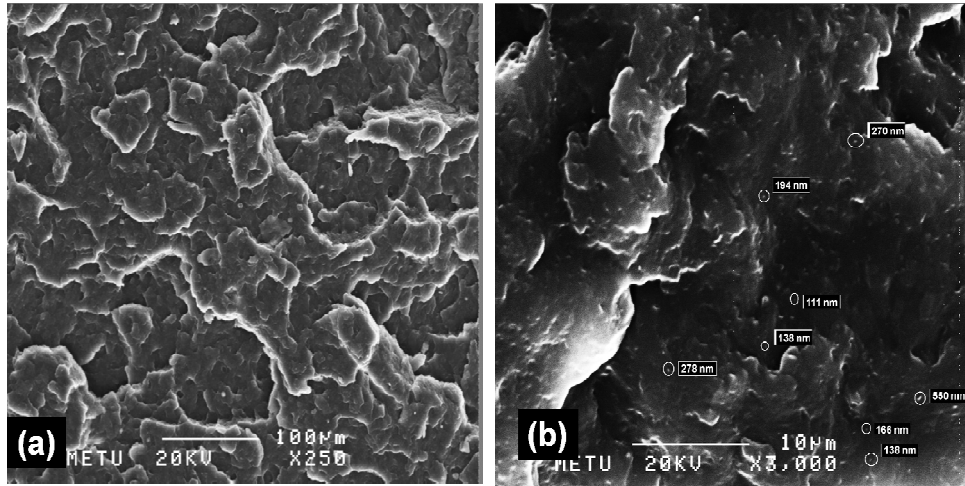


Figure 4.54 Fracture surface of PPE/TKA50-2/MAPP5 (a) x 250 magnification (b) x3000 magnification

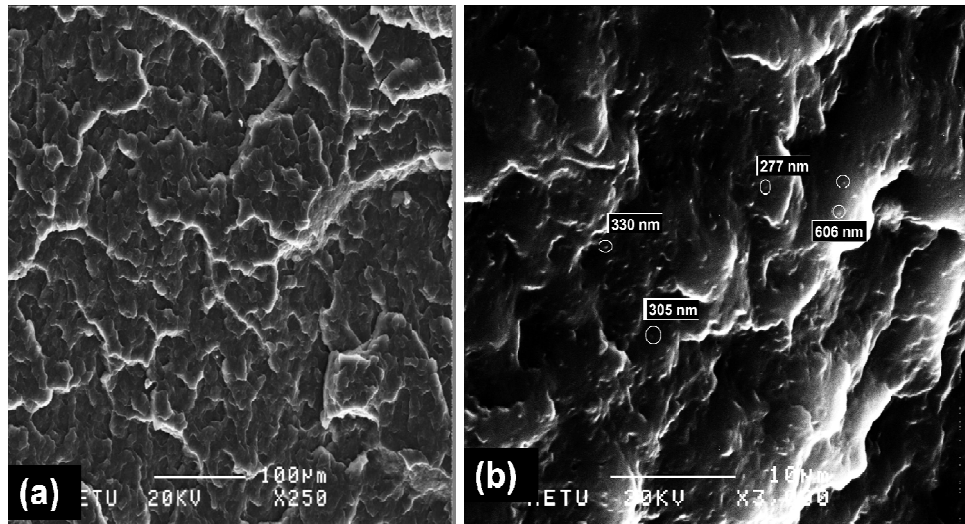


Figure 4.55 Fracture surface of PPE/TKA2/MAPP5 (a) x 250 magnification (b) x 3000 magnification

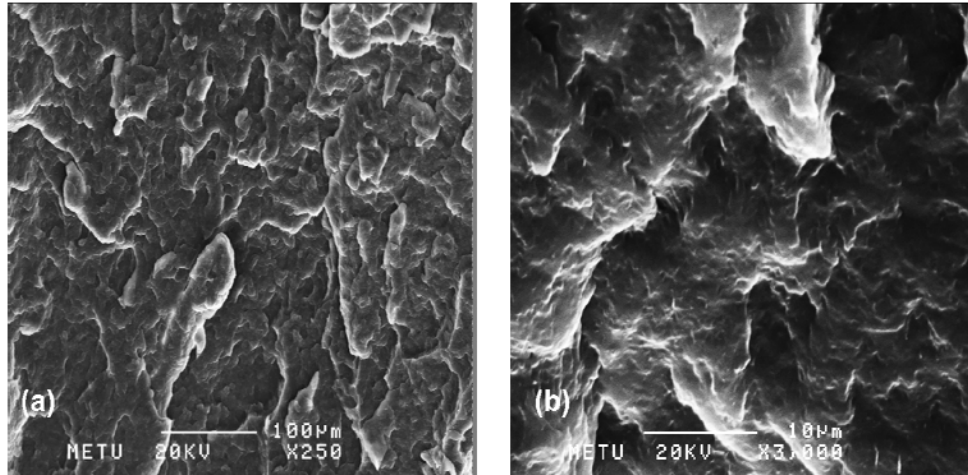


Figure 4.56 Fracture surface of PPE/PGWTKA2/MAPP5 (a) x 250 magnification (b) x3000 magnification

4.2.3.3 SEM Analysis for SET-4

Figure 4.57 through Figure 4.60 show the composites of PPE/Organoclay2/MAPP5-M prepared by “extrusion followed by batch mixing”. SEM micrographs of ternary composites show that featureless surface property of PP definitely changed and crack lines became shorter and denser with the addition of organoclay and MAPP. Observation of Fig.4.58 reveals uniformly distributed tactoids of DMDA clay particles with average lateral dimension of about 150 nm-300 nm. Figure 4.59 shows larger tactoids of STKA clay dispersed relatively in uniform order, and the lateral dimensions of aggregates change from 150 to 700 nm. Aggregates of STKA clay in SEM micrograph confirm the XRD analysis, since d-spacing showed no increase after compounding. Figure 4.60 shows the ternary composites prepared by TBHP clay revealing that clay dispersion is not uniform, but this composition has tactoids smaller than STKA clay, supporting XRD analysis. Figure 4.60 shows some microvoid formation, also known as domains, which are formed by the pull-out of elastomeric regions of MAPP. Dispersion of elastomeric particles are also important and their sizes are formed at the final level depending upon the viscosity

of the environment, melt elasticity of components, shear stresses and shear rate, the mobility of interphase and the surface tension [Contreras et al., 2006].

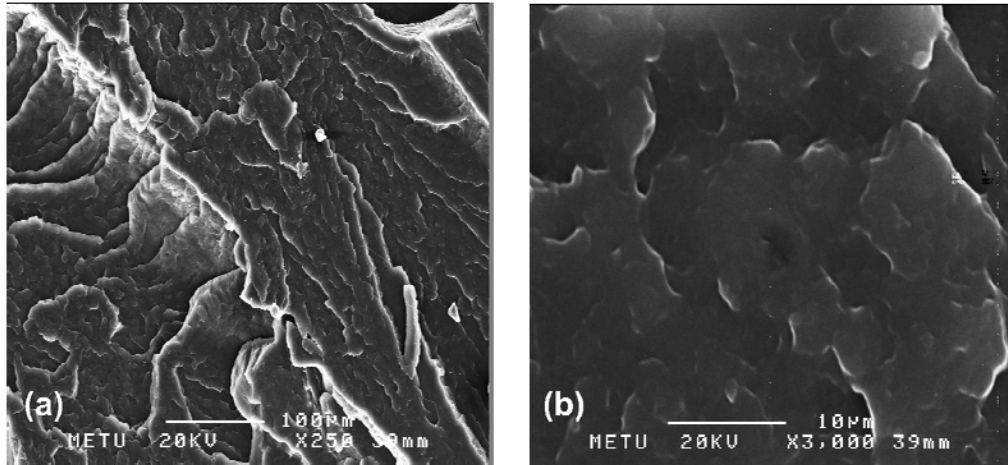


Figure 4.57 Fracture surface of PPE-M (a) x 250 magnification (b) x3000 magnification

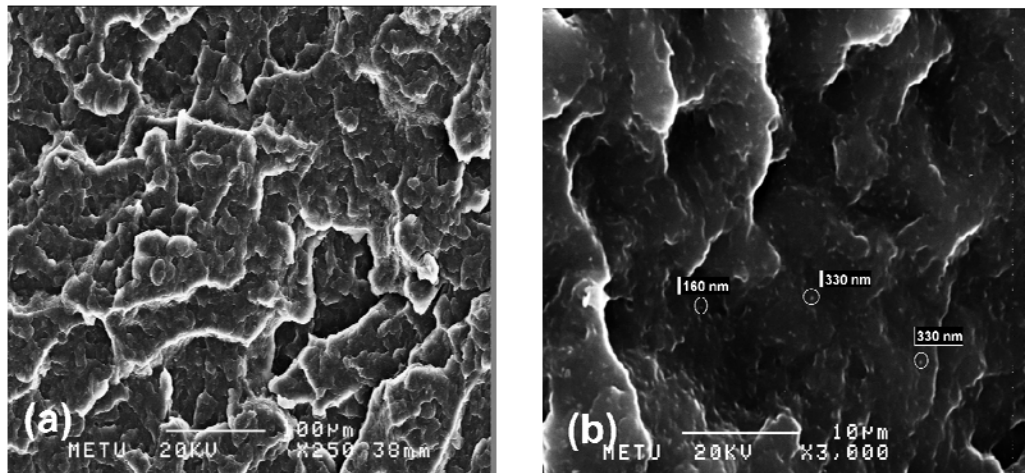


Figure 4.58 Fracture surface of PPE/DMDA2/MAPP5-M (a) x 250 magnification (b) x3000 magnification

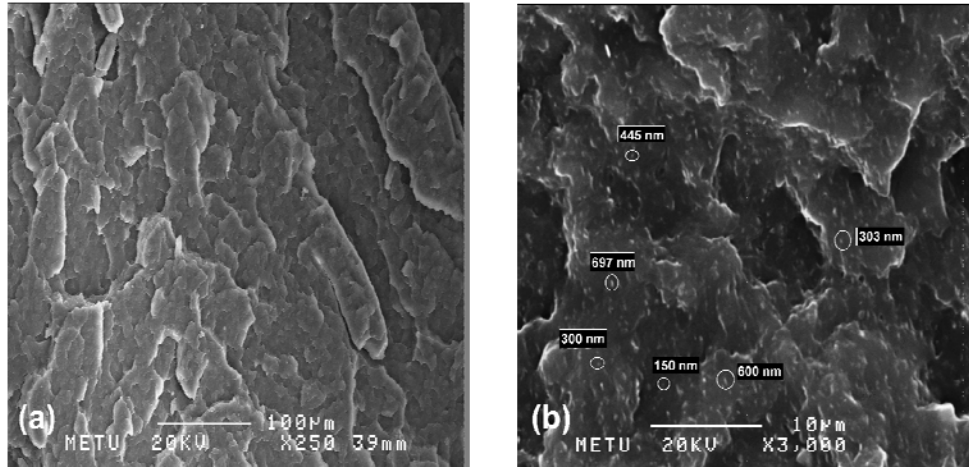


Figure 4.59 Fracture surface of PPE/STKA2/MAPP5-M (a) x 250 magnification (b) x3000 magnification

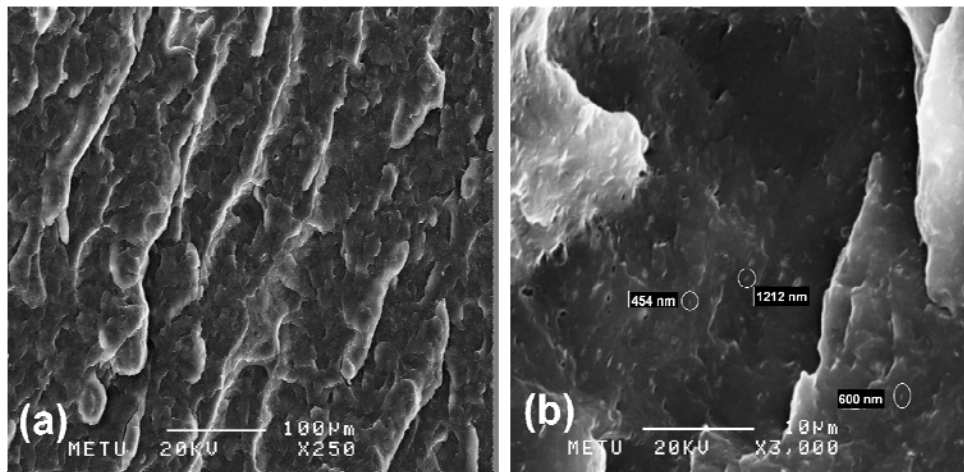


Figure 4.60 Fracture surface of PPE/TBHP2/MAPP5-M (a) x 250 magnification (b) x3000 magnification.

4.2.3.4 SEM Analysis for SET 6

Figure 4.61 shows the fractured surface of neat LLDPE. Since LLDPE samples could not be fractured by the Charpy impact test equipment, samples were immersed into liquid nitrogen and then fractured by a hammer with hand. Smooth surface of LLDPE is observed from the micrograph together with few crack propagation lines. Figure 4.62 shows blends of LLDPE-LOT prepared by 5% of LOT. Addition of 5 wt % LOT caused numerous microvoids in the LLDPE matrix associated with pull-out of LOT particles. SEM micrograph of LLDPE-LOT blend with 12.5 wt % LOT is shown in Figure 4.63. Although the LOT content is increased, no remarkable difference is detectable in the morphology of LLDPE/compatibilizer blend. The continuous and interpenetrated phases seen in the micrograph indicate that the compatibilizer is compatible with LLDPE as also confirmed by rheological analysis which will be given later.

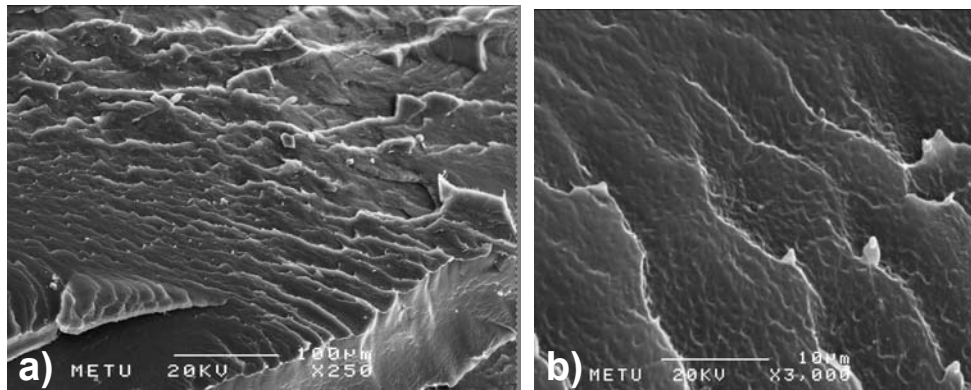


Figure 4.61 Fracture surface of LLDPE (a) x 250 magnification (b) x3000 magnification

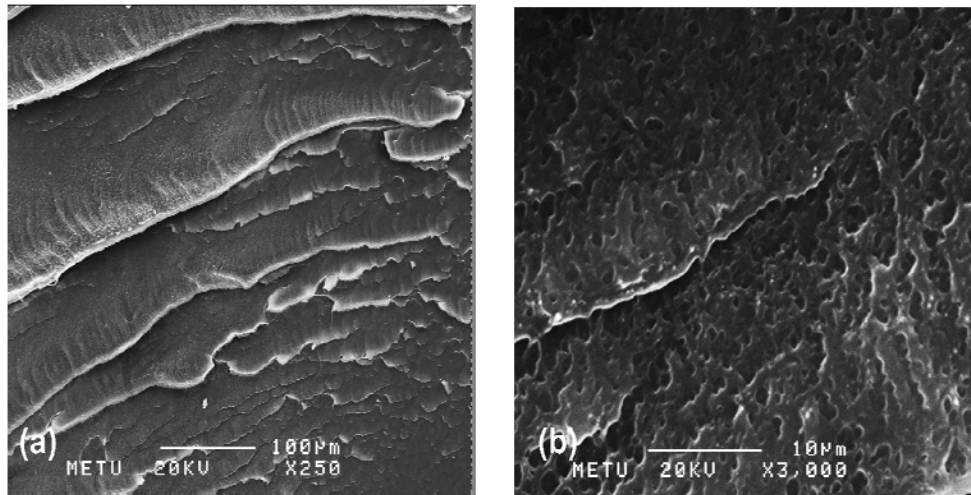


Figure 4.62 Fracture surface of LLDPE95/LOT5 (a) x 250 magnification (b) x3000 magnification

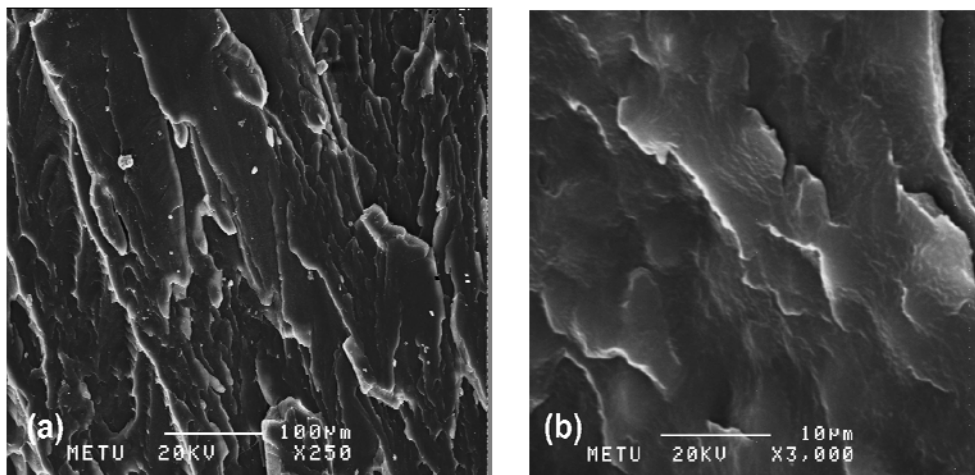


Figure 4.63 Fracture surface of LLDPE87.5/LOT12.5 (a) x 250 magnification (b) x3000 magnification

Figures 4.64 and 4.65 show the ternary composites prepared with 2 and 5 wt % of DMDA clay respectively. Compared to neat LLDPE, smooth surface is not detected and the crack propagation lines of nanocomposite surfaces are not straight lines. Through the well dispersed organoclay layers, many shorter and closer, circular, crack domains are formed and

these nonlinear cracks tend to grow until they interfere with each other. At these points, the stress fields at the tips of the crack lines interact and prevent further growth or cracks by reducing the stress at the tips of the cracks [Isik F, 2005].

The micrographs display that the incorporation of organoclay caused the crack lines on the surface of the matrix to become shorter and denser compared to the LLDPE-LOT blends, and this phenomenon was increased as clay content was increased. These tortuous paths obstruct easy propagation of the cracks. As the crack lines are smaller, the material can bear higher impact stresses. Figure 4.65 with high DMDA content shows more homogeneously distributed clay particles and elastomer phases compared to Figure 4.64. Improved mechanical properties and rheological functions of the sample with 5 wt % of DMDA also support the homogeneous dispersion of clay layers compared to the one prepared with 2 wt % of DMDA.

Figures 4.66 and 4.67 show the SEM micrographs of nanocomposites prepared with 2 and 5 wt % of TBHP organoclay respectively. While tactoids or agglomerates with a dimension ranging from 300-600 nm are observable when 2 wt % was used, these dimensions diminish to 300 nm when 5 wt % of organoclay was used. Spherical microvoids, defined as domains (caused by the pull-out of elastomeric particles), are seen in the both micrographs. They are more clearly seen, in higher numbers and are homogeneously dispersed in the sample LL/TBHP5/LOT12.5 compared to LL/TBHP2/LOT5.

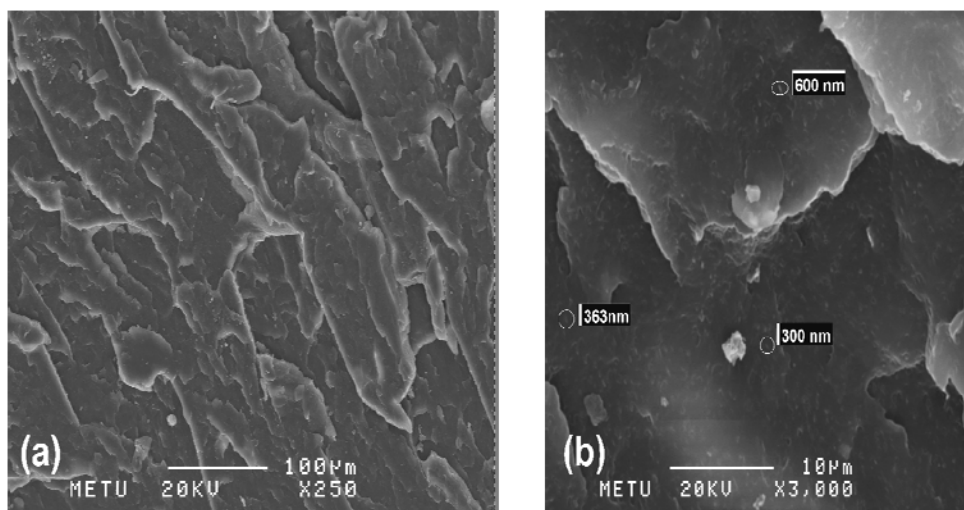


Figure 4.64 Fracture surface of LL/DMDA2/LOT5 (a) x 250 magnification (b) x3000 magnification

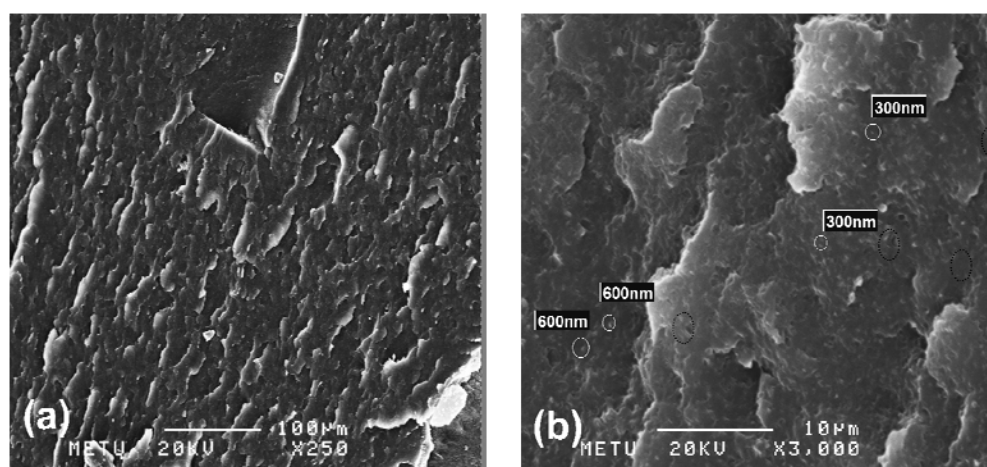


Figure 4.65 Fracture surface of LL/DMDA5/LOT12.5 (a) x 250 magnification (b) x3000 magnification

Tactoids in the composites with TBHP are more observable than in the composites prepared with DMDA, indicating that finer level of dispersion was achieved with DMDA when 5% of organoclay used.

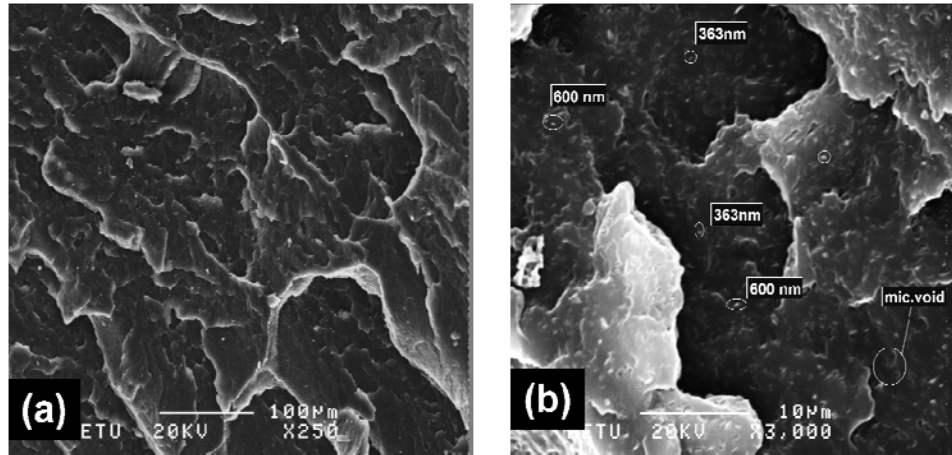


Figure 4.66 Fracture surface of LL/TBHP2/LOT5 (a) x 250 magnification (b) x3000 magnification

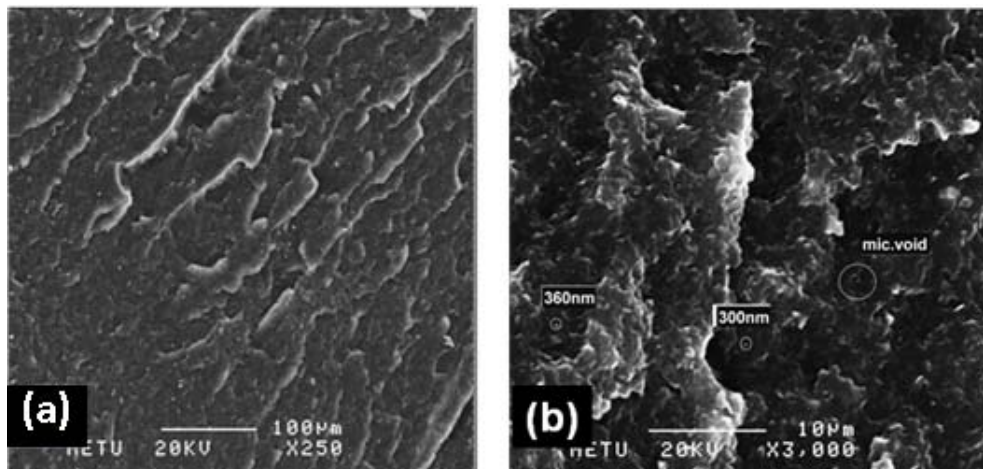


Figure 4.67 Fracture surface of LL/TBHP5/LOT12.5 (a) x 250 magnification (b) x3000 magnification

Figure 4.68 shows SEM micrograph of LL/I34-2/LOT nanocomposite. Clay particles are not clearly observable, but a few tactoids with dimensions of 600 nm are seen in the micrograph. Figures 4.69 and 4.70 show ternary composites prepared with 5 wt % of I34 with LOT concentration of 5 and 12.5 wt % respectively. Thicker clay tactoids are observable in the case of low LOT concentration compared to one with higher content of LOT indicating that clay tactoids are dispersed more in the case of high

compatibilizer concentration. Comparison of Figures 4.69 and 4.70 shows that high concentration of elastomer (LOT) usage gives rise to more homogeneous dispersion of clay layers through the matrix. As LOT concentration is increased to % 12.5 at a fixed organoclay concentration (5 w %) (Figure 4.70), the silicate layers get closer to each other and form micron sized rough surfaces. More homogeneously distributed clay networks in the case of % 12.5 LOT usage give rise to higher values of rheological functions, i.e., storage modulus and complex viscosity of the sample which will be given in subsequent parts of this study.

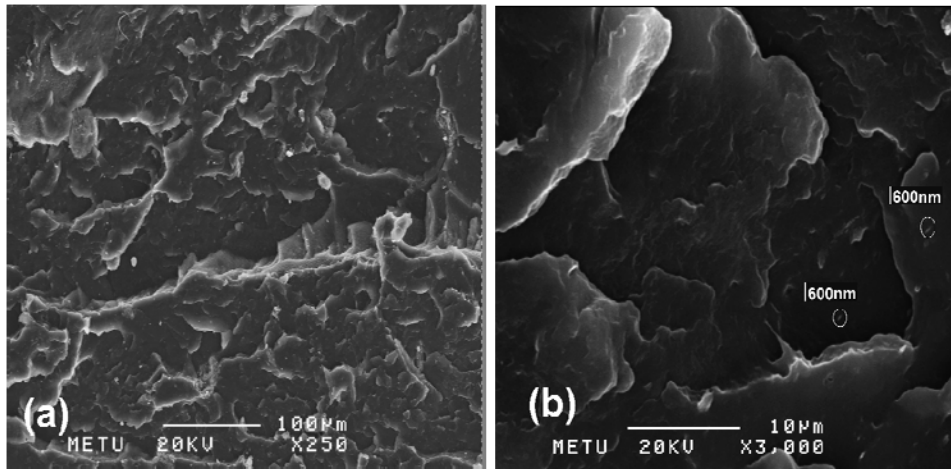


Figure 4.68 Fracture surface of LL/I34-2/LOT5 (a) x 250 magnification (b) x3000 magnification

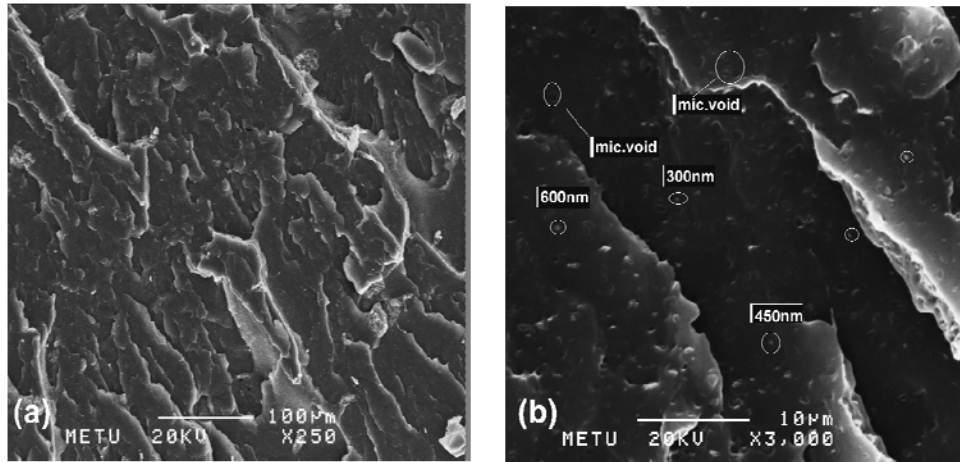


Figure 4.69 Fracture surface of LL/I34-5/LOT5 (a) x 250 magnification (b) x3000 magnification

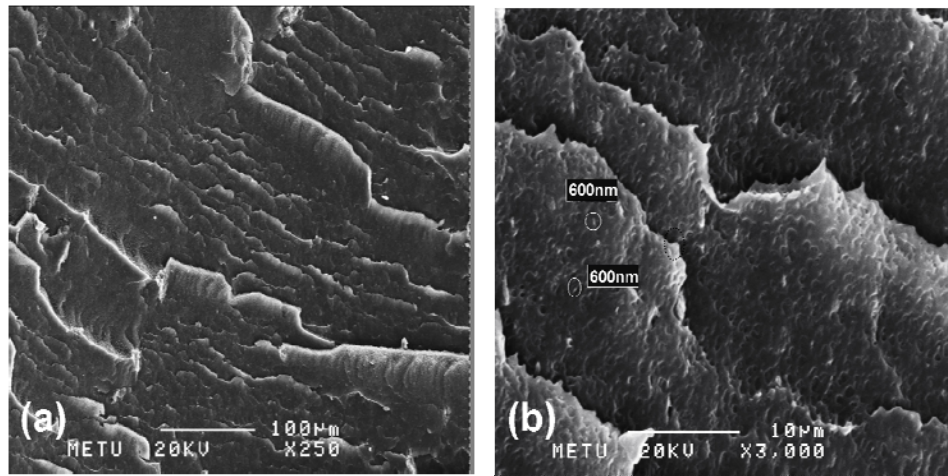


Figure 4.70 Fracture surface of LL/I34-5/LOT12.5 (a) x 250 magnification (b) x3000 magnification

4.2.4 DSC Analysis

4.2.4.1 DSC Results of PPM and PPE Based Composites (SETs 1-4)

Thermal characteristics of PPM, PPM/MAPP blends and PPM/organoclay/MAPP composites were investigated using DSC. Table 4.5 summarizes the DSC results of PPM based composites in terms of melting temperature, T_m , heat of fusion of the sample ($\Delta H(J/g)$) and % crystallinity. DSC thermographs of the samples are given in Appendix A.1. In the binary blend, addition of MAPP to PPM slightly increased the crystallinity of the PPM. Ternary composites of PPM/organoclay2/MAPP2 with MAPP/organoclay ratio, α , of 1 generally showed slight increase in the crystallinity. This could be due to nucleation effect of the clay. When the clay content was lower, as in PPM/TKA1/MAPP3 no significant increase was observed in the crystallinity, and it did not show any dispersion as observed by XRD.

However, in the PPM/HMA1/MAPP3 ternary nanocomposites the clay exhibited intercalation/exfoliation and owing to the nucleation effect of the clay, the crystallinity is significantly higher than that of PPM.

Table 4.5 DSC results of PPM, PPM/MAPP blend and PPM/MAPP based composites prepared in SET-1

	T_m (°C)	PPM wt %	ΔH (J/g)	X_c (%)
PPM	166.5	100	82.00	39.23
PPM98/MAPP2	165.3	98	85.33	41.66
PPM/TBA2/MAPP2	168.6	96	78.78	39.26
PPM/TBP2/MAPP2	166.0	96	80.65	40.195
PPM/HMA2/MAPP2	165.3	96	85.96	42.84
PPM/TKA2/MAPP2	166.1	96	82.92	40.88
PPM/Cloisite®25A2/MAPP2	167.0	96	80.42	40.08
PPM/HMA1/MAPP3	164.6	96	93.82	46.76
PPM/TKA1/MAPP3	164.7	96	77.14	38.45

Tables 4.6 and 4.7 show the DSC results of the samples prepared in SET-2 and SET-3-4 respectively. DSC thermograms of these sets are given in Appendices A.2, 3 and 4 respectively. Ternary composites of PPE/organoclay2/MAPP5 samples show slight increase in crystallinity due to the nucleation effect of the clay. Melting temperatures of the ternary composites decrease slightly as observed from Tables 4.6 and 4.7 probably due to the impurity effect of MAPP on PPE, similar to “freezing point depression”.

Table 4.6 DSC results PPM and its composites prepared in SET-2

	T_m (°C)	PPE wt %	ΔH (J/g)	X_c (%)
PPE	167.2	100	85.42	40.87
PPE/HMA2/MAPP5	167.2	93	79.62	40.97
PPE/TKA2/MAPP5	167.2	93	86.41	44.46
PPE/TKA50-2/MAPP5	165.9	93	83.06	42.73
PPE/PGWTKA2/MAPP5	166.2	93	80.45	41.39

Table 4.7 DSC results PPE and its blend and composites prepared in SETs 3-4

	T_m (°C)	PPE wt %	ΔH (J/g)	X_c (%)
PPE	167.2	100	85.42	40.87
PPE-M	166.8	100	90.17	43.14
PPE/DMDA2/MAPP5	165.9	93	84.70	43.58
PPE/DMDA2/MAPP5-M	164.8	93	84.69	43.57
PPE/TBHP2/MAPP5	165.8	93	83.51	42.97
PPE/TBHP2/MAPP5-M	165.7	93	86.49	44.50
PPE/STKA2/MAPP5	166.8	93	83.82	43.12
PPE/STKA2/MAPP5-M	165.9	93	85.29	43.88

Thermal characteristics of LLDPE, LLDPE/LOT blends and the LL/organoclay/LOT ternary nanocomposites were investigated using DSC.

Table 4.8 summarizes the DSC results of LLDPE based composites in terms of melting temperature, T_m , heat of fusion of the sample (ΔH (J/g)) and % crystallinity. DSC thermographs of the samples are given in

Appendix A.5. Thermographs show that the crystallization of LLDPE/LOT blend and LL/organoclay/LOT composites are similar in shape, and melting temperatures are similar to that of neat LLDPE.

Table 4.8 shows 5 wt % of LOT addition lowers crystallinity and heat of fusion of LLDPE considerably. Surprisingly 12.5 wt % addition of LOT did not have much effect on crystallinity of LLDPE. This is valid in the LLDPE/LOT blend as well as in the ternary nanocomposites. In the case of nanocomposites with 12.5 wt % LOT, the organoclay contents is also higher (5 wt %) and the dispersion of clay is better. All of these factors lead to the nucleation effect, thus increasing the crystallinity.

Table 4.8 DSC results LLDPE and its blend and composites prepared in SET-6

	T_m (°C)	LLDPE wt %	ΔH (J/g)	X_c (%)
LLDPE	122.1	100	104.4	35.63
LL95/LOT5	123.0	95	85.43	30.60
LL87.5/LOT12.5	124.0	87.5	93.68	36.54
LL93/DMDA2/LOT5	121.2	93	85.65	31.40
LL82.5/DMDA5/LOT12.5	122.6	82.5	72.9	35.10
LL893/TBHP2/LOT5	121.5	93	81.9	30.10
LL82.5/TBHP5/LOT12.5	121.6	82.5	77.5	32.10
LL93/I34-2/LOT5	121.5	93	84.3	30.90
LL93/I34-5/LOT5	121.2	90	87.53	33.19
LL82.5/I34-5/LOT12.5	121.5	82.5	78.3	32.40

4.2.5 Mechanical Characterization

“The mechanical behavior of a polymer composite system relies on the type and the amount of the deformation mode that dominates during sample loading up to ultimate failure. Strength and toughness mainly depend on the molecular properties of base polymer, on molecular packing, (density, phase structure, micro-morphology), on the way stress is transmitted between them and on the features and intensity of relaxation mechanism” [Michler, 2005]. The mechanical properties of filled polymer systems mainly depend on the degree of dispersion of the reinforcing material, degree of forces that binds atoms together, thus the quality of the interfacial adhesion.

In the case of addition of fillers to a matrix in order to have reinforcement, the filler component which is strong and stiff bears most of the load or stress applied to the matrix while the polymer matrix which is of low strength, quite tough and extensible effectively transmits the load to the filler. This load transfer necessitates matrix to have sufficiently high cohesive and interfacial shear strength. Thus, in addition to the filler and the polymer, the interphase, inevitable region between two, plays a crucial role in the fabrication and subsequent behavior of the filled polymer systems. The interphase is the region separating the filler from the polymer and comprises the area in the vicinity of the interface [Shenoy, 1999].

This section presents the tensile properties of the samples prepared in different set of composites. In this respect, Young’s modulus (YM), tensile strength (TS), yield stress (YS), % elongation at break (% ϵ -break), % elongation at yield (% ϵ -yield) measurements of the composites are given.

4.2.5.1 Tensile Tests of PPM Based Composites (SET-1)

Typical stress-strain diagram of PPM based composites are shown in Figure 4.71. PPM shows ductile behavior and yields at a particular strain. After yielding, material experiences a period of cold drawing, and then strain hardening occurs due to stretching of polymer chains in the direction of load. Twice extruded neat PPM has tensile strength, Young's modulus, % elongation at break values of 39 MPa, 1512 MPa and 422 respectively. Neat, (unprocessed, just injection molded) PPM shows slightly higher values compared to twice extruded PPM. Addition of MAPP into the PPM decreased its Young's modulus (YM) due to its elastometric, dilution character, since MAPP has lower modulus compared to PPM. YM and TS of MAPP are given as 991 MPa and 32 Mpa, respectively by Cengiz, 2008. While MAPP decreases YM, at the same time, it enhances the elongation at break of PPM.

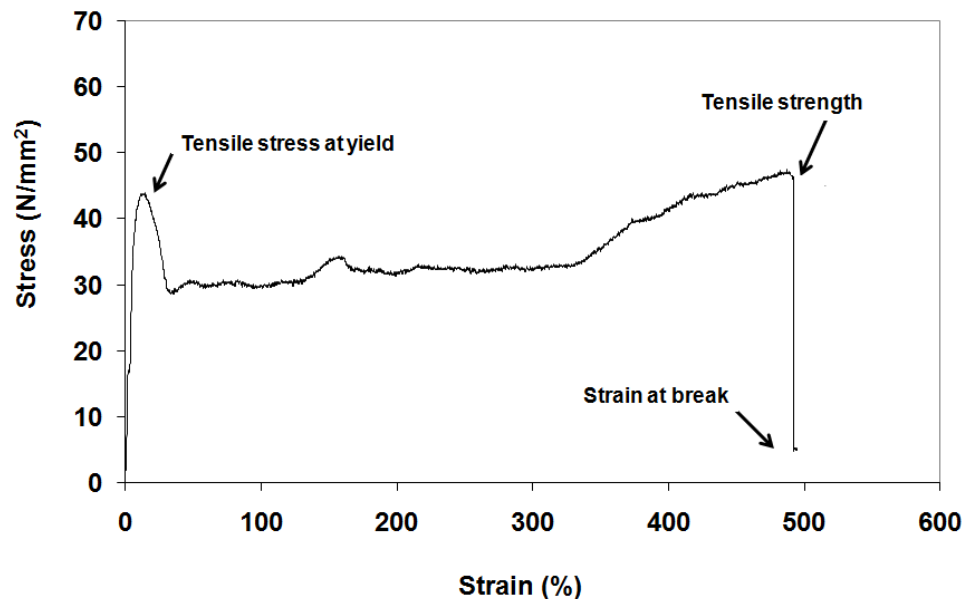


Figure 4.71 Typical stress-strain diagram of PPM

Effect of organoclay type and different ratio of MAPP/organoclay (α) on TS can be seen in Figure 4.72 for composites prepared in SET-1. The first three bars in the figures represent neat PPM, extruded PPM and PPE98/MAPP2 mixture respectively. Following bars with same shade

effect show the composites prepared with same organoclay but with different α values, where first one represents the composites of PPM/Organoclay2/MAPP2 ($\alpha = 1$), second one represents the composites of PPM/Organoclay1/MAPP3 ($\alpha = 3$) samples. Last bar represents the results obtained with Cloisite®25 A. TBA and TBP had little increase in the d-spacing compared to TKA and HMA, therefore samples with $\alpha = 3$ were prepared with only TKA and HMA, since low d-spacing indicates low degree of dispersion of the clay layers in matrix [Tjong, 2006]. X-Ray data of composites (Figures 4.13 through 4.16) showed limited dispersion of clays through the PPM matrix, and this effect can be seen in tensile strength properties as well (Figures 4.72 and 4.73). If clay particles had exfoliated, larger surface would have formed between the clay particles and the polymer, making the stress transfer to the clay layers more effective, resulting increase in the tensile properties [Velasco et al., 2005]. Figure 4.74 shows enhancements in the Young's modulus of the nanocomposites regardless of the clay type. For samples with $\alpha = 1$, Young's modulus of the PPM increases with melt mixing with organoclay and elastomer in the case of TBA, TBP, HMA but not much with TKA. Young's modulus enhancements obtained in SET-1 with $\alpha = 1$ may be attributed to orientation of clay layers and polymer crystals in addition to other factors such as the concentration of clay, adhesion between the clay-polymer-compatible interfaces, the way stress is transferred through the matrix. Also, tactoids of clay particles residing in the matrix may have a high aspect ratio leading the reinforcement effect. Surprisingly, organoclays with small d-spacing obtained with short alkyl tail surfactant, TBA and TBP showed higher modulus values compared to TKA and HMA whose d-spacings are much higher. Since lower d-spacing does not mean that the aspect ratio is lower, enhancements are attributed to possible high aspect ratio of TBA and TBP organoclays.

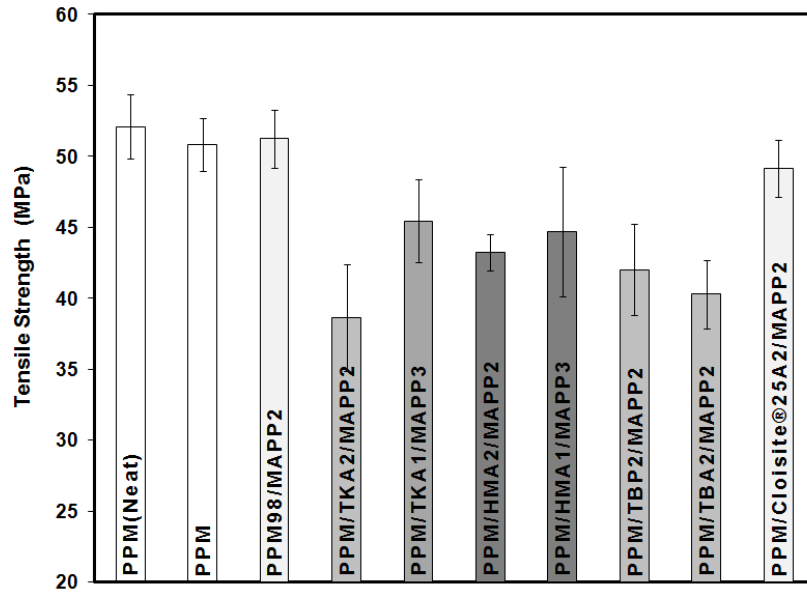


Figure 4.72 Effect of organoclay type on tensile strength of PPM/Organoclay2/MAPP2 and PPM/Organoclay1/MAPP3 composites prepared in SET-1

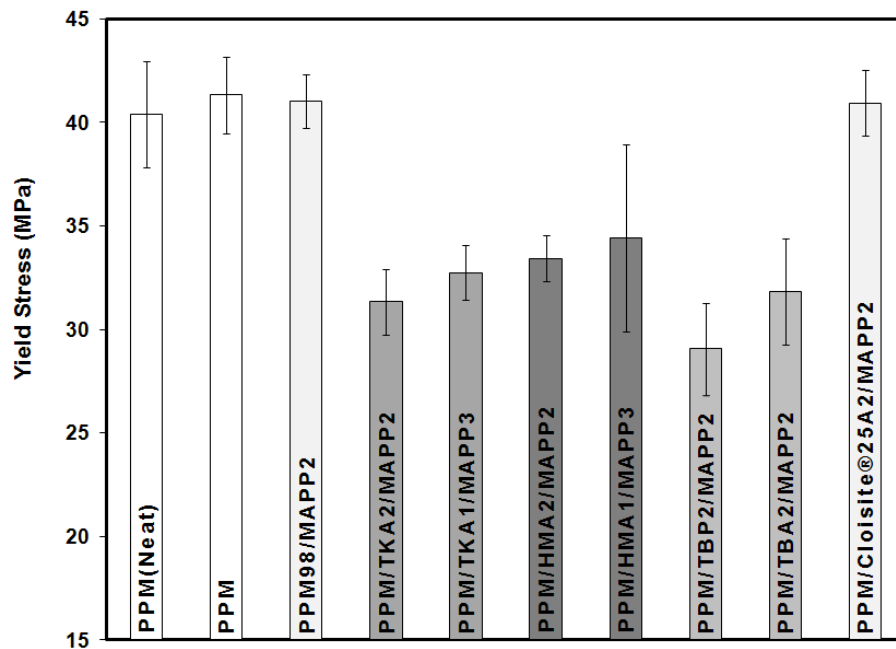


Figure 4.73 Effect of organoclay type on tensile stress at yield of PPM/Organoclay2/MAPP2 and PPM/Organoclay1/MAPP3 composites prepared in SET-1.

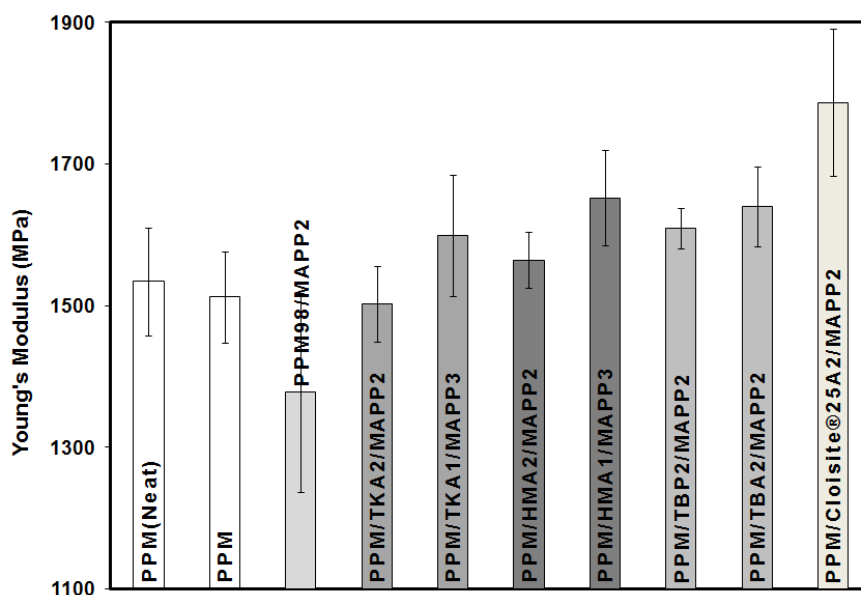


Figure 4.74 Effect of organoclay type on Young's modulus of PPM/Organoclay2/MAPP2 and PPM/Organoclay1/MAPP3 composites (SET1).

Young's modulus of the samples with $\alpha = 3$ are higher compared to sample with $\alpha = 1$, possibly due to high concentration of MAPP used. Increase in the MAPP concentration was found to increase the dispersion of clay layers due to increased adhesion between compatibilizer and organoclay [Hotta and Paul, 2004]. XRD analysis of composite (Figure 4.17) prepared with HMA with $\alpha = 3$ showed broadened and reduced intensity of the clay, also proving the presence of increased adhesion and higher number of delaminated clay layers. Kim et al., 2007 studied PP/organoclay/MAPP nanocomposites with TEM using different MAPP/organoclay ratios and observed that the degree of dispersion was evidently increased as the MAPP/organoclay ratio increased regardless of the total clay concentration. High concentration of MAPP leads to better clay dispersion and adhesion corresponding to increase in the reinforcement as seen in Figure 4.74. Improved properties due to MAPP

may also be explained in terms of the imide bond formation between nucleophilic ammonium/phosphonium groups of the clay and maleic anhydride (MA) groups. Organoclay surfaces exist in an acid-base equilibrium which is ready to react as nucleophile with the carbonyl groups on the MAPP. These interactions yield increase in the adhesion [Quintanilla, 2006]. In addition, enhancement in the case of HMA clay may be attributed to increase in the degree of crystallinity of the composites with the addition of organoclay. Table 4.5 shows that % crystallinity of PPM increased from 39 to 46.76 with ternary composite formation when α was equal to 3 for the HMA organoclay.

It is mentioned in the literature that, interfacial adhesion has an important effect on strength; on the other hand, modulus is much less affected by the nature of the interface [Fornes et al., 2002]. XRD analysis of composites prepared in SET-1 had shown limited dispersion in the matrix and tensile strength of the ternary composites (Figure 4.72) were lower compared to that of, pure PPM, most probably due to weak interfacial attraction between the silicate layers and the matrix. Also, organoclays used in SET-1 were prepared from unpurified bentonite samples, which contain non-clay impurities. In the absence of impurities and flaws, the mechanical properties of PLSN depend on the degree of forces that binds the atoms together. But in this case, raw bentonite used contains contaminants such as quartz, silica, feldspar, sodium carbonate, and chlorite and so on [Gupta, 2010]. These particles probably caused poor adhesion of the polymeric matrix to the clay particles, forming holes at the interphase, which act as defects and stress concentrators in the matrix assisting the failure mechanism [Gupta, 2010]. Also, plasticization effect which may arise from the unintercalated alkyl surfactants may cause contamination at the processing temperature. As also mentioned previously in the XRD part, modifiers with bulky alkyl tails (TKA and HMA) may locate between the particles of clay layers and not in between the galleries inducing plasticization effect at the processing temperature and decreasing the composite properties.

Poor tensile strength values of ternary composites may also be attributed to high viscosity, in other words high molecular weight of PPM, which has an MFI between 4-6 g/10 min. This high viscosity matrix may cause clay layers to be fragmented under high shear stress during compounding which further may cause reduction in the aspect ratio of the filler. Highly viscous matrix may also limit the diffusion of clay layers through the matrix. Also, chemical degradation due to decomposition of organoclays or moisture, can reduce the molecular weight of the PPM, thus partially decrease the mechanical properties such as tensile strength.

Samples prepared with the commercial organoclay Cloisite®25 A shows higher YM compared to one prepared with modified organoclays prepared in this study as well as pure PPM. Comparison of structure of Cloisite®25A with HMA, shows that Cloisite®25A with two long alkyl tails may favor intercalation owing to its higher d-spacing. Also, higher purity MMT used in the Cloisite®25A can be taken as another reason for a more strong clay network. Compatibility between the phases in turn enhances the YM. Nevertheless, it also has limited capability in increasing the TS and stress at yield as shown in Figures 4.72 and 4.73. The results point out to the difficulty of dispersing the clay particles in PPM which has high viscosity.

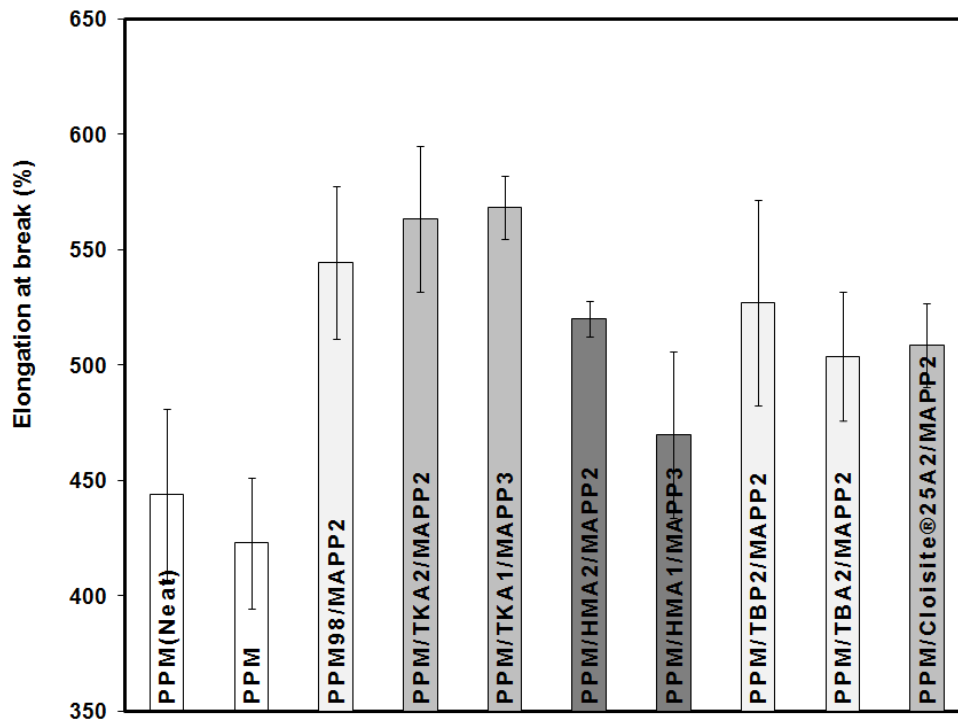


Figure 4.75 Effect of organoclay type on elongation at break of PPM/Organoclay2/MAPP2 and PPM/Organoclay1/MAPP3 composites prepared in SET-1.

Figure 4.75 shows the elongation at break of the samples. Organoclay addition to PP/MAPP binary blend has positive effect on % elongation at break, which may be due to high extensibility of the MAPP domains. Nielsen notes the sensitivity of elongation at break to adhesion between the constituents or partial miscibility at the interface of blend components in phase separated systems. Thus, enhancements in the % elongation at break in ternary nanocomposites may be attributed to adhesion between by the clay particles and the compatibilizer. In ternary nanocomposites, dispersed clay layers act as crack stoppers leading to high ϵ_B . Elongation at break values of composites prepared with TKA, given in Figure 4.75, (both with $\alpha = 1$ and 3) are higher compared to that of the composite prepared with Cloisite ®25 A.

4.2.5.2 Tensile Tests of PPE Based Composites (SET-2)

In this set of experiments, PPE based ternary composites with 2 wt % of organoclay and 5 wt % of MAPP were prepared at screw speed of 350 rpm and at a temperature of 180°C. PPE used in SET-2 has an MFI value between 20-24 g/10 min which is much higher than that of PPM which has an MFI between 4-6 g/10 min. In addition, organoclay prepared with high surfactant concentration (TKA50) was also used in preparation of ternary composites to understand the effect of high concentration of salt usage. Pure commercial MMT was also modified with TKA (PGWTKA) to see if delamination could be obtained by the use of it.

Figures 4.76 – 4.80 show the tensile properties of ternary composites of PPE/organoclay2/MAPP5 samples. Ternary composites prepared with HMA, TKA and TKA50 clay show enhanced YM and yield stress, while reduction was observed in tensile strength and elongation at break and elongation at yield. Fig. 4.76 show the YM of ternary composites with different organoclay types. The composites showed higher YM compared to pure PPE. When HMA and TKA organoclays are analyzed, both have a positive effect in modulus, while TS of the matrix was lowered in the case of HMA (Fig. 4.78). XRD analysis had shown that composites with TKA and HMA had no intercalation. However, even in microcomposites, owing to better interfacial interactions and the effects of shearing forces, a reduction in the tactoid thickness and hence increase in the aspect ratio can be assumed [Mittal, 2007(a)]. This high aspect ratio may lead to increase in interfacial area and stress transfer mechanism enhancing the YM. XRD analysis had shown that organoclay HMA had a d-spacing of 1.78 nm, while organoclay TKA had higher d-spacing, 2.56 nm. Higher gallery distance of TKA may aid dispersion of clay layers and insertion and diffusion of polymer chains between the high interspace.

Since XRD analysis of composites prepared with TKA showed decrease in the d-spacing, enhancements in the YM and TS can also be explained

by increased crystallinity (measured by DSC analysis) and reduction in the spherulite size [Dashmene et al., 2007; Vlasveld et al., 2005]. Higher nucleation density provided by the clay decreases the spherulite size [Dashmene et al., 2007]. While % crystallinity of pure PPE is 40.9, it is 44.5 in the PPM/TKA2/MAPP5 nanocomposite. Increased crystallinity increases YM and TS but it decreases the ductility. However, % elongation at break value of composite of TKA is slightly higher than that of PPE as shown in Fig.4.79. Increased interfacial adhesion between organoclay and matrix increases the elongation at break, showing materials ability to absorb more energy, while clay particles provide a tortuous path for crack propagation. Assessing the degree of delamination of clay layers solely on XRD may lead to wrong conclusion as in this case, while mechanical properties and DSC results indicate relatively better dispersion or adhesion of the TKA organoclay in the matrix.

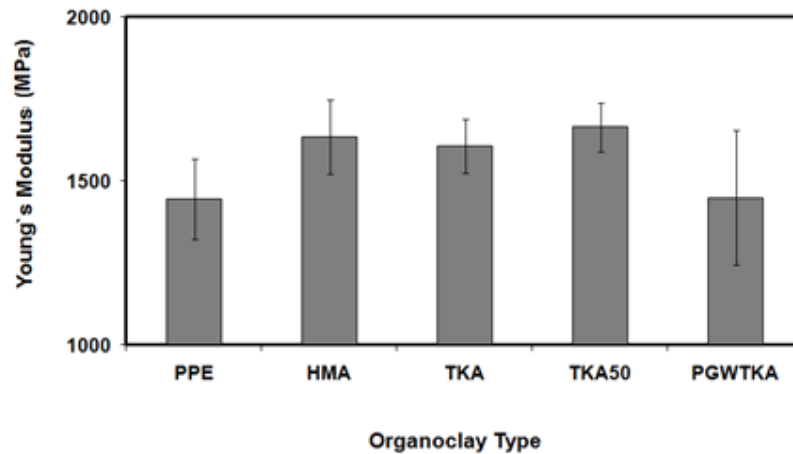


Figure 4.76 Effect of organoclay type on Young's modulus of PPE/Organoclay2/MAPP5 composites prepared in SET2.

When XRD of composites prepared in this set are considered, a contradiction arises between the mechanical properties and XRD results of composites prepared by HMA and TKA50 when modulus is considered. These enhancements can be explained by the flow induced clay

orientation during injection molding. Modulus of PLSN mainly depend on the degree of delamination of clay layers, modulus of polymer and clay platelets, clay loading, degree of crystallinity, orientation of clay layers, orientation of polymer crystallites and interfacial stress transfer mechanism [Galgali et al., 2004]. Since DSC of composites prepared with HMA and TKA50 did not show much change in the % crystallinity, enhancement may be explained by the reinforcement effect of high aspect ratio clay platelets due to fractured clay agglomerates or tactoids. As previously mentioned, modulus is less sensitive to interfacial adhesion compared to TS. Fig. 4.78 shows that the TS of the composites prepared with HMA and TKA50 are slightly lower than that of TKA implying lower interfacial adhesion compared to TKA.

PGWTKA with high basal spacing (2.83 nm) did not enhance the modulus and tensile strength (Figure 4.78) of the PPE, while it increased at yield stress value (Fig. 4.77) of the composite. These enhancements are attributed to flow induced clay orientation during injection molding. Since its XRD analysis showed no intercalation, mechanical properties also indicate poor dispersion of this clay within PPE matrix.

% elongation at break of composites given in Figure 4.80 show lower values for composites prepared with HMA and TKA50, indicating poor adhesion compared to TKA. Generally TS, YM and % elongation at break values of composites prepared with TKA showed enhancement compared to pure PPE. Tensile strength is higher than those of the composite prepared with TKA50 showing the adverse effect of using excess surfactant during the modification process, which was also confirmed by XRD analysis.

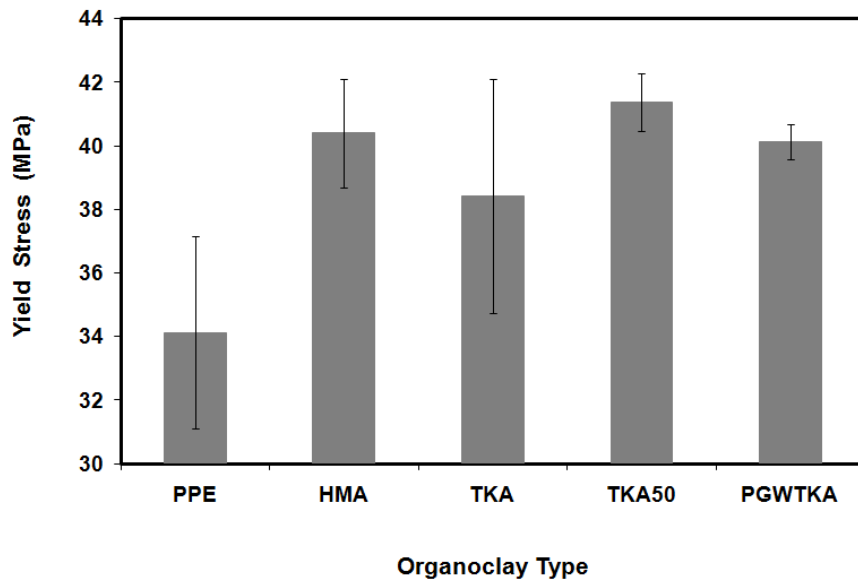


Figure 4.77 Effect of organoclay type on yield stress of PPE/Organoclay2/MAPP5 composites prepared in SET-2.

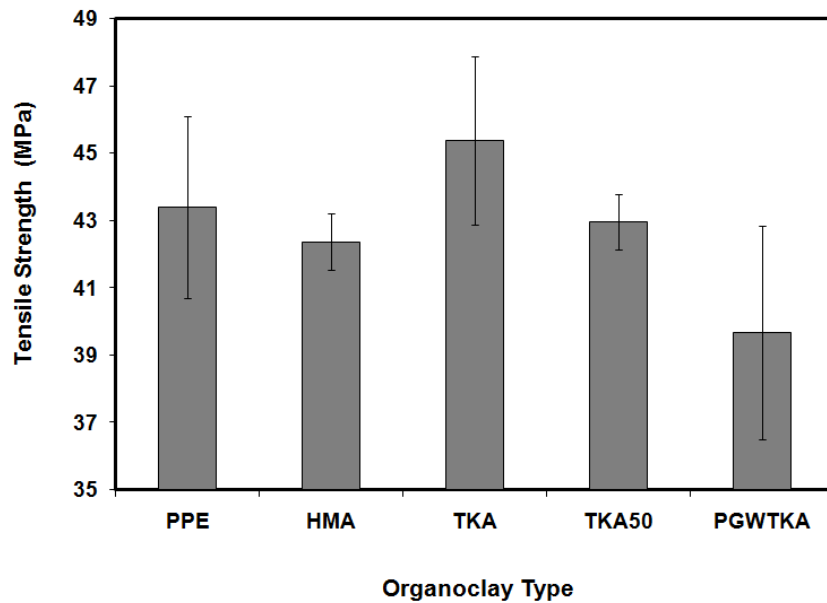


Figure 4.78 Effect of organoclay type on tensile strength of PPE/Organoclay2/MAPP5 composites prepared in SET-2.

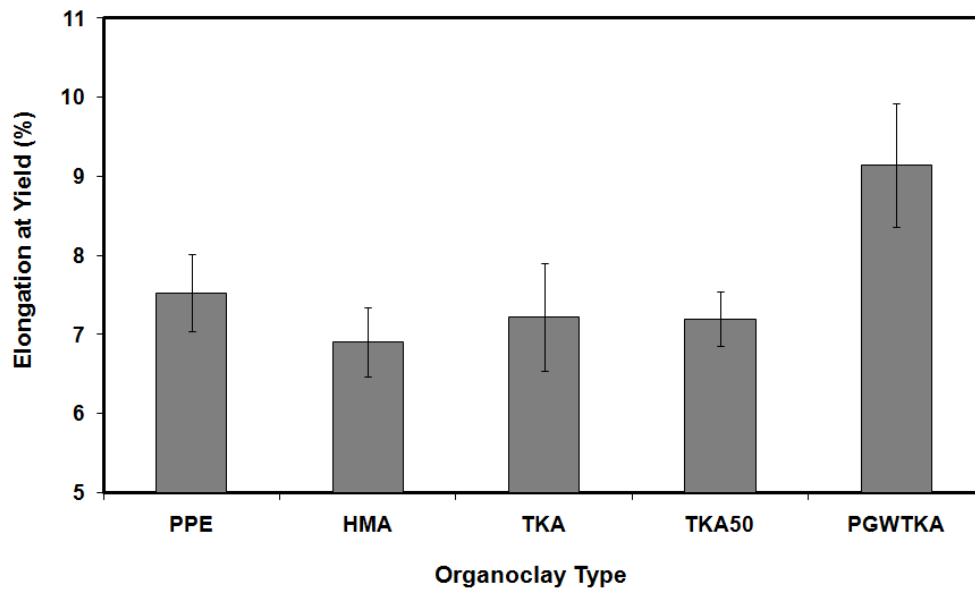


Figure 4.79 Effect of organoclay type on elongation yield of PPE/Organoclay2/MAPP5 composites prepared in SET-2

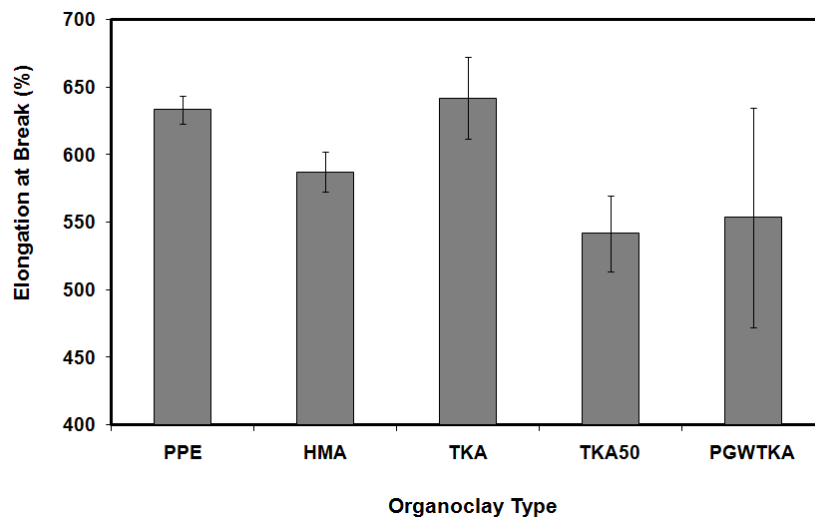


Figure 4.80 Effect of organoclay type on elongation at break of PPE/Organoclay2/MAPP5 composites prepared in SET-2

4.2.5.3 Tensile Tests of PPE Based Composites (SET-3 and 4)

Representative stress-strain diagram of composites prepared in this set is given in Figure 4.81. In sample preparation, 2 wt % of organoclay prepared from purified bentonite and 5 wt % of MAPP were processed in extruder and then further mixed in the batch mixer. Sample prepared by extrusion followed by batch mixing are abbreviated with M at the end of composite concentration. “Extruded only” samples have no M at the end of their abbreviations. In the figures, the first column represents “extruded only” samples, while second ones represent extruded + batch mixed samples.

While PPE shows a yield point at a specific strain and then elongates due to cold drawing and strain hardening, ternary composites composed of DMDA and STKA clay do not show strain hardening. TBHP also shows strain hardening, but the tensile stress values at break is the same or lower than the yield stress. PPE-M has tensile strength at break and stress at yield values of 54 MPa and 43.1 MPa respectively. “Extruded only” PPE has tensile strength at break and stress at yield of 52.24 MPa and 39.8 MPa. Young`s modulus of PPE-M and PPE are 1302.5 MPa and 1351 MPa, respectively.

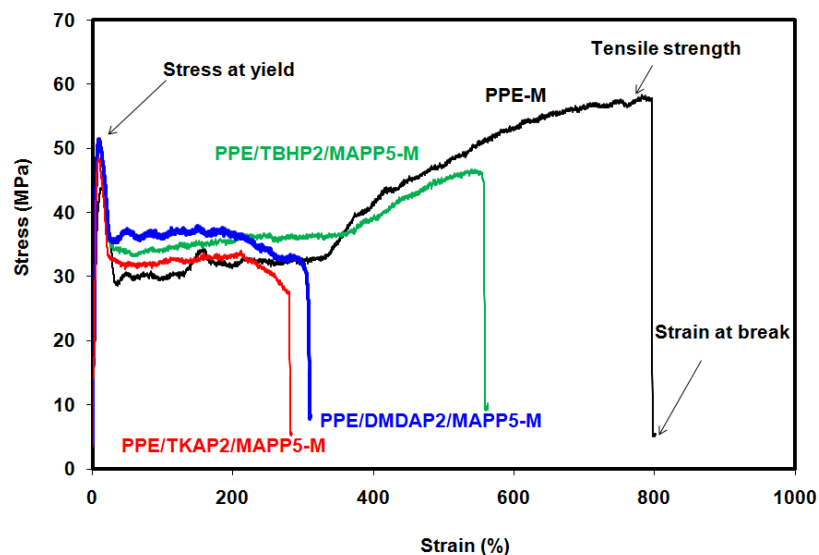


Figure 4.81 Representative stress-strain diagram of PPE-M based composites.

Figure 4.82 and Figure 4.83 show the variation in yield stress and Young's modulus with respect to organoclay type. Since previous studies on PP/Organoclay/MAPP composites, either conducted in the previous thesis studies [Cengiz, 2008; Yayla, 2007] and in the literature [Hasegawa et al., 2006; Kim et al., 2007] focused on the effect of MAPP or elastomeric materials on PPE in detail, binary composites of PPE and MAPP were not studied in this respect.

Figures 4.82 and 4.83 show increase in the yield stress (YS) and modulus obtained by addition of compatibilizer and organoclay regardless of the type organoclay used (except PPM/DMDA2/MAPP5), meanwhile decreases were seen at the same time (Figures 4.84 and 4.85) in elongation at yield and break values. An increase in yield stress and YM due to decreased elongation ability is known for clay incorporation in PLSN, because inorganic particles cannot be strained by external stresses but behave as stress concentrators in the matrix during the straining process [Contreras et al., 2006]. All ternary nanocomposites showed an increase in yield stress and YM after more shear was applied

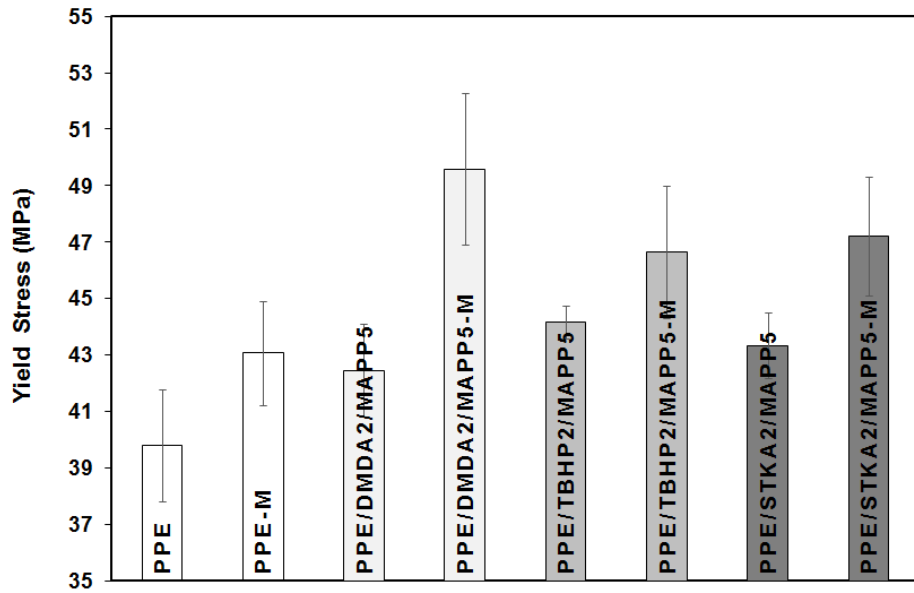


Figure 4.82 Effect of organoclay type on yield stress of PPE/Organoclay2/MAPP5-M composites prepared in SETs-3 and 4.

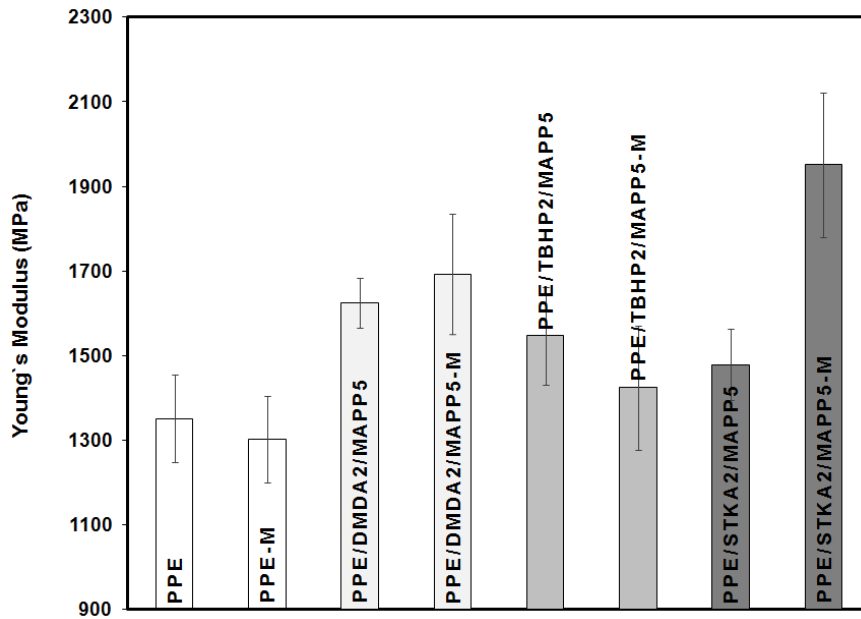


Figure 4.83 Effect of organoclay type on Young's modulus of PPE/Organoclay2/MAPP5-M composites prepared in SETs-3 and 4.

by melt mixing as explained by increased organoclay dispersion observed by XRD analysis. XRD results of composites prepared by DMDA and TBHP showed increase in the d-spacing of the material compared to “extruded only” samples, meaning intercalation had occurred owing to more applied shear. As previously mentioned, the degree of delamination of clay layers depends on the compatibility between the particle and matrix, d-spacing of clay, (chemical structure of organoclay modifier, elastomer and matrix) [Vaia et al. 1995; Vaia and Giannelis, 1997; Balazs et al, 1998; Isik, 2007] and also severe processing conditions, and applied shear during the processing [Lertwimolnun et al., 2006; Modesti et al., 2005; Isik et al., 2008; Demirkol and Kalyon, 2007]. From processing point of view, two parameters are important. During melt blending of clay into a polymer, organoclay layers slide apart from each other. Clay layer delamination can also be increased by diffusion of polymer chains into the spacing between the clay layers [Modesti et al., 2005]. Diffusion mechanism may be taken as less significant, probably due to high melt flow index of polypropylene, PPE, used in this set of experiments. Compatibility between the phases was shown to increase by more applied shear by XRD and TEM analyses. More applied shear and long residence time are the key factors enhancing the dispersion of clay layers and the tensile properties of the PPE-M based nanocomposites. As more shear reduces the tactoid particles or the size of the intercalated stacks, more delamination occurs in the case of high adhesion and compatibility between the clay layers and matrix [Cho and Paul, 2001]. For intercalation to occur, polymer must be transported from the agglomerate/polymer interphase to the primary particles and then to the edges of the tactoids [Vaia et al., 1995], where oblong shaped primary particles form the agglomerates. Primary particles consist of condensed face-to-face stacking of individual tactoids. Mentioned transportation may also be enhanced by applied shear besides chemical compatibility.

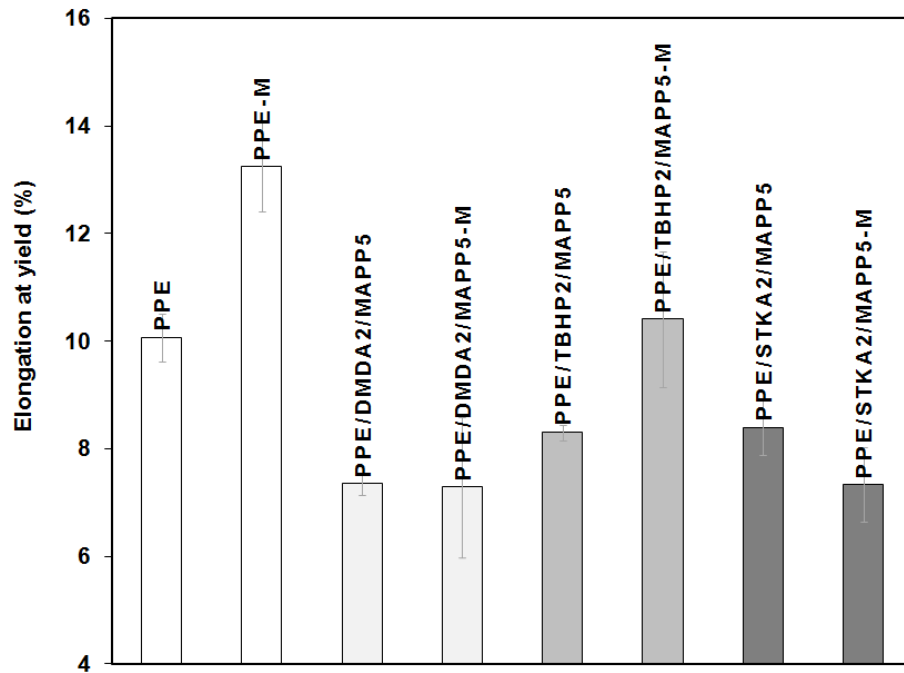


Figure 4.84 Effect of organoclay type on elongation at yield of PPE/Organoclay2/MAPP5-M composites prepared in SETs-3 and 4

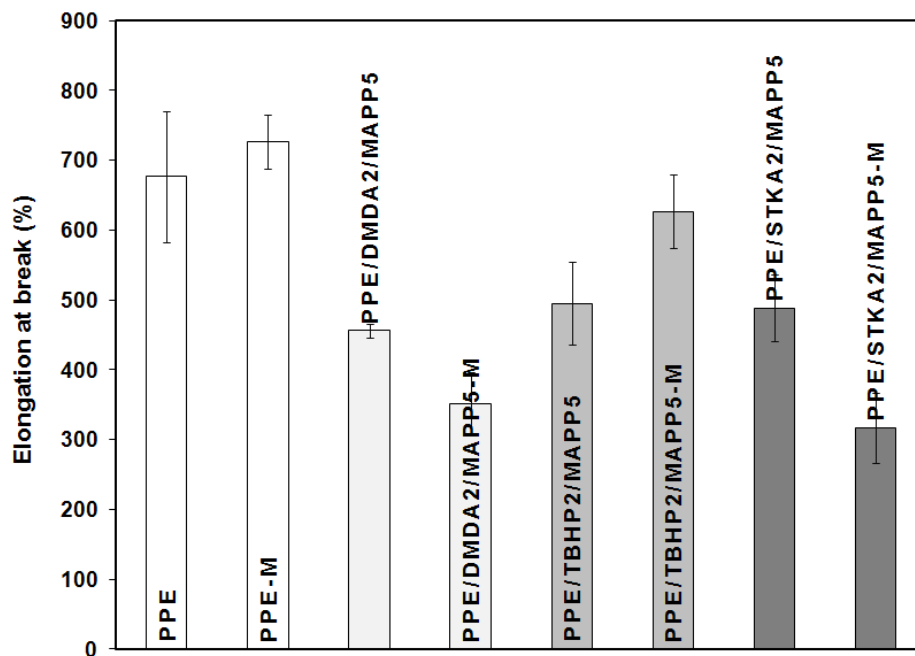


Figure 4.85 Effect of organoclay type on elongation at break of PPE/Organoclay2/MAPP5-M composites prepared in SETs 3 and 4.

Ratio of surface area to volume of the filler increases enhancements in the mechanical properties of samples. Induced and increased specific energy input (given by Eq. 3.3, a measure of energy generated by mixing), increases as exfoliation takes place which also give rise to elasticity and shear viscosity of the sample [Kalyon et al., 2006].

Figures 4.84 and 4.85 show the % elongation at yield and break for the composites in this set, where a reduction is observed due to formation of nanocomposites compared to neat PPE matrix. In classical analysis of the effect of fillers on elongation, it is thought that the extension is due to the matrix, and the filler cannot extend much. Thus, the elongation at yield and break decreases with the filler content. When elongation at break of the ternary composites are analyzed, nanocomposites prepared with both extrusion and batch mixing exhibit higher results compared to “extruded only counterparts”, which is attributed to higher dispersion and strong interfacial interactions between the clay and matrix obtained by high shear. Again, it should be noted that elongation at break is sensitive to increased adhesion between the phases.

4.2.5.3.1 Effect of Organoclay Type

Composites prepared with DMDA show superior properties in modulus and yield stress (Figures 4.82 and 4.83) compared to one prepared with TBHP and STKA. XRD analysis of composites prepared with DMDA show intercalation of clay layers, while TEM analysis show partially intercalated clay layers, few exfoliated layers and tactoids present in the system. Meanwhile the same conclusions can be envisaged for the TBHP; even more ordered layers are present in this system compared to DMDA based on TEM results. When structure of DMDA and TBHP cations are compared, DMDA has two long alkyl tails with 18 C in each of them, TBHP has one long alkyl tail with 16 C atoms. In addition, TBHP has three more alkyl tails with 4 C in each of them, while DMDA has rather short methyl groups in two tails. As previously mentioned, it gets harder to enter

between the clay layers for polymers as alkyl tails of the surfactant increases. As the number of alkyl tails increases, it limits the entry of polymer segments into the clay layers more, sheltering the polymer-organoclay interactions and generating a more hydrocarbon-like environment [Fornes et al., 2002].

In contrast to XRD analysis, composites produced by STKA clay show higher modulus and tensile strength compared to TBHP and TKA. In addition, rheological analysis of composites with STKA shows similar enhancements in the properties as TBHP. Mechanical and rheological analysis both point to increased clay dispersion and adhesion between the clay and the matrix in contradiction to XRD analysis. XRD analysis must be supported with either mechanical or rheological characterization to assess the degree of clay dispersion, in addition to TEM analysis.

4.2.5.4 Mechanical Tests on LLDPE Nanocomposites

Mechanical properties of the PLSN do not only depend on the clay delamination, but also on the miscibility between LLDPE and compatibilizer, and the dispersion of clay particles in matrix.

Representative stress-strain curves of LLDPE, binary blends of LOT and LLDPE and ternary composites of LLDPE, organoclay and LOT are shown in Fig. 4.86. Addition of 5 wt % elastomer LOT to LLDPE increased the YM by 13 % and TS by 5 %, but decreased these properties as LOT content was increased to 12.5 wt %. Addition of 12.5 wt % LOT to LLDPE did not increase TS, but it increased the YM by 8 %. Hotta and Paul, 2004 found similar trends in LLDPE and maleic anhydride grafted polyethylene (LLDPE-g-MA) blends. In their study, 5, 8.5, 16.5 wt % addition of LLDPE-g-MA to LLDPE increased the TS and YM while 33 wt % addition of LLDPE-g-MA decreased the YM from 168 MPa to 190 MPa. Decrease in the YM and TS are attributed to dilution effect of LOT, since it has lower TS compared to LLDPE [Isik et al., 2008]. It can be seen that in

ternary nanocomposites, addition of clay to LLDPE/LOT not only increased the TS and YM, but also increased the elongation at break considerably. When the clay concentration was 5 wt %, there was high ductility in the samples.

The Young's modulus (YM) of the samples were determined from the tangent of the each plot in initial elastic region. The tensile yield point of the samples are not so clear in many cases, except for the ternary composites of LLDPE, thus maximum stress values read from the plots are given as the tensile strength (TS) values. Only ternary composites with DMDA show TS at break as a maximum, while composites with TBHP and I34 show TS at break values lower than the yield stress. A summary of the tensile results of LLDPE composites are given in Appendix B. The YM (Fig. 4.87) and TS (Fig.4.88) of the LLDPE were calculated as 170 MPa and 22 MPa, respectively. The YM of the LLDPE (MFI =3.2 g/10 min, $\rho= 0.9175 \text{ g/cm}^3$) samples used by Durmus et al., 2008 were computed as 64 MPa with a yield stress of 9.9 MPa. Hotta and Paul, 2004 gives YM of the LLDPE (MFI =2 g/10 min, $\rho= 0.926 \text{ g/cm}^3$) sample as 190 MPa with a tensile yield stress of 11.8 MPa.

Figure 4.87 shows the variation in the Young's modulus of the composites with respect to clay type, clay content and LOT content. Higher clay content increased the YM as expected, since higher the clay content higher the reinforcement effect of clay is. 5 wt % addition of DMDA, TBHP and I34 enhanced the YM of the blends approximately 33 %, 41 % and 65 % respectively compared to neat LLDPE. Also shown by TEM and rheological characterization, well dispersed clay platelets of TBHP with high aspect ratio lead to high contact surface area between the filler and the polymer matrix providing enhancement in the modulus of the material.

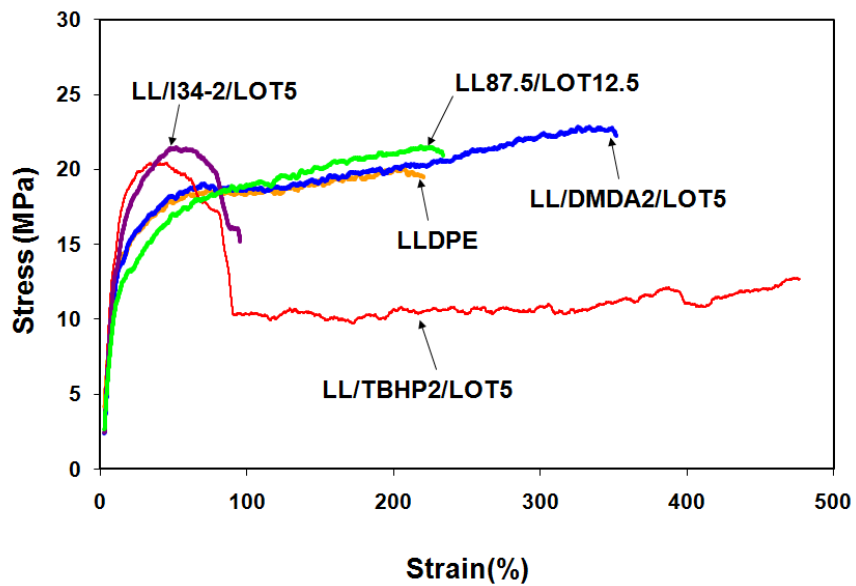


Figure 4.86 Representative stress-strain diagram of LLDPE based composites

Note that organoclay TBHP produced from bentonite gave YM results similar to that of commercial organoclay I34, showing effectiveness of the modification procedure and local bentonite usage in this polymer matrix. Although DMDA showed high extent of intercalation, i.e., high d-spacing in XRD measurement, rheological analysis showed that it is less compatible with LLDPE compared to the organoclay TBHP. This behavior is also seen in the results of YM since enhancement in modulus of DMDA is lower than that of TBHP and I34 clays. This may be due to a lesser degree of exfoliation and reduced aspect ratio of clay platelets [Saminathan et al., 2008] which may be attributed to low interaction between the filler and the organoclay due to its different chemical modifier. Hotta and Paul, 2004 studied LLDPE/Organoclay/LLDPE-g-MA nanocomposites and found that LLDPE matrix with low polarity has high affinity to organoclays with two alkyl tails, and maximizing the alkyl tails, should lead to better dispersion in this polar polymer. The present situation is somewhat different than this conclusion. DMDA [2(Me)N⁺2C18] has two long alkyl tails with 18 C atoms in each and two

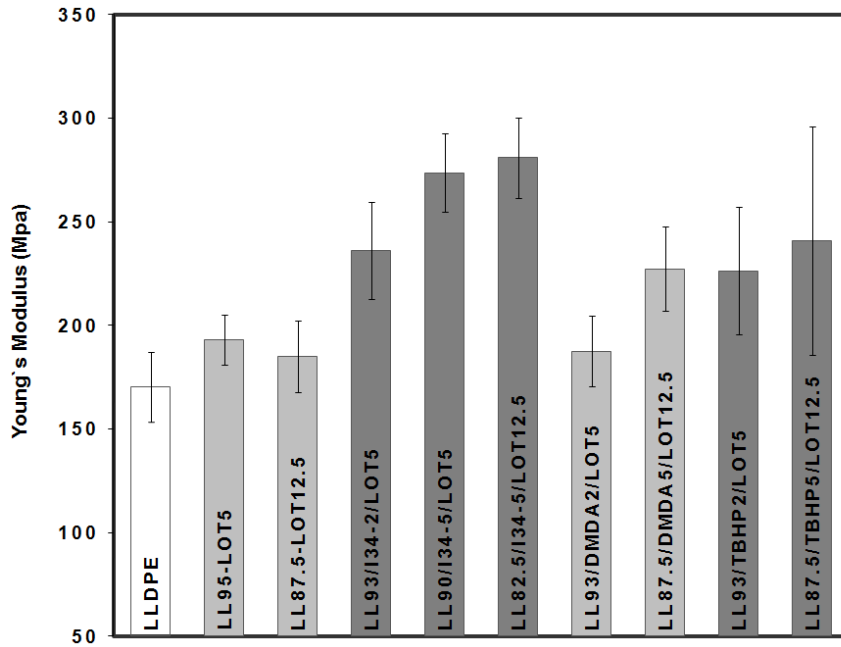


Figure 4.87 Effect of organoclay type and concentration on Young's modulus of LLDPE based composites prepared in SET-6

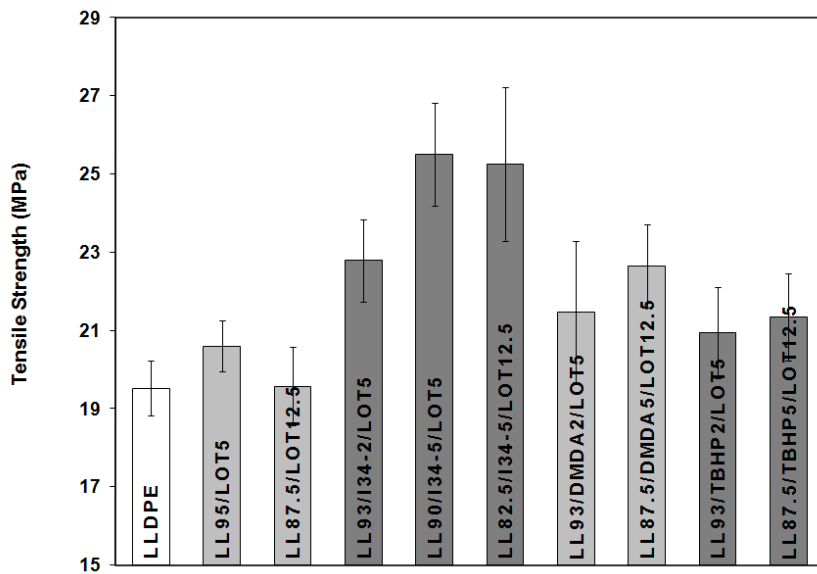


Figure 4.88 Effect of organoclay type and concentration on tensile strength of LLDPE based composites (SET-6)

methyl groups (Me). TBHP [3(Butyl) N⁺C16] has one long alkyl tail with 16 C atoms and also has three tails with 4 C atoms (Butyl groups), meanwhile I34 [2(EthOH) (Me) N⁺-HT] has one long alkyl tail [HT: hydrogenated tallow], one methyl and two ethyl hydroxyl groups. Owing to differences between the chemical modifiers of organoclays, differences in enhancement of modulus can be attributed to specific interactions between different types of clay (e.g., modifier type of the clay) and compatibilizer [Stoeffler et al., 2008].

Effect of LOT/organoclay ratio can be deduced from Figure 4.34 in which LOT/organoclay ratio, ξ , is 1 in LL/I34-5/LOT5 and $\xi = 2.5$ in LL/I34-5/LOT12.5 samples and clay concentrations are the same (5 wt %) in both compositions. As ξ increases to 2.5, YM (Fig. 4.87) and TS (Fig. 4.88) of the composites do not significantly differ than the values obtained by $\xi=1$.

Figure 4.88 shows the variation in the tensile strength of the composites with respect to clay type, clay content and LOT content. TS increases for all types of clays, and the enhancement is the highest in the case of I34 clay. For these organoclays, XRD (for DMDA), TEM and rheological characterization showed intercalated and partially intercalated clay layers through the matrix. Again, increased interfacial area between the clay and matrix induced by high aspect ratio of clay layers promotes the TS of the samples. Tensile strength values of the samples prepared with DMDA are higher than those prepared with TBHP organoclay. This can be confirmed also by SEM analysis (Fig.4.64 and Fig.4.66). As the clay tactoids get smaller, higher dispersion and adhesion can be achieved between the phases. Increased chemical adhesion and compatibility in turn give rise to the enhancements in mechanical properties.

Figure 4.89 shows elongation at break of the nanocomposites. An increase in TS and YM due to decreased ductility is known through clay incorporation, because inorganic particles cannot be strained by external stresses but behave as stress concentrators of matrix during the strain

process [Contreras et al., 2006]. Situation is similar in the nanocomposites with I34, since their elongation at break values are lower than the LLDPE matrix and also from other composites; while they have the highest TS values. Immiscible aggregates of clay platelets (as also shown by TEM) may act as defects and stress concentrators leading to the failure mechanism. Increasing I34 content from 2 % to 5 % further reduced the elongation values of ternary composites, which can be attributed to increased micro void (SEM analysis of samples shows higher microvoids in Figure 4.70) formation due to higher clay content which might cause tearing and failure in the composite as shown.

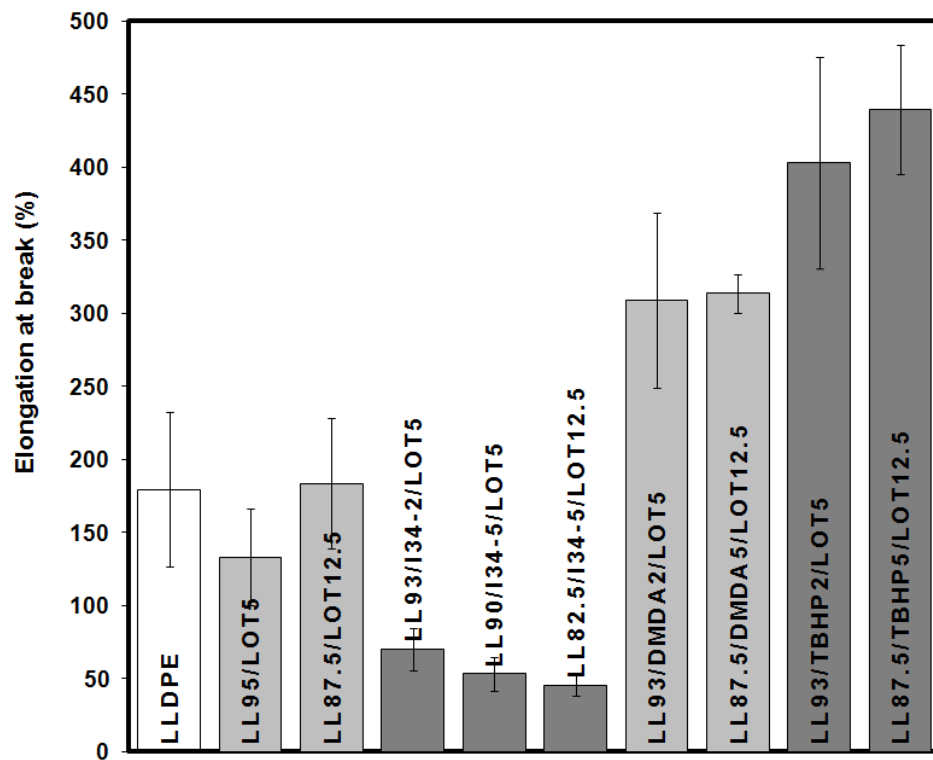


Figure 4.89 Effect of organoclay type and concentration on elongation at break of LLDPE based composites (SET-6).

The relation between elongation at break and TS of the samples mentioned above is confirmed in the case of TBHP clay, where its

composites show higher elongation at break but lower TS compared to composites of DMDA. In the case of DMDA, and especially in TBHP, elongation at break values are much higher than I34, showing enhancement in the materials' high ability to absorb energy with these bentonite modified organoclays owing to good adhesion between the filler and the matrix. This increase in the elongation at break is in contrast to much of the published literature, since generally addition of organoclay can increase the TS of the neat polymer, but decreases its ductility [Fornes et al., 2001; Hotta and Paul, 2004]. In addition, Zhang and Sundararaj, 2006 found similar results to the current study, i.e., increase in the ductility of LLDPE/PEMA/ organoclay composites. In the current ternary composites, organoclays DMDA and TBHP acted as crack stoppers and material could elongate to higher extent. Since area under the stress-strain curves can be taken as a measure for the energy that is dissipated by plastic deformation within the sample, the results in Figure 4.89 confirm that TBHP is superior to DMDA in terms of ductility. Higher elongation at break values compared to commercial organoclay I34 also confirms the superior properties of organoclays prepared in this study. Regarding the elongation ability, TBHP increased elongation at break values of composites by 144 % compared to neat LLDPE.

Increase in the ductility upon organoclay incorporation can also be attributed to molecular similarity between the LLDPE and LOT phases which take an important part in linking the interaction between organoclay and LLDPE. Since LLDPE and LOT are comparable in molecular structure, they can interact with each other, and higher intercalation can be formed in this system and better bonding can take place between the phases [Zhang and Sundararaj, 2006]. This compatibility results in higher ductility values in addition to the expected enhanced YM and TS. In addition to the molecular similarity, rheological results, which will be mentioned in subsequent parts, confirm the miscibility of LLDPE and LOT, since blends of LLDPE95/LOT5 show similar loss in G'' (Pa), storage

modulus, G' (Pa) and complex viscosity η^* (Pa.s) in comparison to the properties of neat LLDPE (Figure 4.104).

4.2.6. Linear Viscoelastic Behavior in the Melt State

Rheological behavior of the composites in melt state present indirect data on the degree of the clay layer dispersion, with the material functions changing significantly through the aggregates, intercalated tactoids and or partially exfoliated clay particles.

Importance of rheology stem from the lack of information provided by XRD. TEM gives chance on direct observation to assess the degree of delamination, but the main problem with TEM is that the volume investigated is very small and does not represent the composite morphology as a whole. Thus, the bulk properties such as rheology together with mechanical testing should be analyzed complementary to TEM and XRD observations.

Rheological behavior of composites PPE/Organoclay2/MAPP5-M (SET-3) and LLDPE based (SET-6) were investigated in this part of the study. The small amplitude oscillatory shear flow was used in order to characterize the linear viscoelastic behavior of PLSN as a function of time, strain and frequency. Firstly, thermal degradation behavior of samples and the matrices were studied by time sweep tests. Depending on this test, samples were mixed for an optimum time in which heat stability was conserved. Storage modulus, loss modulus and complex viscosity of the samples were determined. Storage modulus, G' (Pa), indicates the energy stored as elastic energy during cyclic deformation; loss modulus, G'' (Pa), indicates the energy dissipated as heat during a cyclic deformation and complex viscosity, η^* (Pa.s), is the value which approaches the steady shear viscosity of the suspension as the shear rate and the frequency are reduced to zero [Demirkol and Kalyon, 2007].

4.2.6.1 Rheological Characterization of PP Based Composites

4.2.6.1.1 Time Sweep Test of the Samples

Figures 4.90 and 4.91 show complex viscosities (η^*) of PPE different in three forms. These are ``just pellet`` (unprocessed just molded), PPE mixed for 15 min with 1 phr % Irganox®B225 and PPE mixed for 15 min without heat stabilizer Irganox®B225 forms. Possible degradation of PPE because of the chain scission of PP itself can be directly seen from Fig. 4.90. Polyolefins may undergo chain scission reactions leading to a decrease in molecular weight at high temperature and applied shear. However, even when chain scission occurs, under strictly controlled conditions useful products of uniform quality can be obtained. [Zweifel, 2001]. Heat stabilizer Irganox®B225 addition increased the viscosity of PP and provided a stable thermal stability. For this reason, Irganox®B225 was used in the batch mixer for mixing previously extruded

PPE based composites to avoid possible degradation mechanism. It can also be seen from Fig. 4.90 that, if ``just molded`` sample would be subjected to shear for a longer time, its viscosity would most probably reach the viscosity of PP without Irganox®B225. Mixture of PP95/MAPP5 was also prepared to observe the behavior of binder itself without clay. Samples were taken at different time intervals to observe the effect of mixing time on the binder.

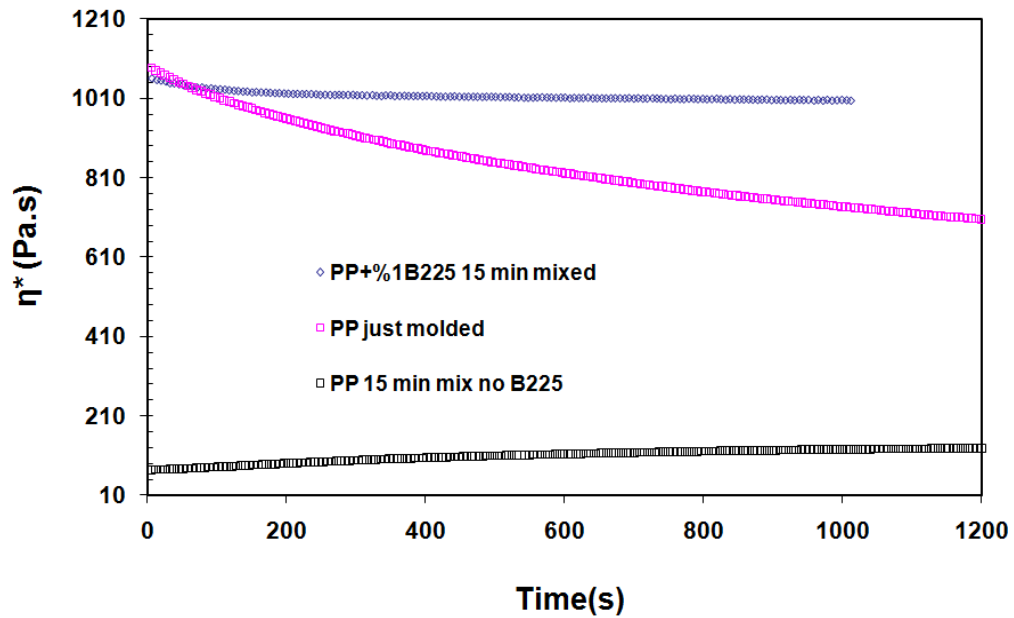


Figure 4.90 Time sweep test of PPE subjected to different temperature histories

Figure 4.91 shows the time dependence of η^* and the effect of stabilizer Irganox®B225 in PP95/MAPP5 and compares it with PPE. For this aim, 95 wt % PP and %5 wt MAPP were mixed with the heat stabilizer Irganox®B225 and samples were taken at different time intervals (10, 15, 20 and 25 min). As time proceeds, effect of thermal degradation shows itself by lowering the viscosity of the blend. Addition of highly viscous MAPP to PPE decreases its viscosity. While PPE has a viscosity of 1061 Pa.s, its viscosity decreased to 968 Pa.s with the addition of the MAPP. It is also seen from this figure that the optimum mixing time is 15 min for the PPE to have the lowest degree of degradation during the mixing.

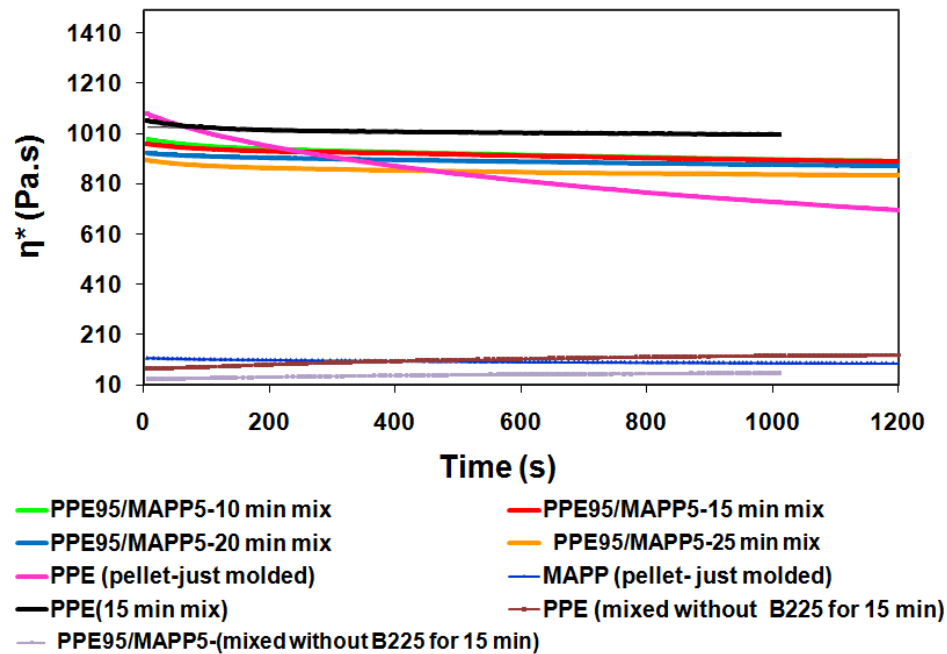


Figure 4.91 Time dependence of complex viscosity of PP, MAPP and their mixtures PP%95-MAPP%5.

4.2.6.1.2 Strain Sweep Tests

In order to determine the linear strain range of response of each material, firstly strain sweep tests were conducted. The idea behind this analysis is to avoid the application of large strains that may stimulate the alignment of the clay particles [Rohlmann et al., 2006]. Strain dependence of storage modulus, G' , and complex viscosity, η^* , of samples were measured at 190°C at a frequency of 5 rad/s.

Figure 4.92 shows the strain dependence of PPE/organoclay2/MAPP5-M samples. Storage modulus (G') of all the samples exhibits a linear region (Newtonian plateau) at low strains and non-linear region at high strain amplitudes. The deviation of G' (Pa) from linear viscoelastic behavior occurs at approximately 40% in the case of PPE based composites. The dynamic frequency tests that follow were conducted at a strain of 40 %.

TBHP and TKA composites show a higher G' compared to DMDA composites. It's surprising that DMDA has lower G' than TBHP and TKA, since it has an intercalated clay structure as shown by X-Ray analysis. Structural differences in the surfactants, such as the number of long alkyl chain lengths, maybe the cause of this contradictory rheological results. Rheological properties are affected by many factors, i.e., volume concentration, viscosity, size, size distribution, surface chemistry and agglomerates of the filler or the dispersed phase [Shenoy, 1999].

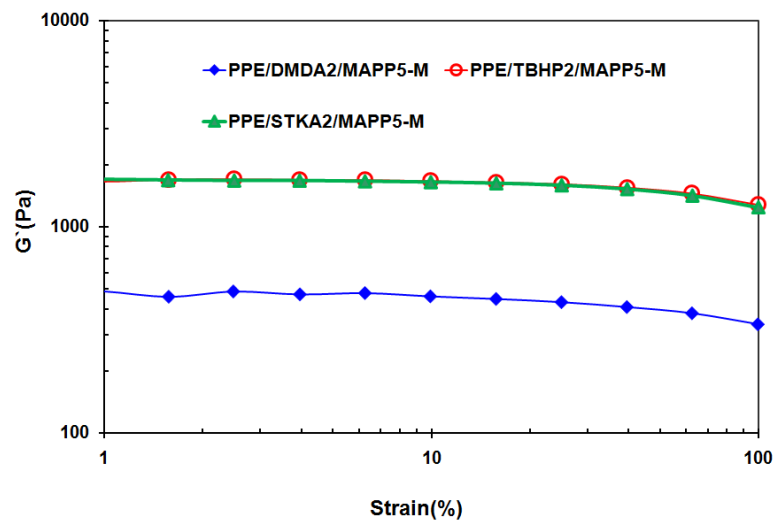


Figure 4.92 Strain dependence of storage modulus of PPE/Organoclay2/MAPP5-M samples

4.2.6.1.3 Effect of Heat Stabilizer on Rheology

Fig. 4.93 through Figure 4.95 show η^* , G' and G'' of PPE, PPE95/MAPP5 samples batch mixed for 15 minutes with and without heat stabilizer Irganox B225, respectively. 1 phr addition of heat stabilizer clearly alters the rheological properties of PPE. Addition of MAPP to PPE definitely lowers the η^* , G' and G'' of the sample owing to its plasticizing effect since viscosity of MAPP is much lower than that of PPE.

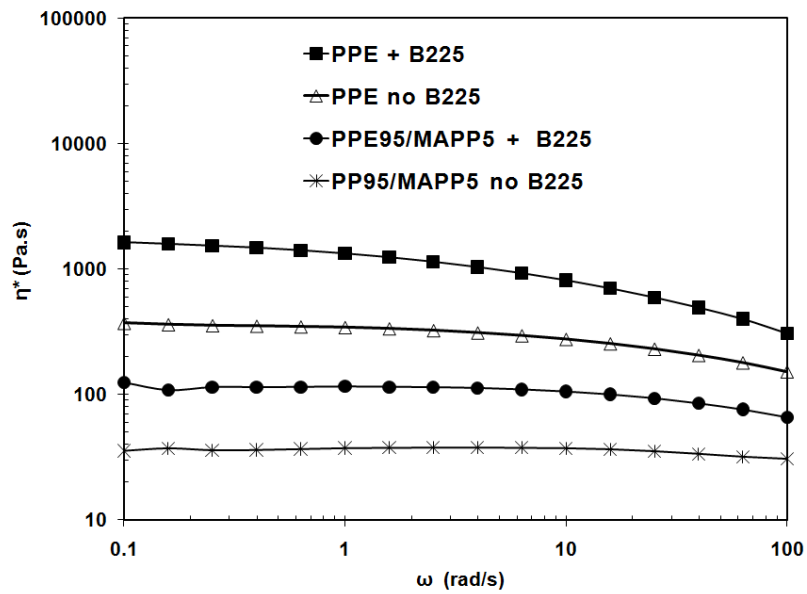


Figure 4.93 Frequency dependence of complex viscosity of PP, MAPP and their mixtures PP%95-MAPP%5 with and without heat stabilizer B225

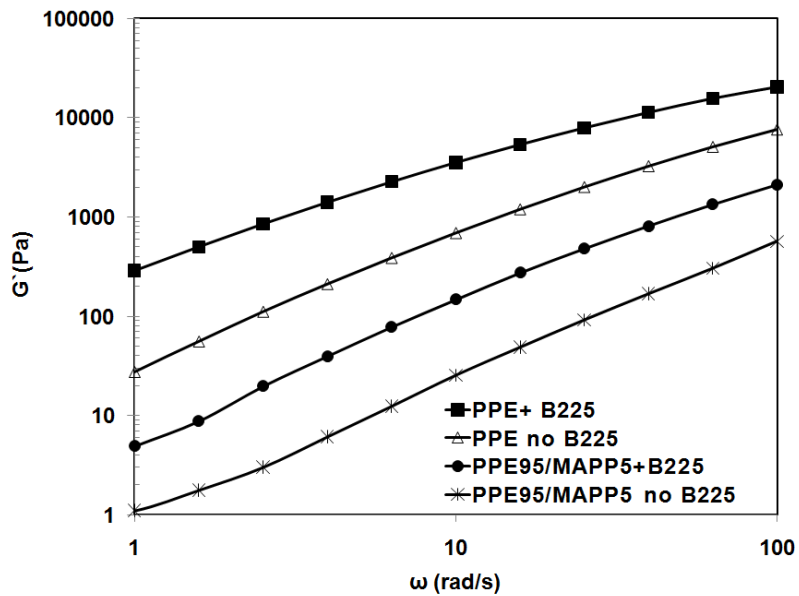


Figure 4.94 Frequency dependence of storage modulus, G' (Pa), of PP, MAPP and their mixtures PP%95-MAPP%5 with and without heat stabilizer B225

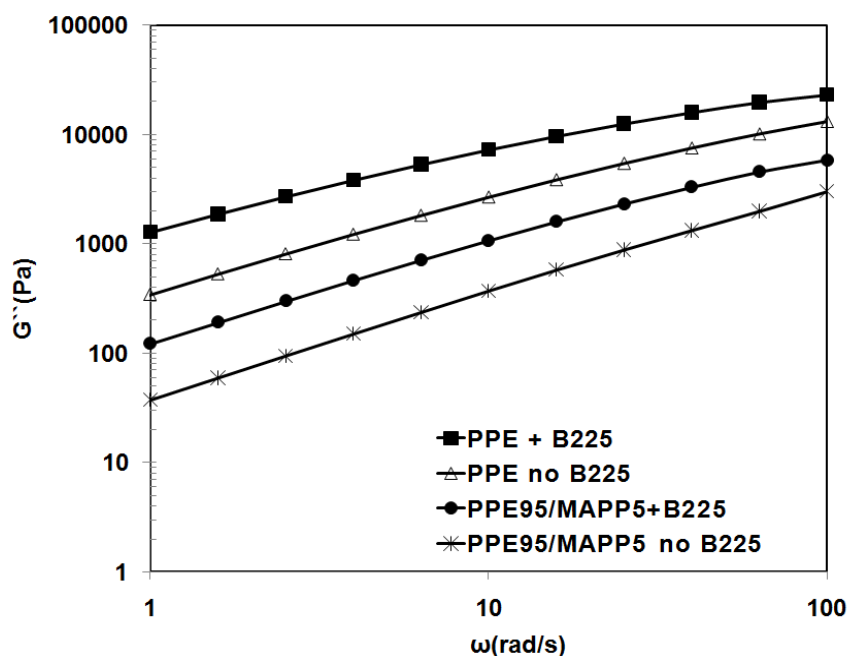


Figure 4.95 Frequency dependence of loss modulus, G'' (Pa), of PP, MAPP and their mixtures PP%95-MAPP%5 with and without heat stabilizer B225

4.2.6.2 Frequency Test of PPE/Organoclay2/MAPP5-M Composites

Figure 4.96 shows the frequency dependence of storage and loss modulus of the PPE/Organoclay2/MAPP5-M samples prepared by mixing for 15 minutes. It is seen that G' and G'' of the composites with STKA and TBHP are higher than those of the composites with DMDA. Similar trend is observed in η^* of the samples given in Figure 4.97. XRD analysis had shown intercalation in the case of TBHP and DMDA while basal spacing of the clay did not change in the composite with STKA. Stoeffler et al., 2008 (a) and Smart et al., 2008 found similar trends in compatibilized clay composites where rheological properties were enhanced, although XRD revealed neither intercalation nor exfoliation. This enhancements may be attributed to specific interactions between the clay and the compatibilizer. In addition, it is probable that a small quantity of dispersed layers coexist with the microparticles, contributing to the differences observed in rheological properties [Stoeffler et al., 2008 (a)]. This conflicting situation

can also be attributed to the deficiency of XRD technique where preferred orientation can give the false impression that intercalation/exfoliation has not occurred [Smart et al., 2008].

Comparison of TEM analysis of PPE/DMDA2/MAPP5 and PPE/TBHP2/MAPP5 clearly show that average L_{clay} of PPE/DMDA2/MAPP5 samples is 119 ± 21 nm, whereas TBHP contains tactoids with L_{clay} of 100-300 nm (Table 4.4). Length of a MMT layer is given as 100 nm in the literature showing that in TBHP clays in the PPE based composites are longer.

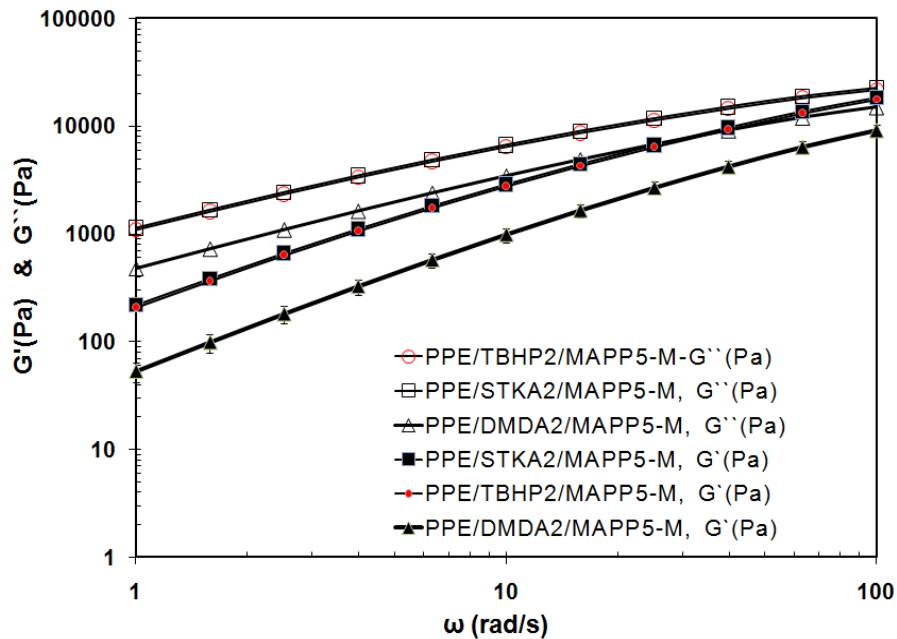


Figure 4.96 Frequency dependence of storage, G' (Pa), and loss modulus, G'' (Pa), of ternary composites of PPE/organoclay2/MAPP5-M.

In the case of PPE/TBHP2/MAPP5-M composites, increased interactions between the tactoids lead to more effective load transferability between them, in other words, tactoids could 'feel' each other through the matrix due to the strong interfacial adhesion and good dispersion which in turn enhances the rheological functions such as G' , G'' and complex viscosity η^* .

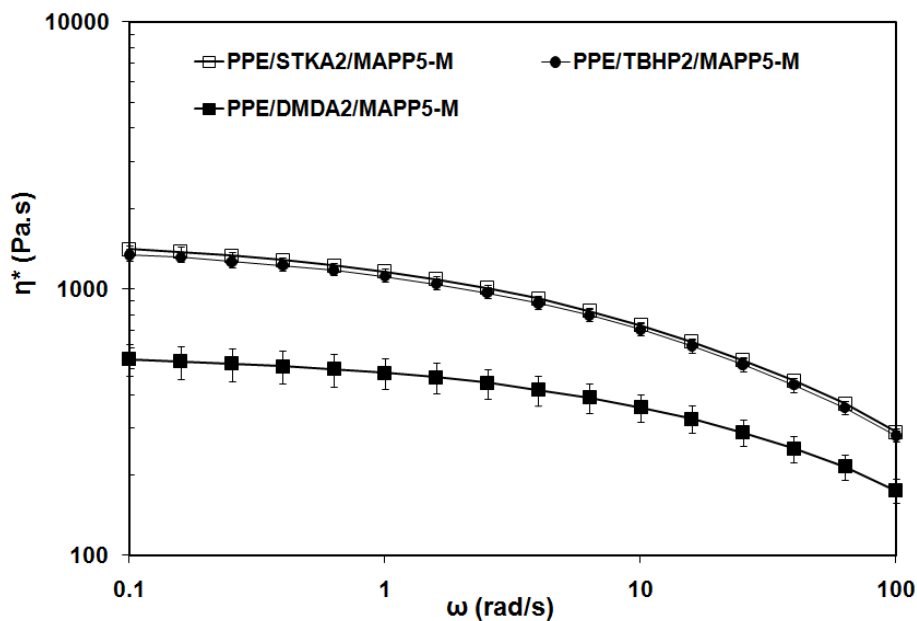


Figure 4.97 Frequency dependence of complex viscosity, η^* (Pa.s), of ternary composites of PPE/organoclay2/MAPP5-M composites.

Figure 4.98 shows the frequency dependence of PPE based composites prepared by “extrusion only” and by “extrusion followed by batch mixing”, giving the opportunity to see how the application of more shear affects the rheological response of the composites. Figures show an increase in the storage and complex viscosity (Appendix C, Fig. C1-C3) of samples prepared by “extrusion followed by batch mixing” compared to the one prepared with “extrusion only”. These enhancements may be related to extended degree of delamination or intercalation of clay layers. In addition, it should be noted that, during batch mixing 1 phr of heat stabilizer was used which affected the rheology of neat PPE samples as shown previously (Figure 4.93-4.95). Addition of heat stabilizer enhanced the G' and η^* of the PPE and PPE95/MAPP5 significantly.

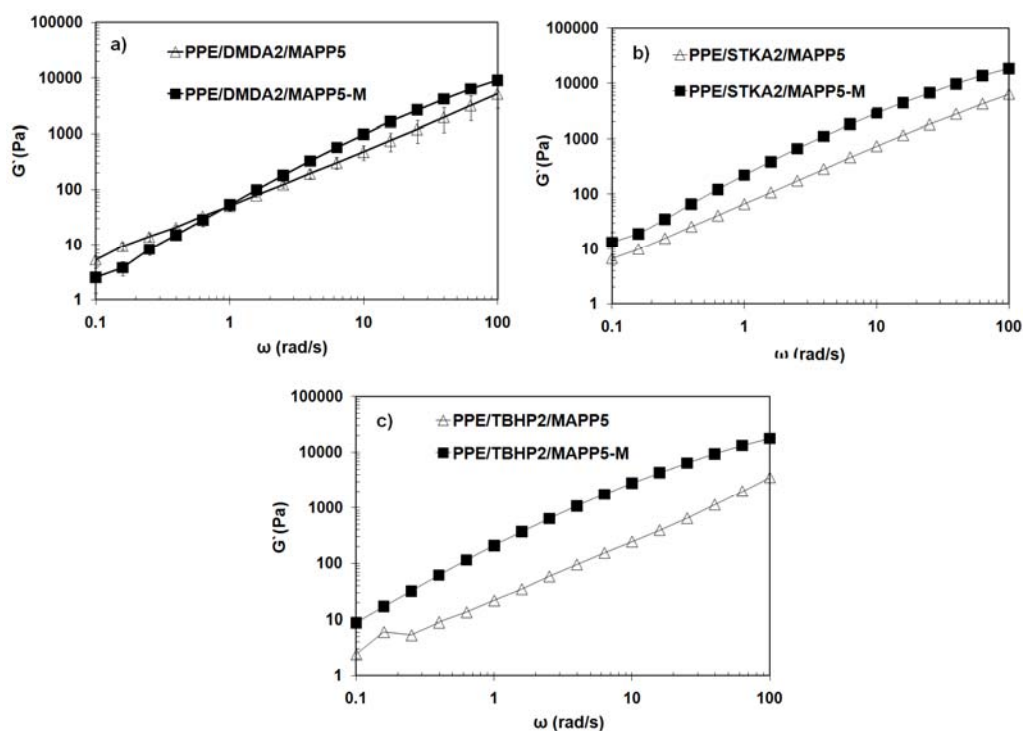


Figure 4.98 Frequency dependence of storage modulus, G' (Pa), of PPE/organoclay2/MAPP5 samples prepared by extrusion only and by extrusion followed by batch mixing. Samples prepared with organoclay a) DMDA, b) STKA and c) TBHP.

4.2.6.3 Rheological Characterization of LLDPE Based Composites

4.2.6.3.1 Time Sweep Test of LLDPE Based Nanocomposites

During processing, materials, like dispersions and polymers, may undergo macro or micro morphological rearrangement with time. These newly formations affect the rheological behavior significantly. Polymeric materials can undergo degradation with time. Oscillatory time sweep tests give data reflecting the changes with time. With the help of data gathered by time sweep tests, optimum processing time can be found. Polymer properties can change so drastically with time that precise and reproducible testing may become troublesome. In this study, polymer

composite samples and especially the polymer matrix was tested by time sweep tests showing the changes as time advances.

Figure 4.99 shows the change of complex viscosity, η^* (Pa.s), of the LLDPE sample batch mixed for different times. Time tags given in the name of the sample indicate the duration of mixing in the batch mixer. Two different runs were done for 5 and 20 min mixed samples. Figure 4.99 shows that, as duration of mixing increases, the complex viscosity decreases. After 15 min mixing, LLDPE-25 min and LLDPE-30 min samples show a significant reduction in the viscosity indicative of a degradation process. 15 min mixed LLDPE sample shows an almost constant viscosity up to 1200 s showing the stability of the matrix. Samples mixed for 25 min and 30 min show an increase in the viscosity at the startup which is probably indicative of a possible crosslinking process. LOT mixed for 15 min also shows heat stability over the time tested.

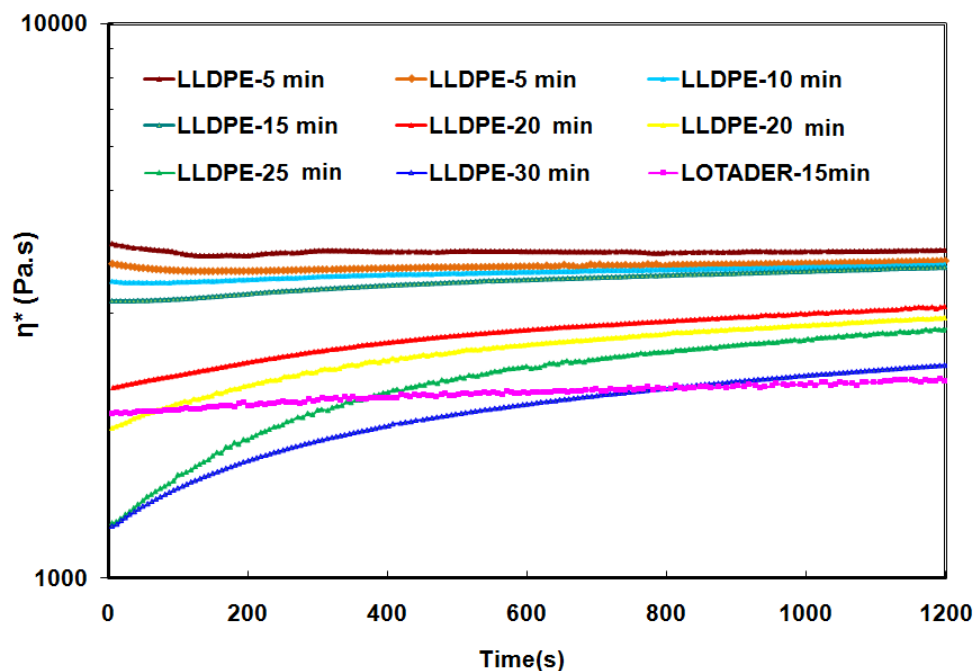


Figure 4.99 Time dependence of complex viscosity, η^* (Pa.s), of LLDPE and LOT mixed for different times.

Figure 4.100 shows the time dependence of η^* (Pa.s) of the binary blends of LLDPE95/LOT5 and LLDPE samples mixed for different durations. Low viscosity LOT decreases the viscosity of LLDPE for all mixing durations. Based on the time sweep tests, ternary composites were batch mixed for 15 min at 190 °C in further experiments to avoid possible degradation of matrix. Frequency dependence of G' and η^* of LLDPE samples mixed for different time intervals are given in Appendix C in Figures C.4 and C.5.

Figure 4.101 (a) shows the frequency dependence of LL/I34-2/LOT5 samples taken during the batch mixing at different time intervals. The sample mixed for 15 min shows higher viscosity compared to sample mixed for 5 min indicating formation of a network structure due to increased dispersion of clay layers in a more uniform fashion. As mixing continues for 25 min, sample viscosity decreases indicating structural breakdown in the system and possible degradation process. Frequency tests also indicated that 15 min of mixing is enough to have sufficient shear for dispersion of clay layers. Frequency tests of LL/DMDA2/LOT5 [Fig.4.101 (b)] composites batch mixed for different time durations display similar trend observed with I34, that 15 min mixing results higher enhancement compared to 5 min mixing. Fig.101 (b) show that 25 and 30 min mixing cause decrease in the viscosity of ternary composite even lower than LLDPE95/LOT5 mixture indicating possible degradation mechanism.

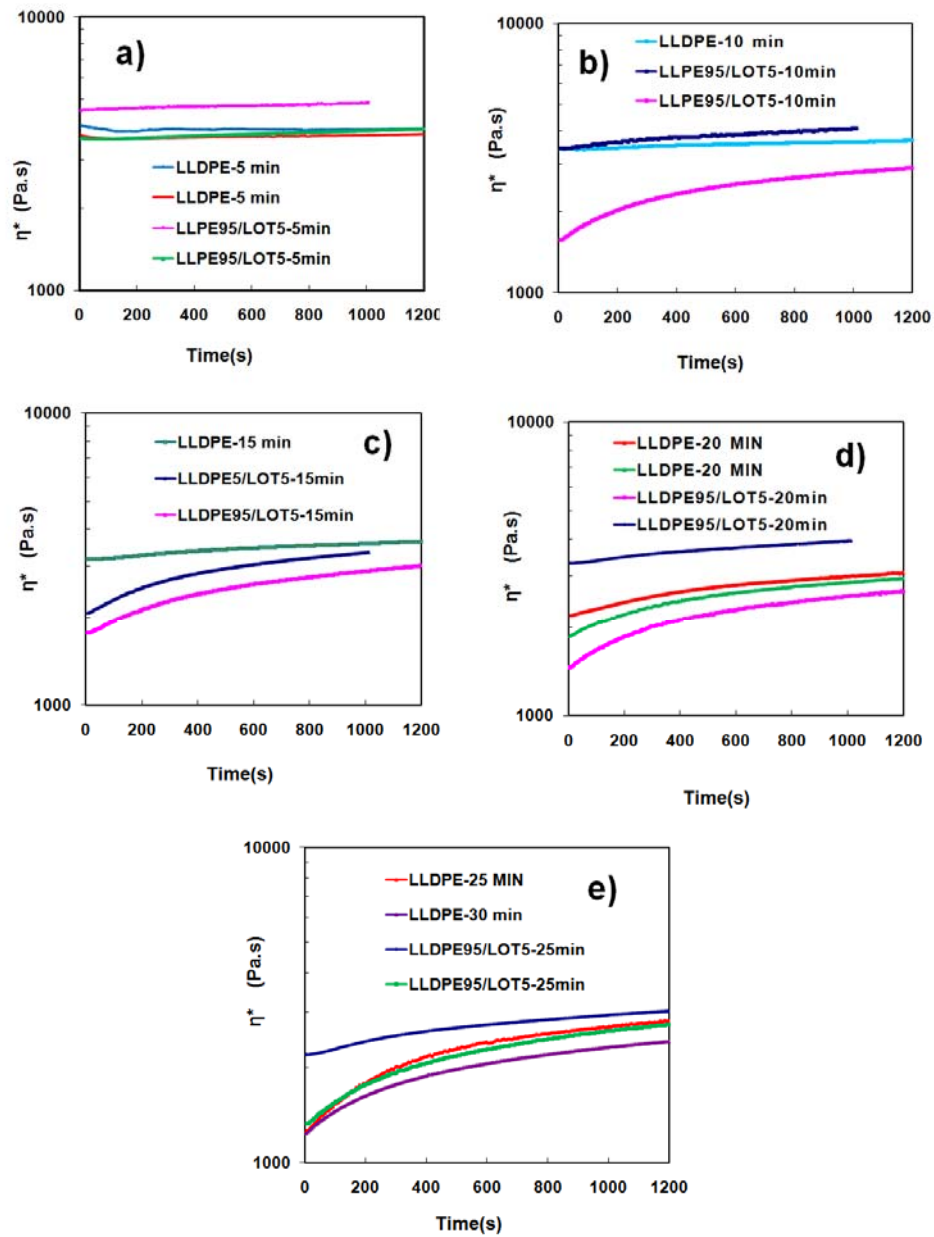


Figure 4.100 Time dependence of complex viscosity, η^* (Pa.s), of LLDPE and LLDPE95/LOT5 binary mixtures batch mixed for different time intervals. a) 5 min mix, b) 10 min mix, c) 15 min mix, d) 20 min mix and e) 25 min mix.

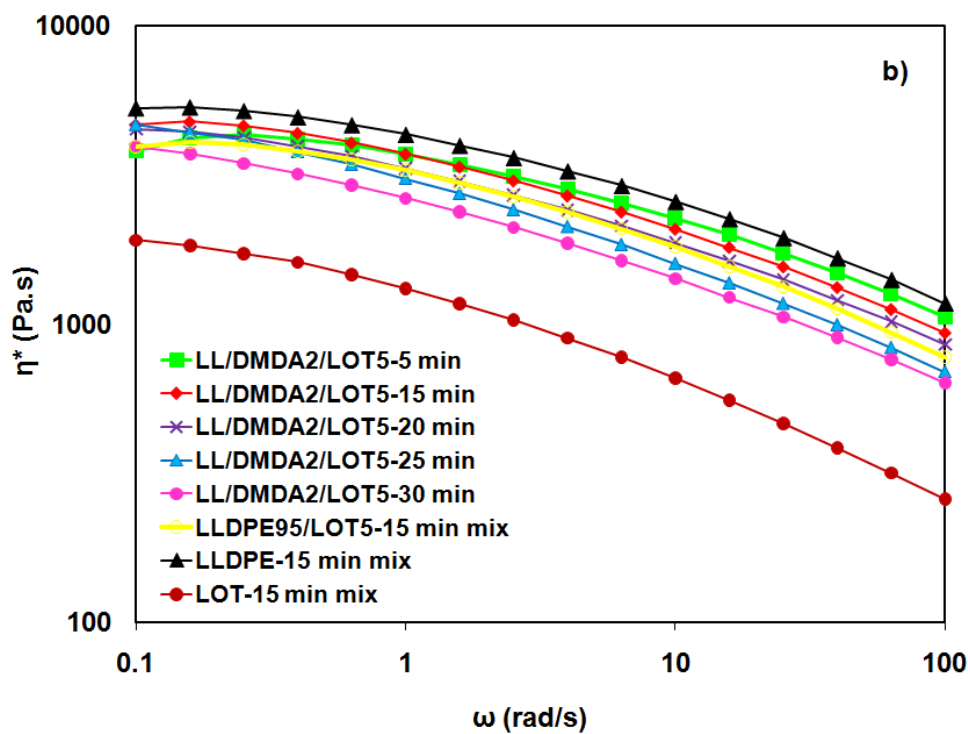
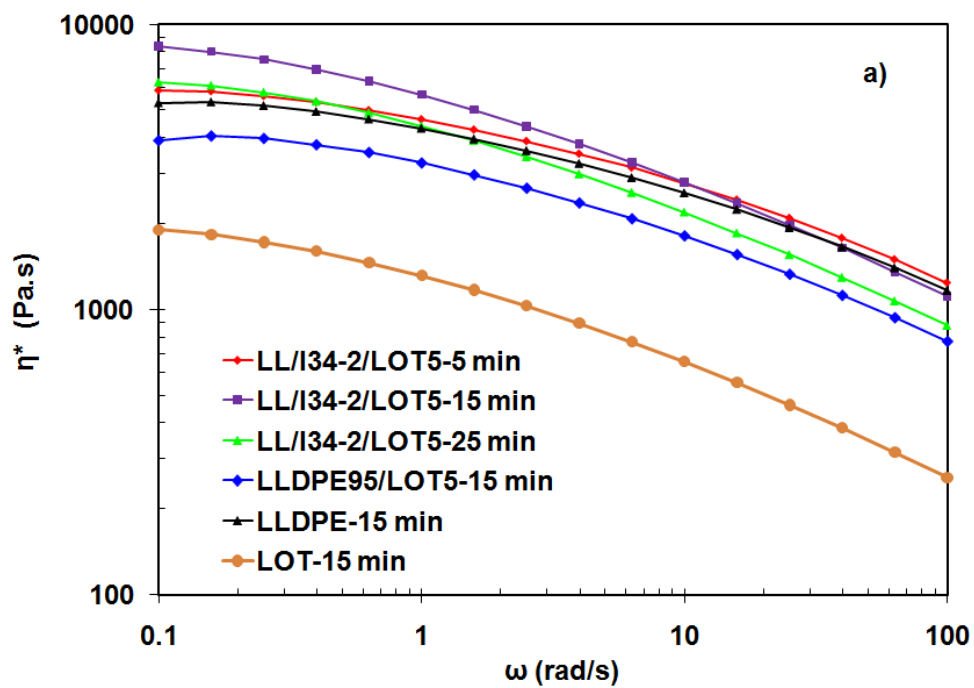


Figure 4.101 Frequency dependence of η^* (Pa.s), of LLDPE, LLDPE/LOT mixtures, LL/organoclay2/LOT5 composites batch mixed for different time durations with a) I34, b) DMDA

4.2.6.3.2 Strain Sweep Test of LLDPE Based Composites

In order to determine the linear range of strain response of each material, firstly strain sweep tests were conducted. Strain dependence of G' and η^* for samples was measured at 190°C at a frequency of 5 rad/s. The idea behind this analysis is to avoid the application of large strains that may stimulate the alignment of the clay particles [Rohlmann et al., 2006]. Since the storage modulus (G') is a more sensitive rheological function than the loss modulus (G'') to the structural changes of the nanocomposites [Durmus et al., 2007], only the storage modulus curves are given for the strain sweep tests. Fig. 4.102 shows the storage modulus for LLDPE and its composites with respect to strain. Storage modulus (G') of all the samples show linear behavior at low strains and non-linear behavior at high strains. Fig. 4.102 shows that G' of LLDPE95/LOT5 binary mixture is between the G' of LLDPE and LOT confirming the effects of low viscosity LOT in the LLDPE. Presence of LOT does not have much effect on the extent of linear region of the LLDPE in LLDPE95/LOT5 blends, while addition of clay shortens the extent of the linear region profoundly in all the samples with clay showing sensitivity of viscoelastic behavior to the presence of clay. The deviation of the G' (Pa) from linear viscoelastic behavior occurs at approximately 10% in the case of LLDPE and it is reduced by the presence of the clay and by the increase in the clay content. The dynamic frequency tests that follow were conducted at a strain of 10 %. It is of primary importance in frequency sweep tests to keep the strain as low as possible within the system constraint, in order to be in the linear viscoelastic region [Shenoy, 1999].

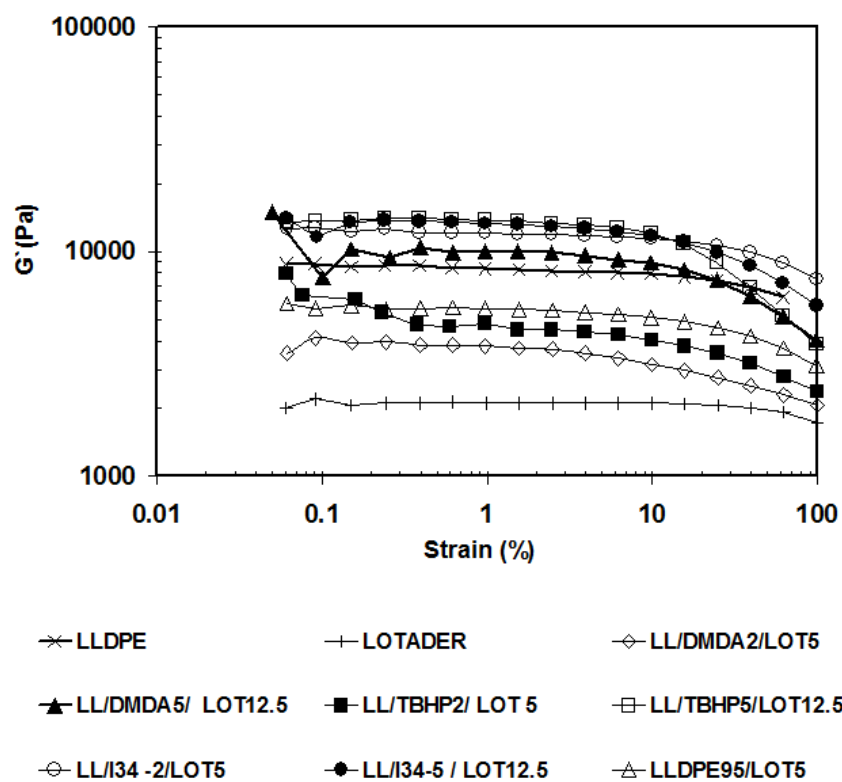


Figure 4.102 Strain dependence of storage modulus (G') of LLDPE and LL/Organoclay/LOT composites ($T=190\text{ }^{\circ}\text{C}$, $\omega = 5\text{ rad/s}$).

Figure 4.103 shows the strain dependence of storage modulus (G') of the composites composed of 98 wt % LOT and 2 wt % organoclay. In this figure, the extent of linear region decreases with addition of the clay compared to pure LOT. Enhancement in G' is highest in the case of DMDA which shows higher compatibility with LOT compared to TBHP and STKA.

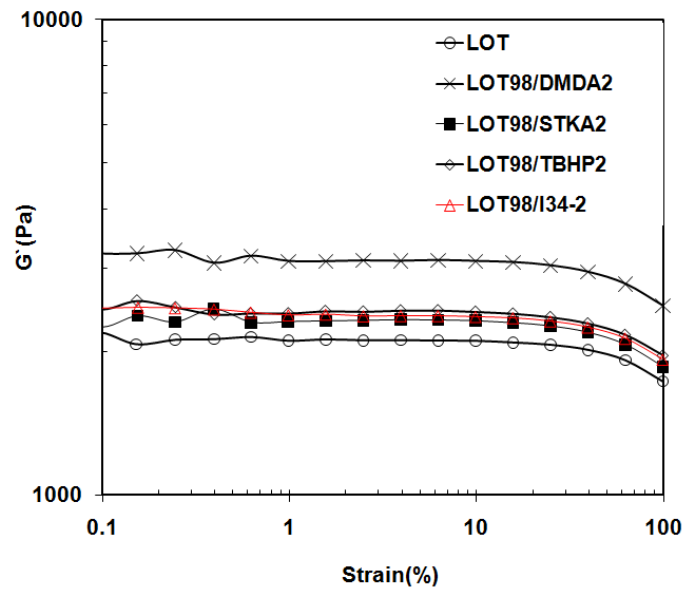


Figure 4.103 Strain dependence of storage modulus of LOT and LOT 98/Organoclay2 nanocomposites.

4.2.6.3.3 Frequency Sweep and Strain Amplitude Tests of LLDPE Based Composites

Figure 4.104 shows that addition of LOT to LLDPE does not have much effect on the viscoelastic behavior especially in the storage (G') and loss modulus (G'') of the LLDPE, thus the differences in the rheological parameters of compatibilized composites can be attributed to the presence of clay [Stoeffler et al, 2008]. LOT has little effect on loss modulus, G'' , and it increases the storage modulus, G' , slightly in the low frequency region. Although G' is increased in low frequencies, the characteristic shoulder encountered in immiscible blends is not observed [Zhang and Sundararaj, 2006]. LLDPE, LOT and the blend LLDPE95/LOT5 displayed viscous-liquid behavior since $G' < G''$ as shown in Figure 4.104. Since a small amount of (5 wt %) LOT was added to the LLDPE, a marginal decrease in the complex viscosity (η^*) of LLDPE was observed at high frequencies. This result together with the fact that G' and

G'' behavior of LLDPE/LOT blend are similar to those of LLDPE implies that there is no liquid-liquid separation between LLDPE and LOT [Zhang and Sundararaj, 2006].

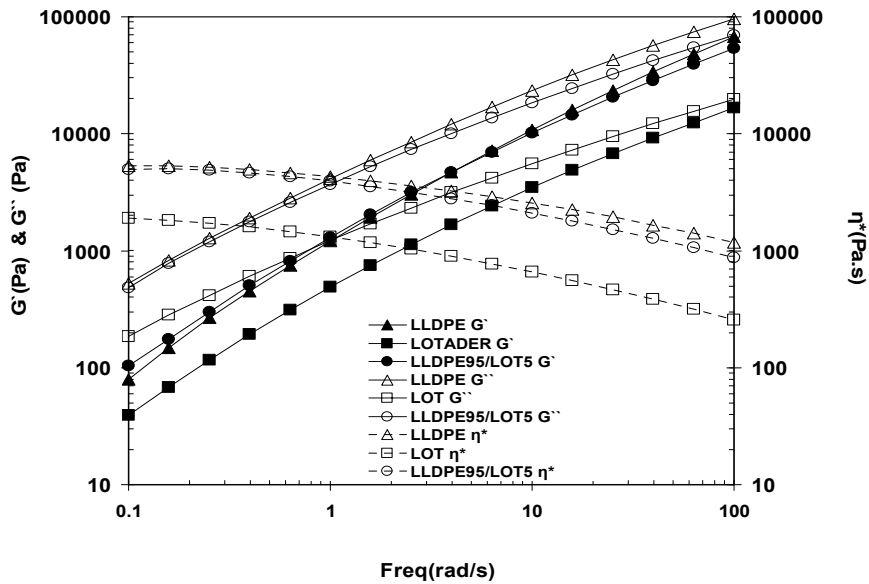


Figure 4.104 Frequency dependence of storage modulus G' (Pa), loss modulus G'' (Pa) and complex viscosity η^* (Pa.s) of LLDPE, LOT and the blend LLDPE95-LOT5

4.2.6.3.3.1 Effect of Organoclay Content on Rheology

Fig. 4.105 shows the frequency dependence of G' and η^* of composites prepared with DMDA clay at different clay contents. Fig. 4.106 shows the same data given in Fig. 4.105 in terms of ratio $G'(\omega)/G'_m(\omega)$ of nanocomposites prepared, where G'_m is the storage (elastic) modulus of the base LLDPE at corresponding frequency. This way of representing the data is useful in understanding the viscoelastic behavior more clearly. The analogous figures obtained for nanocomposites prepared by TBHP and I34 are given through Fig. 4.107-4.108 and Fig. 4.109-4.110 respectively.

Fig.4.105 and Fig. 4.106 indicate that, 2 wt % of DMDA organoclay is not enough for an enhancement, compared to pristine LLDPE, in the G' and η^* , in the entire range of frequency, indicating no physical network formation at this clay content. As shown in Fig. 4.105 (η^* - ω) of the nanocomposite of DMDA (Fig. 4.105 (b)), sample with low clay content showed Newtonian behavior similar to pristine LLDPE. Increasing the clay content to 5% increases the $G'(\omega)/G'_m(\omega)$ (Fig. 4.106 (a)) especially in the low frequency region. The large surface area of clay particles produces colloidal interactions that enhance the G' (Fig. 4.105 (a)) at clay content of 5 % especially at low frequency region [Rohlmann et al., 2008]. At low frequencies, G' is broadly separated, while the data gather in the high frequency region.

In the PLSN rheology, above a certain fraction of organoclay, defined as percolation threshold, G' becomes frequency independent ($G' \propto \omega^0$) in the low frequency region. This solid-like behavior formation is attributed to the percolation network superstructure formation due to strong interactions between the filler and polymer phase and thus to the exfoliated layers or stacks of intercalated layers as reported by other researchers [Galgali et al., 2001; Ren et al., 2001; Wu et al 2005(a, b, c); Zhang and Sundararaj, 2006; Durmus et al., 2007; Rohlmann et al., 2006; Solomon et al., 2001]. Thus, delamination of clay layers causes enhancements in G' at lower frequencies since greater dispersion results in high surface area and aspect ratio. Therefore, in DMDA based organoclays, 2 wt % of clay is not sufficient for the formation of percolation network structure. SEM micrograph shown in Figure 4.64 also indicates that a physical network was not present when 2 wt % DMDA was used. Moreover, composite with 5 wt % of DMDA (Fig.4.65) organoclay shows that denser silicate layers were dispersed through the matrix and this property manifests itself in higher values of rheological functions, i.e., $G'(P)$ and complex viscosity (η)

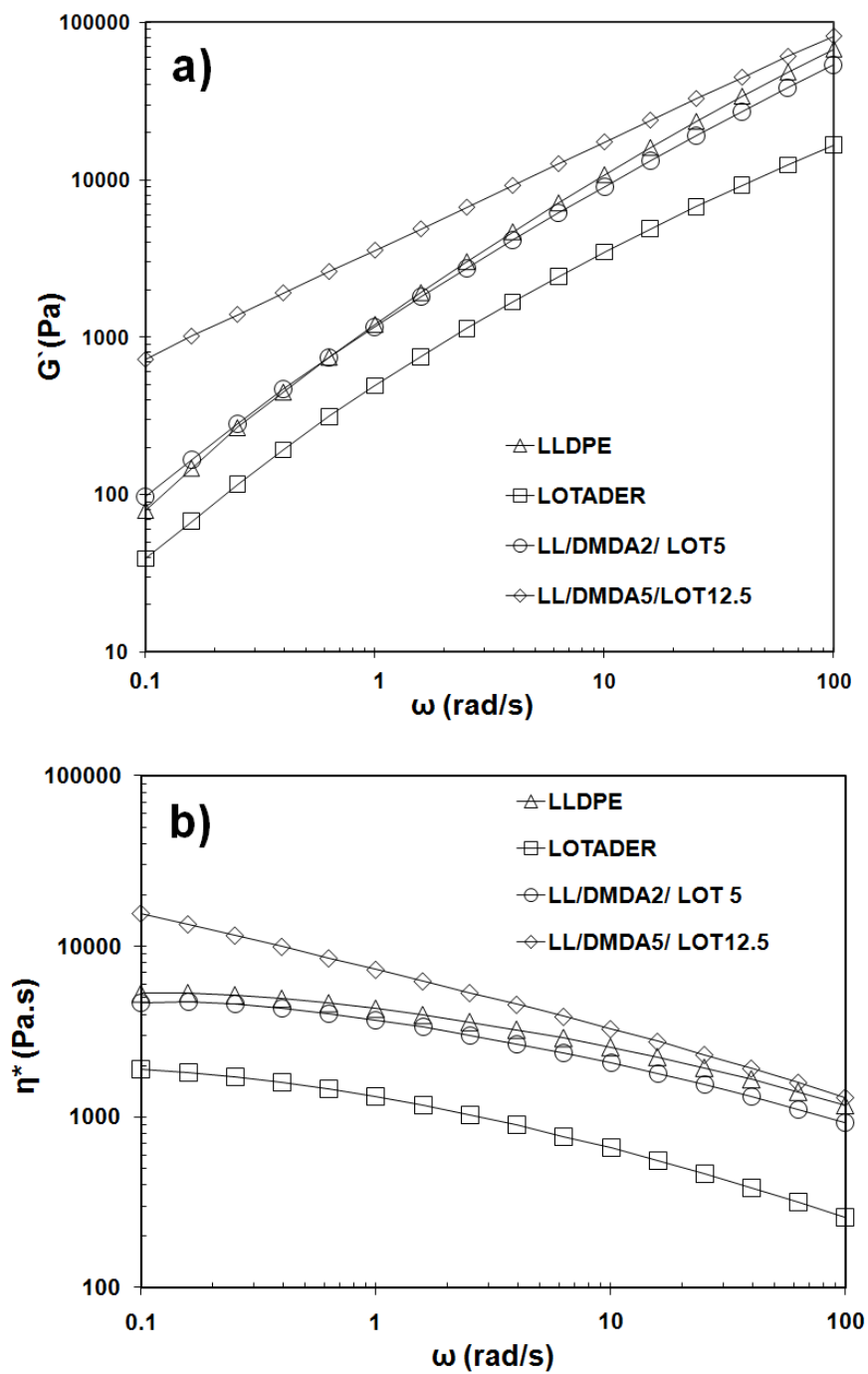


Figure 4.105 Frequency dependence of a) G' (Pa); b) η^* (Pa.s) of LLDPE/DMDA/LOT composites with 2 wt % and 5 wt % clay

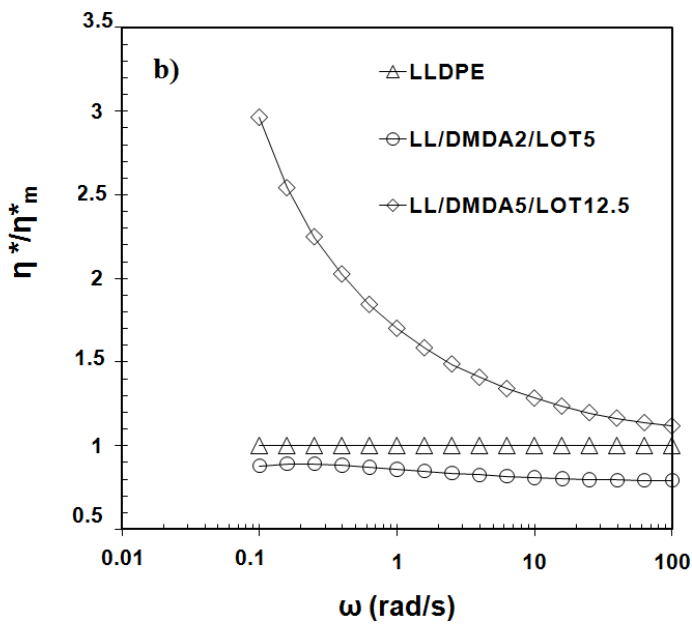
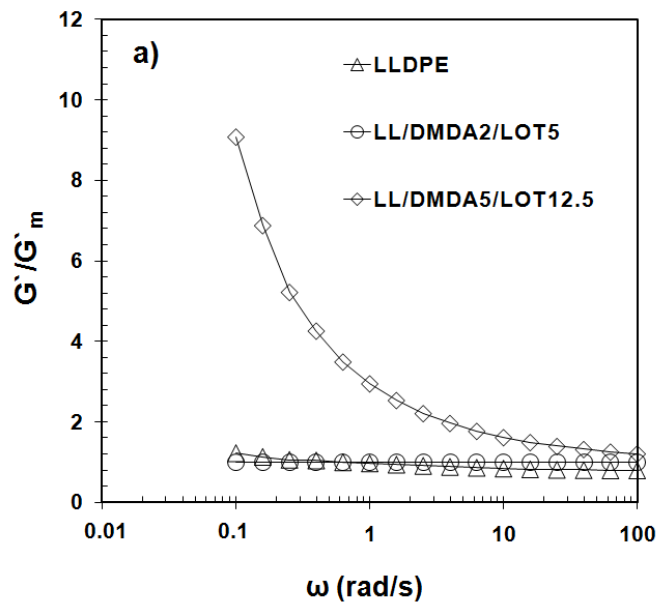


Figure 4.106 Frequency dependence of a) G' of PLSN containing DMDA relative to the $G'(\omega)$ of the matrix. b) η^* of PLSN containing DMDA relative to the $\eta^*(\omega)$ of the matrix

Fig 4.107 and Fig.4.108 indicate a slight enhancement in G' and η^* at low frequency with TBHP clay at a clay content of 2 %, whereas the data increase more as clay content increases to 5 %. Enhancements in the G' at low frequency region and at high clay content are attributed to strong filler–polymer interactions, clay-matrix tethering, uniform nanoscale dispersion, and much larger surface area of clay particles exposed to polymer chains [Barick et al., 2010]. A very slight transition from liquid-like to pseudo solid-like behavior can be observed for the nanocomposites with 2 % of TBHP at the low frequency region, but this transition is more clear with 5% of clay content as observed from part a of Fig.4.107 and Fig.4.108. Figures 4.107 and 4.108 indicate that a solid-like transition could be observed at clay content of 5 % for TBHP. The term “solid-like” is related with the behavior of an elastic solid, whose storage modulus is free of frequency, whereas “pseudo” means that the low-frequency plateau may be damaged by severe pre-loading [Drozdov et al., 2008]. In addition, with 2 % of TBHP, a crossover is seen (Fig. 4.107(b)) at a frequency of 4 rad/s and then elastic behavior of the sample becomes dominant.

Fig. 4.110 gives the frequency dependence of the ratios $G'(\omega)/G'_m(\omega)$ and $\eta^*(\omega)/\eta_m^*(\omega)$ of nanocomposites prepared by I34 organoclay. Results show similar trends with TBHP organoclay, since G' and η^* of the nanocomposites increases with clay content. At a clay content of 5 %, solid-like transition or percolation network was formed for the nanocomposites prepared with I34 organoclay. Effect of LOT/organoclay ratio can be deduced from Fig. 109 and 4.110 in which LOT/organoclay ratio, ξ , is 1 for LL/I34-5/LOT5 and $\xi = 2.5$ for LL/I34-5/LOT12.5 samples, since clay concentrations are the same (5 wt %) in both compositions. Results indicate more LOT enhances the G' , which may be attributed to higher dispersion of clay layers at high LOT concentration. In the presence of high LOT concentration, chance of formation of physical bonds between the phases increases. Maleic anhydride (MA) oligomer present in the LOT can interact with the layers of I34 clay through strong hydrogen bonding

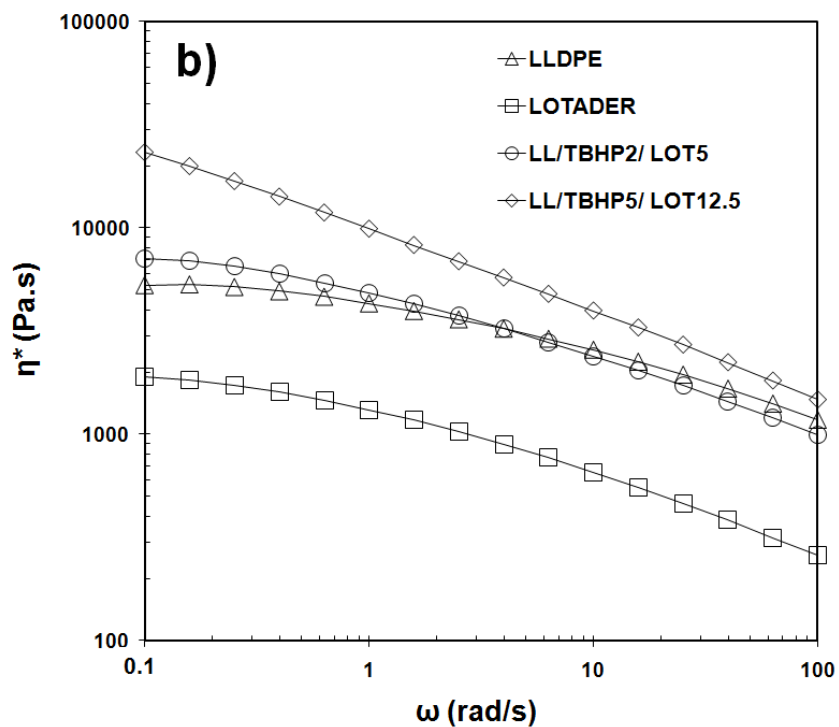
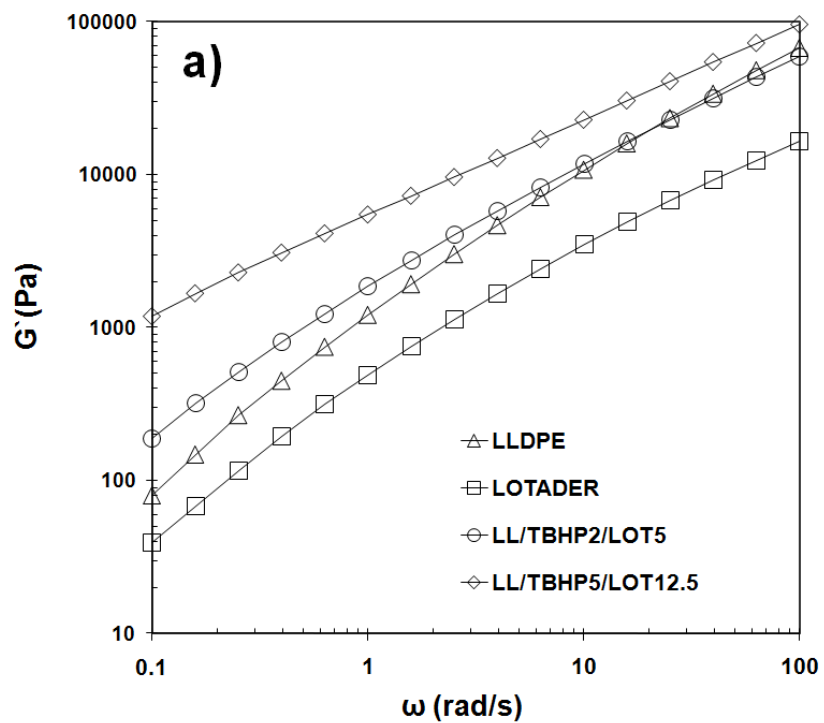


Figure 4.107 Frequency dependence of a) G' (Pa); b) η^* (Pa.s) of LLDPE/TBHP/LOT composites with 2 wt % and 5 wt % clay

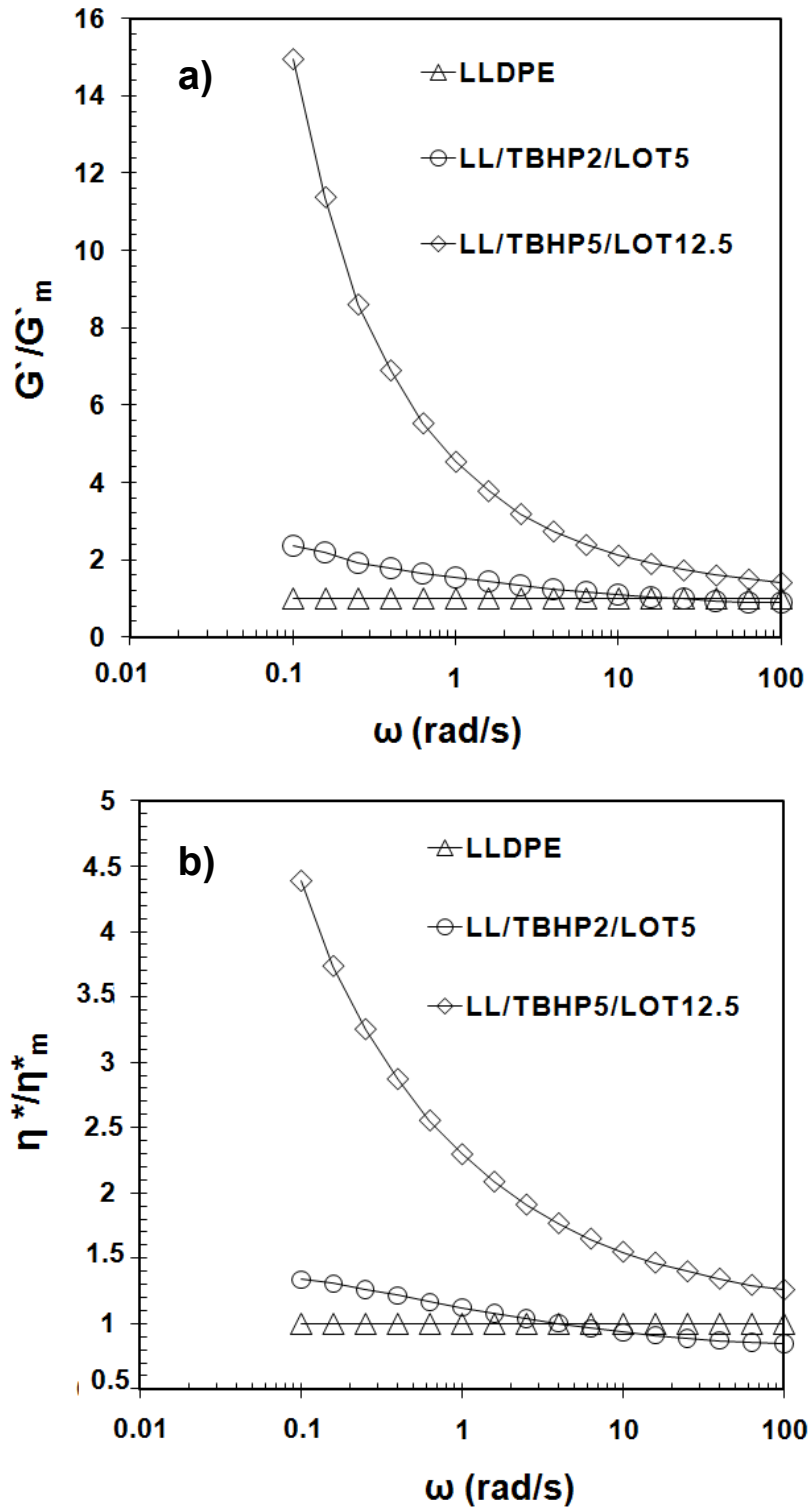


Figure 4.108 Frequency dependence a) G' of PLSN containing TBHP relative to the $G'(\omega)$ of the matrix. b) η^* of PLSN containing TBHP relative to the $\eta^*(\omega)$ of the matrix

between the polar functional group of -MA and the OH group of I34 [Galgali et al., 2001]. The relatively strong polymer–filler interaction present in the I34 system, compared to one prepared with TBHP and DMDA, resulting from the hydrogen bonding between the polymer and organoclay is likely to contribute to the restricted molecular motion, thus higher G' and η^* can be observed [Barick et al., 2010]. This increase is higher than that observed from mechanical properties which show high sensitivity of rheology to interfacial interactions compared to mechanical characterization.

Galgali et al., 2001 attributed typical rheological response, i.e., solid-like behavior, of the clay-polymer nanocomposites to the frictional interactions between the silicate layers and not due to immobilization of confined polymer chains between the silicate layers. The large anisotropy of the tactoids, specific surface area and the individual layers prevent the free rotation of these elements and is the main cause of the relatively lower value of the percolation threshold compared to traditional filled composites [Li. et al, 2003 (a); Rohlmann et al., 2006].

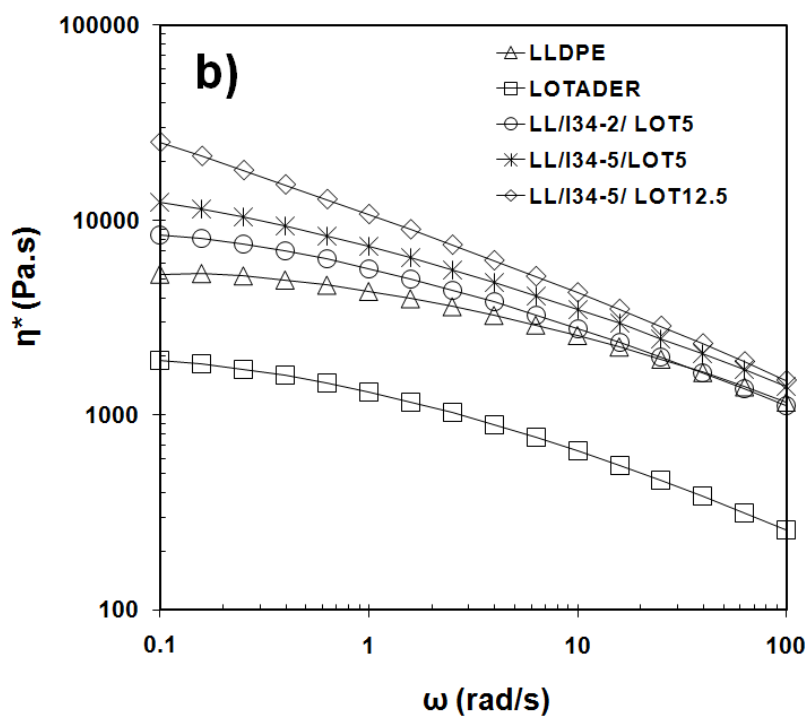
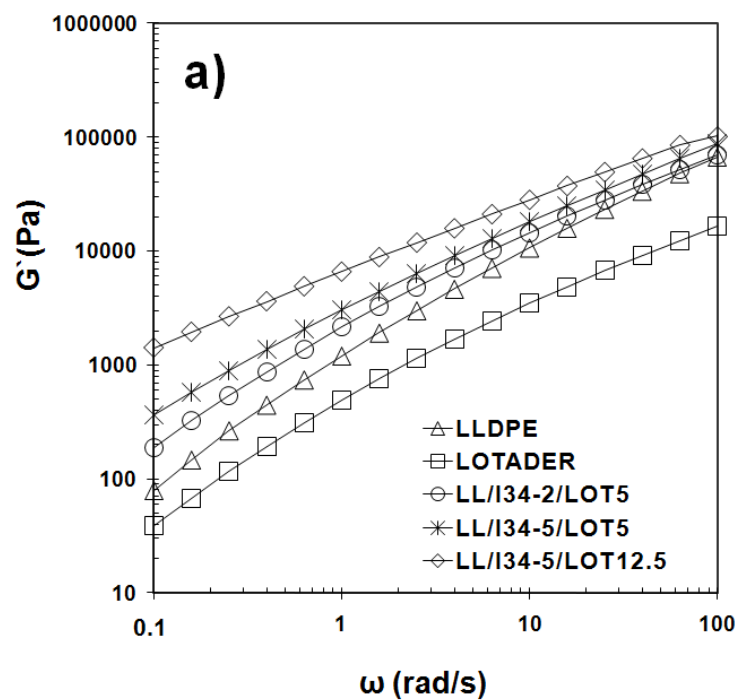


Figure 4.109 Frequency dependence of a) storage modulus, G' (Pa); b) complex viscosity, η^* (Pa.s) of LLDPE/I34/LOT composites with 2 wt % and 5 wt % clay

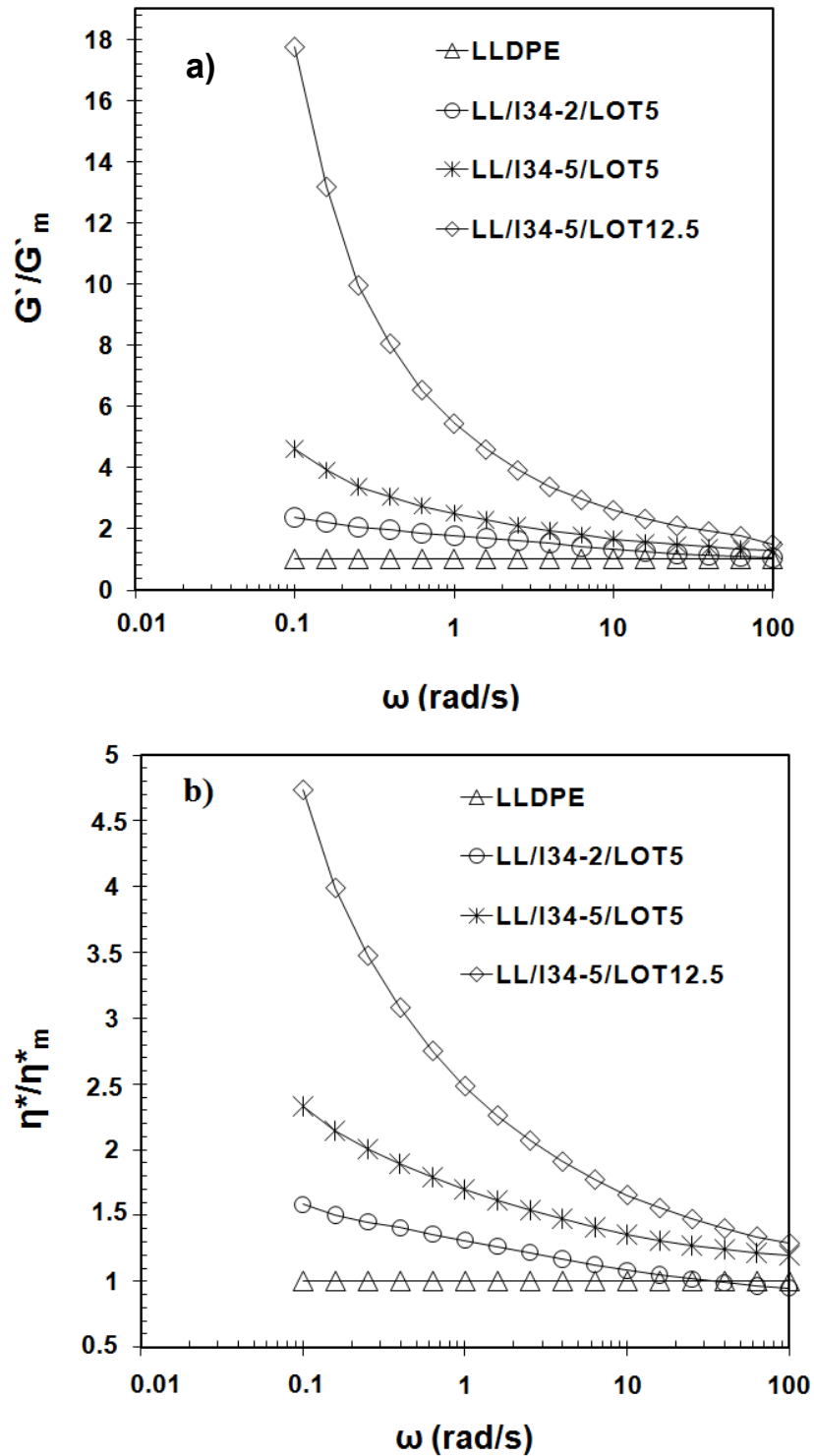


Figure 4.110. Frequency dependence a) G' of PLSN containing I34 relative to the $G'(\omega)$ of the matrix. b) η^* of PLSN containing I34 relative to the $\eta^*(\omega)$ of the matrix

Jian et al., 2003 defined the contribution of intercalated clay to G' of the nanocomposites (G'_{nano}) by two terms: the confinement effect (G'_{conf}) and the interparticle interactions (G'_{inter}), which result in the enhancement of low-frequency G' in comparison with the polymer matrix, i.e.,

$$G'_{\text{nano}} = G'_{\text{matrix}} + G'_{\text{conf}} + G'_{\text{inter}} \quad (\text{Eq.4.2})$$

where G'_{conf} arises from the confinement of silicate layers with an interlayer distance smaller than or the same order of the size of the chain coils that may lead to the alternation of the relaxing dynamic of the intercalated polymers. G'_{inter} arises from frictional interactions between the tactoids. These interactions become more pronounced as the clay content is increased, as can be seen in parts (a) of Fig. 4.106, 108 and 110. Enhancements are attributed to the formation of much stronger interfacial adhesion between the tactoids and the matrix while these increased interactions yield to the more homogeneous dispersion of the tactoids. Due to this enhanced interactions, the load is transferred between the tactoids, i.e., the tactoids can 'feel' each other through the matrix.

4.2.6.3.3.2. Effect of Modifier Type on Rheology

It is a fact that chemistry of the salts used in clay modification affect the linear viscoelastic properties of the PLSN. These effects may be attributed to changes in mesoscopic clay structure, short-long range clay ordering or surface interactions between the clay and the polymer matrix [Solomon et al, 2001]. Therefore it is important to study the effect of organoclay chemistry on rheology of PLSN considering such interactions and structures. Figures 4.111 and 4.113 show the frequency dependence of G' and η^* for the nanocomposites prepared with different organoclays at constant clay content. Parts (a) and (b) of the Figures 4.112 and 4.114 show frequency dependence of $G'(\omega)/G'_m(\omega)$ and $\eta^*(\omega)/\eta^*_m(\omega)$ ratios of

the samples prepared with different organoclays at a constant clay content respectively. These figures indicate that the type of organoclay definitely has an effect on the rheological response of composites.

Effect of I34 in the low frequency region is more pronounced compared to DMDA and TBHP (Fig. 4. 111), at a clay content of 2 wt % revealing good adhesion and strong interfacial interactions between the clay layers and the matrix for this clay. In PLSN rheological functions are affected mainly by filler-filler and polymer-filler interactions. "Filler-filler interactions arise through electrostatic and van der Waals' forces and may result in the arrangement of particle aggregates and eventually of fractal agglomerated structures. The polymer-particle interactions indicate the attachment/detachment of chains to/from the filler surface, process controlled by the effective surface affinity" [Sarvestani and Picu, 2004; Kohl and Beaucage, 2002]. It is probable that hydroxyl groups of I34 have capability of formation of H bond with LLDPE/LOT matrix. Therefore, enhanced filler-polymer interactions result in enhanced G' and η^* in composites with I34, compared to TBHP and DMDA. LLDPE nanocomposite with 2 w% of TBHP showed enhanced G'/G'_m compared to 2% of DMDA as can be seen from Fig. 112 (a) and (b). TEM analysis had also confirmed higher degree of dispersion with TBHP. DMDA organoclay with 2 w% could not form strong clay network.

Figures 4.113 and 4.114 show frequency dependence of nanocomposites prepared with 5 % of organoclay. At a clay content of 5 %, composites prepared with TBHP clay show similar storage modulus (G') and complex viscosity (η^*) to that prepared with commercial clay I34 and show the success of modification. Composites prepared with DMDA also show enhancement in the G' (at a clay content of 5 wt %) not as high as those of TBHP and I34, but still higher compared to LLDPE showing intercalated structure also in this clay. Low frequency enhancements of LL/DMDA5/LOT12.5 in G' and η^* are also higher than those observed in LL/I345/LOT5. These results reveal that, organoclays DMDA, TBHP and

I34 used in this set resulted in percolation network at 5 w % organoclay. While XRD analysis is not much sensitive to the differences in the chemistry, G' is a strong function of chemistry as also can be depicted through Figures 113-114. Solomon et al., 2001 explained this difference by two arguments. Surfactants adsorbed by the exterior surface of the tactoids' area may intercede differences in the attractive interparticle interactions that cause increase in the hybrid network. In addition, the size and shape of the multiplatelet domains may depend on surfactant chemistry. These delicate changes in the mesoscopic structure are poorly characterized by XRD yet could yield substantial rheological effects.

Through the formation of nanocomposites, surface area of the resulting clay particles are orders of magnitude greater than the surface area of the aggregates, which cause increase in the number of platelets that are detached from each other. Increase in the surface area as well as the aspect ratio of the clay particles would enhance the elasticity and the shear viscosity of the suspension [Demirkol and Kalyon, 2007]. Rheological results together with mechanical tests reveal that composites prepared with TBHP and I34 show enhanced properties probably due to better interfacial attraction between the matrix and clay tactoids owing to higher level of dispersion of clay layers through the matrix. Although LL/DMDA2/LOT5 shows similar rheological results to LLDPE, it still has higher mechanical properties in comparison to those of LLDPE.

TEM analysis of composites prepared with 2 wt % of TBHP composites had shown more intercalated/partially exfoliated structure compared to DMDA. Better dispersion of clay in TBHP composites providing higher surface area and aspect ratio could lead to the increase in the G' at lower frequencies. G' of the samples prepared with I34 is highest among the ternary composites, as it is also observed in Young's modulus (Fig.4.87) and tensile strength (Figure 4.88).

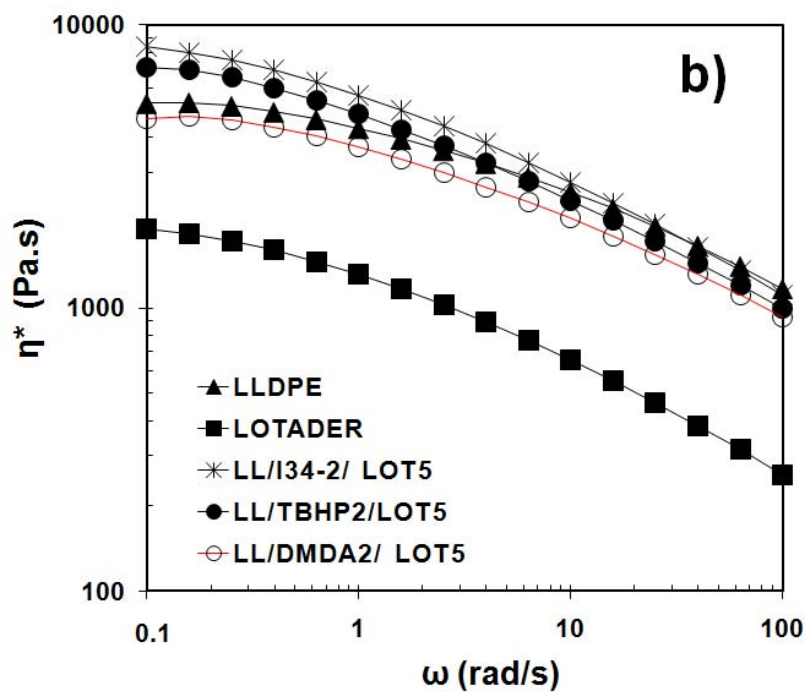
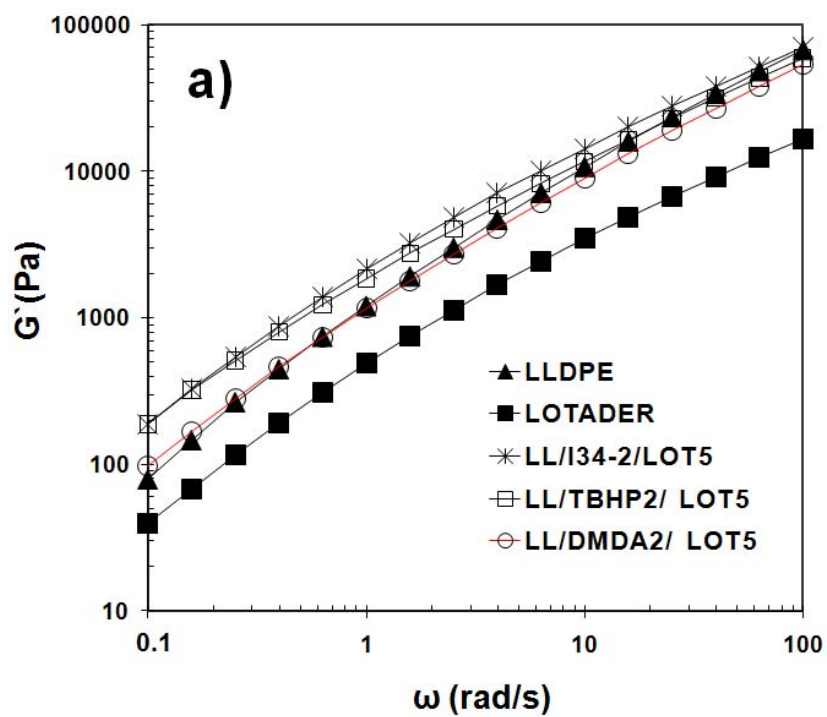


Figure 4.111 Frequency dependence of a) G' (Pa); b) η^* (Pa.s) of LLDPE/Organoclay2/LOT5 composites

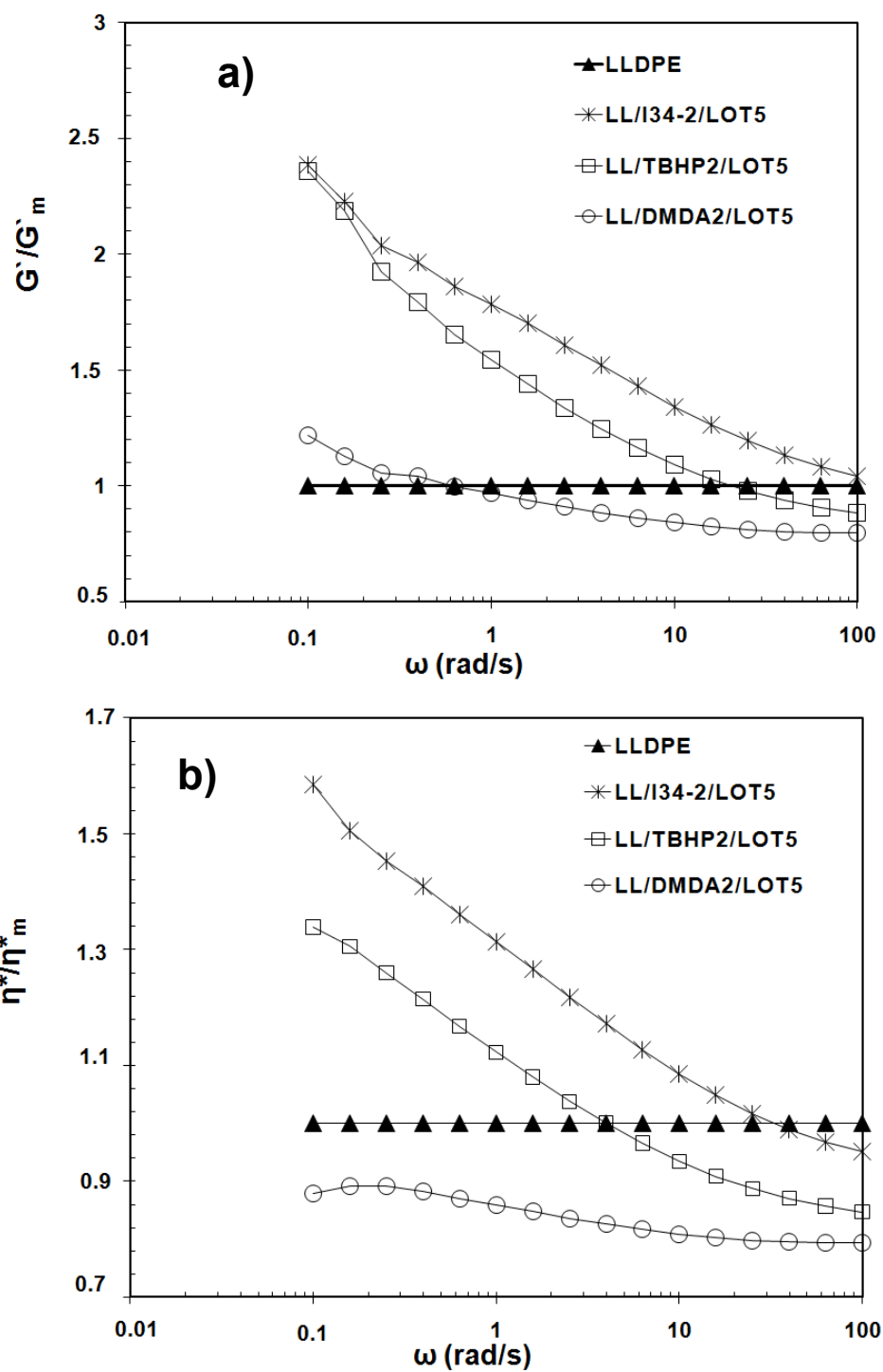


Figure 4.112 Frequency dependence of a) G' of PLSN containing 2 % of clay relative to the $G'(\omega)$ of the matrix. b) η^* of PLSN containing 2 % of clay

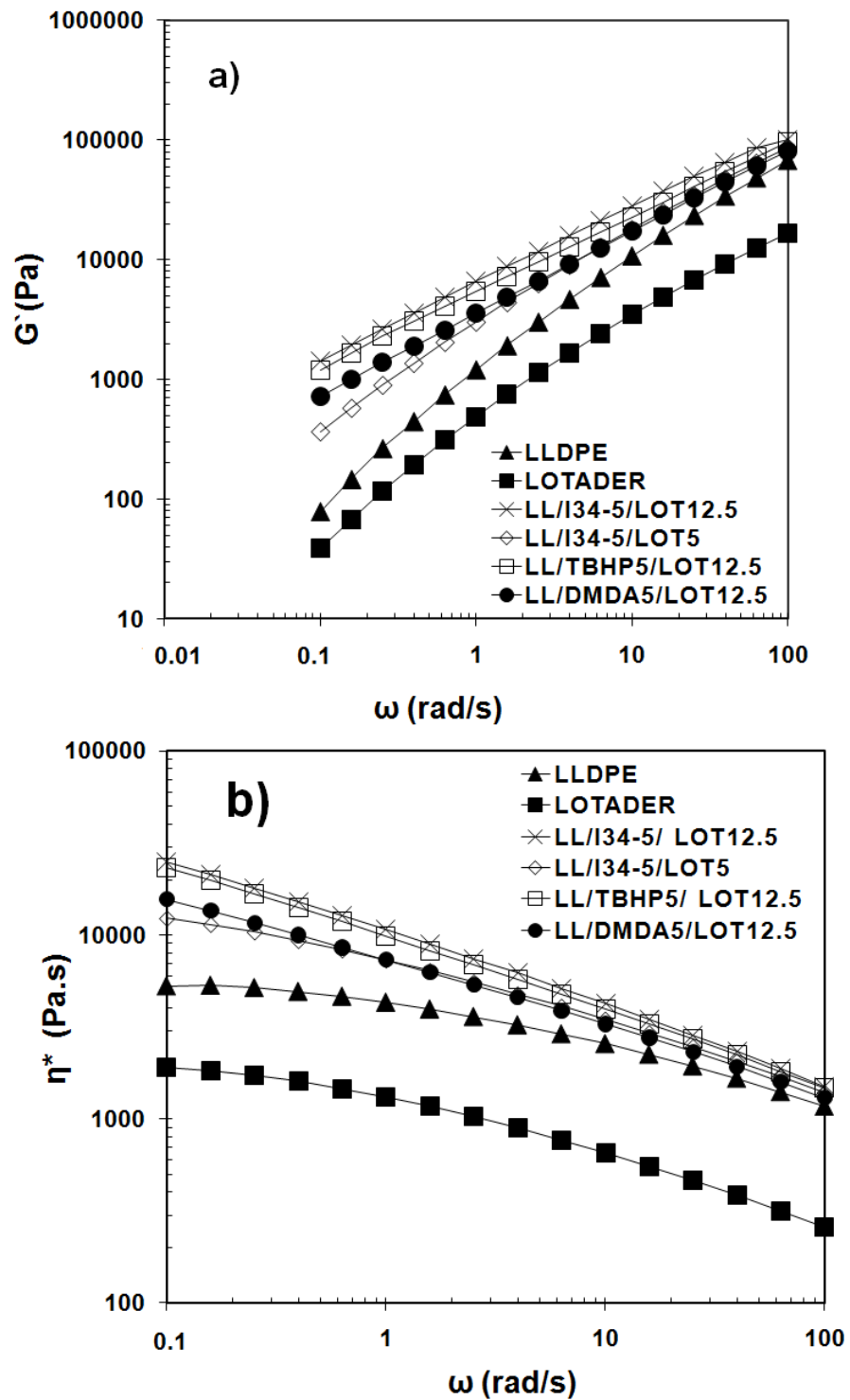


Figure 4.113 Frequency dependence of a) G' (Pa); b) η^* (Pa.s) of LLDPE/Organoclay5/LOT12.5 composites

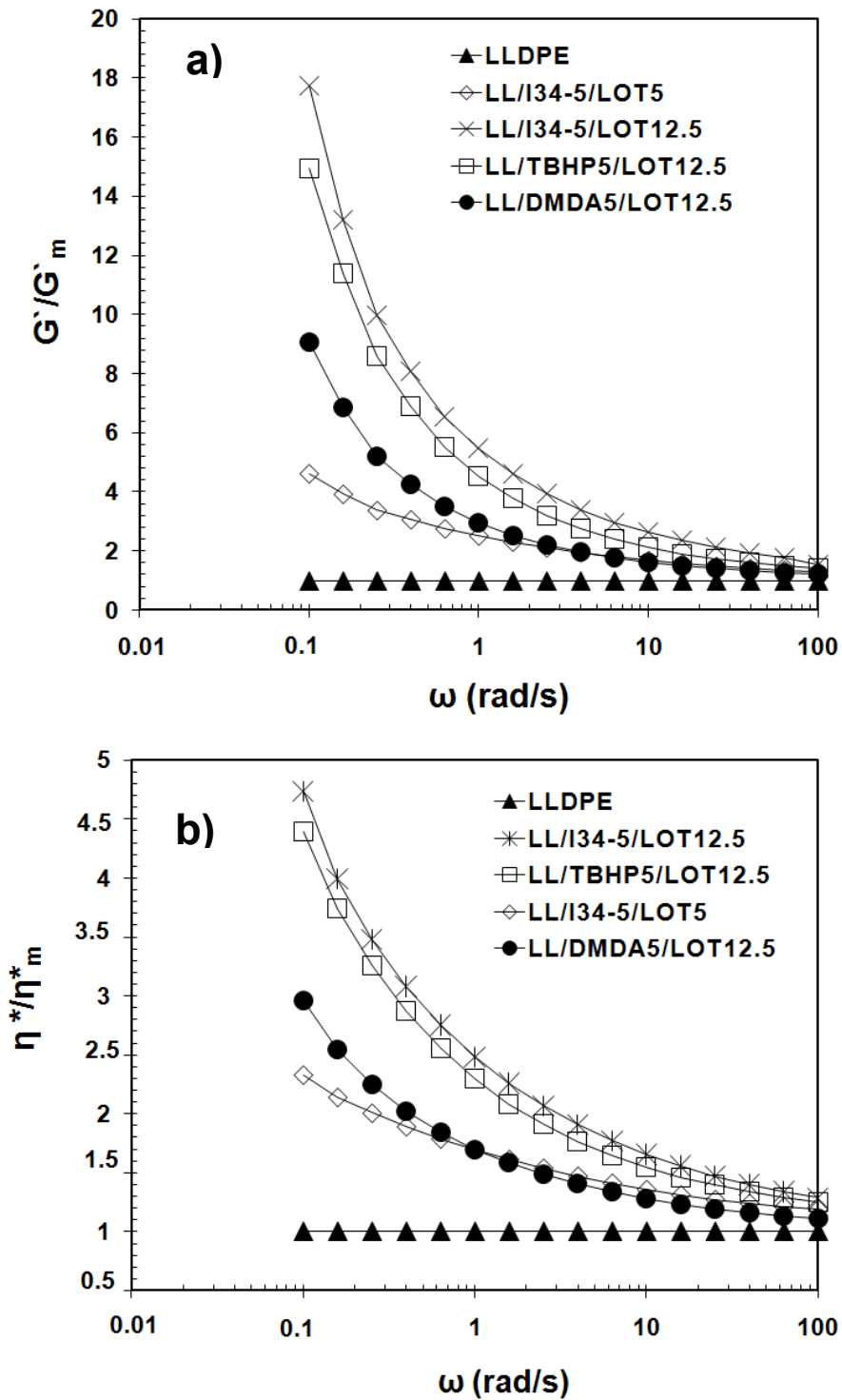


Figure 4. 114 Frequency dependence of a) G' of PLSN containing 5 % of clay relative to the $G'(\omega)$ of the matrix. b) η^* of PLSN containing 5 % of clay relative to the $\eta^*(\omega)$ of the matrix

Figure 4.115 shows G'' versus G' for LLDPE nanocomposites prepared with 2 wt % of clay. The dashed line in the figure shows $G'' = G'$ and is called as the equi-moduli line. LLDPE is on the very left side of the equi-moduli line indicating liquid-like behavior. It becomes more elastic as it is compounded with LOT (LLDPE95/LOT5). LOT is more elastic than LLDPE since it is near the equi-moduli line. Composites with TBHP is more elastic than composites with I34 and DMDA.

Figure 4.116 shows G'' versus G' for LLDPE composites with 5 wt % of clay. Liquid like behavior of LLDPE becomes pseudo solid-like as it is mixed with LOT and organoclays. DMDA based nanocomposite is the most elastic material among the ternary nanocomposites. Comparison of Figures 4. 110 and 4.111 indicate that composites with 5 wt % of clays show higher elastic property compared to composites prepared with 2 wt % clay.

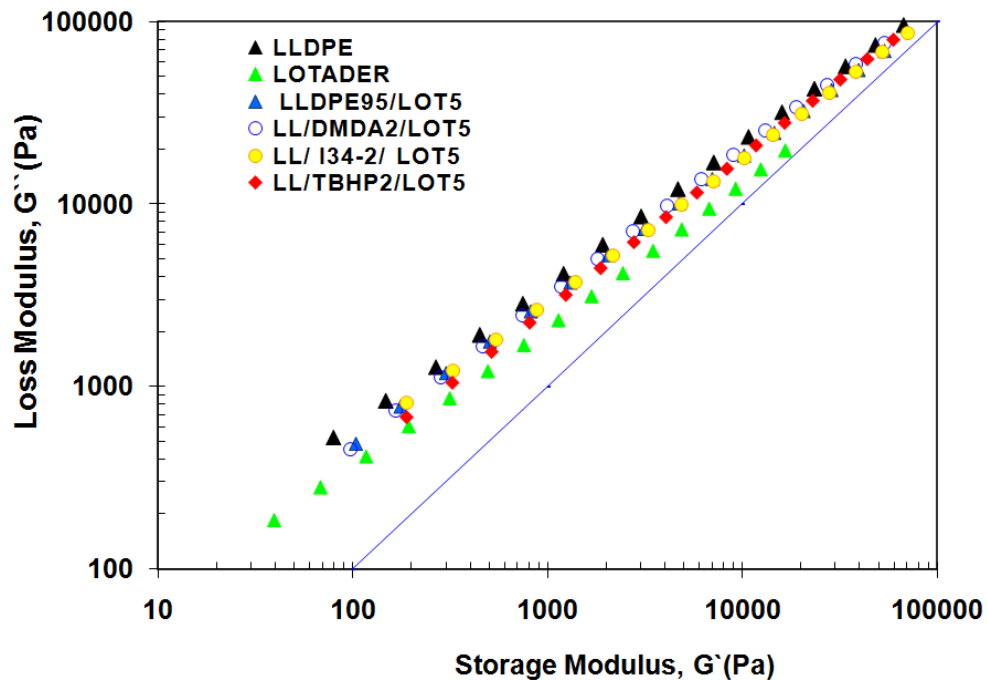


Figure 4.115 Loss modulus as a function of storage modulus for LLDPE/Organoclay2/LOT5 composites

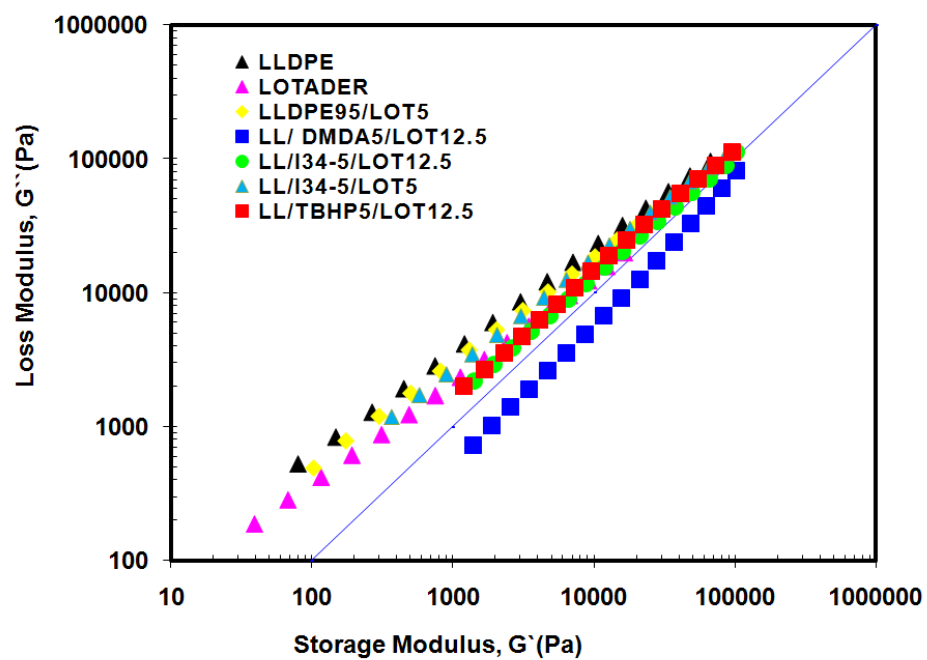


Figure 4.116 Loss modulus as a function of storage modulus for LLDPE/Organoclay5/LOT12.5 composites

CHAPTER 5

CONCLUSIONS

5.1 Composites Prepared by Organoclays Derived from Raw Bentonite (RB)

5.1.1 Purification of Reşadiye Bentonite

Reşadiye bentonite clay was purified by sedimentation in distilled water to have a clay mineral which is rich in Na⁺-MMT content. Afterwards, purified bentonite (PB) was modified and organophilized by quaternary alkyl and phosphonium salts with long alkyl tails.

Chemical analysis of RB and PB showed that Ca⁺² content was reduced (CaO) from 2.6 to 0.33 % because of replacement of Ca⁺² ions with Na⁺ in the suspension rich in Na due to added Na₄(P₂O₇).

Cation exchange capacity (CEC), i.e., the maximum amount of cations that can be taken up, increased from 65 to 100 mmol/100 g of clay after purification, indicating success of purification.

XRD analysis of PB showed that the amount of non-clay parts decreased upon purification, and PB had peaks similar to PGW. Analysis indicated that non-clay parts of RB, i.e., clinoptilolite, feldspar, calcite were mainly sedimented and purification was successful.

5.2 Modification of Bentonite

Both RB and PB were used in modification procedure to observe if purified sample usage makes a difference in the level of clay dispersion in the polymer matrixes.

XRD analysis of organobentonites showed increases in the interlayer spacing of the bentonite, revealing the presence of alkyl cations between the layers of bentonite, thus supporting the intercalation and formation of nanoclays. Results showed that longer and bulkier the cations of modifier are, the higher is the d-spacing of the organoclay.

TGA of PB and organomodified samples indicated that the weight-loss due to water desorption in the initial stages of the organomodified bentonites was much smaller than that of (PB), indicating that the PB was changed to organophilic clay by treating with the long alkyl surfactants.

FTIR spectra of modified bentonites showed different absorption bands from PB and RB near 2931cm^{-1} ($\nu_{\text{as}}(\text{CH}_2)$, asymmetric stretching of CH_2) and 2854cm^{-1} ($\nu_{\text{s}}(\text{CH}_2)$, symmetric stretching). New absorption band in modified bentonites at 1487cm^{-1} is attributed to flexural vibrations of CH_3 . FTIR analysis supported the intercalation of alkyl cations within the bentonite layers with these new bands observed in the modified bentonites.

5.3 PPM Based Nanocomposites (SET-1)

Ternary composites of PPM/Organoclay/MAPP were prepared by extruding the mixture twice. Ternary composites of PPM/Organoclay/MAPP with a clay content of 2 % and MAPP/organoclay ratio of (α) 1, and with a clay content of 1 % and $\alpha=3$ resulted in microcomposite formation as revealed by the XRD analysis. These sets of composites were prepared by organoclays produced from unpurified bentonite, indicating that poor dispersion of clay layers through the matrix is due to the flaws present in it. In addition, high viscosity of PPM limited the diffusion of polymer matrix through the clay layers during applied shear in the extruder. Although high screw speed can increase delamination of clay layers, it also results in low residence time in the extruder and in turn reduces the chance of intercalation of the polymer into the organoclay phase.

Young`s modulus increased in these ternary composites possibly due to the reinforcement effect of the organoclays. Besides this, preferential orientation during high pressure injection molding could be another reason for increased Young`s modulus (YM). Tensile strength (TS) and yield stress (YS) of the composites were lower compared to those of neat PPM due to presence of clay layers that were not delaminated as confirmed by XRD analysis. Although these results were lower compared to neat PPM, when the effect of α was taken into consideration, increase in α caused enhancements in YM and TS due to increased surface area of the clay and adhesion between the clay and polymer phases.

DSC analysis of ternary samples showed slight enhancements in crystallinity.

5.4 PPE Based Nanocomposites (SET-2)

In this set, PPE/Organoclay2/MAPP5 compositions were prepared with HMA, TKA and TKA50 organoclays produced from RB. In addition commercial MMT, PGW, was modified by TKA cation (PGWTKA) and used in ternary composites. PPE used in this set had higher MFI compared to PPM. XRD analyses of this set of samples also showed limited dispersion in the matrix possibly due to lower viscosity and applied shear stress. When cations of HMA and TKA are compared, TKA with 40 C atom (4Cx10) in its backbone is believed to shelter the possible entry of polymer segments through the clay layers. In addition, bulkier alkyl groups of TKA cation may have increased the interaction energy of clay and intercalants and produced relatively less organophilic organoclay. HMA with one long (16 C) alkyl tail also resulted in microcomposite formation as shown by XRD analysis. Comparison of TKA and TKA50 showed that use of excess surfactant during modification process is unnecessary, since composites prepared from both of the TKA contents displayed microcomposite structure as shown by XRD analysis. Organobentonite prepared by PGW, which is a commercial pure MMT, also showed microcomposite formation. From these results, it was concluded that TKA is not a suitable cation for preparation of PPE-clay nanocomposites.

Generally YM and YS of these composites increased compared to neat PPE; while TS was enhanced in the case of TKA clay. Differing from the use of PPM matrix, elongation at break values of the composites were lower compared to that of neat PPE.

5.5 Composites Prepared from Organoclays Derived from PB

5.5.1 PPE Matrix Nanocomposites

Organoclays used in this set of composites were DMDA, TBHP and STKA. Composites of PPE/Organoclay2/MAPP5 were produced by

extrusion followed by batch mixing. Increased duration of shear significantly affected the final properties of composites as confirmed by XRD and mechanical testing. Increased d-spacings and mechanical property enhancements were obtained by batch mixing of the samples. These results indicated the sensitivity of clay dispersion to processing conditions. XRD analysis showed increased interlayer spacing with organoclays DMDA and TBHP, while STKA did not show a dispersed structure. Young`s modulus and yield stress of composites prepared with all the three clays showed enhancements compared to neat PPE. As in the previous part of the conclusions, composites of STKA showed contradictions between XRD and mechanical characterization, pointing to the effect of orientation of clay layers during injection molding. SEM analysis showed that STKA resulted in tactoids that had the same thickness but were longer than the tactoids of samples prepared with DMDA and TBHP.

TEM analysis of DMDA and TBHP clay showed intercalated structures as also shown by XRD analysis.

5.5.2 LLDPE Matrix Nanocomposites

Organoclays DMDA, TBHP, STKA and I34, were used in the LLDPE based composites at two different concentrations, i.e., 2 and 5 %. LOT/organoclay ratio was kept constant at 2.5. Binary composites of LOT98/Organoclay2 were also prepared to observe the compatibility between the two phases. Organoclay STKA showed incompatibility as shown by the XRD analysis, thus ternary composites of STKA were not prepared. XRD analysis of DMDA and I34 showed partially intercalated clay dispersion, as also confirmed by TEM analysis.

XRD of composite with TBHP clay showed neither intercalation nor exfoliation, while TEM analysis showed that intercalated, partially intercalated and even exfoliated layers were present in it. Rheological

analysis of composites of TBHP showed enhancements in storage modulus and complex viscosity compared to neat LLDPE matrix also pointing to better dispersion of clay layers. Tensile strength and modulus of the LLDPE were also increased by addition of TBHP. In conclusion, in contrast to XRD analysis, TEM, rheology and mechanical analyses results indicated nanocomposite formation with TBHP clay. XRD and TEM analysis also confirmed the existence of nanocomposite formation with DMDA organoclay.

Commercial clay I34 showed partially intercalated layers in XRD analysis while its TEM analysis also indicated intercalation. Rheological functions, G' , G'' and η^* , of composites prepared by I34 clay showed higher enhancements compared to organoclays prepared with DMDA and TBHP. Young's modulus and tensile strength indicated higher degree of enhancements compared to neat LLDPE and other organoclays. Composites with LOT/I34=1 were also prepared and the results indicated that XRD peak intensities were reduced with more LOT addition in comparison to the one prepared with same clay concentration (5 wt %) but higher LOT (LOT/I34=2.5). G' , G'' and η^* responses also increased in composites with LOT/I34=2.5. Sensitivity of mechanical analysis was lower compared to rheology and almost identical results were obtained when LOT/I34 ratio was 1 and 2.5. Results indicated that higher compatibilizer addition increased the adhesion between the phases and gave rise to the increase in the surface area of dispersed clay layers.

Composites prepared with DMDA and TBHP showed much higher elongation at break values compared to one prepared with I34. Since area under the stress-strain curves can be taken as a measure for the energy that is dissipated by plastic deformation within the sample, the results confirmed the superiority of TBHP and DMDA. In addition, for composites of DMDA and TBHP Young's modulus and tensile strength of the matrix were higher compared to the LLDPE matrix. Nevertheless, composites

prepared with commercial clay I34 showed higher improvements in YM and TS compared to those of DMDA and TBHP.

In the light of the present study, potential use of Turkish Reşadiye bentonite in the production of polymer nanocomposites with enhanced mechanical properties was confirmed; when appropriate surface modifier is used and clay concentration and processing conditions are optimized. Results also showed that XRD analysis must be supported by both TEM, mechanical testing and rheology in assessing the degree of dispersion of clay layers in the polymer matrix.

REFERENCES

- Akçay, M., 2006. Characterization and Adsorption Properties of Tetrabutylammonium Montmorillonite (TBAM) Clay: Thermodynamic and Kinetic Calculations. *J. Colloid Interface Science*, 296, 16–21.
- Alexandre M., Dubois P., 2000, Polymer-Layered Silicate Nanocomposites: Preparation, Properties and Uses of a New Class of Materials, *Materials Science and Engineering*, 28, 1-63.
- ASTM D638-03, 2004. Standard Test Methods for Tensile Properties of Plastics.
- ASTM/C837 – 99, 2003, Standard Test Method for Methylene Blue Index of Clay. Annual Book of ASTM Standards, 08.01, Philadelphia, PA.
- Arroyo, M., López-Manchado, M.A., Herrero, B., 2003. Organomontmorillonite as Substitute of Carbon Black in Natural Rubber Compounds, *Polymer*, 44, 2447–2453.
- Awad W. H., Gilman J.W., Nydena M., Harris R. H., Sutto T.E., Callahan J., Trulove P. C., DeLong H. C., Fox D. M., 2004. Thermal Degradation Studies of Alkyl-Imidazolium Salts and Their Application in Nanocomposites, *Thermochimica Acta*, 409, 3-11.
- Bafna A. A., 2004. Polyethylene-Clay Nanocomposites: Processing-Structure-Property Relationship, Ph.D. Thesis, University of Cincinnati, Ohio, USA.
- Bailey SW, 1980. Summary of recommendations of AIPEA [Association Internationale Pour l'Étude des Argiles] Nomenclature Committee on Clay. *Am. Mineral*, 65, 1-7.
- Bao S. P., Tjong S. C., 2007. Impact Essential Work of Fracture of Polypropylene/Montmorillonite Nanocomposites Toughened with SEBS-g-MA Elastomer, *Composites*, 38, 378-387.
- Barick A. K., Tripathy D. K., 2010, Effect of Organoclay on the Morphology, Mechanical, Thermal, and Rheological Properties of Organophilic Montmorillonite Nanoclay Based Thermoplastic Polyurethane Nanocomposites Prepared by Melt Blending, *Polymer Engineering and Science*, DOI 10.1002/pen.21556.
- Basara C., Yilmazer U., Bayram G., 2005. Synthesis and Characterization of Epoxy Based Nanocomposites, *Journal of Applied Polymer Science*, 98, 1081–1086.

Bergaya F., Theng B.K.G and Lagaly G., 2006. Handbook of Clay Science, e-book, Elsevier, Chapter-5, p. 152.

Billmeyer, F.W., 1984. Textbook of Polymer Science, John Wiley & Sons. New York, USA.

Boylu F., Cinku K., Cetinel T., Erkan I. and Demirer N., 2007. The Separation Efficiency of Reşadiye Na-Bentonite by Hydrocyclone, 13th Clay Symposium (Isparta, Turkey) Catalogue, pages 213-227.

Bower, D.I., 2002. An Introduction to Polymer Physics., Cambridge University Press., USA.

Caine M.A., McCabe R.W., Wang L., Brown A.G. and Hepworth, 2001. The Influence of Single Oxygen in the Fading of Carbonless Copy Paper Primary Dyes on Clay, Dyes and Pigments, 49, 135-143.

Callister W., 1997. Materials Science and Engineering: An Introduction, 4th Edition, John-Wiley & Sons, USA.

Callister, J., and William D., 2003. Materials Science and Engineering: An Introduction. 6th ed., John Wiley & Sons, New York, USA.

Calderon J.U., Lennox B., Kamal M.R., 2008. Thermally Stable Phosphonium-Montmorillonite Organoclays, Applied Clay Science, 40, 90-98.

Can M.F, Erkan I., Yıldız E., Karakaş F., 2007. Organoclay Preparation and Characterization from Na-Bentonites Modified with Cetyl Pyridinium Chloride (CPC) Monohydride”, 13th Clay Symposium Catalogue, Isparta, Turkey, pages 365-375.

Cao G., 2004. Nanostructures and Nanomaterials: Synthesis, Properties and Applications, Imperial College Press, 2004.

Carretero M.I., Pozo M., 2009. Clay and Non-clay Minerals in the Pharmaceutical Industry Part I: Excipients and Medical Applications, Applied Clay Science, 46, 73-80.c.

Cengiz, F., Preparation and Characterization of Recycled Polypropylene Based Nanocomposites, 2008. MS Thesis, Chemical Engineering Department, Middle East Technical University, Ankara, Turkey.

Cinku K., Ozkan G., Çetinel T., Can F., Boylu F., 2007. Effects of the Mechanical Activation of the Rheological Properties of Reşadiye Bentonites, 13th Clay Symposium (Isparta, Turkey) Catalogue, pages 130-135.

Celik M , Onal M., 2004. Synthesis and Characterization of Poly(glycidyl

methacrylate)/Na-Montmorillonite Nanocomposite, *Journal of Applied Polymer Science*, 94, 1532–1538.

Chawla K. K., 1998. *Composite Materials: Science and Engineering*, Springer Science Business Media Inc., USA.

Chen B., Evans J. R.G., 2005. X-ray Diffraction Studies and Phase Volume Determinations in Poly(ethylene glycol)–Montmorillonite Nanocomposites, *Polymer International*, 54, 807-813.

Chen J.H., Zhong J.C., Cai Y.H., Su W.B., Yang Y.B., 2007. Morphology and Thermal Properties in the Binary Blends of Poly (propylene-co-ethylene) copolymer and Isotactic Polypropylene with Polyethylene, *Polymer*, 48, 2946-2957.

Cho J.W. and Paul D.R., 2001. Nylon 6 Nanocomposites by Melt Compounding, *Polymer*, 42, 1083.1094.

Chow W. S., Mohd I. Z. A., Karger-Kocsis J., Apostolov A. A., Ishiaku U.S., 2003. Compatibilizing Effect of Maleated Polypropylene on the Mechanical Properties and Morphology of Injection Molded Polyamide 6/Polypropylene/Organoclay Nanocomposites, *Polymer*, 44, 7427.

Contreras V., Cafiero M., Silva S. Da, Rosales C., Perera R., Matos M., 2006. Characterization and Tensile Properties of Ternary Blends with PA-6 Nanocomposites, *Polymer Engineering and Science*, DOI 10.1002/pen.20572.

Crozier, R.D. 1992, *Flotation: Theory, Reagents and Ore Testing*, Pergamon, Oxford, UK.

Deborah D.L. Chung, *Composite Materials: Science and Applications, Functional Materials for Modern Technologies*, 2004, Springer-Verlag London Limited, Great Britain.

Demirkol E.A., Kalyon D. M., 2007. Batch and Continuous Processing of Polymer Layered Organoclay Nanocomposites, *Journal of Applied Polymer Science*, 104, 1391–1398.

Demirkol E.A., *Processing and Rheological Behavior of Organomodified Clay/Polymer Nanocomposites*, December 2005. MSc Thesis, Stevens Institute of Technology, Hoboken, New Jersey, USA.

Dennis, H.R., Hunter, D.L., Chang, D., Kim, S., White, J.L., Cho, J.W. and Paul, D.R., 2001. Effect of Melt Processing Conditions on the Extent of Exfoliation in Organoclay- Based Nanocomposites, *Polymer*, 42, 9513–9522.

Deshmane C., Yuan Q., Perkins R.S., Misra R.D.K., 2007. On Striking Variation in Impact Toughness of Polyethylene–Clay and Polypropylene–Clay Nanocomposite Systems: The Effect of Clay–Polymer Interaction, *Materials Science and Engineering A*, 458, 150–157.

Ding Y., Guo C., Dong J., Wang Z., 2006. Novel Organic Modification of Montmorillonite in Hydrocarbon Solvent Using Ionic Liquid-Type Surfactant for the Preparation of Polyolefin–Clay Nanocomposites, *Journal of Applied Polymer Science*, Vol. 102, 4314–4320.

Drozdov A.D., Jensen E.A., and Christiansen J.C., 2008. Pseudo-Solid-like Behavior of Nanocomposite Melts, *International Journal of Nanotechnology and Applications* ISSN 0973-631X, 2, Number 1, 1–14

Durmus A., Kasgoz A, Macosko, 2007. Linear Low Density Polyethylene (LLDPE)/clay Nanocomposites. Part I: Structural Characterization and Quantifying Clay Dispersion by Melt Rheology, *Polymer*, 48, 4492-4502.

Durmus A., Kasgoz A., Macosko C.W., 2008. Mechanical Properties of Linear Low-density Polyethylene (LLDPE)/Clay Nanocomposites: Estimation of Aspect Ratio and Interfacial Strength by Composite Models, *Journal of Macromolecular Science, Part B: Physics*, 47, 608-619.

Eckel D F., Balogh M. P., Fasulo P. D., Rodgers W. R., 2004. Assessing Organo-Clay Dispersion in Polymer Nanocomposites, *Journal of Applied Polymer Science*, 93, 1110–1117.

Erol O., Unal H.I., Sari B., 2010. Synthesis, Electrorheology, and Creep Behaviors of In Situ Intercalated Polyindole/Organo-Montmorillonite Conducting Nanocomposite, *Polymer Composite*, 31, 471-481.

Filho F.G.R., Melo T. J. S., Marcelo R., Suedina S., 2005. Thermal Stability of Nanocomposites Based on Polypropylene and Bentonite, *Polymer Degradation and Stability*, 89, 383-392.

Fornes T.D., Yoon P.J., Hunter D.L., Keskkula H., Paul D.R , 2001. Nylon-6 Nanocomposites: The Effect of Matrix Molecular Weight, *Polymer*, 42, 9929-9940

Fornes T.D., Yoon P.J., Hunter D.L., Keskkula H., Paul D.R., 2002. Effect of Organoclay Structure on Nylon 6 Nanocomposite Morphology and Properties, *Polymer*, 43, 5915-5933.

Fried J.R., 1995. *Polymer Science and Technology*, Prentice Hall PTR, USA.

Furumiya A., Akana Y., Ushida Y., Masuda T. and Nakajima A., 1985. Relationship Between Molecular Characteristics and Physical Properties

of Linear Low Density Polyethylenes, 1985, *Pure & Applied Chemistry*, 57, 6, 823–832.

Galgali G, Ramesh C, Ashish L., 2001. A Rheological Study on the Kinetics of Hybrid Formation in Polypropylene Nanocomposites, *Macromolecules*, 34, 852–8.

Galgali G., Agarwal S., Lele A, 2004. Effect of Clay Orientation on the Tensile Modulus of Polypropylene-Nanoclay Composites, *Polymer*, 45, 17, 6059-6069

Goodhew P.J., Humphreys F.J., Beanland R., 1975. *Electron Microscopy and Analysis*, 3rd Edition, Taylor & Francis.

Gupta, R. K., Kennel E., Kim K.J., 2010. *Polymer Nanocomposites Handbook*, CRC Press, Taylor & Francis Group, USA.

Hambir S., Bulakh N. and Jog J. P., 2002. Polypropylene/Clay Nanocomposites: Effect of Compatibilizer on the Thermal, Crystallization and Dynamic Mechanical Behavior, *Polymer Engineering and Science*, 42, No. 9, 1800-1807.

Hasegawa N., Kawasumi M., Kato M., Usuki A., Okada A., 1998. Preparation and Mechanical Properties of Polypropylene- Clay Hybrids Using Maleic Anhydride-Modified Polypropylene Oligomer, *Journal of Applied Polymer Science*, 67, 87-92.

Hasegawa N., Okamoto H., Kato M., Usuki A., 2000. Preparation and Mechanical Properties of Polypropylene - Clay Hybrids on Modified Polypropylene and Organophilic Clay, *Journal of Applied Polymer Science*, 78, 1918-1922.

Hedley C.B., G. Yuan, B.K.G. Theng, 2007. Thermal Analysis of Montmorillonites Modified with Quaternary Phosphonium and Ammonium Surfactants, *Applied Clay Science*, 35, 180–188.

Hoffman U., K. Endell, and D. Wilm, 1933. Kristallstruktur und Quellung von Montmorillonit, *Z. Krist.*, 86, 340-348.

Hotta S., Paul D.R., 2004. Nanocomposites Formed from Linear Low Density Polyethylene and Organoclays, *Polymer*, 45, 7639–7654.

Ishida H., Campbell S., Blackwell J, 2000. General Approach to Nanocomposite Preparation, *Chemistry of Materials* 12, 1260-1267.

Isik I, Yilmazer U., Bayram G., 2008. Impact Modified Polyamide-6/Organoclay Nanocomposites: Processing and Characterization, *Polymer Composites*, 29, (2008), p.133-141

Isik I., 2007, Impact Modified Polyamide-Organoclay Nanocomposites. PhD Thesis, Chemical Engineering Department Middle East Technical University, Ankara, Turkey.

Isik F., 2005. Nanocomposites Based on Blends of Polyethylene, MSc Thesis, Chemical Engineering Department Middle East Technical University, Ankara, Turkey.

Janek, M., Lagaly, G., 2003. Interaction of a Cationic Surfactant with Bentonite: a Colloid Chemistry Study, *Colloidal Polymer Science*, 281, 293–301.

Jens, A.N., and McMorro D., *Elements of Modern X-ray Physics*. 2001, New York: John Wiley & Sons.

Jian L., Zhou C., Wang G., Zhao D., 2003 (a). Study on Rheological Behavior of Polypropylene/Clay Nanocomposites, *Journal of Applied Polymer Science*, 89, 3609–3617.

Jian L., Zhou C., Wang G., Wei W, Tao Ying, 2003 (b). Preparation and Linear Rheological Behavior of Polypropylene/MMT Nanocomposites, *Polymer Composites*, 24, No. 323-331.

Jin D.W., Seol S.M., Kim G.H., 2009. New Compatibilizer for Linear Low-Density Polyethylene (LLDPE)/Clay Nanocomposites, *Journal of Applied Polymer Science*, 114, 25–31.

Kadar F., Szazdi L., Fekete E., Pukanszky B., 2006. Surface Characteristics of Layered Silicates: Influence on the Properties of Clay/Polymer Nanocomposites, *Langmuir*, 22, 7848-7854.

Kalyon, D. M. and Sangani H., 1989. An Experimental Study of Distributive Mixing in Fully Intermeshing Co-rotating Twin Screw Extruders, *Polymer Engineering Science*, 29 (15), 1018-1026.

Kalyon D. M., Dalwadi D., Erol M., Birinci E., Christos Tsenoglu, 2006. Rheological Behavior of Concentrated Suspensions as Affected by the Dynamics of the Mixing Process, *Rheol Acta*, 45, 641–658.

Kannan P., Sevel R., Rajagopal S., 1997. Oxidation of Organic Sulfides with Clay-Supported Iodosylbenzene as Oxygen Donor, *Tetrahedron*, 53, 7635-7640.

Kato M, Usuki A., Okada A., 1997. Synthesis of Polypropylene Oligomer – Clay Intercalation Compounds, *Journal of Applied Polymer Science*, 66, 1781-1785.

Kaw A. K., *Mechanics of Composite Materials*, 1997, CRC Press LLC, USA

- Kawasumi M., Hasegawa N., Kato M., Usuki A., Okada A., 1997. Preparation and Mechanical Properties of Polypropylene- Clay Hybrids, *30*, 6333-6338.
- Kim G.M., Michler G.H., Rosch J., Mulhaupt R., 1998. Micromechanical Deformation Process in Toughened PP/PA/SEBS-g-MA Blends Prepared by Reactive Processing, *Acta Polymer*, *49*, 88-95.
- Kim K, Kim H, Lee J., Effect of Interlayer Structure, 2001. Matrix Viscosity and Composition of a Functionalized Polymer on the Phase Structure of Polypropylene–Montmorillonite Nanocomposites, *Polymer Engineering Science*, *41*:1963–9.
- Kim N.H., Maltora S.V., Xanthos M., 2006. Modification of Cationic Nanoclays with Ionic Liquids, *Microporous and Mesoporous Materials*, *96*, 29-35.
- Kim D.H., Fasulo P.D., Rodgers W.R, Paul D.R., 2007. Structure and Properties of Polypropylene Based Nanocomposites: Effect of PP-g-MA to Organoclay Ratio, *Polymer*, *48*, 5308-5323.
- Klug, H. P., Alexander, L. E. X-Ray Diffraction Procedures, Wiley, New York, 1974.
- Kohls D.J., Beaucage G., 2002. Rational Design of Reinforced Rubber, *Current Opinion in Solid State and Materials Science* *6*, 183–194.
- Kozak M., L. Domka, 2004. Adsorption of the Quaternary Ammonium Salts on Montmorillonite, *Journal of Physics and Chemistry of Solids*, *65*, 441–445.
- Kornmann, X., 2001. PhD Thesis, Synthesis and Characterization of Thermoset-Clay Nanocomposites, Division of Polymer Engineering, Luleå University of Technology: Luleå, Sweden.
- Kroschwitz J.I., Mark H.F., 2003. *Encyclopedia of Polymer Science and Technology*, 3rd Ed., Wiley Interscience.
- Krishnammoorti R, Giannelis EP., 1997. Rheology of End-Tethered Polymer Layered Silicate Nanocomposites. *Macromolecules*, *30*, 4097–102.
- Kulshreshtha A. K., Maiti A. K., Choudhary M. S., Rao K. V., 2006. Nano-Addition of Raw Bentonite Enhances Polypropylene (PP) Properties, *Journal of Applied Polymer Science*, *99*, 1004–1009.
- Lagaly, G., 1981. Characterization of Clays by Organic Compounds, *Journal of Clay Minerals*, *16*, pp. 1-21.

Lagaly, G., Ogawa, M., Dékány, I., 2006 (a). Clay Mineral-Organic Interactions. In: Bergaya, F., Theng, B.K.G., Lagaly, G. (Eds.), Handbook of Clay Science. Elsevier, Amsterdam, pp. 309–377.

Lagaly, G., Ogawa, M., Dékány, I., 2006 (b). Colloid Clay Science, In: Bergaya, F., Theng, B.K.G., Lagaly, G. (Eds.), Handbook of Clay Science. Elsevier, Amsterdam, pp. 152.

Lan T, Kaviratna P.D. and Pinnavaia T.J., 1995. Mechanism of Clay Tactoid Exfoliation in Epoxy-Clay Nanocomposites, Chemistry of Materials, 7, 2144-2150.

Lee J.Y., Lee H.K., 2004. Characterization of Organobentonites Used for Polymer Nanocomposites, Materials Chemistry and Physics, 85, 410-415.

Lee W.J., Eung S.K., Hun S.K., Jin-San Y., 2005. Preparation and Characterization of Polypropylene/Clay Nanocomposites with Polypropylene-graft-Maleic Anhydride, Journal of Applied Polymer Science, 98, 1229-1234.

Leuteritz A., Kretschmar B., Willeke M., Jehnichen D., Jentsch U., 2005. Grundke K., Janke A., PP-Clay Nanocomposites: Comparison of Different Layered Silicates, Macromolecular Symposium, 221, 53-61.

Lertwimolnun W., Vergnes B., 2006. Effect of Processing Conditions on the Formation of Polypropylene/Organoclay Nanocomposites in a Twin Screw Extruder, Polymer Engineering and Science, DOI 10.1002/pen.

Li C., Kong Q., Zhao J., Zhao D., Fan Q., Xia Y., 2004. Crystallization of partially Miscible Linear Low-Density Polyethylene/Poly(ethylene-co-vinylacetate) Blends, Materials. Letters, 58, 3613.

Lim Y. T., Park O., 2000. Rheological Evidence for the Microstructure of Intercalated Polymer/Layered Silicate Nanocomposites, Macromolecular Rapid Communication, 21, 231–235.

Liangxiong L., Whitworth T.T, Lee R., 2003. Construction of an Ultrathin, Compacted Clay Membrane for Use in Reverse Osmosis, Applied Clay Science, 24, 59-68.

Lopez D. G., Picazo O., Merino J.C., Pastor J.M., 2003. Polypropylene–Clay Nanocomposites: Effect of Compatibilizing Agents on Clay Dispersion, European Polymer Journal, 39, 945–950.

Lopez D. G., Mitre I., Fernandez J.F., Merino J.C., Pastor J.M., Influence of Clay Modification Process in PA6-Layered Silicate Nanocomposite Properties, 2005. Polymer, 26, 2758-2765.

- Ma Jisheng, Shimin Z., Zongneng Q., Ge L., Youliang H., 2002. Crystallization Behaviors of Polypropylene/Montmorillonite Nanocomposites, *Journal of Applied Polymer Science*, 83, 1978–1985.
- Mravčáková M., Boukerma K., Omastova M., Chehimi M.M., 2006. Montmorillonite/Polypyrrole Nanocomposites. The Effect of Organic Modification of Clay on the Chemical and Electrical Properties, *Materials and Science Engineering C*, 26, 306-313.
- Maiti,P., Nam, P.H., Okamoto, M., Hasegawa, N. and Usuki, A., 2002. Influence of Crystallization on Intercalation, Morphology, and Mechanical Properties of Polypropylene/Clay Nanocomposites, *Macromolecules.*, 35(6): 2042-2049.
- Massinga, P.H., et al., 2010. Alkyl Ammonium Intercalation of Mozambican Bentonite, *Applied Clay Science*, doi:10.1016/j.clay.2010.04.017.
- Met I., Akgun H., 2005. Composite landfill liner design with Ankara clay, Turkey, *Environ Geol* (2005) 47: 795–803.
- Michler G.H., Calleja F.J.B., 2005. Mechanical Properties of Polymers Based on Nanostructure and Morphology, Taylor-Franchis Group, CRC Press, USA.
- Mittal V, 2007(a). Gas Permeation and Mechanical Properties of Polypropylene Nanocomposites with Thermally-Stable Imidazolium Modified Clay. *European Polymer Journal* 43, 3727–3736.
- Mittal V, 2007(b). Polypropylene-Layered Silicate Nanocomposites: Filler Matrix Interactions and Mechanical Properties, *Journal of Thermoplastic Composite Materials*, 20, 575-599.
- Mittal V., 2010. Optimization of Polymer Nanocomposite Properties, Wiley-VCH Verlag GmbH & Co. KGaA, Weinheim, Germany.
- Modesti M., Lorenzetti A., Bon D., Besco S., 2005. Effect of Processing Conditions on Morphology and Mechanical Properties of Compatibilized Polypropylene Nanocomposites, *Polymer*, 46, 10237–10245.
- Morgan A. B., Gilman J. W., 2003. Characterization of Polymer-Layered Silicate (Clay) Nanocomposites by Transmission Electron Microscopy and X-Ray Diffraction: A Comparative Study, *Journal of Applied Polymer Science*, 87, 1329–1338.
- Nam, P.H., Maiti,P., Okamoto M., Kotaka T., Hasegawa, N., and Usuki, A., 2001. A Hierarchical Structure and Properties of Intercalated Polypropylene/Clay Nanocomposites, *Polymer*, 42, 9633-9640.

Navarchian A. H., Ardakani K. M., 2009. Processing of Transmission Electron Microscope Images for Quantification of the Layer Dispersion Degree in Polymer-Clay Nanocomposites, *Journal of Applied Polymer Science*, 114, 531–542.

Nielsen L.E., Landel R.F., 1994. *Mechanical Properties of Polymers and Composites*, Marcel-Dekker Inc., USA.

Okamotoa M., Moritaa S., Kima Y.H., Kotakaa T., Tateyamab H., 2001. Dispersed Structure Change of Smectic Clay/Poly(methyl methacrylate) Nanocomposites by Copolymerization with Polar Comonomers, *Polymer*, 42, 1201-1206.

Onal M, Sarıkaya Y., Alemdaroglu T., Bozdogan I., 2003. Isolation and Characterization of a Smectite as a Micro-Mesoporous Material from Bentonite, *Turkish Journal of Chemistry*, 27, 683-693.

Osman M.A., Mittal V., 2004. The Aspect Ratio and Gas Permeation in Polymer-Layered Silicate Nanocomposites, *Macromol. Rapid Commun.* 25, 1145–1149.

Osman M. A., Rupp J.E.P., 2005. Interfacial Interactions and Properties of Polyethylene-Layered Silicate Nanocomposites, *Macromolecular Rapid Communication*, 26, 880–884.

Osman M.A., Mittal V., Suter, U.W., 2007. Poly(propylene)-Layered Silicate Nanocomposites: Gas Permeation Properties and Clay Exfoliation, *Macromolecular Chemistry and Physics*, 208(1): 68–75.

Patel H.A, Somani R.S., Bajaj H.C and Jasra R.V., 2006. Nanoclays for Polymer Nanocomposites, Paints, Inks, Greases and Cosmetics Formulations, Drug Delivery Vehicle and Waste Water Treatment. *Bulletin of Material Science* 29, 133–145.

Patel H. A., Somani R. S., Bajaj H. C., Jasra R. V., 2007. Preparation and Characterization of Phosphonium Montmorillonite with Enhanced Thermal Stability, *Applied Clay Science*, 35, 194–200.

Panek G., S. Schleidt, Q. Mao, M. Wolkenhauer, H. W. Spiess, and G. Jeschke, 2006. Heterogeneity of the Surfactant Layer in Organically Modified Silicates and Polymer/Layered Silicate Composites, *Macromolecules*, 39, 2191-2200.

Peacock A.J., 2000. *Handbook of Polyethylene: Structures, Properties and Applications*, Marcel Dekker Inc., USA.

Perrin-Sarazin F., Ton-That M.-T., Bureau M.N., Denault J., 2005. Micro- and Nano-Structure in Polypropylene/Clay Nanocomposites, *Polymer* 46 (2005) 11624–11634

Prasad R., Gupta R. K., Cser F., Bhattacharya S. N., 2006. Experimental Investigation of the Linear Viscoelastic Response of EVA-Based Nanocomposites, *Journal of Applied Polymer Science*, Vol. 101, 2127–2135.

Qin H., Zhang S., Zhao C., Hu G., Yang M., 2005. Flame Retardant Mechanism of Polymer/Clay Nanocomposites Based on Polypropylene, *Polymer*, 46, 8386-8395.

Quintanilla L.M.L., Valdes S.S., Valle L.F.R., Rodriguez F.J.M., 2006. Effect of Some Compatibilizing Agents on Clay Dispersion of Polypropylene-Clay Nanocomposites, *Journal of Applied Polymer Science*, 100, 4748-4756.

Rahaman M.N., 2007. *Ceramic Processing*, Taylor-Francis, USA.

Ramakrishna, S., 2005. *An Introduction to Electrospinning and Nanofibers*, World Scientific Publishing Company, River Edge, NJ, USA.

Ratnayake U.N., Hawort B., 2006. Polypropylene-Clay Nanocomposites: Influence of Low Molecular Weight Polar Additives on Intercalation and Exfoliation Behavior, *Polymer Engineering and Science*, DOI 10.1002/pen.20573, 1008-1015.

Ray S.S. and Okamoto M., 2003. *Polymer/layered Silicate Nanocomposites: A Review from Preparation to Processing*, *Progress in Polymer Science*, 2003.

Reichert P, Nitz H., Klinke S., Brandsch R., Thomann R., Mülhaupt R., 2000. Poly(propylene)/Organoclay Nanocomposite Formation: Influence of Compatibilizer Functionality and Organoclay Modification, *Macromolecular Material Engineering*. 275, 8–17.

Ren J., Silva A.S., and Krishnamoorti R., 2000. Linear Viscoelasticity of Disordered Polystyrene-Polyisoprene Block Copolymer Based Layered-Silicate Nanocomposites, *Macromolecules*, 33, 3739-3746.

Reynolds, R. C. Jr., 1989. Diffraction by Small and Disordered Crystals in *Modern Powder Diffraction*, *Reviews in Mineralogy* Vol. 20, Mineralogical Society of America, Washington, DC, USA, p 144.

Rieder M., Cavazzini G., D'yakonov YS., Frank-Kamenetskii VA., Gottardi G., Guggenheim S., Koval PV., Müller G., Neiva AMR., Radoslovich EW., Robert J-L., Sassi FP., Takeda H., Weiss Z., and Wones DR., 1998. Nomenclature of micas, *Clays Clay Miner*, 46: 586–595.

Rohlmann CO., Failla MD., Quinzani LM., 2006. Linear Viscoelasticity and Structure of Polypropylene–Montmorillonite Nanocomposites, *Polymer*, 47, 7795–804.

- Rohlmann C. O., Horst M. F., Quinzani L. M., Failla M. D., 2008. Comparative Analysis of Nanocomposites based on Polypropylene and Different Montmorillonites, *European Polymer Journal*, 44 2749–2760.
- Rosen S., 1993. *Fundamental Principles of Polymeric Materials*, 2nd Ed., John Wiley and Sons, Inc, New York, USA.
- Ruiz-Hitzkya E. and Meerbeek A. Van, 2006. Clay Mineral and Organoclay–Polymer Nanocomposite, In: Bergaya, F., Theng, B.K.G., Lagaly, G. (Eds.), *Handbook Of Clay Science*. Elsevier, Amsterdam, Pp. 583-621.
- Saminathan K., P. Selvakumar and Nerash Bhatnagar, 2008. Fracture Studies of PP/Nanoclay Composite. Part I: Effect of Loading Rates on Essential Work of Fracture, *Polymer Testing*, 27-3, 296-307.
- Samyn F., Bourbigot S., Jama C., Bellayer S., Nazare S., Hull R., Castrovinci A., Fina A., Camino G., 2008. Crossed Characterisation of Polymer-Layered Silicate (PLS) Nanocomposite Morphology: TEM, X-ray diffraction, Rheology and Solid-State Nuclear Magnetic Resonance Measurements, *European Polymer Journal*, *Macromolecular Nanotechnology*, 44, 1642–1653.
- Sandler S.R, 1998. *Polymer Synthesis and Characterization: A Laboratory Manual*, Academic Press, San Diego, USA.
- Sarvestani A. S., Picu C. R., 2004. Network Model for the Viscoelastic Behavior of Polymer Nanocomposites, *Polymer* 45, 7779–7790.
- Seymour R.B., 1996. *Polymer Chemistry: An Introduction*, 4th Edition, Marrel Dekker, New York, USA.
- Seymour R.B. and Carraher C.E.Jr, 1984. *Structure-Property Relationships in Polymers*, Plenum Press, New York and London.
- Shelley J. S., Mather P. T. and Devries K. L., 2001. Reinforcement and Environmental Degradation of Nylon-6/Clay Nanocomposites, *Polymer*, 42, 5849-5858.
- Shenoy A.V., 1999. *Rheology of Filled Polymer Systems*, Kluwer Academic Publishers, Great Britain.
- Smart G., Kandola B. K., Horrocks A.R., Nazare S. and Marney D., 2008. Polypropylene Fibers Containing Dispersed Clays Having Improved Fire Performance. Part II: Characterization of Fibers and Fabrics from PP–Nanoclay Blends, *Polymers for Advanced Technologies*, 19, 658–670.
- Solomon M.J., Almusallam A.S., Kurt F, 2001. Rheology of Polypropylene/Clay Hybrid Materials, *Macromolecules* , 34, 6, 1864-1872.

- Somwangthanaroj A., Lee E. C. and Solomon M. J., 2003. Early Stage Quiescent and Flow-induced Crystallization of Intercalated Polypropylene Nanocomposites by Time-resolved Light Scattering, *Macromolecules*, 36 (7), 2333-2342.
- Song S., Zhang Y., Liu T. and Zhang M, 2005. Beneficiation of Montmorillonite from Ores by Dispersion Processing, *Journal of Dispersion Science and Technology*, 26:375–379.
- Sperling, L.H., 2006. *Introduction to Physical Polymer Science*, 4th Edition, Wiley.
- Stoeffler K., Lafleur P.G. and Denault J., 2008 (a). Effect of Intercalating Agents on Clay Dispersion and Thermal Properties in Polyethylene/Montmorillonite Nanocomposites, *Polymer Engineering and Science*, 48, 1449-1466.
- Stoeffler K., Lafleur P.G. and Denault J., 2008 (b). The Effect of Clay Dispersion on the Properties of LLDPE/LLDPE-g-MAH/Montmorillonite Nanocomposites, *Polymer Engineering and Science*, DOI 10.1002/pen.21204.
- Tabak A., Afsin B, Caglar B., Koksal E., 2007. Characterization and Pillaring of a Turkish Bentonite (Reşadiye), *Journal of Colloid and Interface Science* 313, 5–11.
- Tajammul Hussain S., 1996. Transmission Electron Microscopy (TEM) Study of Polycrystalline Ru: Ag/Alumina Supported Catalyst System, *Turkish Journal of Chemistry* 20, 33-37, TÜBİTAK Yayınları.
- Tang Y., Hu Y., Song L., Zong R., Gui Z., Chen Z., Fan W., 2003. Preparation and Thermal Stability of Polypropylene/Montmorillonite Nanocomposites, *Polymer Degradation and Stability* 82, 127–13.
- Tjong S.C., 2006. Structural and Mechanical Properties of Polymer Nanocomposites, *Materials Science and Engineering R.*, 53, 73–197.
- Tjong S. C., Ruan Y. H., 2008. Fracture Behavior of Thermoplastic Polyolefin/Clay Nanocomposites, *Journal of Applied Polymer Science*, Vol. 110, 864–871.
- Ton-That MT, Perrin-Sarazin F, Cole KC, Bureau MN, Denault J., 2004. Polyolefin Nanocomposites: Formulation and Development, *Polymer Engineering Science*, 44:1212–9.
- Tyagi B., Chudasama C. D., Jasra R. V., 2006. Determination of Structural Modification in Acid Activated Montmorillonite Clay by FT-IR Spectroscopy, *Spectrochimica Acta Part A*, 64, 273–278.

Usuki A, Kawasumi M, Kojima Y, Okada A, Kurauchi T, Kamigaito O., 1993. Swelling Behaviour of Montmorillonite Cation Exchanged for Omega-Amino Acids by Epsilon-Caprolactam, *Journal of Materials Research*, 8, 1174–1178.

Vaia R. A., Jandt K.D., Edward J. K. and Giannelis E. P., 1994. Interlayer Structure and Molecular Environment of Alkylammonium Layered Silicates, *Chemistry of Materials*, 6, 1017-1022.

Vaia R. A., Jandt K.D., Edward J. K. and Giannelis E. P., 1995. Kinetics of Polymer Melt Intercalation, *Macromolecules* 1995,28, 8080-8085.

Vaia R. A., Jandt K.D., Edward J. K. and Giannelis E. P., 1996. Microstructural Evolution of Melt Intercalated Polymer-Organically Modified Layered Silicates Nanocomposites, *Chemistry of Materials*, 8, 2628-2635.

Vaia R.A., Liu W., 2002. X-Ray Powder Diffraction of Polymer/Layered Silicate Nanocomposites: Model and Practice, *Journal of Polymer Science: Part B: Polymer Physics*, 40, 1590–1600.

Vaia, R.A., Liu W., Koerner H., 2003. Analysis of Small-Angle Scattering of Suspensions of Organically Modified Montmorillonite: Implications to Phase Behavior of Polymer Nanocomposites, *Journal of Polymer Science: Part B: Polymer Physics*, Vol. 41, 3214–3236.

Velasco J.I., Ardanuy M., Miralles L., Ortiz S., Maspoch M.L., Soto M.S., Santan O., 2005. PP/PET/Undecyl Ammonium Montmorillonite Nanocomposites Synthesis and Characterization, *Macromolecular Symposium*, 221, 63-73.

Velasco J.I., Ardanuy M., Realinho V., Antunes M., Fernandez A.I., Pena G.J.I., Perez M.A.R., Saja J.A., 2006. PP/Clay Nanocomposites: Combined Effects of Clay Treatment and Compatibilizer Polymers on the Structure and Properties, *Journal of Applied Polymer Science*, 102, 1213-1223.

Vlasveld D.P.N, Vaidya S.G., Bersee H.E.N, Picken S.J, 2005. A Comparison of the Temperature Dependence of the Modulus, Yield Stress and Ductility of Nanocomposites Based on High and Low MW PA6 and PA66, *Polymer*, 46, 3452- 3461

University of California, Introduction to X-Ray Diffraction <http://www.mrl.ucsb.edu/mrl/centralfacilities/xray/xray-basics/index.html>., last visited on 24 May, 2010.

Nobelprize, TEM, http://nobelprize.org/educational_games/physics/microscopes/tem/index.html, last visited on: 12 April, 2010.

Materials Evolution and Engineering, Handbook of Analytical Methods, SEM, <http://www.mee-inc.com/sem.html>, last visited on: 15 April 2010.

Iowa State University SEM, <http://www.mse.iastate.edu/microscopy/whatsem.html>, last visited on: 22 April 2010.

www.cartage.org.lb/.../OrganicCompound.htm, last visited on: 12 May 2010.

http://en.wikipedia.org/wiki/Differential_scanning_calorimetry, last visited on: 15 May 2010, Wang L. Z., 2001. Characterization of Nanophase Materials, Wiley-VCH, Germany.

Wang H., Chen S., Zhang J., 2009. Surface Treatment of LLDPE and LDPE Blends by Nitric Acid, Sulfuric Acid, and Chromic Acid Etching, Colloid Polymer Science, 287, 541–548.

Wanga Y., Chena F.-B., Lib Y.C., Wua K.C., 2004. Melt Processing of Polypropylene/Clay Nanocomposites Modified with Maleated Polypropylene Compatibilizers, Composites: Part B, 35, 111–124.

Weiss, A. 1962, In Proceedings of the Tenth National Conference on Clays and Clay Minerals; Pergamon Press: New York, pp 191-224. Weiss, A. Angew. Chem., Znt. Ed. 1963, 2, 134.

Wiles M., Huebner H.J., McDonald T.J., Donnelly K.C., Philips T. D., 2005. Matrix-immobilized Organoclay for the Sorbtion of Polycyclic Aromatic Hydrocarbons and Pentachlorophenol from Groundwater, Chemosphere, 59, 1455-1464.

Wilkinson A.N., Ryan A.J., 1998. Polymer Processing and Structure Development, Kluwer Academic Publishers, Netherlands.

Wu X., Xiaobing Wu, Jiaqi Chen, and Xingrong Zeng, 1991. The Application of DSC in Identification of LDPE/LLDPE Blends Mulching Film, Die Angewandte Makromolekulare Chemie, 189, 183 -193.

Wu D., Zhou C., Fan X., Mao D., Bian Z., 2005 (a). Linear Rheological Behaviour and Thermal Stability of Poly(Butylene Terephthalate)/Epoxy/Clay Ternary Nanocomposites, Polymer Degradation and Stability, 87, 511-519.

Wu Defeng, Zhou C., Hong Z., Mao D., Bian Z., 2005 (b). Study on Rheological Behaviour of Poly(Butylene Terephthalate)/Montmorillonite Nanocomposites, European Polymer Journal, 41, 2199–2207.

Wu D., Zhou C., Yu W., Fan X., 2005 (c). Effect of Flocculated Structure on Rheology of Poly(butylene terephthalate)/Clay Nanocomposites, Journal of Polymer Science: Part B: Polymer Physics, 43, 2807–2818.

Xie W, Gao Z, Pan W, Hunter D, Singh A, Vaia R., 2001. Thermal Degradation Chemistry of Alkyl Quaternary Ammonium Montmorillonite, *Chemistry of Materials*, 13, 2979-2990.

Xie W., Xie R., Pan W.P., Hunter D., Koene, Tan L. S., Vaia R., 2002. Thermal Stability of Quaternary Phosphonium Modified Montmorillonites, *Chemistry of Materials*, 14, 4837-4845.

Yapar, S., Özbudak, V., Lopes, A., 2005. Yapar, S., Özbudak, V., Lopes, A., 2005. Effect of Adsorbent Concentration to the Adsorption of Phenol on Hexadecyl Trimethyl Ammonium–Bentonite. *J. Hazardous Materials*, 121, 135–139.

Yuan Q. and Misra R.D.K., 2006. Impact Fracture Behavior of Clay–Reinforced Polypropylene Nanocomposites, *Polymer*, 47, 4421–4433.

Yuzer H., Sarioglan S., Koral M., Dogan H, Celik M.S., Karahan S., Development of Solvent-Based Bentonites from Reşadiye Bentonite., 13th Clay Symposium (Isparta, Turkey) Catalogue, pages 195-202.

Yoon P.J., Hunter DL, Paul DR., 2003. Polycarbonate Nanocomposites. Part 1, Effect of Organoclay Structure on Morphology and Properties, *Polymer*, 44, 5323.

Zhang M., Sundararaj U., 2006. Thermal, Rheological, and Mechanical Behaviors of LLDPE/PEMA/Clay Nanocomposites: Effect of Interaction Between Polymer, Compatibilizer, and Nanofiller, *Macromolecular Materials and Engineering*, 291, 697-706.

Zweifel H., 2001, *Plastic Additives Handbook*, Hanser Publisher, Munich, Germany.

APPENDIX A

DSC ANALYSIS

A.1 DSC of samples prepared in SET-1 (PPM/Organoclay/MAPP)

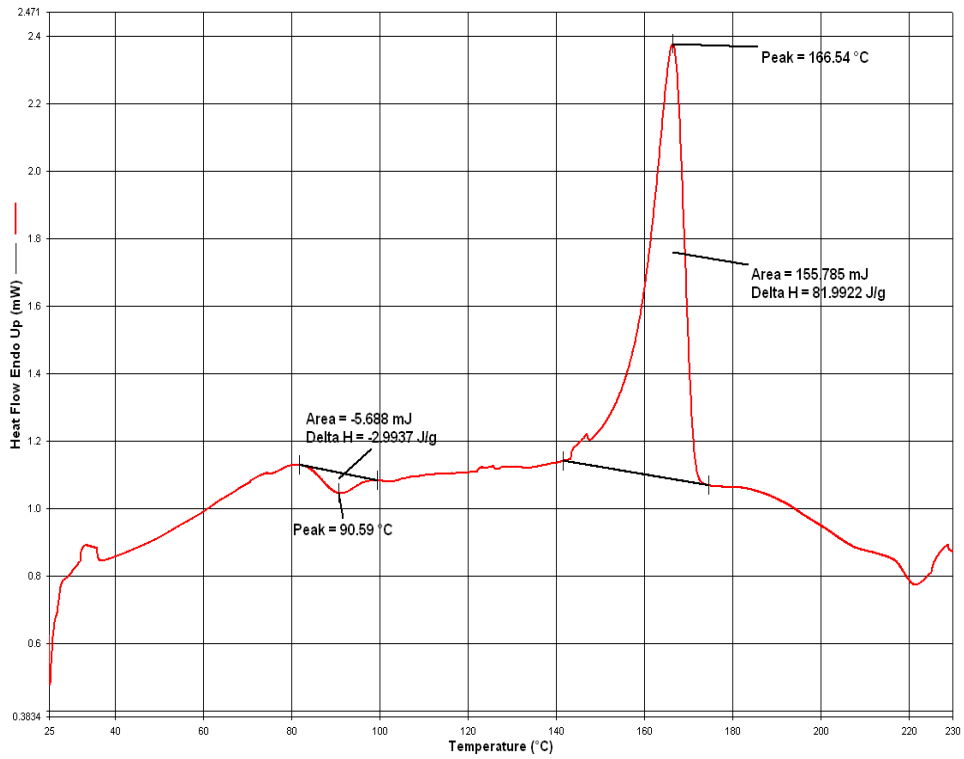


Figure A.1 DSC thermogram of PPM

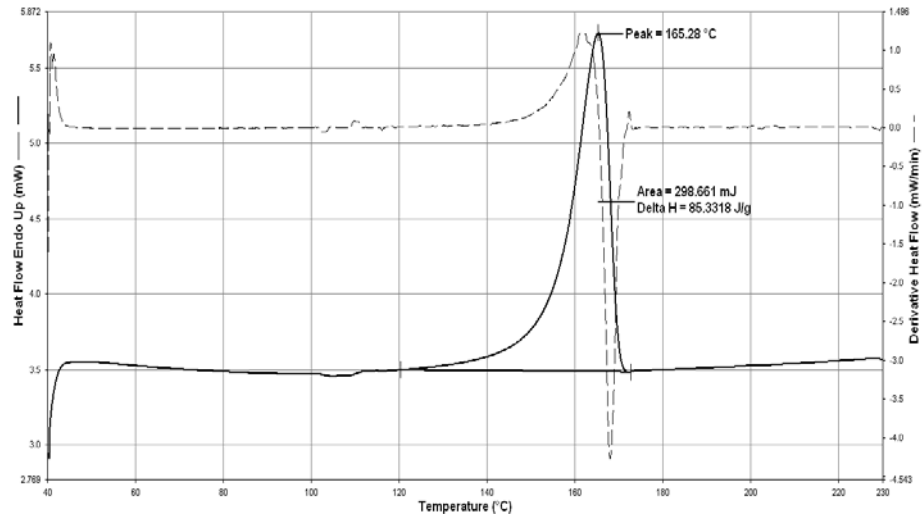


Figure A.2 DSC thermogram of PPM98/MAPP2

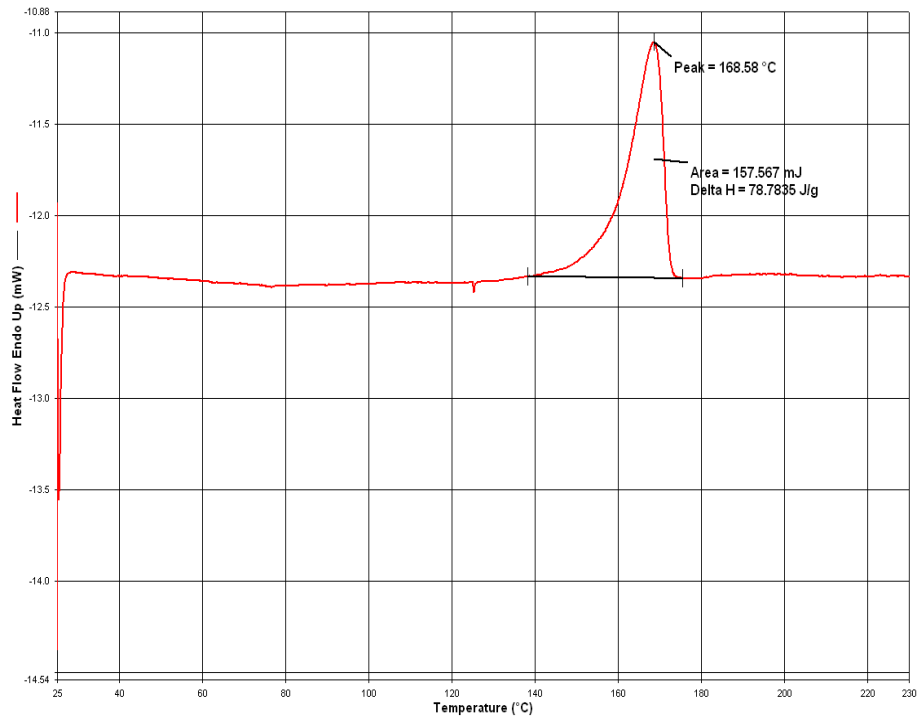


Figure A.3 DSC thermogram of PPM/TBA2/MAPP2

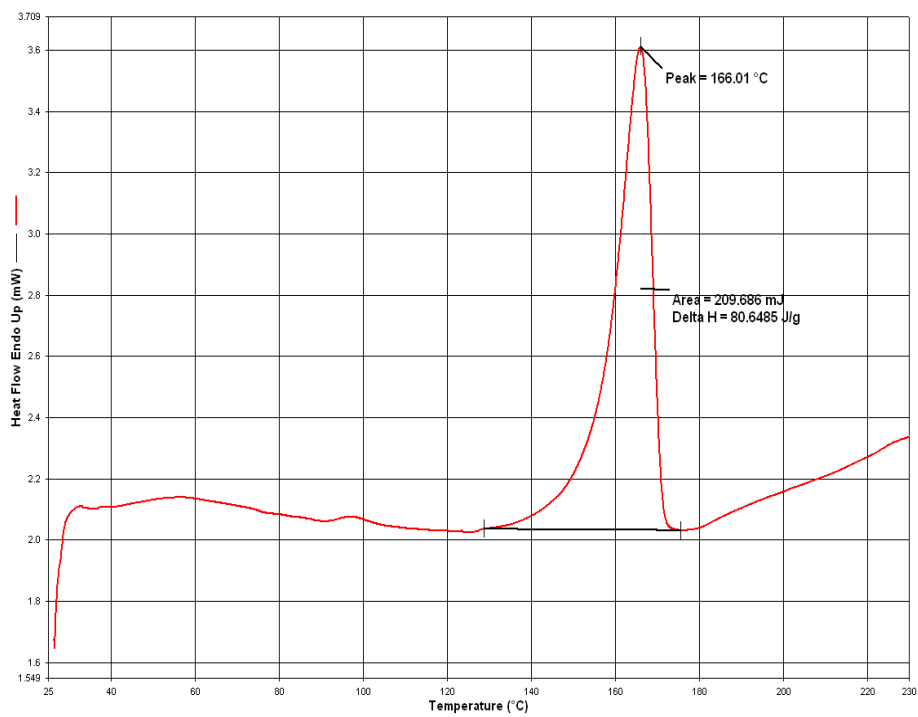


Figure A.4 DSC thermogram of PPM/TBP2/MAPP2

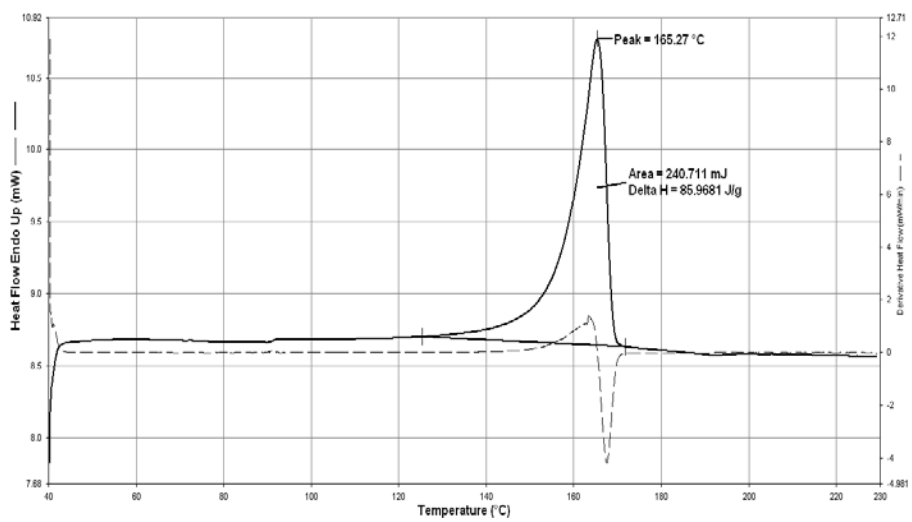


Figure A.5 DSC thermogram of PPM/HMA2/MAPP2

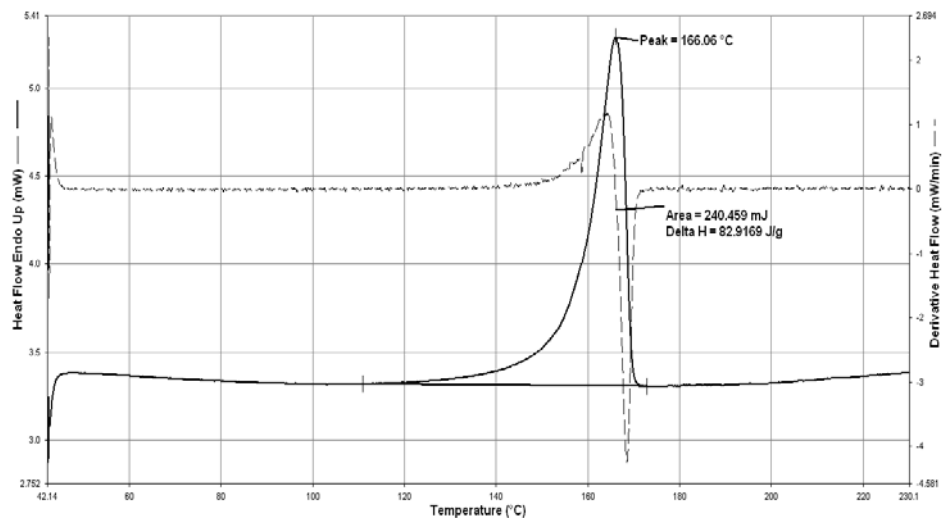


Figure A.6 DSC thermogram of PPM/TKA2/MAPP2

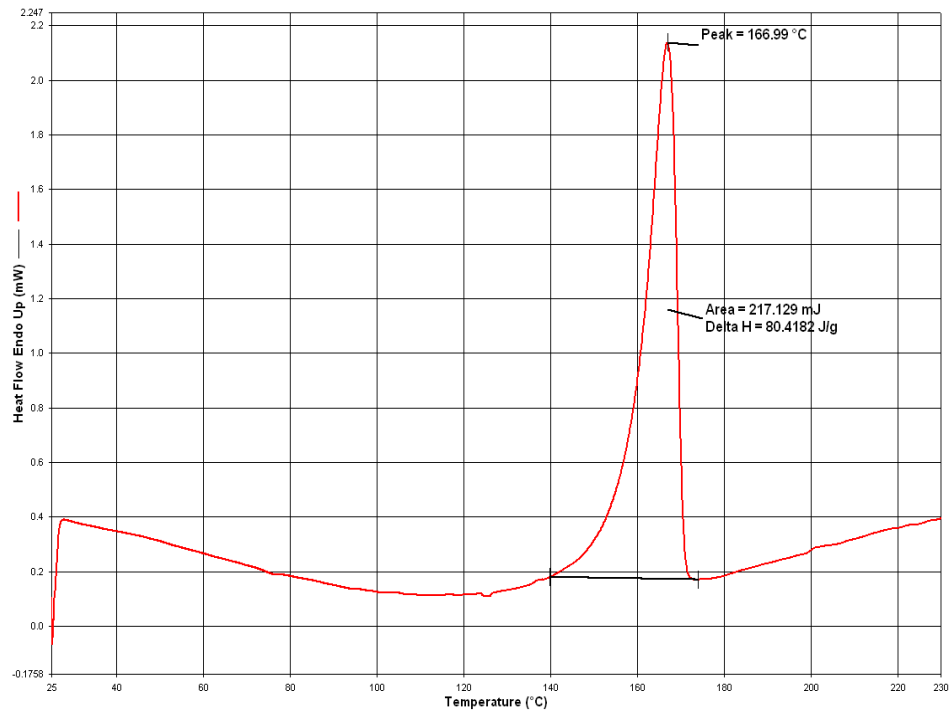


Figure A.7 DSC thermogram of PPM/Cloisite25A2/MAPP2

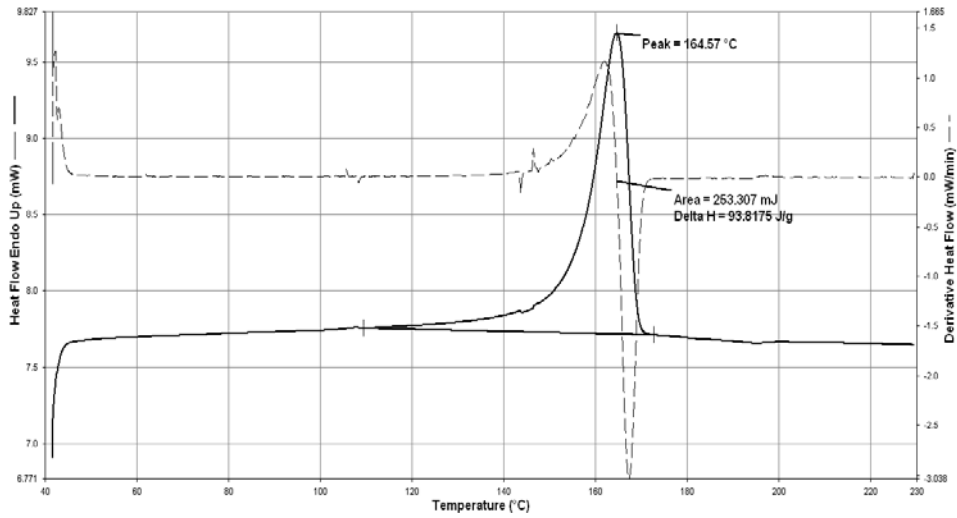


Figure A.8 DSC thermogram of PPM/HMA1/MAPP3

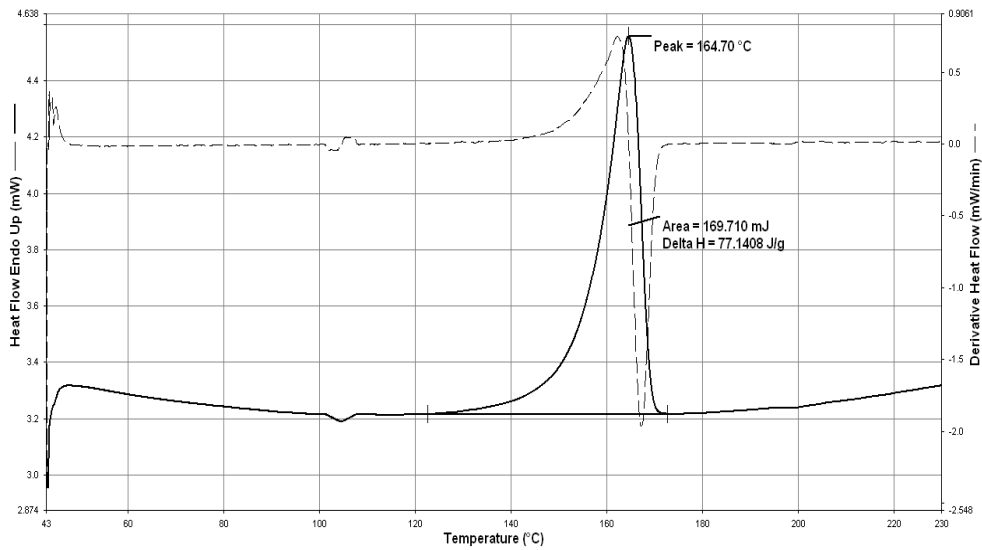


Figure A.9 DSC thermogram of PP/TKA1/MAPP3

A.2. DSC thermograms of samples prepared in SET-2.

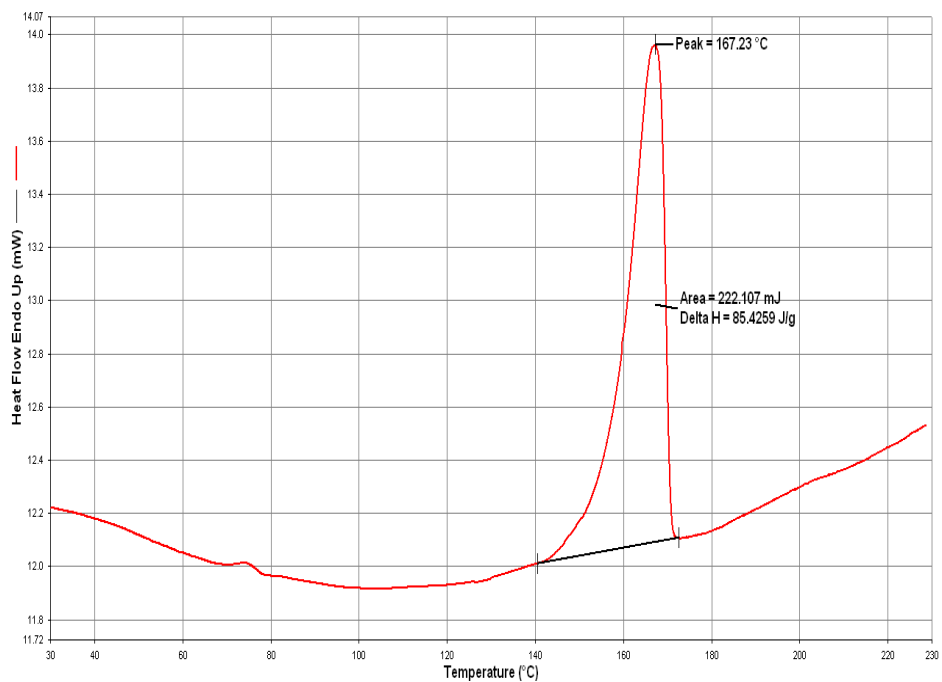


Figure A.10 DSC thermogram of PPE

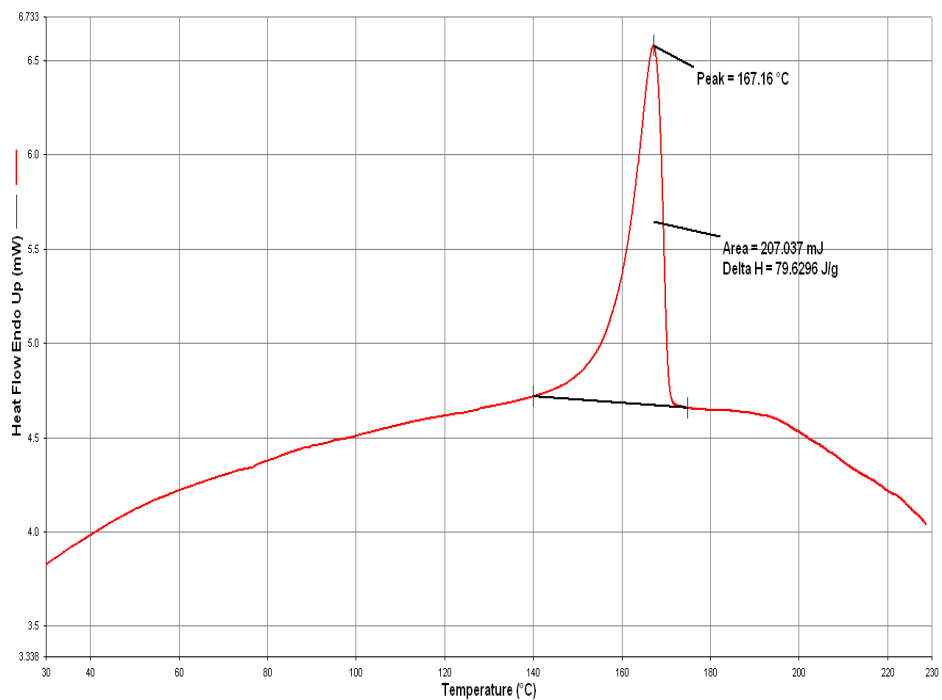


Figure A.11 DSC thermogram of PPE/HMA2/MAPP5

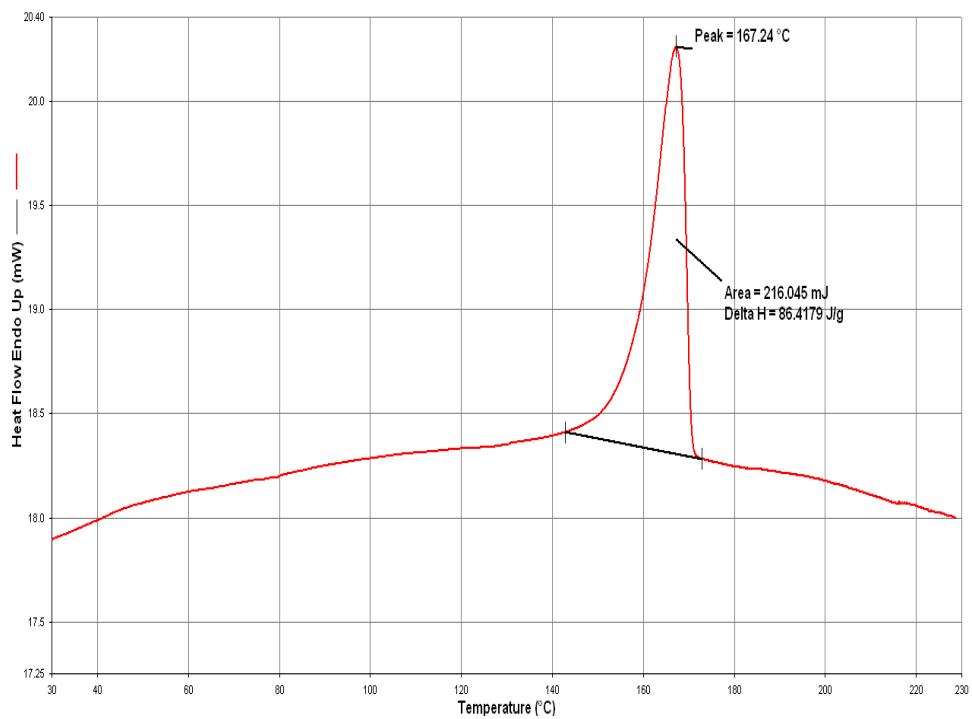


Figure A.12 DSC thermogram of PPE/TKA2/MAPP5

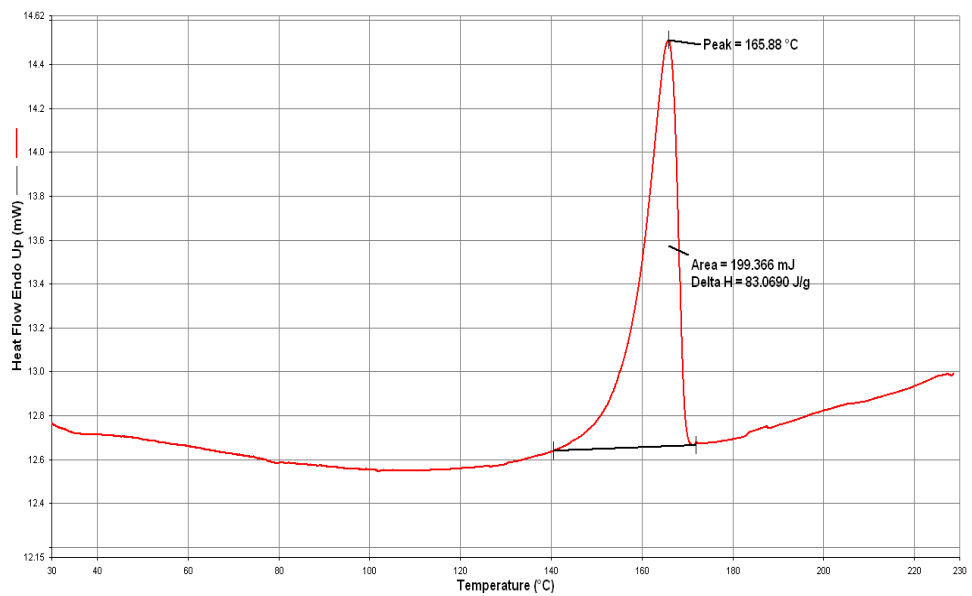


Figure A.13 DSC thermogram of PPE/TKA50-2/MAPP5

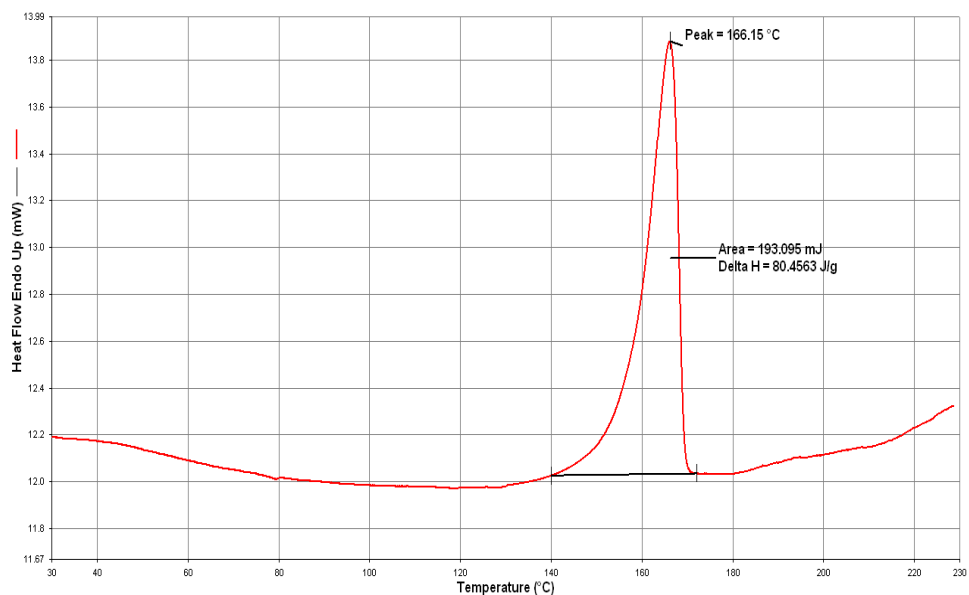


Figure A.14 DSC thermogram of PPE/PGWKIS2/MAPP5

A.3. DSC thermograms of samples prepared in SET-3

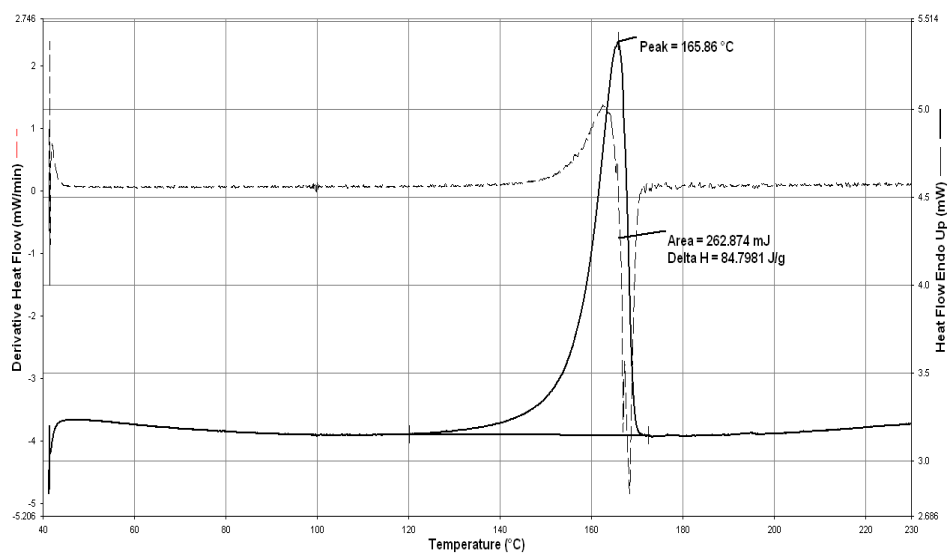


Figure A.15 DSC thermogram of PPE/DMDA2/MAPP5

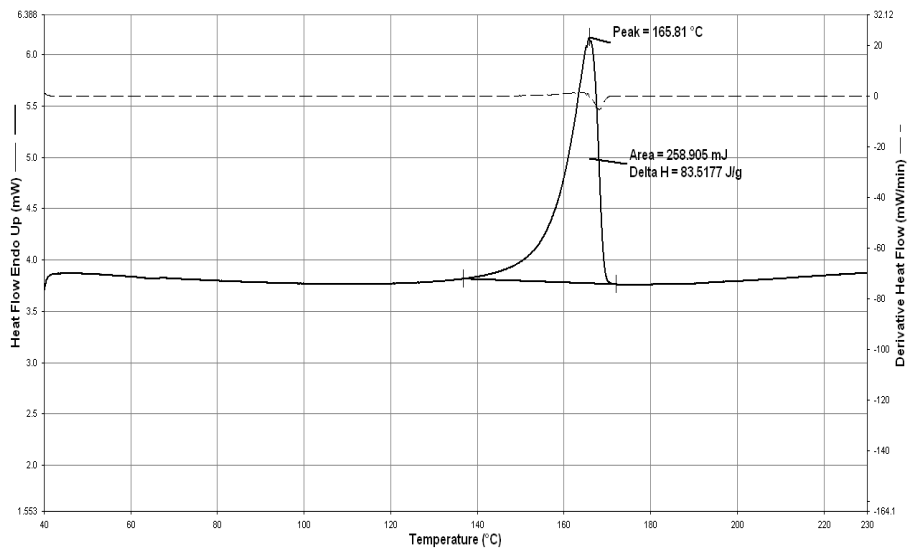


Figure A.16 DSC thermogram of PPE/TBHP2/MAPP5

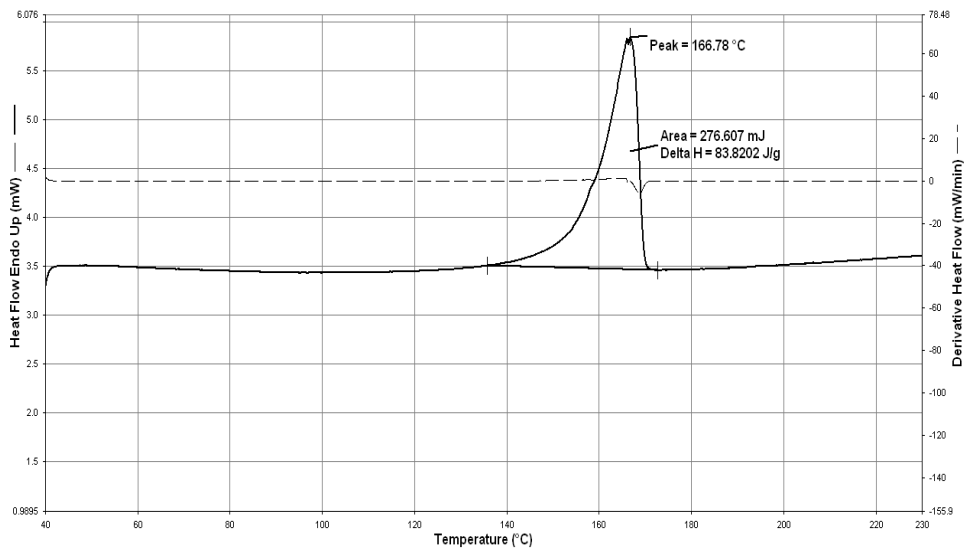


Figure A.17 DSC thermogram of PPE/STKA2/MAPP5

A.4 DSC thermograms of samples prepared in SET-4

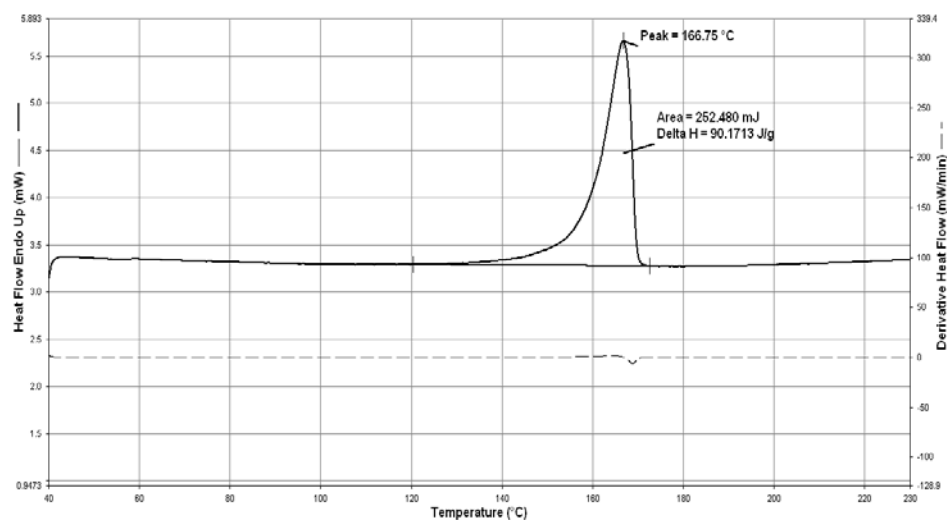


Figure A.18 DSC thermogram of PPE-M

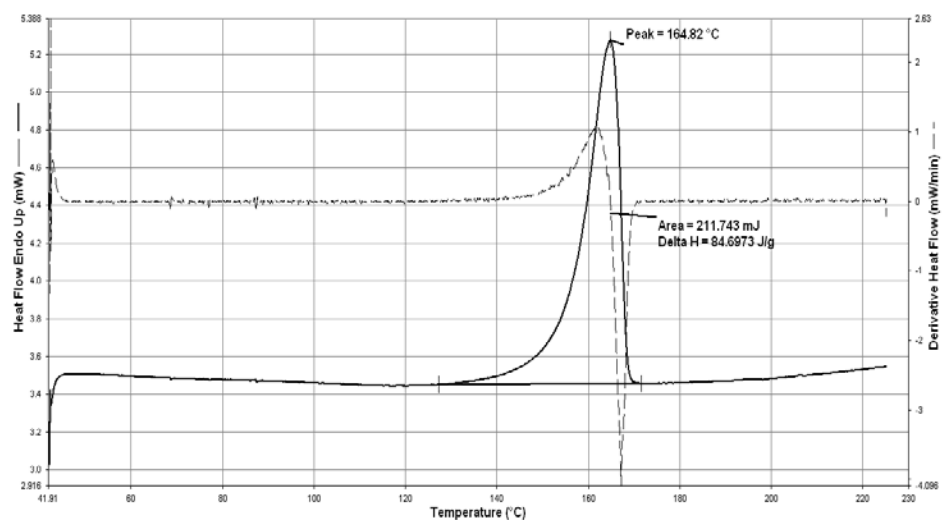


Figure A.19 DSC thermogram of PPE/DMDA2/MAPP5-M

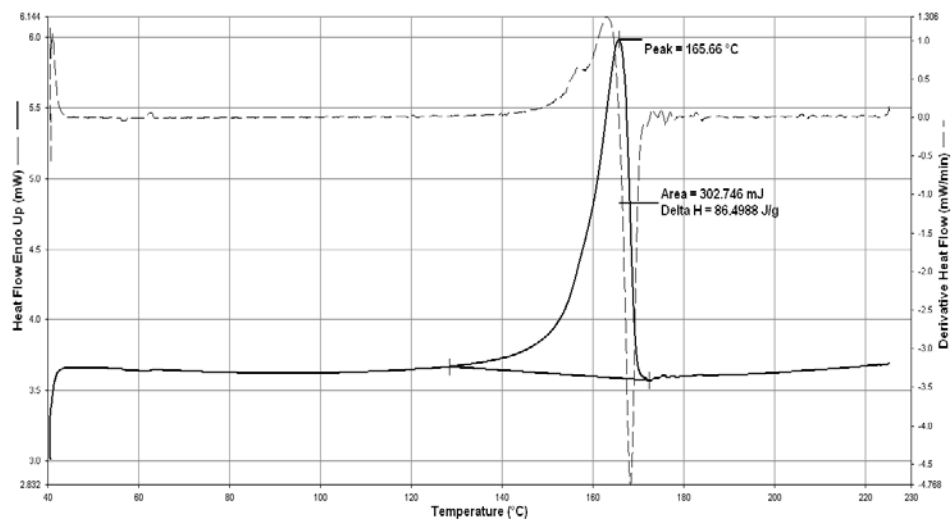


Figure A.20 DSC thermogram of PPE/TBHP2/MAPP5-M

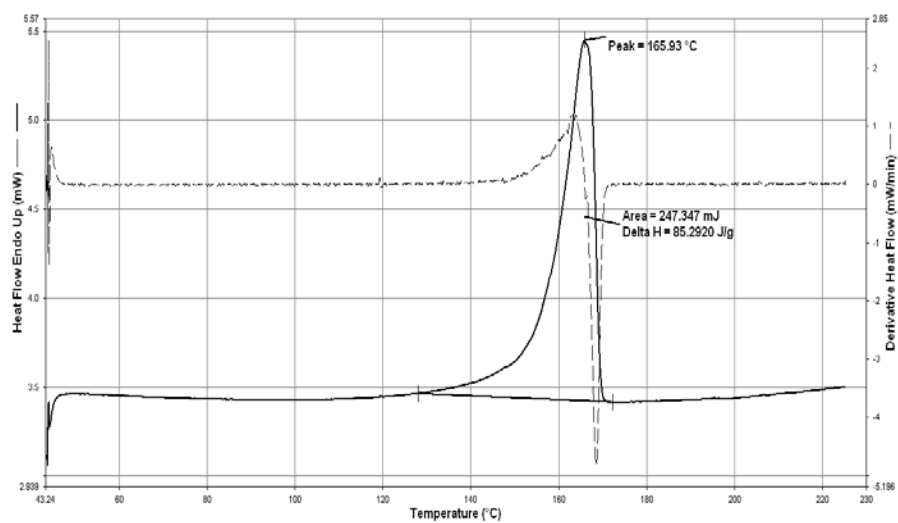


Figure A.21 DSC thermogram of PPE/STKA2/MAPP5-M

A.5 DSC thermograms of samples prepared in SET-6

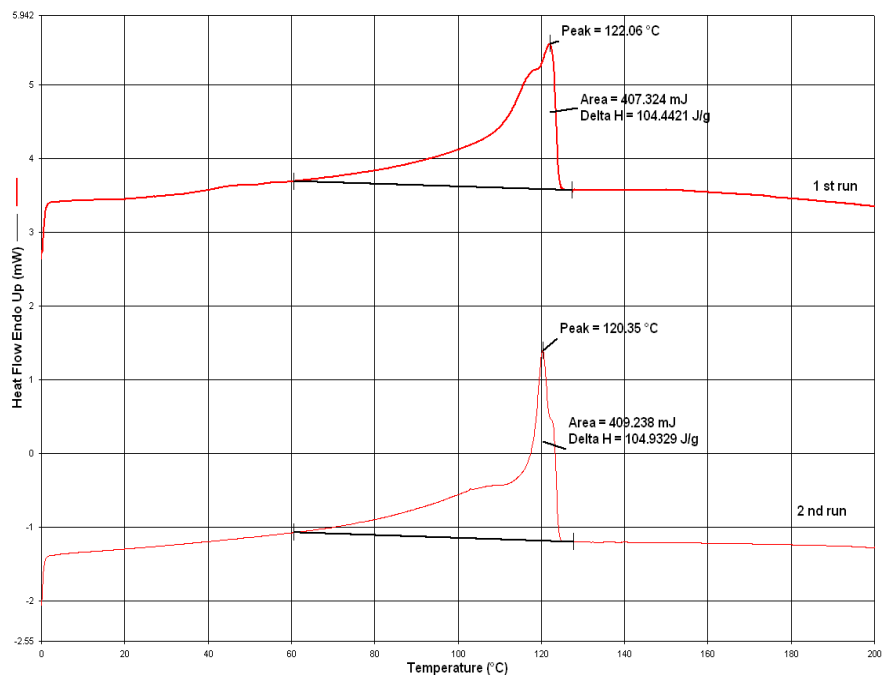


Figure A.22 DSC thermogram of LLDPE

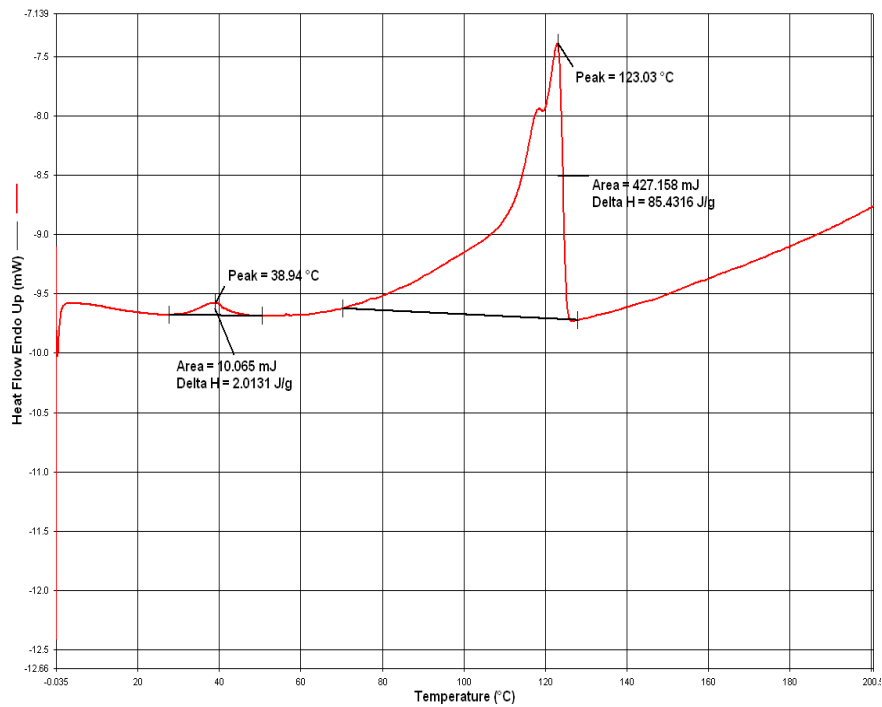


Figure A.23 DSC thermogram of LLDPE95/LOT5

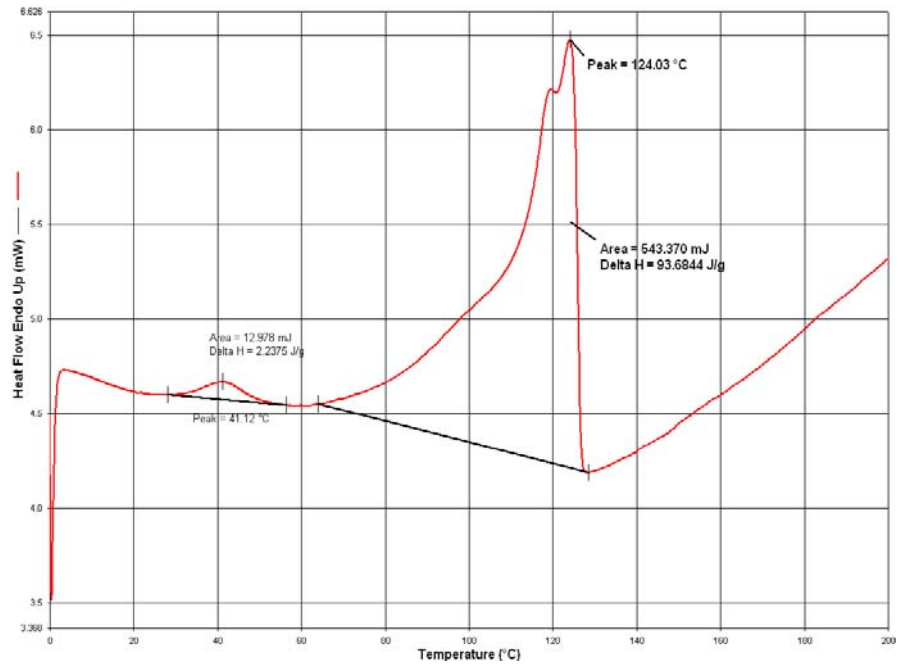


Figure A.24 DSC thermogram of LLDPE87.5/LOT12.5

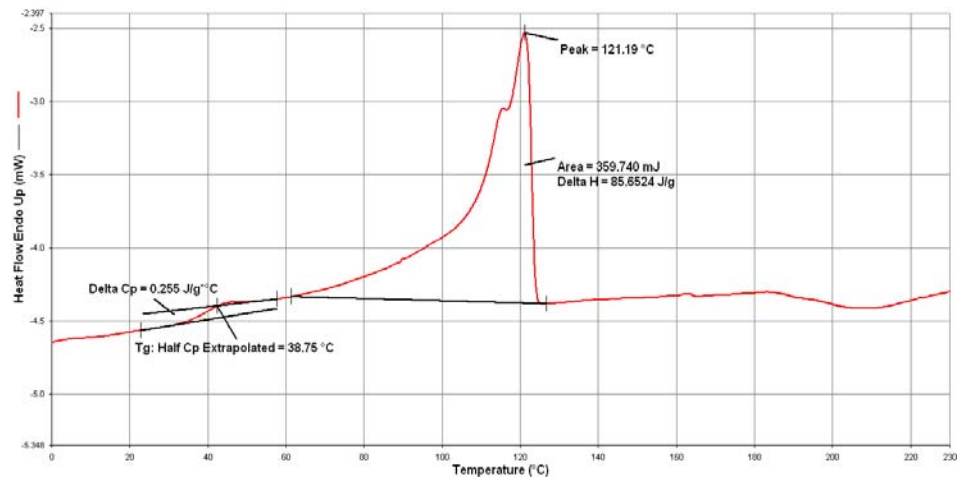


Figure A.25 DSC thermogram of LL/DMDA2/LOT5

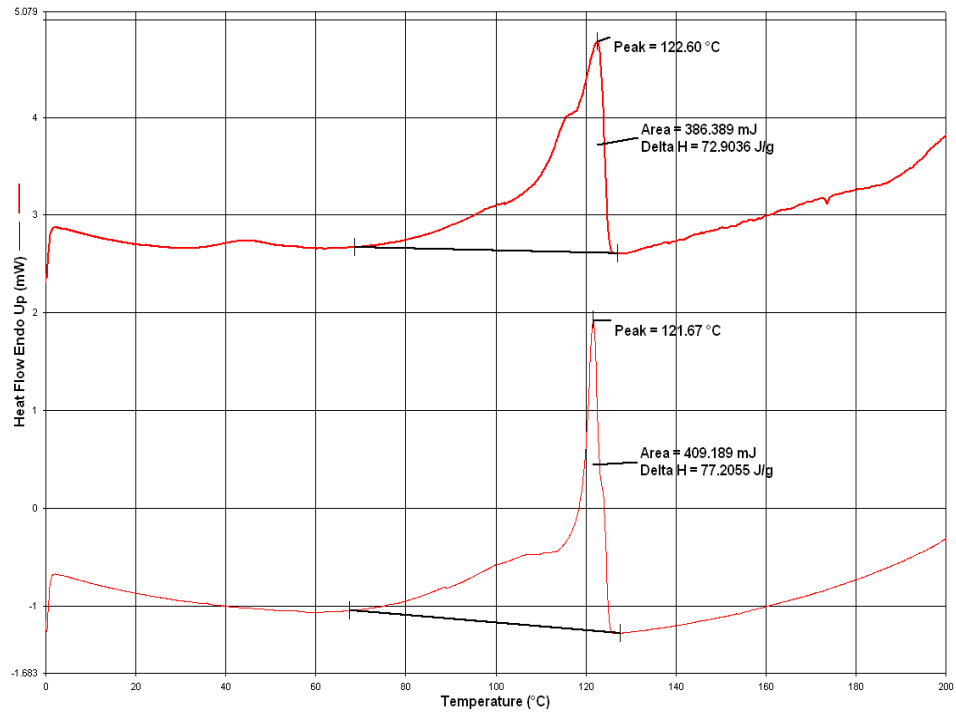


Figure A.26 DSC thermogram of LL/DMDA5/LOT12.5

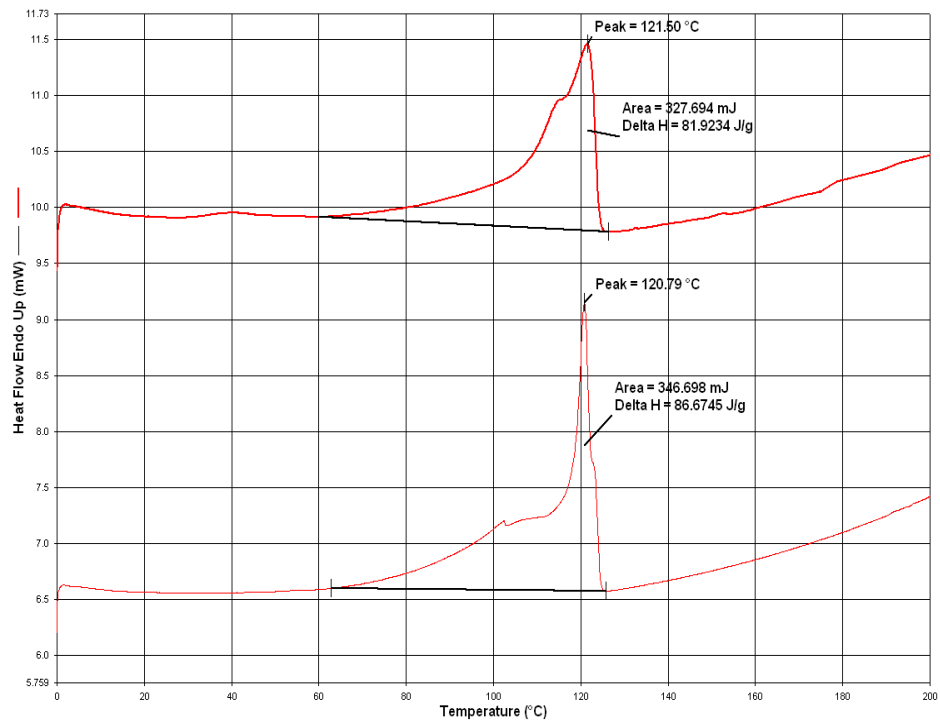


Figure A.27 DSC thermogram of LL/TBHP2/LOT5

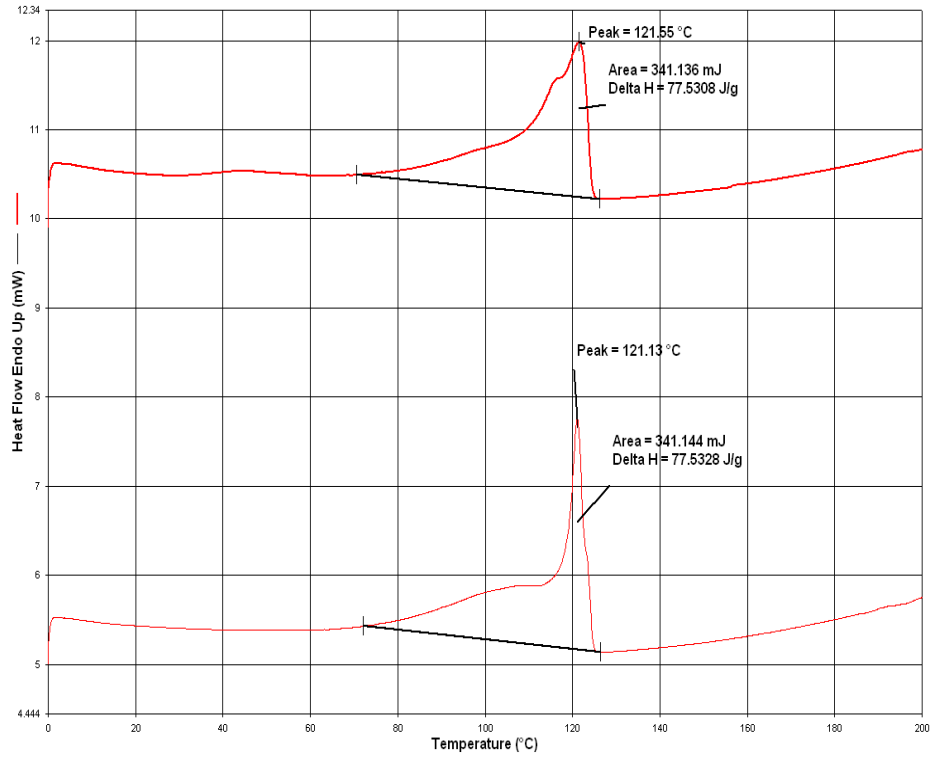


Figure A.28 DSC thermogram of LL/TBHP5/LOT12.5

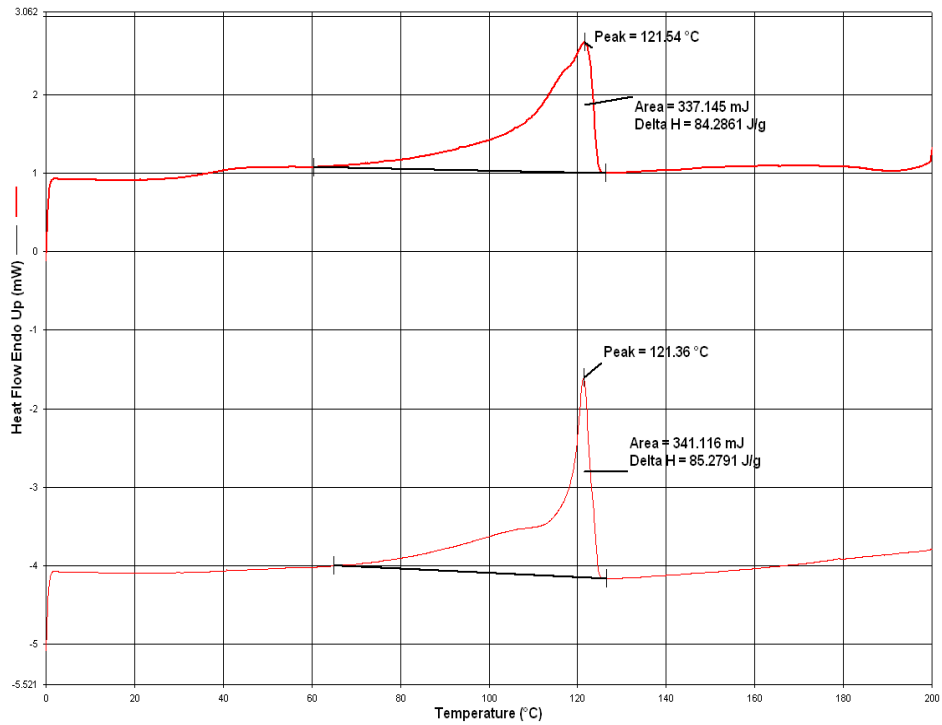


Figure A.29 DSC thermogram of LL/I34-2/LOT5

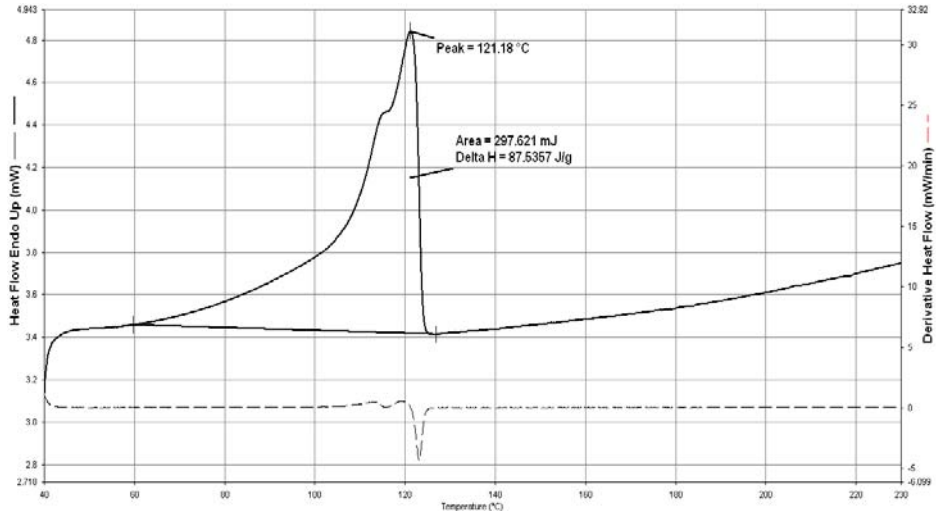


Figure A.30 DSC thermogram of LL/I34-5/LOT5

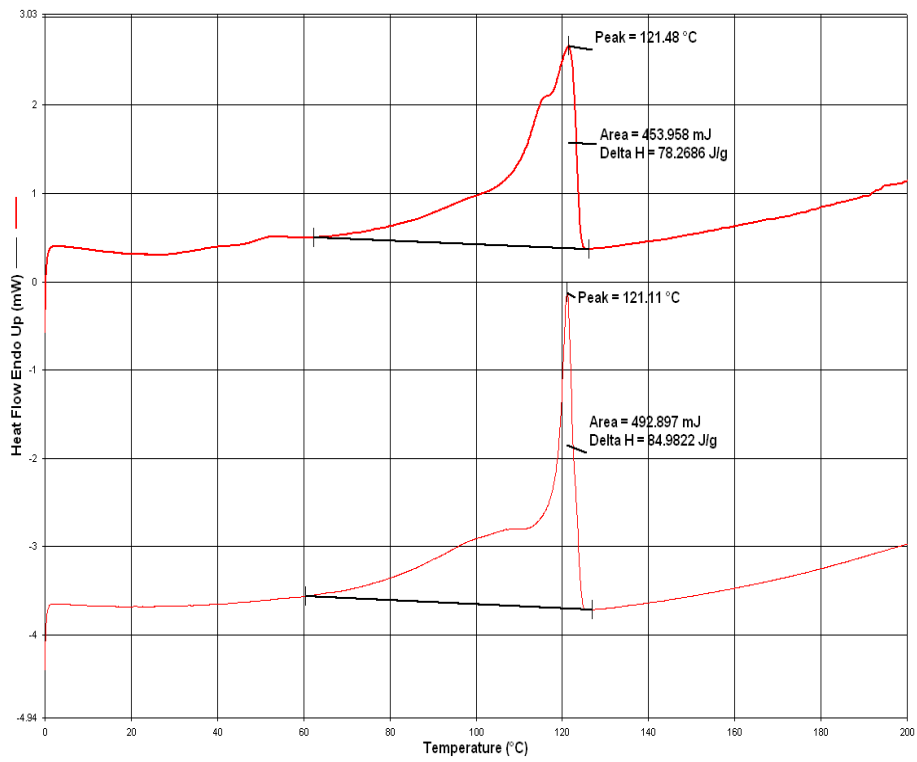


Figure A.31 DSC thermogram of LL/I34-5/LOT12.5

APPENDIX B

MECHANICAL TEST RESULTS

Table B. 1 Tensile strength data for SET-1 and SET-2

SET1			
Two Step Extrusion-150 rpm and 80 rpm during 1st and 2nd extrusion steps, 210°C			
Composition	PPM	Tensile Strength (MPa)	St. Dev. (MPa)
PPM (neat)	100	52.09	2.27
PPM	100	50.82	1.85
PPM95/MAPP5	98	51.24	2.06
PPM/TBA2/MAPP2	96	40.29	2.42
PPM/TBP2/MAPP2	96	42.01	3.21
PPM/HMA2/MAPP2	96	43.23	1.29
PPM/TKA2/MAPP2	96	38.62	3.79
PPM/Cloisite®25A2/MAPP2	96	49.15	1.98
PPM/HMA1/MAPP3	96	44.69	4.58
PPM/TKA1/MAPP3	96	45.46	2.93
SET2			
Two Step Extrusion-350 rpm 180°C			
Composition	PPE	Tensile Strength (MPa)	St. Dv. (MPa)
PPE	100	43.39	2.70
PPE/HMA2/MAPP5	93	42.37	0.85
PPE/TKA2/MAPP5	93	45.37	2.50
PPE/TKA50-2/MAPP5	93	42.96	0.83
PPE/PGWTKA2/MAPP5	93	39.67	3.20

Table B.2 Tensile strength data for SET-3, 4 and 6

SET3			
Two Step Extrusion-350 rpm 180°C			
SET4 (Abbreviated with M)			
Melt mixing of composites prepared in SET3 in the batch mixer at 190 °C and 32 rpm for 15 min with 1 phr B225			
Composition	PPE	Yield Stress (MPa)	St. Dev (MPa)
PPE	100	39.80	1.98
PPE-M	100	43.08	1.84
PPE/DMDA2/MAPP5	93	42.46	1.65
PPE/DMDA2/MAPP5-M	93	49.58	2.68
PPE/TBHP2/MAPP5	93	44.16	0.59
PPE/TBHP2/MAPP5-M	93	46.65	2.33
PPE/STKA2/MAPP5	93	43.34	1.14
PPE/STKA2/MAPP5-M	93	47.20	2.10
SET 6			
Melt mixing in the batch mixer at 190 °C and 32 rpm for 15 min			
Composition	LLDPE	Tensile Strength (MPa)	St. Dv. (MPa)
LLDPE	100	19.52	0.70
LLPE95/LOT5	95	20.60	0.65
LL87.5/LOT12.5	87.5	19.57	1.01
LL/DMDA2/LOT5	93	21.47	1.80
LL/DMDA5/LOT12.5	82.5	22.65	1.07
LL/TBHP2/LOT5	93	20.94	1.16
LL/TBHP5/LOT12.5	82.5	21.34	1.11
LL/I34-2/LOT5	93	22.79	1.05
LL/I34-5/LOT12.5	82.5	25.25	1.97
LL/I34-5/LOT5	90	25.50	1.32

Table B.3 Yield stress data for SET-1 and SET-2

SET1			
Two Step Extrusion-150 rpm and 80 rpm during 1st and 2nd extrusion steps, 210°C			
Composition	PPM	Yield Stress (MPa)	St. Dev. (MPa)
PPM (neat)	100	40.40	2.57
PPM	100	41.33	1.85
PPM95/MAPP5	98	41.00	1.30
PPM/TBA2/MAPP2	96	31.80	2.56
PPM/TBP2/MAPP2	96	29.10	2.22
PPM/HMA2/MAPP2	96	33.40	1.10
PPM/TKA2/MAPP2	96	31.30	1.60
PPM/Cloisite®25A2/MAPP2	96	40.90	1.60
PPM/HMA1/MAPP3	96	34.40	4.50
PPM/TKA1/MAPP3	96	32.70	1.30
SET2			
Two Step Extrusion-350 rpm 180°C			
Composition	PPE	Yield Stress (MPa)	St. Dev. (MPa)
PPE	100	34.1	3.02
PPE/HMA2/MAPP5	93	40.4	1.70
PPE/TKA2/MAPP5	93	35.0	2.50
PPE/TKA50-2/MAPP5	93	41.8	0.90
PPE/PGWTKA2/MAPP5	93	40.0	0.56

Table B. 4 Young`s modulus data for SET-1 and SET-2

SET1			
Two Step Extrusion-150 rpm and 80 rpm during 1st and 2nd extrusion steps, 210°C			
Composition	PPM	Young`s modulus (MPa)	St. Dev. (MPa)
PPM (neat)	100	1534	76
PPM	100	1512	65
PPM95/MAPP5	98	1377	140
PPM/TBA2/MAPP2	96	1639	57
PPM/TBP2/MAPP2	96	1609	29
PPM/HMA2/MAPP2	96	1564	39
PPM/TKA2/MAPP2	96	1502	53
PPM/Cloisite®25A2/MAPP2	96	1787	103
PPM/HMA1/MAPP3	96	1652	67
PPM/TKA1/MAPP3	96	1599	86
SET2			
Two Step Extrusion-350 rpm 180°C			
Composition	PPE	Young`s modulus (MPa)	St. Dev. (MPa)
PPE	100	1444	123
PPE/HMA2/MAPP5	93	1635	113
PPE/TKA2/MAPP5	93	1608	82
PPE/TKA50-2/MAPP5	93	1664	75
PPE/PGWTKA2/MAPP5	93	1450	204

Table B. 5 Young's modulus data for SET-3, SET-4 and SET-6

SET3, Two Step Extrusion-350 rpm 180°C			
SET4 (Abbreviated with M)			
Melt mixing of composites prepared in SET3 in the batch mixer at 190 °C and 32 rpm for 15 min with 1 phr B225			
Composition	PPE	Young's Modulus (MPa)	St. Dev. (MPa)
PPE	100	1351	103
PPE-M	100	1302	102
PPE/DMDA2/MAPP5	93	1624	59
PPE/DMDA2/MAPP5-M	93	1692	142
PPE/TBHP2/MAPP5	93	1547	116
PPE/TBHP2/MAPP5-M	93	1424	147
PPE/STKA2/MAPP5	93	1478	84
PPE/STKA2/MAPP5-M	93	1950	171

Table B. 6 Elongation at break data for SET-1, SET-2

SET1			
Two Step Extrusion-150 rpm and 80 rpm during 1st and 2nd extrusion steps, T = 210°C			
Composition	PPM	Elongation at break (%)	St. Dev. (%)
PPM (neat)	100	444	37
PPM	100	423	28
PPM98/MAPP2	98	545	33
PPM/TBA2/MAPP2	96	504	28
PPM/TBP2/MAPP2	96	527	44
PPM/HMA2/MAPP2	96	520	8
PPM/TKA2/MAPP2	96	563	32
PPM/Cloisite®25A2/MAPP2	96	509	18
PPM/HMA1/MAPP3	96	470	36
PPM/TKA1/MAPP3	96	569	14
SET2			
Two Step Extrusion-350 rpm 180°C			
Composition	PPE	Elongation at break (%)	St. Dv. (%)
PPE	100	634	10
PPE/HMA2/MAPP5	93	587	15
PPE/TKA2/MAPP5	93	642	30
PPE/TKA50-2/MAPP5	93	542	28
PPE/PGWTKA2/MAPP5	93	553	81

Table B. 7 Elongation at break for SET-3, SET-4 and SET-6

SET3			
Two Step Extrusion-350 rpm, T= 180°C			
SET4 (Abbreviated with M)			
Melt mixing of composites prepared in SET3 in the batch mixer at 190 °C and 32 rpm for 15 min with 1 phr B225			
Composition	PPE	Elongation at break (%)	St. Dev. (%)
PPE	100	677	94
PPE-M	100	727	38
PPE/DMDA2/MAPP5	93	456	10
PPE/DMDA2/MAPP5-M	93	352	45
PPE/TBHP2/MAPP5	93	495	59
PPE/TBHP2/MAPP5-M	93	627	52
PPE/STKA2/MAPP5	93	488	48
PPE/STKA2/MAPP5-M	93	317	50
SET 6			
Melt mixing in the batch mixer at 190 °C and 32 rpm for 15 min			
Composition	LLDPE	Elongation at break (%)	St. Dev. (%)
LLDPE	100.0	180	53
LLPE95/LOT5	95.0	133	33
LL87.5/LOT12.5	87.5	184	45
LL/DMDA2/LOT5	93.0	309	60
LL/DMDA5/LOT12.5	82.5	314	14
LL/TBHP2/LOT5	93.0	403	72
LL/TBHP5/LOT12.5	82.5	440	44
LL/I34-2/LOT5	93	70	15
LL/I34-5/LOT12.5	82.5	45	7
LL/I34-5/LOT5	90	53	12

Table B. 8 Elongation at yield data for SET-1 and SET-2

SET1			
Two Step Extrusion-150 rpm and 80 rpm during 1st and 2nd extrusion steps, 210°C			
Composition	PPM	Elongation at yield (%)	St. Dev. (%)
PPM (neat)	100	8.5	0.4
PPM	100	9.5	0.3
PPM98/MAPP2	98	11.6	1.8
PPM/TBA2/MAPP2	96	7.4	0.5
PPM/TBP2/MAPP2	96	7.7	0.4
PPM/HMA2/MAPP2	96	7.5	0.5
PPM/TKA2/MAPP2	96	7.4	0.4
PPM/Cloisite®25A2/MAPP2	96	7.4	0.6
PPM/HMA1/MAPP3	96	7.9	0.6
PPM/TKA1/MAPP3	96	7.9	0.5
SET2			
Two Step Extrusion-350 rpm 180°C			
Composition	PPE	Elongation at yield (%)	St. Dv. (%)
PPE	100	7.5	0.5
PPE/HMA2/MAPP5	93	6.9	0.4
PPE/TKA2/MAPP5	93	7.2	0.7
PPE/TKA50-2/MAPP5	93	7.2	0.3
PPE/PGWTKA2/MAPP5	93	9.2	0.8

Table B. 9 Elongation at yield data for SET-3

SET3			
Two Step Extrusion-350 rpm 180°C			
SET4 (Abbreviated with M)			
Melt mixing of composites prepared in SET3 in the batch mixer at 190 °C and 32 rpm for 15 min with 1 phr B225			
Composition	PPE	Elongation at yield (%)	St. Dev (%)
PPE	100	10.0	0.5
PPE-M	100	13.2	0.8
PPE/DMDA2/MAPP5	93	7.3	0.2
PPE/DMDA2/MAPP5-M	93	7.3	1.3
PPE/TBHP2/MAPP5	93	8.3	0.1
PPE/TBHP2/MAPP5-M	93	10.4	1.3
PPE/STKA2/MAPP5	93	8.4	0.5
PPE/STKA2/MAPP5-M	93	7.3	0.7

APPENDIX C

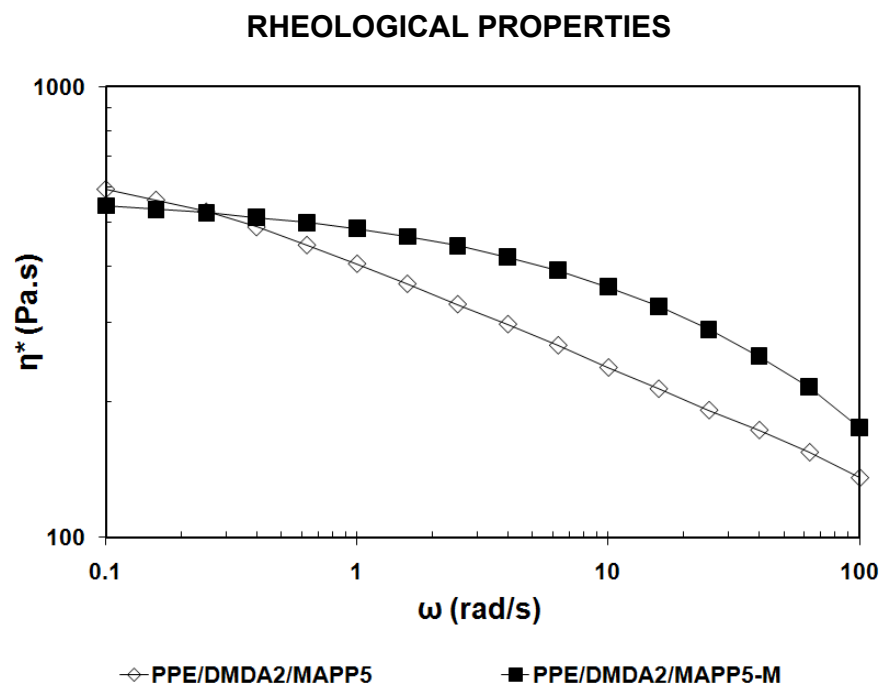


Figure C. 1 Frequency dependence of storage modulus, η^* (Pa.s), of PPE/organoclay2/MAPP5 samples prepared by extrusion only and by extrusion followed by batch mixing. Samples prepared with organoclay DMDA

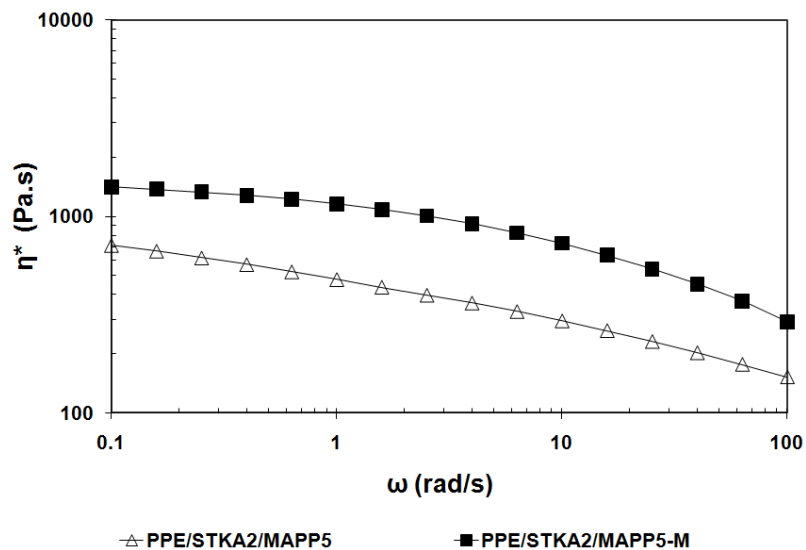


Figure C.2 Frequency dependence of storage modulus, η^* (Pa.s), of PPE/organoclay2/MAPP5 samples prepared by extrusion only and by extrusion followed by batch mixing. Samples prepared with organoclay STKA

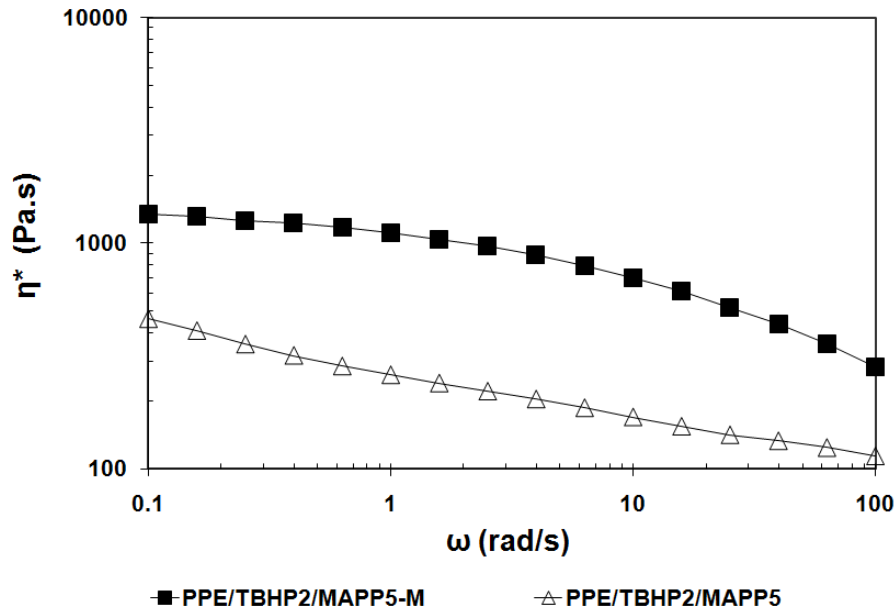


Figure C. 3 Frequency dependence of storage modulus, η^* (Pa.s), of PPE/organoclay2/MAPP5 samples prepared by extrusion only and by extrusion followed by batch mixing. Samples prepared with organoclay TBHP

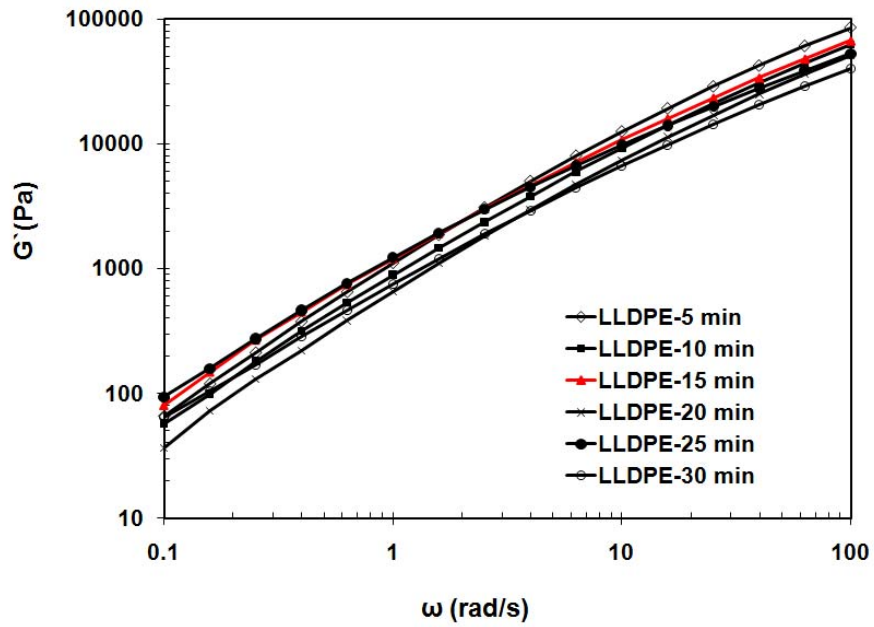


Figure C.4 Frequency dependence of loss modulus, G'' (Pa) of LLDPE mixed for different durations.

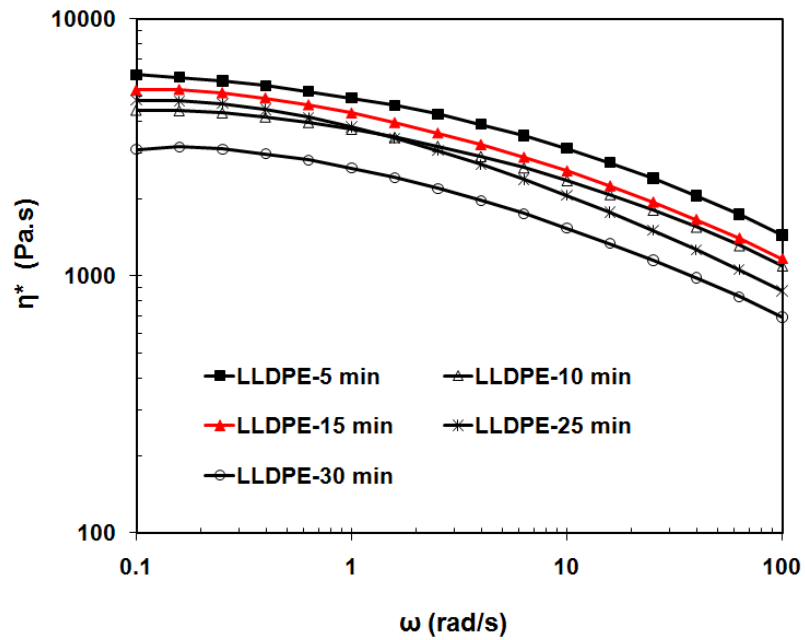


Figure C.5 Frequency dependence of complex viscosity, η^* (Pa.s) of LLDPE mixed for different durations

CURRICULUM VITAE

PERSONAL INFORMATION

Surname, Name: Seyidoglu, Tijen

Nationality: Turkish (TC)

Date and Place of Birth: 13 August 1980, Artvin (TURKEY)

Marital Status: Single

Phone: +90 312 210 43 88

Fax: +90 312 210 26 00

Email: stijen@metu.edu.tr

EDUCATION

<u>Degree</u>	<u>Institution</u>	<u>Year of Graduation</u>
MS	METU, Chemical Engineering	2006
BS	Gazi, Chemical Engineering	2003
High School	Ankara Anittepe Lisesi	1997

WORK EXPERIENCE

<u>Year</u>	<u>Place</u>	<u>Enrollment</u>
2004 December- present	METU, Chemical Engineering	Teaching Assistant
2002, summer	Artvin, Murgul Bakir Fabrikasi	Intern Process Engineer
2001, summer	Ankara, SET Cement Factory	Laboratory Intern

EXPERIENCE ABROAD

<u>Place</u>	<u>Project</u>	<u>Year</u>
Stevens Inst. Tech., Highly Filled Materials Institute, NJ, USA	Production of Polymer- Organoclay Nanocomposites and Their Rheological Characterization	October 2008-April 2009

FOREIGN LANGUAGES

English, Advanced
Intermediate, Georgian

CONFERENCE PRESENTATIONS:

- 1) Tijen Seyidođlu, Ülkü Yılmaz, *Modifiye Edilmiş Kil Üretimi ve Polipropilen Matriks Nanokompozitler İçinde Kullanımı*, Poster Presentation, 2. Ulusal Polimer Bilim ve Teknoloji Kongresi ve Sergisi, Harran Üniversitesi, Sanlıurfa, 30 April-02 May 2008.
- 2) Tijen Seyidođlu, Ülkü Yılmaz, *Modifiye Edilmiş Kil Üretimi Ve Polipropilen Matriks Nanokompozitler İçinde Kullanımı*, Poster Presentation, Sekizinci Ulusal Kimya Mühendisliđi. Kongresi (UKMK-8). İnönü Üniversitesi Kongre ve Kültür Merkezi, Malatya, August 26-29 2008.
- 3) Tijen Seyidođlu, Ulku Yilmazer, Production of Modified Clays and Their Use in Polypropylene Based Nanocomposites, *Oral Presentation*, 24th *Polymer Processing Society Annual Meeting, PPS-24, June 15-19, 2008, Salerno, Italy.*
- 4) Tijen Seyidođlu, Ulku Yilmazer, Dilhan Kalyon, Preparation of Organoclay from Purified Bentonite and Its Use in Organoclay-Compatibilizer-LLDPE Nanocomposites, Poster Presentation, 5th Nanoscience and Nanotechnology Conference (NanoTR5), Anadolu University, Eskişehir, June 08-12, 2009.

- 5) Tijen Seyidođlu, Ulku Yilmazer, Dilhan Kalyon, Linear Low Density Polyethylene/Organoclay/Compatibilizer Ternary Nanocomposites, 6th Chemical Engineering Conference For Collaborative Research In Eastern Mediterranean Countries, EMCC-6, March 7-12, 2010, Belek, Antalya, Turkey,
- 6) Tijen Seyidođlu, Ülkü Yilmazer, Dilhan Kalyon, Safılaştırılmıř Bentonitin Alkil Amonyum/Fosfonyum Tuzları İle Modifiye Edilmesi ve Lineer Alçak Yođunluklu Polietilen Üçlü Nanokompozitlerinde Kullanımı, Oral Presentation, 3.Polimer Bilimi ve Teknolojisi Kongresi ve Sergisi, May 12-14, 2010, Kocaeli Üniversitesi, Kocaeli, Turkey
- 7) Tijen Seyidođlu, Ulku Yilmazer, Polypropylene Matrix Nanocomposites with Organoclays Produced from Turkish Bentonite, Poster Presentation, 6thInternational ECNP Conference on Nanostructured Polymers and Nanocomposites, 27-30 April, 2010, Madrid, Spain.
- 8) Tijen Seyidođlu, Ülkü Yilmazer, Dilhan Kalyon, Organikkillerin Modifiye Edilmesi ve Polipropilen Matris İçinde Kullanımı, Poster Presentation, 9th Ulusal Kimya Mühendisliđi. Kongresi, (UKMK-9), Gazi Üniversitesi Mühendislik-Mimarlık Fakültesi, June 22 – 25, 2010, Ankara, Turkey.
- 9) Ülkü Yilmazer, Tijen Seyidođlu, Faruk Yılmaz, Bitkisel ve Dođal Kaynaklı Dolguların İzolasyon ve İç Trim Parçalarında Kullanımının İncelenmesi, Oral Presentation, The Fifth Automotive Technologies Congress, Otekon, 07-08 June, 2010, Bursa, Turkey.

HOBBIES

Reading, cinema, science, tennis, swimming, dancing, museums, travel